Knowledge-Based Multidisciplinary Sizing and Optimization of Embedded Mechatronic Systems - Application to Aerospace Electro-Mechanical Actuation Systems

Scott Delbecq

THÈSE

En vue de l'obtention du
DOCTORAT DE L'UNIVERSITÉ DE TOULOUSE

Délivré par:
Institut National des Sciences Appliquées de Toulouse (INSA Toulouse)

Discipline ou spécialité:
Génie mécanique, mécanique des matériaux

Présentée et soutenue par
Scott DELBECQ
le: 29 novembre 2018

Titre:
Knowledge-Based Multidisciplinary Sizing and Optimization of Embedded Mechatronic Systems – Application to Aerospace Electro-Mechanical Actuation Systems

---

École doctorale:
Génie mécanique, mécanique des matériaux (MEGEP)

Unité de recherche:
Institut Clément Ader (UMR CNRS 5312)

Directeur de thèse:
Marc BUDINGER

Jury:
Craig LAWSON, Senior Lecturer, Cranfield University, Rapporteur
Johan ÖLVANDER, Professor, Linköping University, Rapporteur
Nathalie BARTOLI, Ingénieur de recherche, ONERA Toulouse, Examinatrice
Marc BUDINGER, Maître de Conférences (HDR), INSA Toulouse, Examinateur
Jean-Charles MARÉ, Professeur, INSA Toulouse, Examinateur
Frank THIELECKE, Professor, Hamburg University of Technology, Examinateur
Benjamin DAGUSÉ, Expert Conception Moteurs Électriques, Safran Electronics & Defense, Invité
Jérôme PIATON, Expert Systèmes Électromécaniques, Safran Electronics & Defense, Invité

To Julian

Acknowledgements

First, I would like to thank the members of the jury for accepting to examine my work. I particularly would like to thank Prof. Craig Lawson and Prof. Johan Ölvander for accepting to review the work presented in this thesis. The quality of their reviews and their suggestions have significantly helped me improve the quality of this dissertation. I am also very thankful to Dr. Nathalie Bartoli and Prof. Frank Thielecke for their relevant remarks and the interesting discussions we had during the oral defense. I wish to thank Prof. Jean-Charles Maré for doing me the honor of presiding this jury.

L'accomplissement de cette thèse n'aurait pas été possible sans l'initiative et l'accompagnement de certaines personnes. Initialement, le sujet de cette thèse a été suggéré par mon ancien tuteur de stage chez Sagem, Nirina Feliste, qui avait identifié très tôt l'intérêt d'une approche système pour le dimensionnement de systèmes d'actionnement. Merci Nirina de m'avoir proposé cette thèse et pour avoir partagé ton expertise en modélisation multi-physique et en automatique appliquée.

Le second initiateur de cette thèse que je souhaite également remercier est mon directeur de thèse, Marc Budinger. Merci Marc pour ton implication naturelle et constante tout au long de cette thèse. Cette implication associée à ta grande expertise technologique et méthodologique ont permis de diriger mes travaux de thèse d'une façon que je trouve exemplaire. Ces trois années de travail sous ta direction ont été particulièrement intenses mais très plaisantes et très enrichissantes à la fois scientifiquement et humainement. J'en garderai un très bon souvenir. J'espère que nous pourrons continuer à collaborer dans le futur.

Je souhaite également remercier mes encadrants industriels, Jérôme Piaton et Benjamin Dagusé. Jérôme, merci de t'être rendu disponible aux moments clés de mes travaux. Tes conseils ont permis de guider ces travaux pour qu'ils répondent à la fois aux problématiques scientifiques et industrielles. Merci également d'avoir partagé une fraction de ta grande expertise et tes expériences en développement de systèmes électromécaniques embarqués. Benjamin, tu as grandement contribué à ce que cette thèse CIFRE se déroule de la meilleure des manières. En tant qu'ancien doctorant tu as su me conseiller à la fois scientifiquement et d'un point de vue organisationnel. Merci pour ta pédagogie les fois où j'ai eu besoin d'un expert de la machine électrique ! J'ai pris beaucoup de plaisir à travailler avec vous et j'espère que nous pourrons continuer à collaborer. Je n'aurais pas pu demander de meilleurs directeurs de thèse et encadrants, merci encore.

Il est maintenant temps de remercier mes collègues de Safran Electronics and Defense. Je ne vais pas énumérer chacun d'eux mais je garderai un bon souvenir de l'ambiance et des personnes que j'ai pu rencontrer. Je voudrais quand même remercier le cercle rapproché de collègues issue de la

naissance de l'équipe Asservissement et Puissance. Cette équipe est pour moi un bel équilibre entre expertise multi-domaine et convivialité, j'en garderai d'excellents souvenirs. Merci à Audrey, Badr, Baptiste, Benjamin, Blaise, Hicham, Jérôme, Medhi, Romain et l'ensemble des stagiaires que j'ai pu rencontrer.

Qui dit thèse dit laboratoire, et ici il est question de l'Institut Clément Ader. Ce fut pour moi un très bon environement de travail, j'ai pu y rencontrer des personnes formidables avec qui j'espère garder contact. Merci à Marc, Pierre et Alain de m'avoir proposé d'effectuer des enseignements. Cela m'a permis de découvrir quelque chose de nouveau et que je souhaite continuer désormais. Je souhaiterais remercier les enseignants-chercheurs de l'équipe actionneurs embarqués, Dimitri, Ion et Jean-Charles qui m'ont apporté des conseils dès qu'ils en ont eu l'occasion. Merci Jean-Charles de m'avoir encourager à me lancer une thèse, comme souvent c'était un très bon conseil de ta part ! J'espère qu'on continuera à se voir pour discuter actionneurs et aviation en général ! Je souhaite aussi remercier l'ensemble des doctorants, enseignants-chercheurs et personnels scientifiques de ce laboratoire à taille humaine. Je vais quand même remercier individuellement le cercle rapproché des collègues et amis: Florent, Florian, Adrien, Simon, Victor, Pierre, Aurélien, Jérôme, Nicolas, Battoul, Ahmad, Laure, Guillaume, Louis, et les animaux, Francesco and Silvio. Je voudrais également remercier les stagiaires, Christophe, Thomas et Luis, que j'ai pu encadrer ainsi que les différents étudiants que j'ai eu en projets à l'INSA et l'ISAE. Leurs travaux ont contribué à différentes thématiques de cette thèse.

La réussite d'une thèse est sans aucun doute conditionnée par un bon équilibre entre travail et vie personnelle. Je vais donc maintenant remercier mes proches et mes amis qui m'ont apporté un soutien inégalable et d'innombrables opportunités de sortir la tête de cette thèse.

Merci à mes amis et famille du Sporting Club Graulhétois que j'ai décidé d'abandonner pour me consacrer pleinement à cette thèse. C'est toujours un plaisir de venir vous voir jouer et de passer quelques soirées avec vous ! Je n'oublierai jamais ces années magiques dans ce club dont l'ambiance est unique.

Parallèlement, je souhaite remercier les Galactics, la génération de juniors reichel qui a marqué l'histoire du club, pour leur précieux conseils pour mener à bien ces travaux de thèse. Non je plaisante ! Merci pour les retrouvailles annuelles qui ne sont que du bonheur. Un grand merci à notre père spirituel à tous, Christian, qui m'a toujours soutenu rugbystiquement et professionnellement.

Je souhaite remercier également tous mes amis de l'INSA, du rugby mais pas que ! C'est toujours un plaisir pour moi de vous voir et de retrouver cette convivialité notamment lors de l'annuelle Foire au Jambon ou au RIRE ! Un merci particulier à Charles, Florent et Greg (la Dream Team) pour les années d'IS et celles qui ont suivies.

Je remercie également "la bande à Marie-Laure" qui m'ont accueilli chaleureusement dans leur groupe et qui ont su apporter le soutien nécessaire à Marie-Laure pour me soutenir à son tour pour le sprint final.

Je ne peux pas oublier "les bon gars" (Adrien, Baptiste, Beard, Charp', Fridjof, Guedot, Lucas, La Bete, Le Corse, La Lope, La Monfe et Rabbi), pour avoir presque cru en moi quand j'ai annoncé me lancer dans une thèse, mais surtout pour ces nombreux souvenirs et les autres à venir. Merci pour

toutes ces émotions collectives ! Une mention spéciale pour Adrien et ses coups de fil hebdomadaire, tu es notre guide à tous !

Merci également à mes amis de très longue date: Brice, Ferry, Crevette, Gonzo, Mael, Nico et Romain. Les années passent, les souvenirs s'accumulent, que ça continue ! Un merci particulier à Nico (et Marine !), "les collocs", pour m'avoir accueilli chaleureusement durant mes périodes sur Paris qui resteront de très bons souvenirs.

Merci aussi aux membres de ma belle famille qui ont cru en moi et qui m'ont également encouragé tout au long de cette thèse.

Enfin, je remercie ma famille étendue, les Delbecq, les Levavasseur, les Malcolm, les McGlade et les Saunders, pour leurs encouragements et tous les bons moments qui résultent de nos retrouvailles. Je remercie particulièrement "la meute" Delbecq pour leur soutien, notamment mes parents à qui je dois beaucoup. Merci pour tous ces précieux moments ensemble et ceux à venir. Je souhaite remercier pour terminer ma compagne, Marie-Laure. Merci pour ton soutien sans faille, et surtout pour l'amour et le bonheur que l'on partage chaque jour.

Résumé

Un défi à court terme pour les industriels de l'aéronautique est de concevoir des produits sûrs, fiables, compactes, basse consommation et à faible impact environnemental due à la forte concurrence et à l'augmentation des attentes des clients et des autorités de certification. Un défi à plus long terme pour ces organisations est de pérenniser leur savoir-faire et leur expertise qui sont menacés par le départ en retraite de générations d'experts, ingénieurs et techniciens. Relever ces défis n'est pas une tâche facile lorsque les produits concernés sont des systèmes mécatroniques embarqués tel que les systèmes d'actionnement électromécaniques. La conception de ces systèmes complexes nécessite l'intégration de savoirs très hétérogènes dû aux interactions entre de nombreux métiers de l'ingénierie, ainsi qu'entre les différentes lois de la physique qui caractérisent leur comportement. De plus, les systèmes mécatroniques embarqués sont constitués de nombreux composants interdépendants. Gérer les dépendances entre composants reste une tâche non-triviale et fondamentale du métier d'ingénieur. Ceci conduit à des itérations coûteuses durant le cycle de conception et des solutions non-optimisées. Les techniques d'optimisation multidisciplinaire fournissent des fondements théoriques et des outils de calculs permettant l'optimisation de systèmes comportant un grand nombre de variables et des couplages multidisciplinaires. Dans le but d'utiliser ces techniques pour un dimensionnement rapide des produits mécatroniques, des tâches doivent être effectuées : représentation du savoir de conception, décomposition et coordination des modèles pour l'évaluation et l'optimisation des performances du système. Les modèles algébriques ont été choisis pour représenter les différents modèles de conception. Une nouvelle formulation d'optimisation multidisciplinaire est proposée. Elle permet des convergences rapides et s'avère robuste au changement d'échelle. Une approche basée sur la théorie des graphes et le calcul symbolique est proposée pour aider les ingénieurs à la mise en place de problèmes à grand nombre de variables et comportant des couplages multidisciplinaires. Une méthodologie de conception et dimensionnement est présentée ainsi que l'outil logiciel associé. L'objectif principal est de permettre un dimensionnement global des systèmes mécatroniques en insistant sur réutilisation du savoir et la prise de décision rapide. La méthodologie est illustrée sur un cas simple de système d'actionnement aéronautique. Ensuite, des systèmes plus complexes sont abordés. Tout d'abord, la conception d'un système d'actionnement électromécanique de commandes de vol primaire est étudié. Enfin, la méthodologie est appliquée à un système d'actionnement d'inverseur de poussée électrique.

Abstract

The critical short term challenge for contemporary aerospace industrial companies is to design safe, reliable, compact, low power consumption and low environmental impact products, forces driven by economic competition and the increasing expectations of customers and certification authorities. A long-term challenge for these organizations is to manage their knowledge and expertise heritage, which is jeopardized due to forthcoming retirement of the current generation of experts, engineers and technicians. Undertaking these challenges is particularly intricate when it comes to embedded mechatronic systems used in electro-mechanical actuation systems. The design of these complex systems involves heterogeneous knowledge due to the interface of multiple engineering specializations and the interacting physical laws that govern their behaviour. Additionally, embedded mechatronic systems are composed of several interdependent components and sub-systems. Dealing with interdependencies remains a non-trivial and fundamental aspect of modern engineering practice. This can result in costly iterations during the design process and final non-optimal solutions. Multidisciplinary System Design Optimization techniques provide theoretical foundations and computational tools for optimizing large and multidisciplinary systems. Tasks must be performed to apply such techniques for rapid initial sizing of mechatronic products: modelling the design knowledge, partitioning and coordinating the models for system performances analysis and optimization. Algebraic analysis functions are chosen to represent the design models. A new Multidisciplinary System Design Optimization formulation for fast and robust analysis is proposed. A theoretic graph approach using symbolic manipulation to assist designers in formulating large and multidisciplinary problems is outlined. A specific design methodology and its associated framework developed are presented. The general objective is to allow holistic sizing of mechatronic engineering systems with emphasis placed on model reusability and rapid decision making. The methodology is illustrated using a simple aerospace actuation system example. More complex actuation systems are then addressed. First, the design of an electro-mechanical primary flight control actuation system is examined, subsequently; the design methodology is applied to an electrical thrust reverser actuation system.

Table of contents

List of figures

List of tables

Nomenclature

Acronyms / Abbreviations

AAO	All At Once
AC	Alternating Current
AD	Automatic Differentiation
AE	Algebraic Equation
ARP	Aerospace Recommend Practice
ATC	Analytical Target Cascading
ATO	Aborted Take Off
ATRU	Autotransformer Rectifier Unit
BFGS	Broyden-Fletcher-Goldfarb-Shanno
BLI	Boundary Layer Ingestion
BLISS	Bilevel Integrated System Synthesis
BOA	BOA framework: Bind your models, Optimize your system, Accelerate your design
CAD	Computer Aided Design
CFD	Computational Fluid Dynamics
CMA-ES	Covariance Matrix Adaptation Evolution Strategy
COBYLA	Constrained Optimization By Linear Approximation
CO	Collaborative Optimization
CS	Complex Step
CSO	Collaborative Subspace Optimization

DAE Differential Algebraic Equation

DC Direct Current

DOE Design of Experiments

DSM Design Structure Matrix

EBHA Electro Back-up Hydrostatic Actuator

EEC Electronic Engine Controller

EHA Electro Hydrostatic Actuator

EMA Electro Mechanical Actuator

EMI Electromagnetic Interference

ETRAS Electrical Thrust Reverser Actuation System

FCC Flight Control Computer

FD Finite Difference

FEM Finite Element Method

FMI Functional Mock-up Interface

FMU Functional Mock-up Unit

FTA Fault Tree Analysis

HSTA Horizontal Stabilizer Trim Electromechanical Actuator

HVDC High Voltage Direct Current

IBC Individual Blade Control

IDF Individual Discipline Feasible

KKT Karush-Kuhn-Tucker

LHS Latin Hypercube Sampling

LoC Lines of Code

MAUD Modular Analysis and Unified Derivatives

MBSE Model-based Systems Engineering

MDA Multidisciplinary Design Analysis

MDAO Multidisciplinary Design Analysis and Optimization

MDF MultiDisciplinary Feasible

MDO Multidisciplinary Design Optimization

MOSFET Metal-Oxide-Semiconductor Field-Effect Transistor

MSDO Multidisciplinary System Design Optimization

MTBF Mean Time Between Failure

NACA National Advisory Committee for Aeronautics

ND Normal Deploy

NSGA2 Non Sorting Genetic Algorithm II

NS Normal Stow

NVH Normalized Variable Hybrid

ODE Ordinary Differential Equations

PbW Power-by-Wire

PCU Power Control Unit

PDE Partial Differential Equation

PDU Power Drive Unit

PFCAS Primary Flight Control Actuation System

PLS Primary Locking System

PSO Particle Swarm Optimization

RSM Response Surface Methodology

SAND Simultaneous Analysis and Design

SbW Signal-by-Wire

SD Symbolic Differentiation

SHA Servo Hydraulic Actuator

SiC Silicon Carbide

SLSQP Sequential Least Square Quadratic Programming

SNOPT Sparse Nonlinear OPTimizer

TB Thrust Bearing

THD Total Harmonic Distorsion

TLS Tertiary Locking System

TRAS Thrust Reverser Actuation System

TRCU Thrust Reverser Controller Unit

TRL Technical Readiness Level

TRS Thrust Reverser System

TVC Thrust Vector Control

UDE Unified Derivatives Equations

XDSM Extended Design Structure Matrix

Chapter 1

Context

1.1 The More Electrical Aircraft

Over the last century, aerospace engineering has evolved increasingly complex aircraft architectures. Today's aircraft are complex systems that can be decomposed into different layers as shown in Figure 1.1.

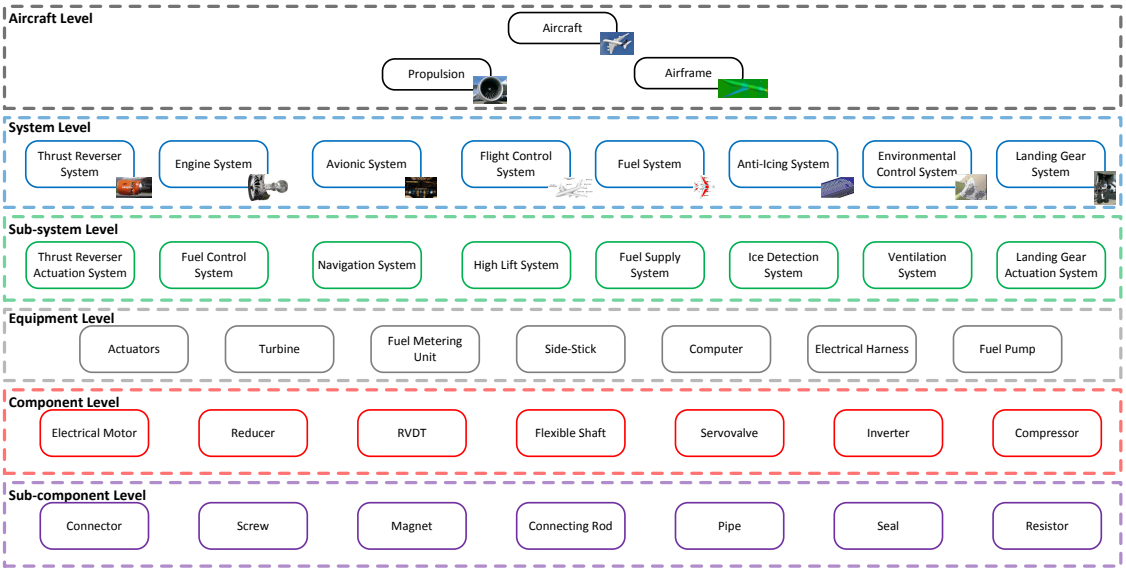

Fig. 1.1 Decomposition of a fixed wing aircraft (Non-exhaustive)

Environmental protection is a key driver for next generation aircraft as one of the goals of Flightpath 2050 are asked by ACARE European Council [121]. In order to drastically reduce fuel burn, emissions and noise, new aircraft concepts have been proposed. They investigated innovative propulsion systems [184], airframes, propulsion-airframe integration for boundary layer ingestion (BLI), and system and equipment architectures. New carbon alloys for structural components have helped reduce aircraft structural weight (the Airbus A350 and Boeing 787) while the use of winglets

has enabled a decrease in fuel consumption. The hybrid electric propulsion system and aft-mounted BLI concept of NASA's Starc-ABL aircraft [91], illustrated in Figure 1.2, and Safran's open-rotor engine architecture [39] illustrate such research trends .

Fig. 1.2 NASA's Starc-ABL aircraft concept [242]

One research direction consists of electrifying propulsion and associated systems equipment by leveraging the advantages of electrical technologies in terms of integration, maintenance and power efficiency. Increasingly, this "more electrical aircraft" course of action is driving both the research and technological focus of the aeronautical industry and academica. The research on non-propulsive systems can be separated in two main themes as illustrated in Figure 1.3. The first theme investigates the replacement of pneumatic systems by electrical systems. The goals are the increase of the overall gas turbine efficiency, easier physical integration and simplified maintenance. The second theme investigates the concept of hydraulics-free aircraft which consists of replacing hydraulics with electrical systems. Particularly for large aircraft, the main goal is to reduce the overall weight while being easier to integrate and maintain. Furthermore, electrical systems are considered more environmentally friendly than hydraulic systems due to the removal of Skydrol fluid.

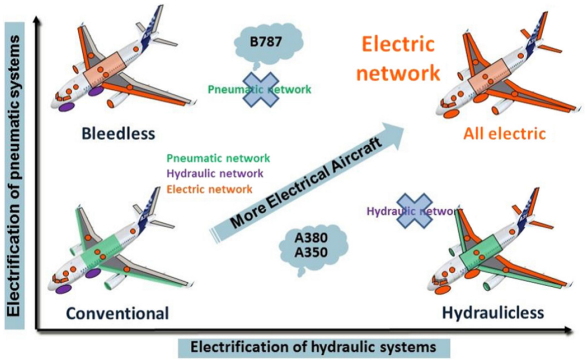

Fig. 1.3 The two axis of More Electrical Aircraft [87]

To date, non-propulsive electrical systems applications cover the complete range of Technical Readiness Levels (TRLs). For improving gas turbine efficiency, bleed valves have been replaced by an electrically driven compressor on the Boeing 787 aircraft [175]. This same aircraft also integrates electrical resistance elements that generate heat under the leading edge surface of the wing which promises lower power consumption than other de-icing technologies that bleed hot air from the engine.

Other major non-propulsive systems are actuation systems. Commercial aircraft need different actuation systems to fulfill their needs as illustrated in Figure 1.4.

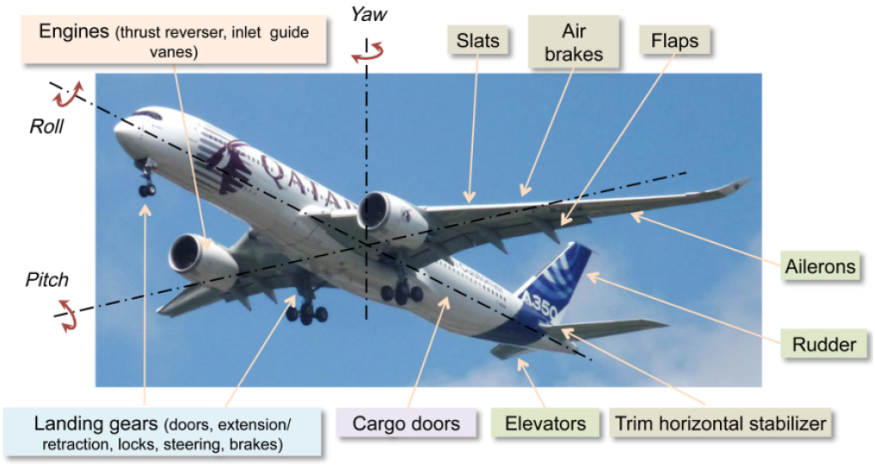

Fig. 1.4 Actuation needs on a commercial aircraft [150]

They are used to deploy and retract the landing gear or to actuate flight control surfaces. Such systems also tend towards electrification. Electrical Thrust Reverser Actuation Systems (ETRAS) are composed of an electro-mechanical power chain and have been introduced on Airbus A380, Airbus A350 and COMAC C919 nacelles. The electrification of aircraft systems and equipment has also impacted flight controls. Fly-by-wire concepts introduced Signal-by-Wire (SbW) actuators using Servo Hydraulic Actuators (SHA) [152]. The hydraulic power used by SHA is generated by engine driven pumps and distributed by hydraulic networks. Power-by-Wire (PbW) actuators such as Electro Back-up Hydrostatic Actuators (EBHAs) and Electro Hydrostatic Actuators (EHAs), shown in Figure 1.5, were introduced in the back line of primary flight control surfaces on the Airbus A380 which enabled to reduce the aircraft overall weight by removing the tertiary hydraulic network [234].

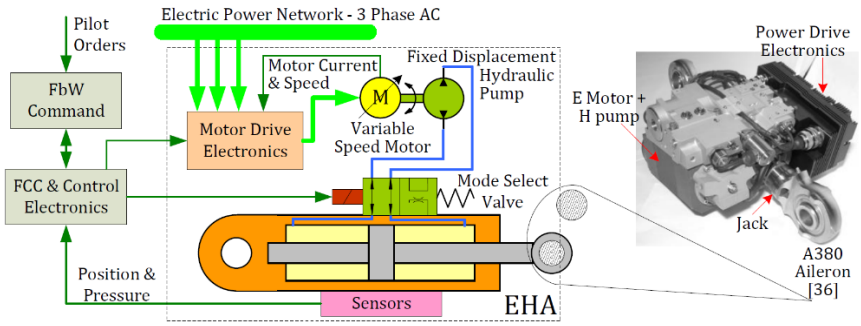

Fig. 1.5 Description of an EHA [240]

The next step was to introduce PbW Electro Mechanical Actuators (EMAs) which enabled the removal of hydraulic fluid of actuators such as those described in Figure 1.6. This technology is currently in front line of two spoilers control surface of the Boeing 787 and Airbus A350-1000.

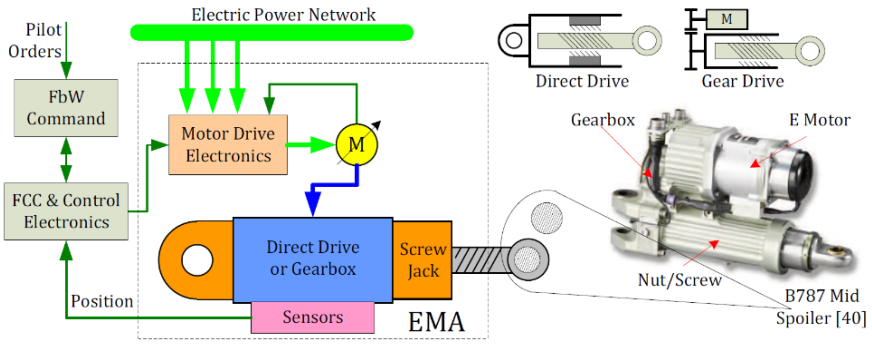

Fig. 1.6 Description of an EMA [240]

Furthermore, new electrical distribution systems are currently investigated to supply these non-propulsive electrical loads [87].

The integration of these new technologies can increase risks of unexpected behaviours of these critical systems leading to costly re-designs. In some investigated concepts, practical electrical technologies do not yet meet performances requirements and integration constraints. Despite being more efficient, these electrical technologies still generate losses. This heat excess has to be managed locally or else it could result in non-acceptable life time degradation or outright failures of boundary equipment and components. Additionally, these new electrical systems have to prove that they meet the stringent reliability and availability requirements of contemporary commercial aircraft. Therefore, one of the challenges for developing a more electrical aircraft is to master the design and integration of the next-generation mechatronic systems for actuation and other needs. For this purpose, several European and French research projects have investigated design methodologies and the development of physical prototypes.

1.2 Previous Research Projects and Previous Theses

Several research projects around the More Electrical Aircraft concept have driven research teams at both Institut Clément Ader in Toulouse and the Safran company.

The first were Electrically Powered Integrated Control Actuators – EPICA [1] (1993-1997) and Electrical Innovative Surface Actuation – ELISA[1] (1999-2001) which concerned alternative power architectures for actuation systems. In the beginning of the 21st century, Power Optimized Aircraft – POA[1] : 2002-2006 seeked ways to optimize the aircraft power architecture. Then projects like More Open Electrical Technologies – MOET[1] (2006-2009) focused on developing methodologies and technologies to enable better flexibility and use of electrical equipments. "Concept Innovant de Systémes d'Actionnement de Commandes de vols secondaires et de Servitudes" – CISACS[1] (2008 - 2012)[1,2] and DRESS on the other hand concerned the electrification of landing gear actuation systems.

[1] Institut Clément Ader projects
[2] Safran projects

COVADIS[2] (2008-2011) was a project between Airbus and Safran which resulted in flight tests of electro-mechanical primary flight control actuators for ailerons [58]. SYRENA[1,2] (2010 - 2013) was a research project that involved industrial partners such as Safran and research laboratories. FRACASS[2] (2011-2014) investigated the concept of control surface splitting with rotary on-hinge electro-mechanical actuators. It also investigated new architectures for regulation functions of gas turbines. Actuation 2015[1,2] (2012-2016) involve a larger number of industrial and academic partners and focused on the standardization of aerospace actuators and power electronics from landing gears to flight control. CORAC Genome[2] (2013-2018) funded by French research funds, had for objective to develop future electrical equipment and systems. SYRENA II[1,2] (2014 - 2018), the successor of this first project is currently under development.

In parallel of the previous research projects, many PhD thesis were involved. Some took place in the Actuation System team of Institut Clément Ader and greatly contributed to the work done in this thesis.

Liscouet-Hanke investigated aircraft power architectures and proposed a design methodology to better size them and enable aircraft level trade-offs [143]. Liscouet was the first PhD student in the laboratory to use scaling laws for the preliminary sizing of actuators [141]. Hospital focused on developing sizing models based on inverse simulation [109]. Giraud developed a methodology for the sizing of aircraft electrical networks [86]. Reysset developed preliminary design tools such as specification generation based on mission profile analysis [194]. Coic proposed a bond-graph based modelling approach to support the design of high dynamic hydraulic servo-actuators [43]. Sanchez proposed a methodology to generate algebraic analysis functions based on Finite Element Method simulations in order to utilize them during the preliminary sizing of actuation systems [207]. Monsimer investigated methods for enabling radical innovation during early preliminary design phases of fuel regulation systems [170]. Thauvin used design exploration of regional hybrid electrical aircraft concepts using multidisciplinary design and optimization methods [229].

On the other side of the atlantic, alternatives for more electrical systems and actuators have early been identified early [139]. Investigations of these alternatives were supported by US research programs such as Electrically Powered Actuator Design (EPAD) which leaded to the development of a primary flight control electro-mechanical actuator [130]. The final outcome was flight tests of the prototype on the F-22 [117]. Significant US military programs have provided the introduction of new technologies such as the F-22 [16] and the F-35 [197]. On the civil program side, the Boeing 787 more electric subsystems introduced the need for higher electrical power generation [19] as well as new electric drive technologies [34].

1.3 Scope of the Thesis

The eco-system and context where this thesis has emerged were previously outlined. They have greatly influenced the investigations in this thesis as well as other research work discovered over three

years. This part describes the scope of this thesis in terms of the studied systems, components and objectives.

1.3.1 Typical Systems

The systems studied in this thesis are in most cases actuation systems of Safran's portfolio. Nevertheless, the methods and approaches developed in this thesis can be applied to other kinds of embedded mechatronic systems but will be here applied to aerospace actuation systems. An example of functional actuation chain is given in Figure 1.7.

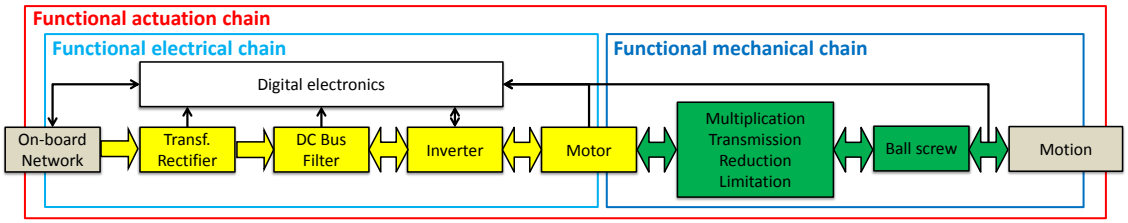

Fig. 1.7 A typical actuation system functional chain

An actuation system functional chain can be decomposed into functional electrical and mechanical chains. The purpose of such systems are to move specific mobile structures such as control surfaces or, for example, a thrust reverser transcowl. The interfaces of such electrical systems are an electrical interface, generally an electric power supply, and mechanical interfaces which generally support where the system is integrated to the mobile structure. The electrical chain is used to transform the aircraft 3-phase electrical network into a local Direct Current (DC) electrical network. It is also in charge of distributing and controlling the required motion. The mechanical chain is there to adapt and distribute the power so that it is capable of the required motion. The electrical motor permits linking the electrical and the mechanical chain by transforming electrical power into rotational mechanical power.

Flight Controls Applications

The purpose of primary flight control systems is to control the aircraft trajectory by acting on movable surfaces. Ailerons are the primary flight control surfaces that act for roll control. They can be actuated by a linear electro-mechanical actuator like Figure 1.8 [58].

Other electro-mechanical topologies have been developed such as rotary electro-mechanical actuators like Figure 1.9.

Secondary flight controls are used to change the aerodynamic configuration of the aircraft during a particular flight phase. For example, the Horizontal Stabilizer Trim electro-mechanical Actuator (HSTA), illustrated in Figure 1.10, ensure the overall equilibrium of the aircraft during the given flight phases (e.g. climb, cruise or approach) [150].

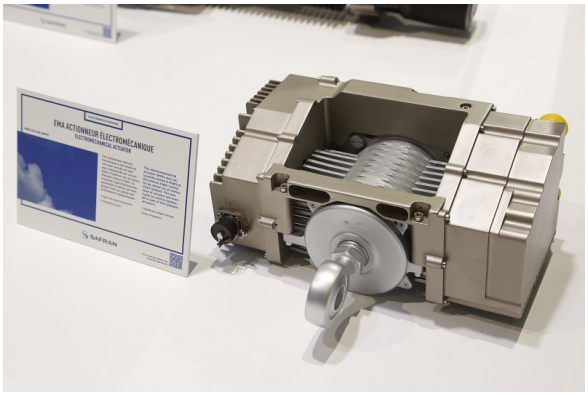

Fig. 1.8 Linear Aileron Electro-Mechanical Actuator (Safran)

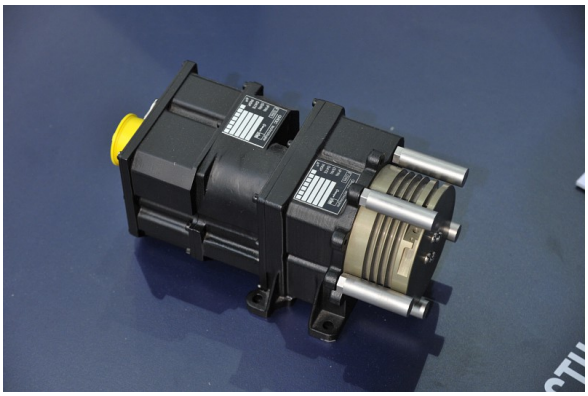

Fig. 1.9 Rotary electro-mechanical Actuator (Safran)

Fig. 1.10 Horizontal Stabilizer Trim electro-mechanical Actuator (Safran)

Thrust Reverser Application

Thrust Reversers are used to reverse the engine thrust just after touchdown during the landing phase in order to enhance wheel brakes sustainability, and land on shorter, wet or icy runways. Electrical thrust reverser actuation systems are one technology for actuation nacelle thrust reversers (Figure 1.11).

Fig. 1.11 Engine, nacelle and actuation system (CFM/Nexcelle/Safran)

The challenges linked to the design of these system examples are given and studied in this thesis.

1.3.2 Typical Components

These typical electro-mechanical systems are composed of mechatronic components required to fulfil the specified functions. The main design drivers (system level) of these components are outlined.

Power Electronics

Power electronics are one main component of electrical actuation systems. The autotransformer is an electrical component that transforms an alternative electrical network into two alternative electrical networks with different voltage and current but the wave form and frequencies remain the same. The 3-phase autotransformer is widely used in aeronautics because of its compactness and is low Total Harmonic Distorsion (THD). They are often associated to rectifier that transform the two 3-phase electrical network into one DC network. In some case, interphase inductors are added to smoothen current pulses on the DC network. Inverters composed of semi-conductors are then used to transform the DC voltage into 1-phase or 3-phase voltage sources depending on the load they have to drive. Figure 1.12 shows pictures of common power electronic components.

The main design drivers of autotransformers and interphase inductors are the magnetic saturation of the core and the maximum temperature of the windings. For inverters, the main design drivers

(a) Example of autotransformer unit (Thales)

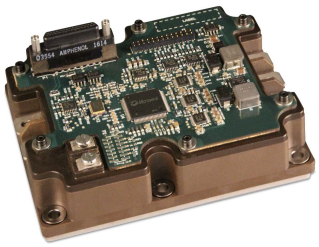

(b) Example of Silicon Carbide (SiC) power core module (Microsemi)

Fig. 1.12 Two main electrical components of aerospace actuation systems

are the switching frequency and the maximum temperatures of diodes and transistors. Generally as the main design drivers include the thermal behaviour of components, the power electronic design includes the cooling system (heat sink, liquid...).

Another power electronics component used in regenerative energy devices is the braking resistor. Whereas as in some systems like electrical vehicles the regenerative energy is stored, some system use this device to transform the energy into heat that must be dissipate. One topology of this component is the planar resistance illustrated in Figure 1.13.

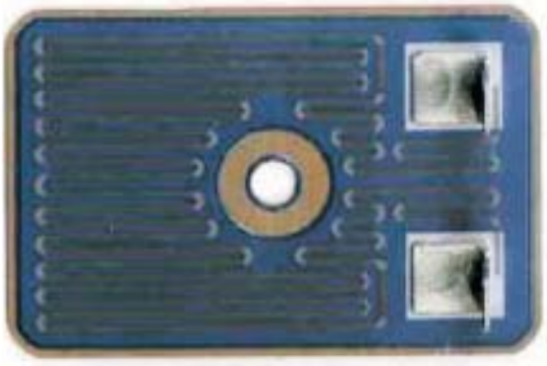

Fig. 1.13 Example of planar braking resistor

The main design drivers of this component are its resistance value and its maximum temperature capability.

Electrical Machines

The function of an electrical motor is to transform electrical power into mechanical power. Most types can operate reversibly as generators and transform mechanical power into electrical power. The most common technology used for embedded actuation systems is the permanent magnet brushless motor because of their reliability and high torque density obtainable [120]. For the power range (100 W - 50 kW) of aerospace actuation systems, the armature is the stator and the inductor is the rotor with its permanent magnets. Applying an alternative voltage to the stator winding terminals produces an

electromagnetic field that interacts with the rotor magnet field which produces an electromagnetic torque that leads to the rotation of the non-fixed part (generally the rotor). Two motor typologies exist for the power range of aerospace actuation systems:

- High torque motor – They generally are capable of generating high torque at low speed. Their ratio factor (Length/Diameter) is low (0.25-1) and the number of pole pairs is large (> 10). They are well suited for direct-drive architectures.
- High speed motor – They are used for high speed applications with high reduction ratios to the load. Their ratio factor (length/diameter) is high (1-3) and the number of pole pairs is small to medium (2 - 10).

(a) Example of high torque motor (Kollmorgen)

(b) Example of high speed motor (Parker)

Fig. 1.14 Two main motor typologies for aerospace actuators

The main design drivers of brushless motors are maximum torque, torque ripple, maximum winding temperature, inertia, maximum speed and flux weakening strategy.

Mechanical Transmission

Mechanical gears or reducers sets adapt the mechanical power from one shaft to another. Multiple technologies of gears are available in aerospace applications with some examples shown in Figure 1.15.

Spur gears are the most common gears with both shafts in parallel. Bevel gears on the other side the two shafts are not parallel but form an angle which is in most cases is equal to 90° as shown in Figure 1.15a. More complex gear such as planetary gears are used for high torque application as it is transmitted through different planet gears but also to have the same input and output shaft axis. Their main design drivers are tooth bending stress and contact stress which respectively lead to tooth breakage and pitting. Contact stress has an effect on the pinion size whereas tooth bending stress has an effect on the tooth shape and size. Other selection parameters such as maximum/fatigue torque and reduction ratio are also design drivers. Harmonic Drives, represented in Figure 1.15c, have advantages such as lack of backlash, compactness and high reduction ratio (30 – 150) compared to classical gears (2.5 – 8).

(a) Example of straight bevel gear

(b) Example of planetary gear

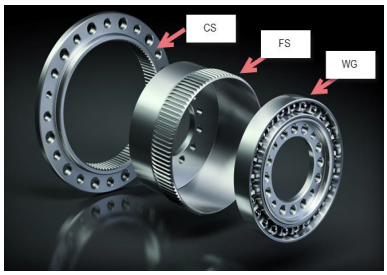

(c) Example of Harmonic Drive gear

Fig. 1.15 Three examples of gear technologies used for aerospace actuators

Compound gears were first developed for aircraft flap systems and can take really high torques due to the fact that the torque is shared between two large teeth. Despite their better torque capacity compared to planetary gears, they have lower direct efficiency. Magnetic gears are also investigated because of their torque limitation function but are not yet flying [111].

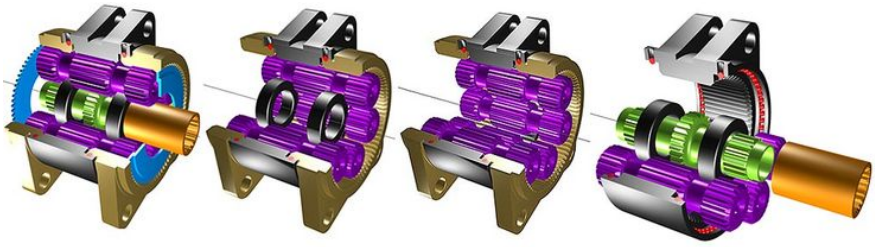

Fig. 1.16 Compound planetary gear [230]

In order to transform a rotational power into a translational power, nut screw devices can be used (Figure 1.17). These devices have four degrees of freedom [123]. Two parts of the device have to be fixed in order to provide the function, either the nut translation or rotation combined with the screw rotation or translation. Roller screws are one main technology of nut screw and have the particularity to handle high torques but with small pitches. On the contrary, ball screws handle smaller torques but can be designed for higher pitches and at lower cost.

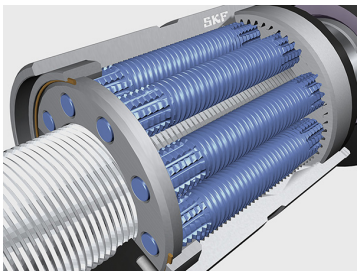

(a) Example of roller screw (SKF)

(b) Example of ball screw (Umbra)

Fig. 1.17 Two main nut screw technologies for aerospace actuators

The main design drivers of nut screws are the maximum/fatigue axial load and buckling load. Pitch is also a design driver and often leads to the technological choice between roller screw and ball screw.

Flexible shafts transmit rotary motion through their high rotational stiffness whilst allowing misalignment between input and outputs shafts, as shown in Figure 1.18.

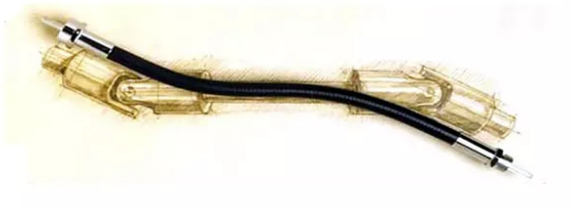

Fig. 1.18 Flexshaft are similar to gimbals (S. S. White)

Their main designs drivers are maximum speed, stiffness, fatigue and peak torque.

1.3.3 Objectives

The design of actuation systems at Safran is a collaborative process between different teams of the design office: embedded software, digital electronics, power electronics, electrical machine, control, mechanics, system architecture and modelling.

This thesis mainly focuses on the sizing aspects of actuation systems which has implications for the power electronics, electrical machine, control, mechanics, system architecture and modelling teams.

Different design process approaches can be used for teams to interact during the development of actuation systems. The sequential design process illustrated in Figure 1.19 relies on strong hypothesis on subsystems interactions generally based on project post-mortem and designer experience. Such process does not guarantee system performances optimality and has no degree of freedom along the design process.

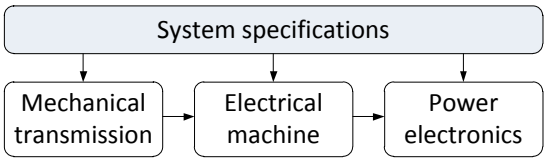

Fig. 1.19 Sequential design process of actuation system

The sequential iterative design process, given in Figure 1.20, enables interactions between subsystem design teams. This process is more efficient that the sequential process but often results in costly human iterations. Additionally, it does not offer enough degree of freedom to obtain system

performances optimality as design decisions are still made without seeing the global effect on the system.

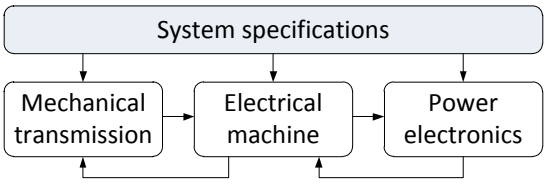

Fig. 1.20 Sequential iterative design process of actuation system

The sequential iterative process is similar to the approaches used in Safran's design office. This process is not optimal for system performance and development costs. There is an industrial need to change this process in order to be more competitive and sustain the design office know-how. Hence, the industrial objectives of this thesis have be explicitly defined:

IO1. *Develop a holistic sizing methodology and an associated software tool.*

IO2. *The methodology shall enable knowledge capitalization and collaboration.*

IO3. *The software tool shall handle analysis and optimization of coupled systems.*

IO4. *The software tool shall provide reasonable analysis and optimization times.*

IO5. *The methodology and software tool shall be tested on a realistic industrial product.*

Therefore, these can be summarize in one main objective which is to propose a practical and more integrated design approach for electro-mechanical actuation systems supported by a software tool which can be deployed in an industrial design office. However, these objectives raise some important research questions:

RQ1. *How should this sizing methodology be incorporated in the overall design process?*

RQ2. *Who will be the users of such software tool?*

RQ3. *How to capitalize knowledge and collaborate in a multidisciplinary design office?*

RQ4. *How to interface different engineering specialization design tools?*

RQ5. *Can Multidisciplinary Design Optimization techniques be made available to unexperienced users?*

RQ6. *What is a reasonable computation time in a design office? What are the potential solutions to reach it?*

RQ7. *Is there a limit in terms of system complexity for using such sizing methodology?*

1.3.4 Applications

The work achieved during this thesis has contributed to different applications and publications that are not all mentioned in this manuscript. Table 1.1 gives a synthesis of these contributions.

Table 1.1 Applications achieved during the thesis and their references.

System	Key topics	References
Fuel Metering Pump	Thermal/Hydraulic	[170]
DC/DC Buck Converter	Thermal/Electric	[208, 207]
Aileron linear EMA	Thermal/Co-simulation	[54]
Thrust Vector Control EMA	High dynamic/Vibrations	Chapter 4
Aileron Rotary EMA with lever arm	Control	[51]
Aileron Rotary EMA	Thermal	[210]
Primary Flight Control Actuation System	Structure	Chapter 5 and [53]
ETRAS	Power chain/Mission profile	Chapter 6 and [52]

1.4 Dissertation Overview

Chapter 1 introduced the context of this thesis in terms of working environment, previous work, typical systems and components. It also outlined the needs which led to the creation of this collaboration between Safran and Institut Clément Ader and the objectives that were defined.

Chapter 2 is a state of the art of engineering design approaches which is then used to determine the methods that can be used during sizing activities. First, intrinsic challenges of mechatronic systems are outlined. The methods and tools used in Model-based Design are studied. Systemic approaches used in engineering design are then presented. Finally, different design optimization methods are investigated.

Chapter 3 proposes a new multidisciplinary system design optimization formulation adapted to sizing optimization problems, and compares it to existing formulations. Graphs and algorithms which help designers in the formulation of design optimization problems are described.

The core of this thesis is the development of a sizing methodology and its associated framework. A detailed description is provided in Chapter 4.

Chapter 5 is a flight control case study. The design of a primary flight control actuation system is achieved. The actuation system is composed of rotary electro-mechanical actuators and control surface structure. The concept of control splitting is investigated.

Chapter 6 is a design case study that concerns an electrical thrust reverser actuation system. First, a conceptual design is achieved. Finally, a more detailed design is performed for mission profile and motor control strategy optimization.

Results and lessons learned are summarized in Chapter 7. Conclusions are made and perspectives are outlined.

Chapter 2

The State of the Art for Engineering Design Approaches

2.1 Introduction

The field of aerospace covers a large variety of products, disciplines and domains. Consequently, aircraft engineering activities cover many design problems. It is proposed to outline four categories of problems, their associated problem indicators and an associated example. The nature of the interfaces between disciplines is considered. The considered nature of disciplinary models throughout the thesis are:

- 3D models correspond to detailed geometry analysis using Finite Element Method (FEM), Computer Aide Design (CAD)
- 1D models represent transient time domain simulations
- 0D models correspond to algebraic modelling

The objective of aircraft conceptual design is to define a specification of aircraft sub-systems and equipment. This requires the participation of four fundamental disciplines: aerodynamics, flight dynamics, propulsion and structures. Furthermore, it must consider a sizable number of specialist disciplines like sizing scenarios (maneuvers, mission profiles, ...) or analysis (aerodynamics, propulsion, ...). It involves high number of empirical models representing the inputs from different disciplines, with a relatively low fidelity based on, previous designed and manufactured aircraft. The nature of the couplings are typically 0D/0D between fundamental discipline analyses and 0D/1D for mission profiles.

Sub-system design has an objective to deliver equipment and component level specifications. For example, the aircraft electrical network design involves a very large number of sizing scenarios (thousands [87]) due to many failure cases (short circuit, fire, ...) and many components (static converters, commuters ...). The nature of couplings is mostly 0D/0D.

The purpose of equipment design is to generate an accurate specification of components. For example, electro-mechanical flight control actuator design requires a relatively high number of disciplines. Sizing scenarios come from operational and failure modes (continuous torque, wind gust, ...) and design drivers at the components level (mechanical stress, maximum temperature capability, ...). They can be represented using differential algebraic equations (0D-1D) or algebraic equations (0D). They require also estimation of component characteristics (inertia, thermal resistance, ...) which can be evaluated using estimation models like scaling laws or surrogate models of FEM simulations (0D) or directly detailed simulations (3D). The nature of couplings range from 0D/0D, 0D/1D, 1D/1D to 0D/3D.

The objective of component design is to justify detail component needs. For example, high fidelity wing design involves some twenty design drivers (wing span, twist, rib thickness, ...) which are represented by the two fundamental disciplines of aerodynamics and structural mechanics. They are evaluated using complex structural mechanics FEM models and aerodynamic Computational Fluid Dynamics (CFD) models [126]. Here the coupling is achieved through commonly held boundary conditions of the FEM and CFD simulations and therefore represents a 3D/3D coupling. Figure 2.1 classifies a non-exhaustive list of problems in terms of number of disciplines, model fidelity and nature of couplings.

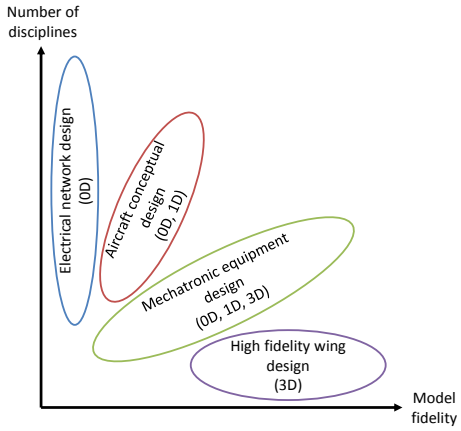

Fig. 2.1 Classification of Aircraft Engineering Design Problems (Non-Exhaustive)

This introduction has outlined that aircraft design introduces a large variety of potential couplings at many levels. Hence, there is a need for design methodologies to deal such multidisciplinary problems.

2.2 Challenges of Embedded Mechatronic System Design

Mechatronics are the synergic and systemic regroupment of mechanical engineering, electronics, control, computer science and systems engineering as illustrated in Figure 2.2. A mechatronic system

is a device composed of elements of these domains which exchange information and energy flows in order to deliver a set of functions.

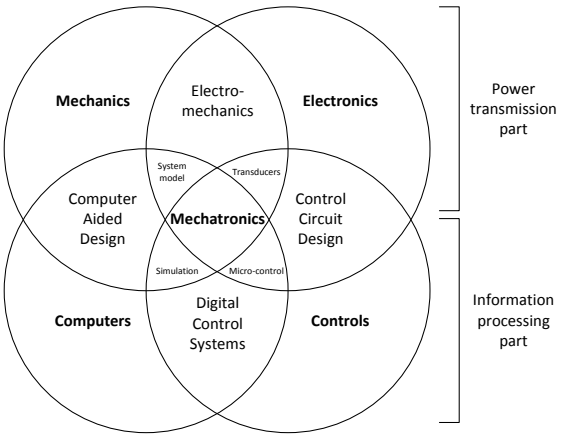

Fig. 2.2 Mechatronics [27]

Mechatronic systems are involved in many industry domains such as automotive, heavy industry and in aerospace. When these systems operate in the automotive or aerospace industry they are considered as embedded because they are supplied and controlled by mobile devices. Aerospace actuation systems are an example of an embedded mechatronic system. The criticality of such systems requires consideration for reliability in their design [150]. Furthermore, they are exposed to harsh environments in terms of thermal management and vibration [110]. Designing these complex systems demands the mastering of different engineering specializations and a multi-level approach to manage the resultant complexity. Hence, technical standards such as Aerospace Recommended Practice (ARP) 4754 [12] provide information to conduct complex system design with certification as a goal. The design of mechatronic components involves multiple physics and has to take care of the multi-scale aspects of component size and physical time constants [27]. Many mechatronic systems are coupled systems. Coupled system raise numerical difficulties during design computational processes [177]. An other challenge of mechatronic system design is knowledge management. As they require different engineering specializations, different engineers contribute to the resultant design. Thus, the knowledge required for their design is heterogeneous and physically distributed among individuals in a design office.

2.2.1 Reliability

The embedded characteristic of embedded mechatronic systems constrains their design to achieve required failure rates. Reliability indicators and assessments for aerospace systems are addressed in a thorough manner in the document ARP4761 [11]. The probability of failure requirements depend on the function criticality that the system has to ensure. Aerospace actuation systems are mainly involved in critical applications such as flight controls or landing gears. For primary flight controls,

one catastrophic event is tolerated per one billion flight hours in commercial aeronautics [150]. This requirement strongly impacts the architecture design.

Some systems may be designed to resist failure. This means that then are designed to never fail during their operational life. It is possible to achieve this by over-sizing components with the introduction of important safety factors during the fatigue design for instance, but at the cost of a weight penalty.

When over-sizing is not advisable or not possible, the system can be designed to be fault tolerant. This means that a failure of a system element does not lead to a system failure. Redundancy enables tolerance to failure and is widely used in aerospace systems. Redundancy can be introduced by adding different load path and components [141]. Figure 2.3 gives a few examples of redundant flight control actuators and their application.

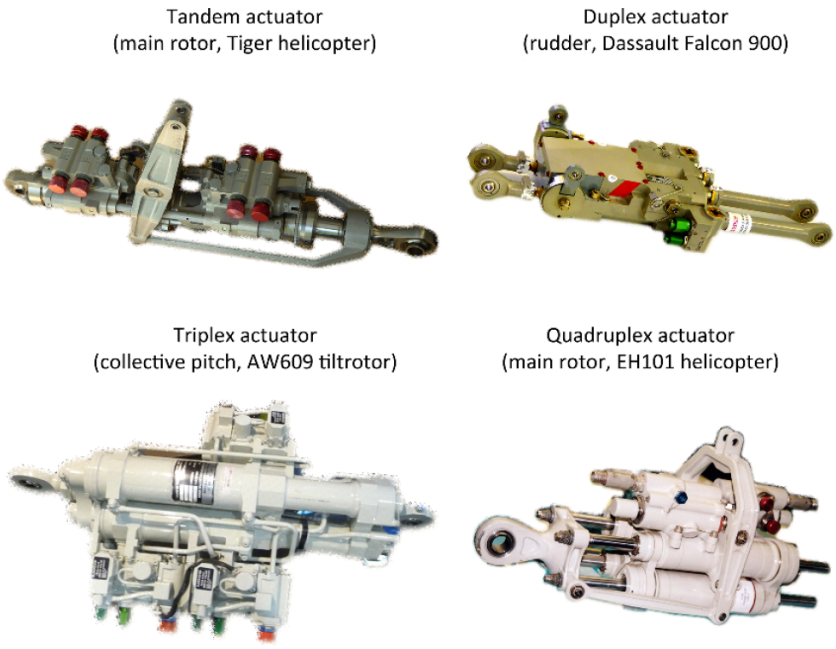

Fig. 2.3 Examples of Aerospace Actuators with Redundancy [150]

Redundancy can also be applied to power electronics design such as a 3-phase inverter by adding an additional arm and passive components which is activated once the short circuit of the faulty arm occurs [196]. Redundancy is also found in sensing and monitoring approaches where additional sensors are added with majority voting to ensure that the correct value is processed [143].

Therefore, the reliability of a system is a targeted requirement and is fulfilled in practical designs when the architecture choice is made either by over-sizing or using redundancy.

2.2.2 Multi-Level and Multi-Engineering Specializations

A challenge in mechatronic system engineering design is its multi-level facets. The design process has to consider all point of views of the stakeholders. A mechatronic system can be decomposed

in system level and component level [195]. An additional level can be the physical level composed of the different physics that rule the behaviour of components. Figure 2.4 shows how two typical mechatronic systems can be represented at system level, component level and physical level.

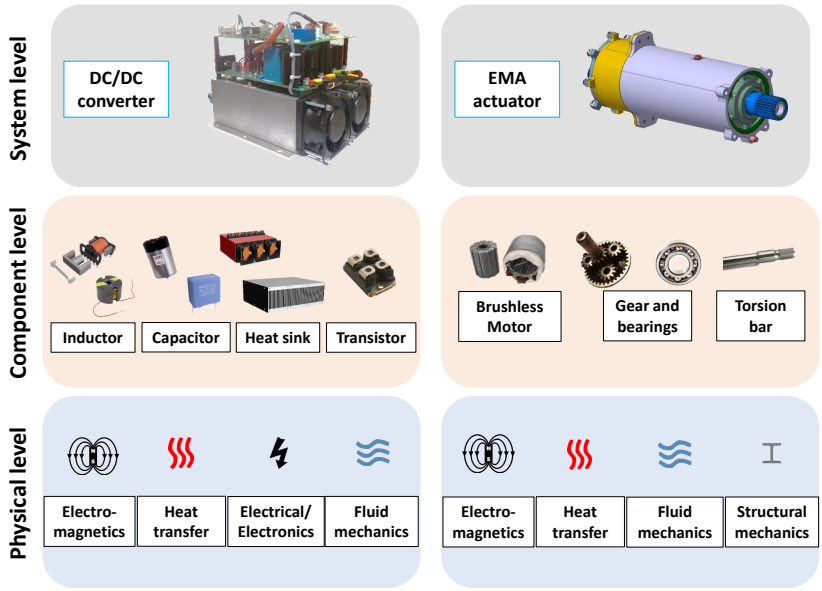

Fig. 2.4 Multi-level aspects of mechatronics systems

This multi-level characteristic has to be managed during the engineering design process especially during the process of information exchange and modelling activities.

In addition to the multi-level complexity of mechatronic systems, the multi-engineering specialization property of such systems increases the complexity of their design. They are composed of several components that require the utilization of different engineering specializations to design them. In a design office engineering specializations correspond to different engineering teams. The digital electronics team is responsible for the controller hardware and software. The power electronics team design the power modules. Machine designers size the electrical drive. The mechanical engineering team is charge of the design of mechanical transmission components. System architects specify the system, lead the system design and make sure that integration is successful.

This situation leads to different difficulties. The engineering teams are sometimes in different locations and interact through e-mails, specification/justification documents or collaborative work environments. To achieve a coherent system design, several human iterations are necessary between the different teams. The knowledge of the different engineering teams is implemented is specific design tools which most of the time do not connect to each other. Therefore, it is difficult to automate these iterations.

Iterations get more important as the needs and constraints of engineering specializations become more numerous. Needs can be the inputs required to design a given part. Constraints can be

technological limits of components, the available materials, manufacturing tools or the supply chain. The system architect has to deal with the coordination of the system design while taking into account needs and constraints of the different teams.

The challenge resulting from multi-level and the multi-engineering specialization aspects is thus to intelligently decompose the system and make heterogeneous engineering teams work together efficiently to deliver on time and compliant products.

2.2.3 Multi-Physical and Multi-Scale

As seen in the previous part, mechatronic systems are composed of several different components that are designed thanks to different engineering specializations. The performance of these components are ruled by the laws of physics. A multi-physical approach is then necessary to design them.

Power electronics design requires electrical, electromagnetic and heat transfer simulations. Machine design requires the same physical simulation but also mechanical considerations for vibrations and manufacturing. The mechanical transmission behaviour is driven by the laws of structural mechanics whereas the material property are temperature dependent. These multi-physical aspects of components lead to numerous and complex evaluation of design drivers during the design process of mechatronic systems. In addition, the integration of the different components in a same system leads to multi-physical coupling as the system can heat (Figure 2.5) or vibrate a whole. The evaluation of the physical behaviour leads to the utilization of sophisticated simulation tools.

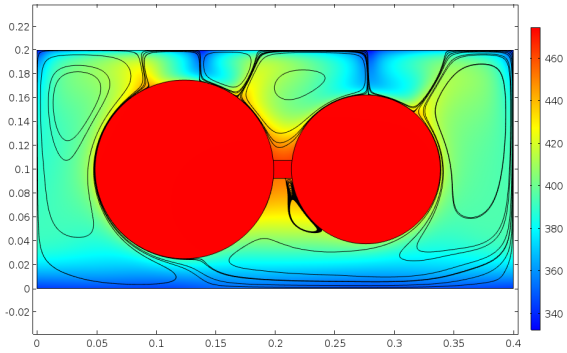

Fig. 2.5 Actuator housing heat transfer and fluid mechanics simulation using COMSOL [207]

As illustrated in Figure 2.6, mechatronic systems obey to multi-physical laws but are also subject the intricate aspects of multi-scale.

The size of component varies from the chip to a large ball screw. When integrating these component together the scale change is a difficulty. Despite the size, the time constant of the physical laws are different. For instance, vibrations can go up to the kHz (ms) whereas time constant of the thermal behaviour are from the minutes to the hours. This leads to different simulation time steps and the decomposition of simulation tasks.

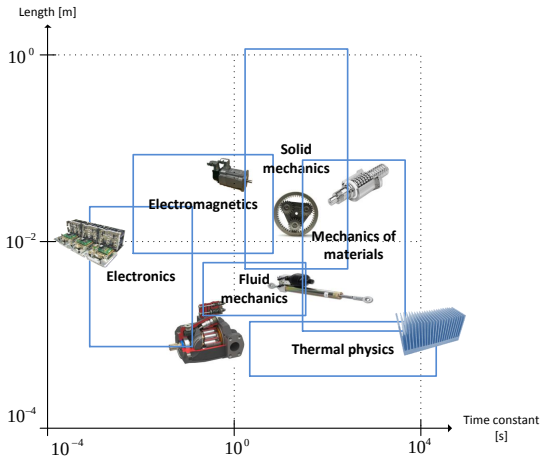

Fig. 2.6 Multi-physical and multi-scale aspects of mechatronics systems

2.2.4 Multidisciplinary Couplings

Numerical models that evaluate engineering systems and components performances are at this date very effective in many engineering areas. From chip design to structural design, all domains have sophisticated free and commercial software. Nevertheless, analysis of coupled systems is intricate. Coupled analysis lead to the handling of loops in the computation data process.

The presence of these multidisciplinary couplings increases the engineering design problem complexity because the performance of the system depends on the interaction performances of the coupled disciplines [216]. The origin of multidisciplinary design analysis and optimization (MDAO) is in aircraft wing design. Wing design includes three coupled disciplines: controls, aerodynamics and structures [94, 126]. MDAO techniques were then extended to aircraft design [132] and other engineering systems like helicopters [40], spacecraft [23] or automobiles [129].

Examples of coupled systems are control-design problem in mechatronic systems [147]. Other examples are couplings through system sizing scenarios. An example of the design of an electro-mechanical drive is given in Figure 3.3. The mechanical components are selected on the maximum torque they have to transmit. The maximum mechanical stress corresponds to the torque generated by the shock on an end-stop due to a position sensor failure. The computation of the equivalent torque generated by the shock requires detailed knowledge of the stiffness and kinetic energy (inertia) stored in each device of the electro-mechanical drive. Hence, the components have to be already selected.

Different strategies exist to deal with multidisciplinary coupling analysis [158]. This is also referred to as Multidisciplinary Design Analysis (MDA). The first possibility is for numerical solvers to converge the residual of state variables to zero for implicit forms or the value of the coupled variables for explicit forms [112]. Another possibility is the use of constrained optimization solvers [216]. Discussions around the resolution of multidisciplinary couplings are the discussed in Section 2.5.5. Therefore, the analysis of multidisciplinary couplings generated by the formulation of the

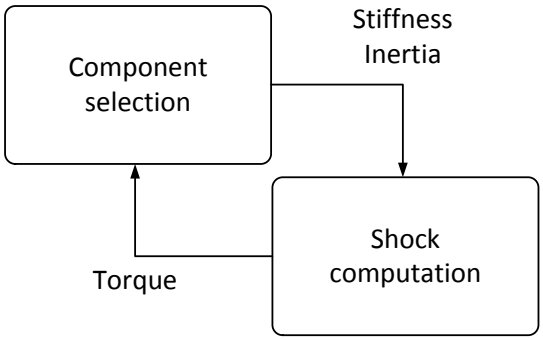

Fig. 2.7 Example of multidisciplinary coupling for electro-mechanical drive component selection

mechatronic system design problem is an additional challenge in the related engineering design context.

2.2.5 Knowledge Management

Knowledge management is a concern for high technology industrial companies as well as organizations in general [61]. They design and manufacture high performance, critical and high quality technological products. This is possible due to decades of problem solving, experience feedback, research and continuous improvement. To capitalize on know-how, each organization has their own methods [4]. Furthermore, knowledge management methods and tools specific to the field of engineering design are present in the literature [164].

Designing mechatronic systems involves several stakeholders whom have different types of engineering specialization knowledge. Hence, knowledge management is a significant challenge. Knowledge is available in different engineering specialization teams of the design office as shown in Figure 2.8. The most challenging difficulty is that in many enterprises these team are in different geographic locations [164].

During system design the design drivers of the system are well known by the system architect which enables him to manage the other engineering specializations (electronics, machine design, machine design, software...) design tasks. The other engineering specialization experts are well aware of technological limits of their components and therefore assess rapidly their performances.

Experienced system architects are able to make system design trade-offs without interacting with other engineering specialization experts. The more expertise there is in a product development the less there will be design iterations [164]. The main focus for organizations is to capture and distribute this expertise.

Formating this technical knowledge is generally done in the form of technical notes that are available for all the design office. Nevertheless, it is difficult to conciliate product development and knowledge capitalization as time is always missing. Therefore, the introduction of non-intrusive and

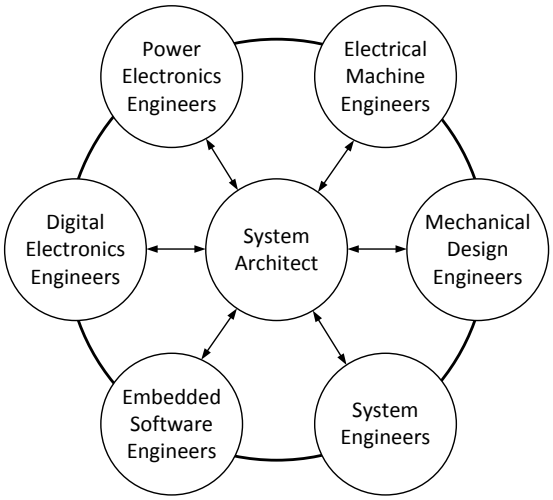

Fig. 2.8 Different engineering teams and knowledge flows

non-time consuming knowledge capitalization methods during the design process remains a challenge for todays high technology organizations.

2.3 Model-Based Design

A model is a physical, mathematical, or logical representation of a system, phenomena, or a process. Simulation numerically implements these models in order to determine the behavior of a system or a process [122]. Thus, it enables us to test or analyze systems or concepts of the real world if a model can represent them. Indeed, modelling and simulation permits the creation of a virtual duplicate of systems and process and characterize their behavior in a given environment for a given operational mode. Due to such capabilities, the use of modelling and simulation offers cost and risk reduction during the life cycle of a product [73, 103]. Modelling and simulation offers significant advantages during the development of a product as shown in Figure 2.9.

The increase of computational capabilities and numerical tools sophistication has allowed companies to spread the approach among different engineering teams. During design activities models can represent links between functional requirements and a physical architecture [238], achieve system preliminary sizing [31], determine performances of components [47], and verify component integration and system performances [181].

In the engineering design context, modelling and simulation coupled with rigorous documentation are an excellent opportunity for knowledge capitalization. In the test and integration context, such activity is an alternative to costly test bench campaigns which are historically necessary for validation and verification of some requirements.

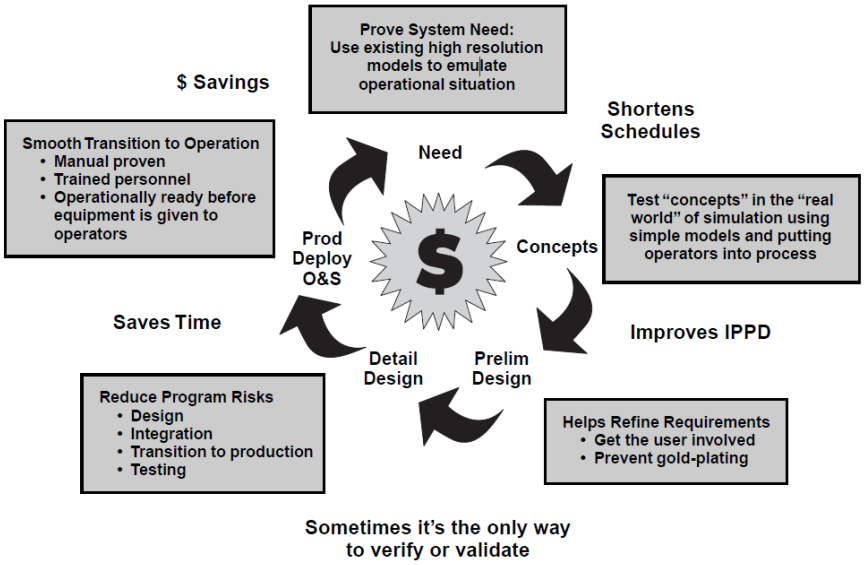

Fig. 2.9 Advantages of modelling and simulations [138]

2.3.1 Requirements Engineering, System Architecture and Reliability

Requirement engineering consists of the definition, documentation and maintenance of requirements throughout the design process. Systems engineering methods are needed to make this critical step successful [73]. The development standards like ISO 26702 and IEEE standard 1220-2005 has proven their usefulness in complex system development [65, 71]. As the number of requirements keeps increasing in aircraft development, requirements analysis can help reduce such number by tracking redundant or conflicting requirements. Once requirements are well defined, functions that enable them have to be determined.

A function can be defined as the act of transforming matter, energy or data in time, shape or space [165, 150]. System preliminary design begins with the search for functional architecture and the physical architectures that enable them. Some criteria of choice can be the use of off the shelf components or existing intellectual property but the main process evaluation is preliminary sizing in order to make assessment about mass, size and cost.

To represent these types of architecture, different methods and tools exist. For system design, the most common one is SysML. Nevertheless, depending on what phase of the development process diverse tools are available [181]: needs analysis and specifications level (APTE method, SysML, Arcadia...), functional level (SADT, SART, SysML, CATIA Systems level F, Arcadia...) and logic/organic level (FAST: Sequential decomposition of the architecture and component allocation, Arcadia...).

The first step in architecture definition is to outline the interfaces of the system with its environment. Another step is to link the functional requirements to the architecture to verify that all the requirements are covered. Many Model-based Systems Engineering (MBSE) tool provide such features [101].

Frameworks to automate system performances simulations and validation with respect to requirements have been developed [174].

Emphasis must be placed on formalization when representing a physical architecture. For example, when the system is multi-physical, the power flows can be represented using different colors to outline the different natures of the flow (electrical, thermal, mechanical, hydraulic, ...) as shown in Figure 2.10. This is fundamental because subsequent design stages will rely on the information developed at the architecture definition stage.

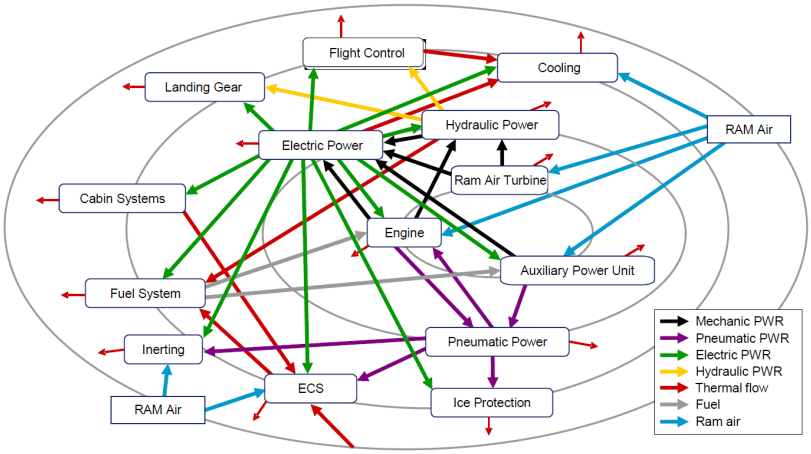

Fig. 2.10 Secondary power flows for an Airbus A230 type single-aisle aircraft [143, 150]

Embedded system preliminary design is the step where reliability analysis of the system is achieved. Equipment and system manufacturers must provide systems which have a probability of failure less than 10^{-9} (in the case of primary flight controls). Such requirements have bearing on the architecture choice. The probability of failure is computed using Fault Tree Analysis (FTA) and the Mean Time Between Failure (MTBF) of components [142]. Todeschi compared standards MIL-HDBK- 217 Plus and FIDES 2009 for predicting the reliability of power electronics in aerospace applications [231]. He underlined the necessity for these tools to improve and enable better considerations of the system's environment like ambient temperature.

Architecture generation is a research topic that provides different architectures based on functional architecture and component data [3]. This topic is also investigated for aircraft level trade-offs [119, 118]. Architecture evaluation can be achieved using reliability techniques. This allows us to eliminate architectures which do not meet reliability requirements. The next step in architecture evaluation is system sizing. It offers the possibility to compare architecture in terms of mass and performance. Nevertheless, the automation of architecture generation and evaluation has still to be investigated as actual software can provide such features but with a low fidelity.

2.3.2 System Sizing

A fundamental difference between system design and system sizing is considered in this work. System design determines what should be the components (architecture) and what should be their performance and the characteristics of sub-systems and components to meet overall system requirements. System sizing is a step of system design that determines what should be a sub-systems and components preliminary geometry so that their performance enable the overall system to meet its requirements. Thus, system sizing is a process that provides component specifications with respect to system specifications, as illustrated in Figure 2.11.

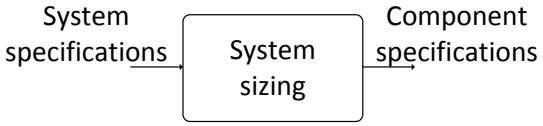

Fig. 2.11 System sizing principle

The core purpose of sizing is to determine the physical characteristics of the system. This particular phase of preliminary design is generally done using analytic models [6]. Two approaches can be chosen. An intuitive approach is only achievable by an expert who masters the disparate links between the physical characteristics. The expert can through a few manual iterations on the inputs make system level trade-offs and provide a solution that meets the requirements. This approach requires a significant learning curve and is similar to trial and error method for problem solving. The other approach is to use model-based methods. Model-based methods for system sizing can be decomposed in three topics: sizing models construction, design procedure definition and design optimization [27].

The establishment of sizing models is a compromise between accuracy and complexity [47]. Estimation models are one type of sizing models used to simplify the system sizing problem. They enable us to determine component geometries with respect to component selection parameters. Budinger proposed to distinguish three categories of sizing parameters at the system level [27]:

- Integration parameters: used to evaluate mass and global dimensions (e.g. length, width, diameter) of components
- Simulation parameters: used to perform analysis of a sizing scenario (e.g. total inertia, thermal resistance and capacity)
- Operating domain parameters: used to verify the usage of components respect their endurance (e.g. mean winding temperature) or peak performances (e.g. maximum torque)

At the component level three other catagories are considered:

- Strutural parameters: used to define the topology

- Material parameters: used to define the material properties
- Geometry parameters: used to define the shape and geometry (e.g. length, angle, ratios)

Scaling laws are widely used estimation models that rely on reference components [30, 124]. The simplification method they use considers three main assumptions [30]: identical physical and material properties, geometric similarity, an the dominance of one design driver.

If a ball bearing like in Figure 2.12 is considered, and that the static load F_{ref} for which the left ball bearing as been sized and its diameter D_{ref} are known, then it is possible using a scaling law to compute the diameter D of the new ball bearing with respect to the required static load F.

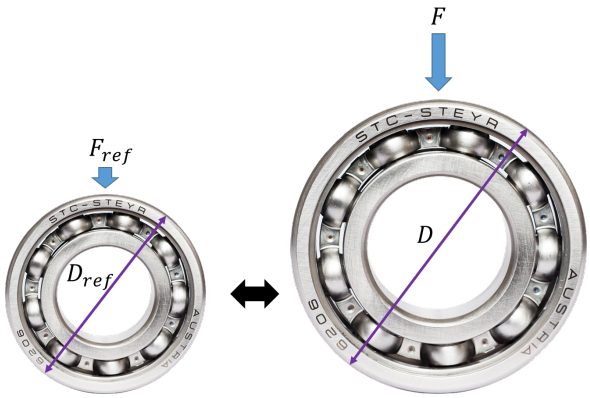

Fig. 2.12 Scaling laws example on ball bearing

The mechanical stress σ is a function of load F and area S,

$$\sigma^* = \frac{F^*}{S^*} \tag{2.1}$$

where $F^* = \frac{F}{F_{ref}}$. As scaling laws assume same material properties and the main design driver of mechanical component is stress, the stress of both bearing must the same $\sigma^* = 1$. Hence,

$$F^* = S^* \tag{2.2}$$

as scaling laws assume geometric similarity $S^* = D^{*2}$. Hence,

$$D^* = F^{*\frac{1}{2}} \tag{2.3}$$

or

$$D = D_{ref} \left(\frac{F}{F_{ref}} \right)^{*\frac{1}{2}} \tag{2.4}$$

This simplification enables us to use a constant aspect ratio instead of several geometrical quantities, and thus reduce the number of variables in the problem. Additionally, such approach reduces the risk of side effects due to unconsidered physical phenomena as the design remains close to the existing. Other sizing approaches define detailed component geometry as variables in order to

guarantee the uniqueness of the design solution [171]. Recent investigations in surrogate modelling of Finite Element Method simulations showed that such models can be used during system sizing [209, 207].

The use of analytic models is very interesting in terms of fidelity but often requires a lot of work effort to be established. In addition, they use many degrees of freedom which is not the purpose at a preliminary level. Other models representing sizing scenarios are necessary for system sizing. They enable to assess system performances (e.g. torque, time response) or technological limits (maximum temperature, maximum stress) by using the parameter of components and system requirements.

The establishment of a design procedure corresponds to the definition of a calculation sequence corresponding to the assembly of the different elementary models representing the system computational model. This is straightforward for experts or devices similar to existing systems but remains an art for new system concepts or additional system requirements. Some graphical tools have been developed in order to assist engineering in the construction of sizing procedure for concurrent engineering [195]. They usually take the form of spreadsheets like Microsoft Excel [166], MITCalc [168] or computer algebra environments. Design graphs are interesting methods for the formulation of sizing procedures [27].

It is possible to consider design problems as an optimization problem [177, 147]. Some of the variables and parameters can be considered as design variables or constraints. This way engineering can rely on powerful optimization algorithms to enable the generation of feasible and optimal design alternatives. Such design optimization approach enables to decrease decision making time and allow engineers to undertake the design of more complex systems. Design by shopping approaches can also be used during system sizing [223]. Some engineers will prefer this approach when compared to optimization as they can better visualize the effect of design variables on the system design alternatives whereas in optimization the final results is the only design alternative. Furthermore, when the sizing model is missing some design drivers the optimization can converged towards strange aspect ratios for instance. A solution, which is often used in that particular case, is to impose a constraint aspect ratio like for a rib in structural optimization.

2.3.3 Engineering Specialization Analysis

Engineering specialization analysis corresponds to the evaluation of component performances. The evaluation of performances requires detailed knowledge of the component. This knowledge leads to the use of numerical models that use detailed geometry components and sophisticated solvers to represent the physical phenomena. The models can be complex analytic models built by hand and tuned using test bench results. They can be also numerical models based on empirical data. Some engineer specialization analysis models are based on Finite Element Method which rely on partial differential equations (PDE).

The engineering specialization analysis is required to assess physical quantities that can not be evaluated at preliminary design stage like the thermal behavior of a capacitor [82], the effect of

magnets on torque ripple of synchronous reluctance motors [189]. The design of EMI filters for instance requires detailed harmonic models [233]. The verification of load distribution in nut/screws devices is often based on Finite Element Methods as illustrated in Figure 2.13 [1, 64].

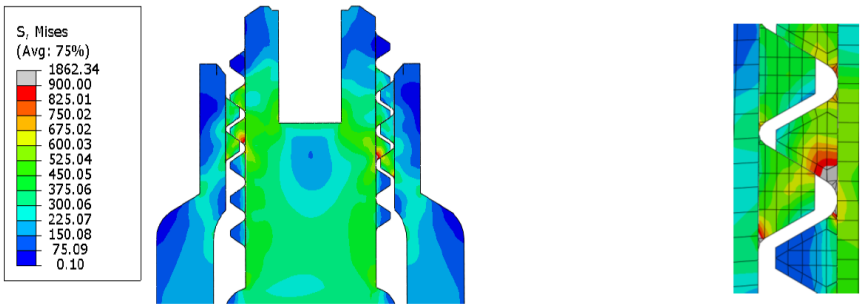

Fig. 2.13 Detailed load distribution in nut screw device [64]

There are a large number of engineering specialization tools either commercial or non-commercial. Some rely on analytical models such as KISSsoft [128] for gear design or MITCalc [168] for buckling computation. Engineers also build their design spreadsheets in Mathcad [161] or Microsoft Excel [166] where they implement algebraic models taken from AGMA standards [14] for instance. For complex physical phenomena like heat transfer or structural mechanics detailed design tools like ANSYS [10], Abaqus [225], Patran [217] or COMSOL [44] are used. This way design drivers such as maximum temperatures or, resonance frequencies can be assessed.

Detailed design or sizing of complete components is also possible using automated simulation workflow environments such as ModelCenter [148]. Indeed, Figure 2.14 shows how different design tools can be integrated in a computation and optimization environment for rotorcraft drive system sizing [13].

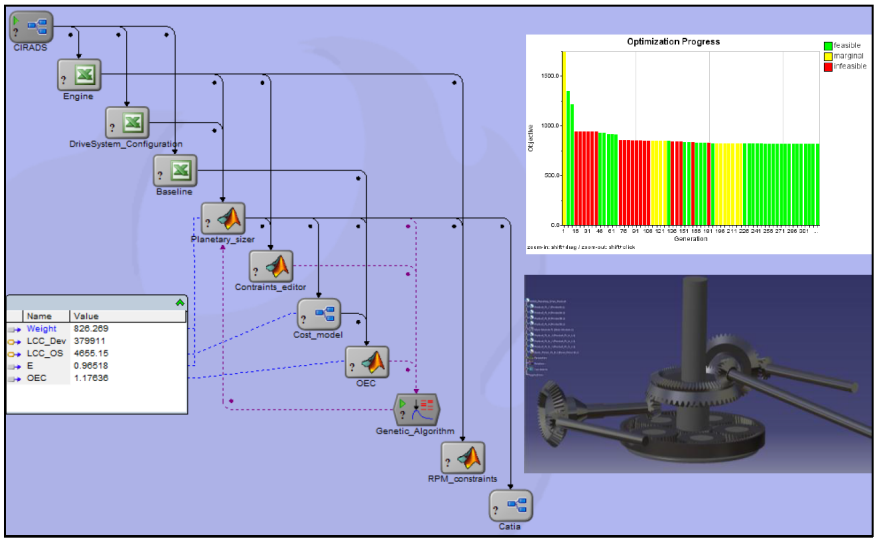

Fig. 2.14 Integration of different design tools in ModelCenter [13]

2.3.4 System Virtual Prototyping and Integration

System virtual prototyping provides the possibility to verify the integration of components and check if the system meets the performance as defined in the requirements [181]. This specific step in the design process uses modelling and simulation to assess the system behaviour. Test bench campaigns are needed to verify integration and performance but virtual prototyping is a first step to quickly and for less cost outline potential design non-conformities.

System virtual prototyping, in opposition to engineering specialization analysis, manipulates lumped parameter simulation models. Lumped parameter models simplify the description of the behaviour of spatially distributed physical systems into a topology consisting of discrete entities [27]. These simulations models are also referred to as 0D-1D model as their computational models use algebraic equations (AE), ordinary differential equations (ODE) or differential algebraic equations (DAE) where the state variables are a function of time. These models allow us to evaluate in a high-level way the functional and physical couplings inside a system. Different implementation of lumped parameters exists in the design context. Each lumped parameter modelling and simulation tools have been developed for specific disciplinary needs (hydraulics, power electronics ...). Nevertheless, many multi-physical simulation tools combine different physics such as AMESim [218], OpenModelica [78], Dymola [226] or Simscape [162]. Such tools combine a graphical approach and procedural approach [178].

Lumped parameter models can be represented using distinct formalism like a block diagram, state space, bond graph (Figure 2.15) or nodal networks [27]. All have a common core: implement the differential algebraic equations that represent the system behaviour, then link them to each other and solve them.

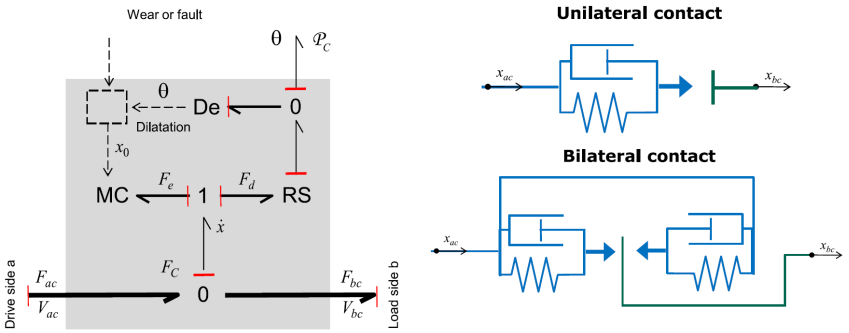

Fig. 2.15 Example of bond graph to model contact in nut screw devices [151]

Bond graph theory supposes causality of models whereas nodal networks like Modelica programming language [79] enable acausal modelling. Acausal modelling permits faster implementation of models and increases reusability of models as both inputs and outputs are flexible.

The use of lumped parameter simulation tools is mainly for evaluating physical characteristics of the system with respect to time. They are also used for evaluating system performances with respect to frequency or pulsation. Frequency solvers for power electronics such as Electromagnetic Interference

(EMI) filter design [56, 171] enable rapid frequency domain simulations that can then be used in optimization processes. Such approach is also used to assess control laws design during the sizing of mechatronic products [147].

The co-simulation between different lumped parameters simulation tools is required for global modelling. Indeed, to interact between discipline specializations such as hydraulics and control or to interact between system integrators and suppliers different simulation tools have to be connected. This need was first expressed by the automotive industry and is at this date well underway. For instance, it is possible to simulate the system behaviour in Simulink [163] using Simulink model for the controller and Dymola [226] for modelling the system and the load.

A solution for co-simulation is to convert models into FMUs (Functional Mock-up Units). FMUs are the implementation of the FMI (Functional Mock-up Interface) standard [219] that allows the exchange and the co-simulation of models created in different simulation environments. FMUs can be exported as a model exchange or co-simulation. Model exchange includes only the computational model, whereas co-simulation also includes a dedicated solver. The Python package pyFMI [9] enables to manipulate an FMU through a python program to modify inputs and parameters, simulate the model and access the simulation results.

2.3.5 Surrogate Modelling

Surrogate models, metamodels or substitution models are simplified models of more complex models. The complexity of models is often due to mathematical form or prerequisite numerical solvers. The surrogate models can take the form of algebraic expression or more complex numerical models. Surrogate modelling approaches are widely used in different engineering specializations. Such models are often used when the quantity of interest cannot be computed easily and accuratly with analytic approaches [27]. Additionally, they are also used to replace simulation models that have high computational cost in order to use them for optimization or Design of Experiments purposes [22]. Indeed, the complexity of development systems keeps increasing and lead to more and more complex mathematical models to represent them. Simulations involving these models generate high simulation run times which justify the usage of surrogate models [239, 75].

Three important criteria can characterize the type of surrogate modelling technique as shown in Figure 2.16 : Design of Experiment choice, model choice to represent the phenomena and the fitting model that lead to different mathematical forms.

Many computational tools enable the usage with high-level interfaces and a large choice of regression model such as the Python library Scikit-learn [180].

For engineering specialization analysis, surrogate models of Finite Element Method simulations have been proposed for structural mechanics [22], aerostructural [140] or electromagnetics [211] and heat transfer [209] . This allows lite-weight models can be directly used in more complex engineering systems design [205]. Surrogate models of lumped parameter transient simulations for design and control co-design are also investigated [59]. Surrogate models for system analysis and integration are

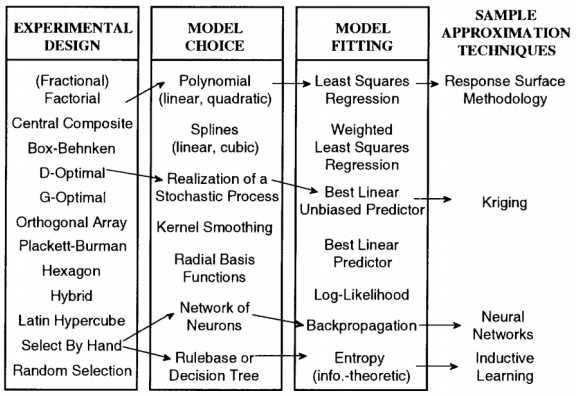

Fig. 2.16 Techniques for surrogate modelling [215]

also under investigation. For instance, non-linear dynamical systems transient simulations have been reduced through surrogate modelling [106]. Multi-body dynamic simulations have been transformed into surrogate models using Response Surface Methodology (RSM) [194]. The mean current passing through a DC bus capacitor surrogate model has been obtained using RSM of transient electrical simulations [87].

2.4 Systemic Approaches in Engineering Design

A system can be defined as a device composed of several interacting sub-systems which fulfills a set of functions in a given environment. A system as a product has a life cycle that involves development, production, usage and disposal [102]. A systemic design approach should then include the needs and requirements of each phase of the product's life cycle. Applying such approach to complex systems like aerospace systems is not straightforward, it requires a set of methods to make it efficient and reachable. The simplest way to represent a system in the block diagram as shown in Figure 2.17.

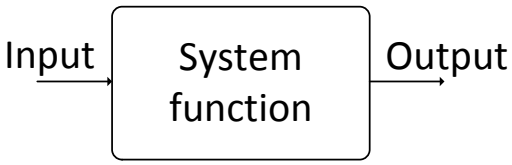

Fig. 2.17 Block diagram of one system function

When it comes to more complex systems that involve multiple functions that are chaotically linked between each other the representation of system is intricate. Thus, the engineering design process is as well. A systemic approach is then mandatory in order to deal with design activities decomposition and coordination.

Many interrogations can appear when trying to achieve a systemic design approach of a product:

- How do I represent my engineering system design problem?
- How should I decompose my design problem?
- How should I coordinate the design process?
- How do I achieve a global system analysis?
- How do I visualize my design alternatives?

This section seeks to present existing methods that answer these questions.

2.4.1 Design Representation

To understand the interactions in engineering design activities, different representation methods are possible.

The Structural Matrix was proposed by Steward for representing the interactions between equations and variables in system of equations [222]. He then extended it to engineering design using what he called Design Structure Matrix (DSM) as illustrated in Figure 2.18. It consists of replacing equations by system elements and variables by element interrelationships.

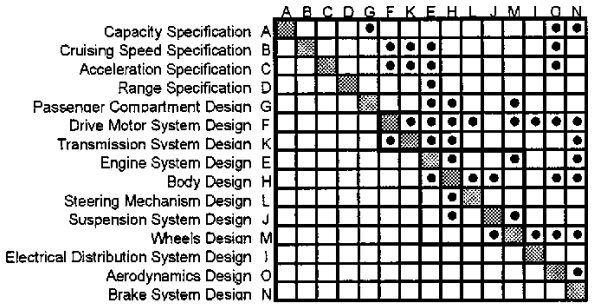

Fig. 2.18 Example of Design Structure Matrix [25]

Another alternative for representing interactions in engineering design process is the Directed Graph [7]. A more specific graph used to represent system of equations is the bipartite graph [63].

N2 diagram or N2 chart, given in Figure 2.19, is a diagram that represents in the shape of a matrix the functional or physical interfaces between system elements. It gives a visualization of how system elements interact in terms of inputs and outputs. It is well suited for data flow representation like in Model-based Design or more generally Modelling and Simulation.

System elements are placed on the diagonal of the matrix. Inputs can enter the element from the top or the bottom where as outputs come out from the left or the right of the element. The data flows in clockwise direction through forward and feedback loops. With this diagram multidisciplinary couplings can easily be highlighted [20].

The Extended Design Structure Matrix (XDSM) is interesting for representing optimization problems in a global and standard manner [136]. In is particularly interesting for problems containing

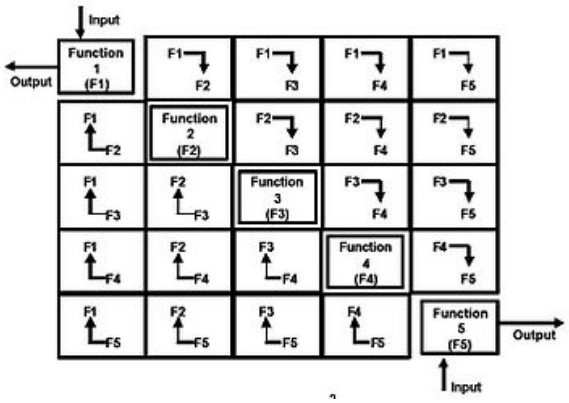

Fig. 2.19 N2 diagram principle [122]

multidisciplinary couplings. It is similar to the N2 chart and the DSM diagram in the sense that components are placed in a grid. Lambe and Martins [136] proposed to distinguish the components that evaluate disciplines (rectangle) and those which which handle an iterative procedure (rounded rectangle). External inputs and outputs can be represented as well as the data connections between components using parallelograms containing the variable name and a thick gray line the connection. In addition, a specific numbering of components enables to highlight the execution sequence of the problem. Furthermore, a thin black line highlights the process flow of the problem. An example of XDSM diagram is given in Figure 2.20.

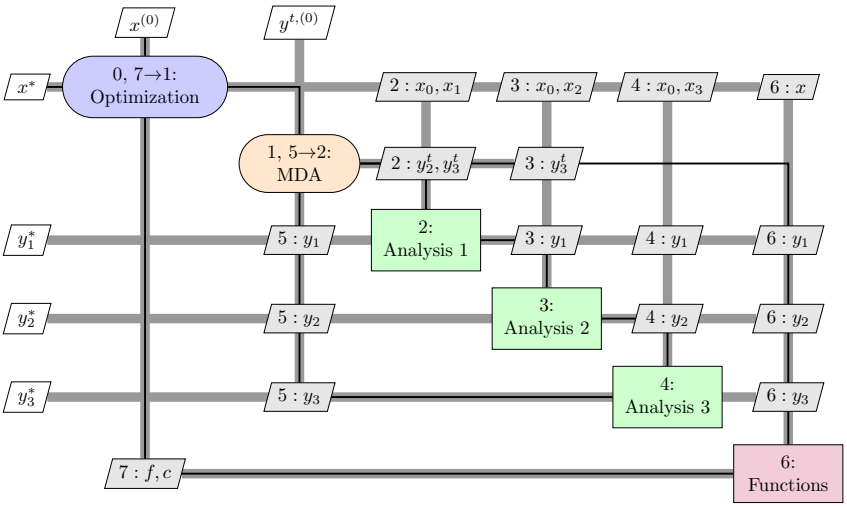

Fig. 2.20 XDSM diagram for the MultiDisciplinary Feasible architecture [158]

In the next chapters, the XDSM is simplified by removing the numbering of components and the thin black line to streamline the diagrams. Nevertheless, for the considered problems the execution order and the process flow are deduced from the order of components in XDSM structure as in the N2 chart.

Gross proposed an interactive chart, illustrated in Figure 2.21, to edit and visualize sub-systems and components interdependencies [93]. The model implementation enables efficient design space exploration and sensitivity analysis between the system variables.

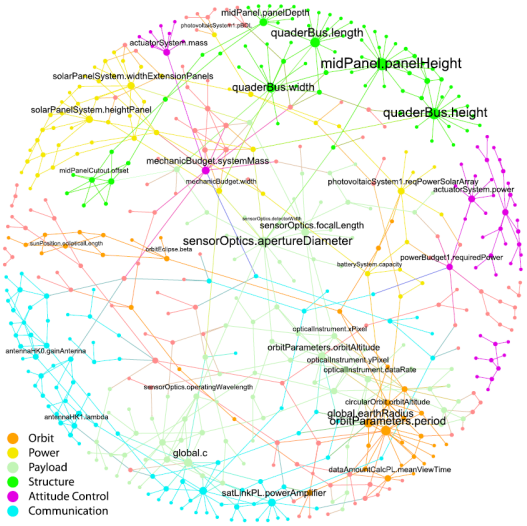

Fig. 2.21 Spacecraft representation using an interactive chart [93]

2.4.2 Design Decomposition

Many engineering systems are heterogeneous, large and multidisciplinary. Determining the possible interactions among the participating sub-systems and their components can require significant time and money. System engineering processes help reduce these costly iterations by decomposing the system design into smaller more manageable design tasks [122]. A good system decomposition can be proven if the design of each sub-system remains independent. In system engineering the design decomposition of a system is often done by analyzing its organic architecture [73]. The system is therefore partitioned into sub-systems themselves split into multiple components and components into parts.

Knowledge-based engineering approaches for mechatronic system design tend to achieve design decomposition by defining two layers of knowledge: system layer and component layer [185]. An example of such approach has been illustrated for mechatronic system design with a domain specific layer which involves multiple engineering specializations and a system layer that represents component interactions as shown in Figure 2.22 [195].

The knowledge-based approaches enable better considerations for design drivers such as technological limits of components whilst assessing system performance.

Rogers underlined the difficulty to decompose an engineering design problem for novel concepts such as spacecraft [198]. Thus, he proposed the utilization of Artificial Intelligence for decomposition by assimilating a design process to an optimization problem composed of analysis functions, design variables and design constraints.

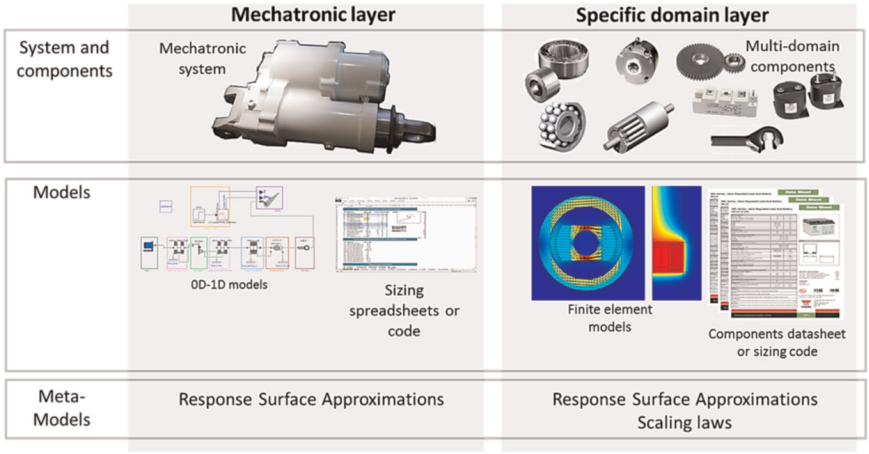

Fig. 2.22 Knowledge-based decomposition of mechatronic systems [195]

Decomposition methods for Design Optimization problems have been investigated for distributed optimization where the design is driven by multiple optimizers like Collaborative Subspace Optimization (CSO) [216]. Other methods like evolutionary algorithms have been proposed to solve decomposition problems [7].

2.4.3 Design Coordination

The challenge of design coordination is to determine the successful ordering of information flows in the design process. If a previous system has had a successful development then the design process can be reused and no decomposition or coordination efforts is necessary. Nevertheless, non-optimal coordination can results in a significant number of iterations between stakeholders or models. Despite that numerical optimization techniques enable to deal with such iterations, the computational cost can be reduced by determining a smarter coordination strategy.

The coordination can be achieved by the order of use of the computational models. If models are acausal it is an additional degrees of freedom for design coordination because models have flexible inputs and outputs [79, 6]

The determination of efficient coordination can be assisted by using graphical tools such as an adjacency matrix [182] or bipartite graphs [33]. Graph tearing methods [68] and DSM matrix triangulation algorithms enable to determine the most effective computational sequence for the system model. Reysset developed a tool that mixes symbolic computation and graph algorithms to determine efficient coordination in the definition of sizing procedure [195]. A usage example is given in Figure 2.23

In engineering design, common coordination issues are the presence of a singularity in the computational model. The computational model can be over-constrained, under-constrained or contain algebraic loops [195]. Dealing with these singularities requires the usage of specific solvers or a reformulation of the computational model.

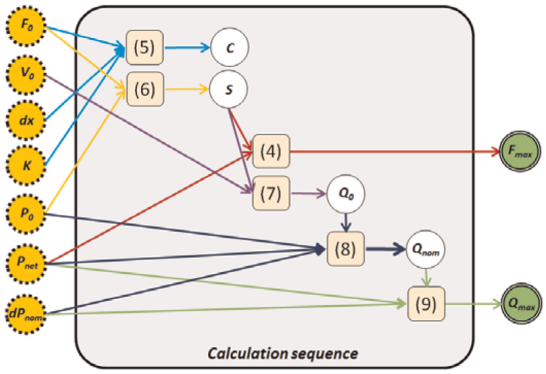

Fig. 2.23 Coordination of a hydraulic actuator design problem [195]

Other techniques that enhance coordination efficiency have been investigated. Bloebaum presented a method based on sensitivity analysis of coupling variables to coordinate multidisciplinary problems [20]. Allison proposed a methodology to simultaneously partition and coordinate complex multidisciplinary systems using heuristic algorithms [7].

2.4.4 System Analysis and Design

System analysis consists of assessing the system performances for a given configuration whilst system design consists of finding the good configuration for the desired performance level. System analysis resides in the capability to determine how elementary analysis models based on engineering science such as structural analysis, heat transfer or electromagnetics are used for component analysis related to each other and how they impact system performance.

Generally, for complex engineering systems determining the interactions between elementary analysis models requires a strong knowledge and expertise of the system. For designs based on existing concepts, sub-systems and their interactions are well established [198] and the designers expertise is usually sufficient. For novel concepts or junior designers system analysis and design is not straightforward but remains an vital task.

Two approaches are possible to achieve a system analysis. Assembling analytic models obtained by fitting empirical or simulation data using surrogate modelling [177, 209] or existing analytical models to form a complete system analysis model is the first. This approach permits faster analysis and enables non-experts of legacy analysis tools to assess performances using relatively simple mathematical models. The second approach consists of connecting different analysis tools together to achieve a global computational workflow [148, 36]. This is often referred to as distributed engineering and is managed by a design environment as shown in Figure 2.24. It generally requires high computational cost for system analysis and often licenses of legacy analysis tools on the same computer.

System analysis of multidisciplinary systems solves the different couplings between variables by utilizing different numerical methods. More details about multidisciplinary systems are given in Section 2.5.5.

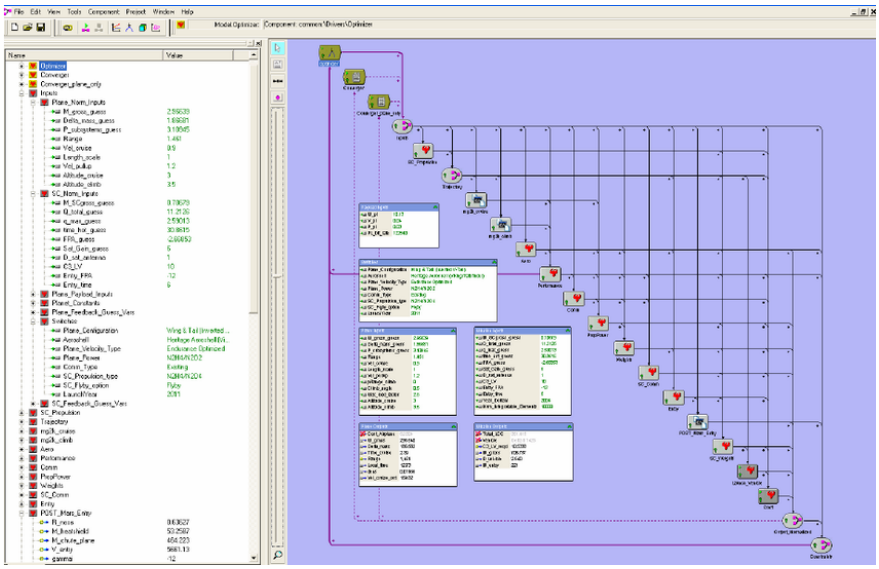

Fig. 2.24 Example of a ModelCenter workflow for mars vehicle design [199]

Numerical tools that predict performances of engineering system are at this date mature and widely used. The challenge now is to determine which design endows optimal performances of the system. This is the purpose of design optimization techniques discussed in Section 2.5.

2.4.5 Design Visualization

Design is a decision making process. It is important to have efficient visualization tools to support such process. In a wider scope than design, data visualization is a concern in many disciplines [125]. Data sciences have accelerated the development of data visualization tools especially using front-end web technologies [21]. Data visualization tools specific to engineering design have also been development such as LIVE [243] and Trade Space Visualizer [223] which is now part of the ModelCenter [148] commercial software.

The most relevant visualization tools for engineering design are: scatter plots, scatter matrices, the correlation matrix and parallel coordinates.

The scatter plot is equivalent to a 2D $y = f(x)$ plot where the behaviour of y with respect to x can be visualized. This plot can be extended by plotting the Pareto frontier of these variables [47]. Furthermore, the effect of x and y on a third variable z can be visualized by introducing different sizes of dots as shown in Figure 2.25. This figure also shows that the effect on a fourth variable u can be visualized by introducing a gradient of colors corresponding to the values of u with respect to the values of x and y.

The scatter matrix is composed of elementary scatter plots that correspond to different combinations of the selected variables. If the two variables have a low correlation then the corresponding scatter plot will have a chaotic or random distribution. Whereas if the scatter plot corresponds to

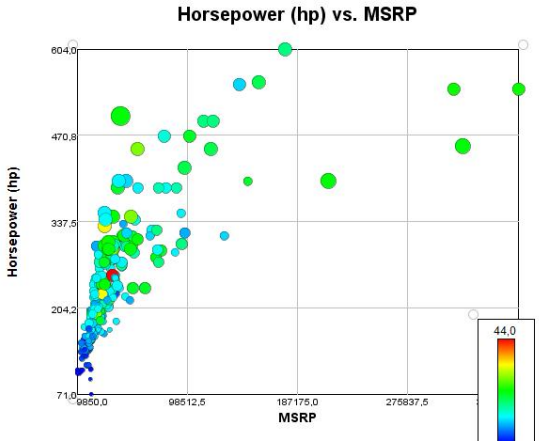

Fig. 2.25 Scatter plot using Trade Space Visualizer

a well shaped curve then the two variables are strongly correlated. Scatter matrix can also use the previous features of scatter plots such as Pareto frontier, dot size and dot color.

Parallel coordinates are widely used for large datasets visualization [115]. Columns corresponds to the variables and each line correspond to a dataset, and in our case of engineering design, a design alternative. Filters and brush can be used to clean the datasets to include only design alternatives that the user finds interesting. Examples of these plots in Trade Space Visualizer [223] are given in Figure 2.26.

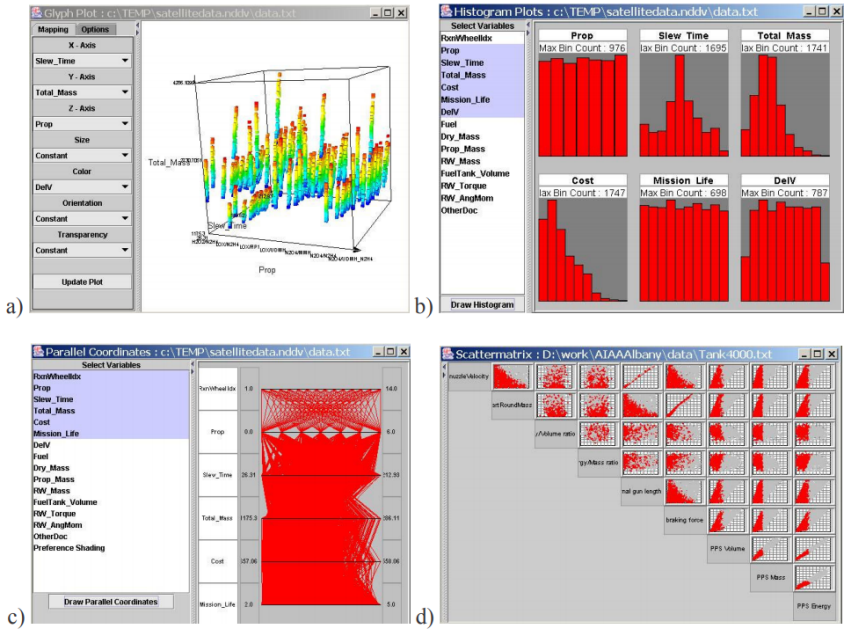

Fig. 2.26 a) Glyph plot, b) Histogram plot, c) Parallel Coordinates, d) Scatter Matrix [223]

Correlation matrix (Figure 2.27) enable to determine the correlation between different design variables by analyzing a dataset. In engineering design they can be used to see the effect of requirements on system or component parameters or to determine which variables in a design problem have to be taken into account. Sensitivity matricies have a similar purpose and are also used in engineering design [133].

		i []	TR [Nm]	nin (max) [min-1]	nav (max) [min-1]	nav (max) [min-1]	Jin [x10-4 kgm2]	m [kg]	dH (max) [mm]	K3 [x103 Nm/rad]	D [mm]	L [mm]
Ratio	i []	1										
Repeatable peak torque	TR [Nm]	0.30682406	1									
Average torque	TA [Nm]	0.35602186	0.98557612									
Kest	K	0.3276811	0.98879708									
Momentary peak torque	TM [Nm]	0.30296353	0.99865771									
Maximum input speed (oi	nin (max) [m	-0.20580877	-0.80148318									
Maximum input speed (gr	nin (max) [m	-0.20656551	-0.87485511	1								
Average input speed (oil i	nav (max) [r	-0.13227901	-0.95654528	0.91103729	1							
Average input speed (gre	nav (max) [r	-0.06710678	-0.83507266	0.63647966	0.78280989	1						
Moment of inertia	Jin [x10-4 kg	0.1079201	0.95993794	-0.82954229	-0.95465143	-0.91335741	1					
Weight	m [kg]	0.13040322	0.96919648	-0.88390933	-0.97143869	-0.88958117	0.99389969	1				
Maximum hollow shaft di	dH (max) [m	0.17329579	0.93395171	-0.95926971	-0.96903126	-0.73110904	0.91331557	0.94954675	1			
Torsional stiffness	K3 [x103 Nm	0.19665716	0.98874239	-0.88266051	-0.97056948	-0.87376364	0.98380053	0.99118094	0.94577501	1		
Diameter	D [mm]	0.20276043	0.95254648	-0.96866694	-0.97944204	-0.75116062	0.93246914	0.96374109	0.98834561	0.96183855	1	
Length	L [mm]	0.16357662	0.95287492	-0.95301812	-0.98290172	-0.77290577	0.94209207	0.97117242	0.99636468	0.96684497	0.9942834	1

Fig. 2.27 Correlation Matrix in Excel

2.5 Optimal Design

Numerical optimization tools have significantly improved in sophistication and helped the industrialization of Optimal Design [177]. Due to increasing competition within the industry, simply meeting the minimum project requirements for a new design does not ensure a contract win. In order to increase competitiveness, emphasis must be placed on optimization of system performance [36]. Optimization enables designers to use mathematical decision-making methods for engineering design activities. Complex systems lead to significant numbers of design variables and design constraints. Design spaces can be so large that all the design alternatives cannot be assessed easily. Using numerical optimization to assist decision-making process such as engineering design empowers designers to undertake large and coupled systems. A large number of numerical optimization methods exist and all have their own pros and cons. The purpose here is to outline the different possibilities that offer optimal design and determine which approaches are interesting for rapid mechatronic system sizing.

2.5.1 Design Optimization

Optimization is commonly used in engineering systems design in order to find the best possible design in terms of performances. Before that, it was widely used to minimize manufacturing costs, obtaining maximum profit or curve fitting [18].

An engineering design optimization problem is a problem in which certain parameters (design variables i.e x) need to be determined to achieve the best measurable performance (objective function i.e $f(x)$) subject to technological limits and requirements (design constraints i.e $c_i(x)$ and $g_j(x)$) as shown in 2.5.

$$\begin{aligned} &\text{minimize} && f(x) \\ &\text{with respect to} && x \in \mathbb{R}^n \\ &\text{subject to} && c_i(x) = 0, \quad i = 1, \ldots, m. \\ & && g_j(x) \leq 0, \quad j = 1, \ldots, k. \end{aligned} \tag{2.5}$$

Engineering design problems are for most products constrained optimization problems as the system has to respect performance, integration, manufacturing and material property constraints. Nevertheless, the convexity and the differentiability of engineering design problems vary depending on the studied product [177].

A wide range of numerical optimization techniques enable to tackle most of engineering system design problems. Different characteristics can define a optimization problem:

- Type of design variables
  - continuous variables
  - integer programming (discrete variables)
  - mixed variables
- Relations among design variables
  - linear programming
  - non-linear programming
- Type of optimization problems
  - unconstrained optimization
  - constrained optimization
- Differentiability
  - Gradient-free optimization
  - Gradient-based optimization

Engineering design problems show a wide range of types as the number of analysis functions or number of design variables varies. Design variables can be continuous or discrete or both in some problems. The relations among design variables can vary due to the mathematical functions used in the design problem and how they are connected in the system design model. This can result in a linear or non-linear programming problem to model the relationship between design variables and the objective function and design constraints in the case of constrained optimization.

Gradient-free optimization, also referred to as black-box optimization, is used when practical design problems do not offer derivatives of model functions. This is the case when design variables take

discrete or integer values, for example the number of teeth in gear design, that lead to discontinuous model functions. If model functions have discontinuities in their slope then they are not derivable at some points. Gradient-free optimization is also interesting when facing design problem composed of several local minima (multi-modal) such as the Eggholder illustrated in Figure 2.28.

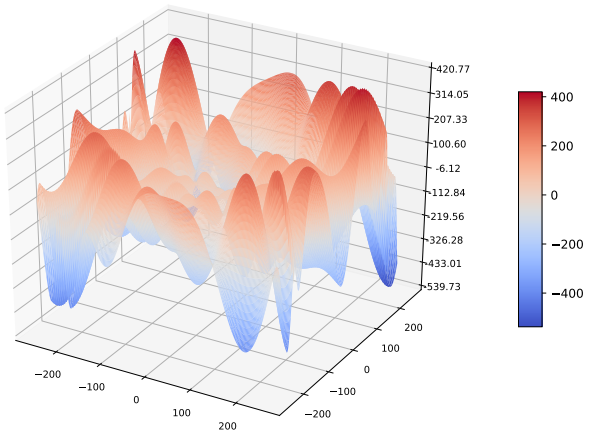

Fig. 2.28 Non-convex optimization problem example: Eggholder function

Gradient-based optimization is very effective for optimization problems composed of a large number of design variables. The number of iterations increase linearly with the number of design variables where as for gradient-free algorithms (Non Sorting Genetic Algorithm II (NSGA2), Particle Swarm Optimization (PSO) it tends to increase quadratically as shown in Figure 2.30. Gradient-based methods are not very robust for multi-modal problems as they tend to terminate on a local minima. Figure 2.29 shows the gradient descent iterations for two different starting point , $x = -0.5$ and $x = 0.5$, when minimizing:

$$f(x) = 0.5x^4 - 16x^2 + 5x \tag{2.6}$$

The two optimization render two different local minima even if the function is less multi-modal than Figure 2.28.

Combining gradient-based optimizers and multi-start capabilities increases chances to find the global optimum by keeping the best feasible sample. The biggest challenge for gradient-based optimization remains the computation of total system derivatives.

Assessing which of optimization methods is the best remains the domain of mathematicians. For engineers the fundamental task in engineering system design optimization is to determine which method is best suited for the actual problem. The principle questions of engineers when facing design optimization problems are:

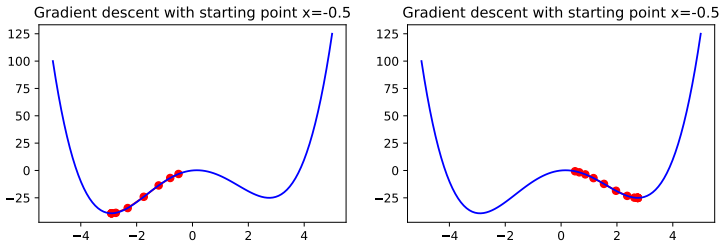

Fig. 2.29 Gradient descent for two different starting points

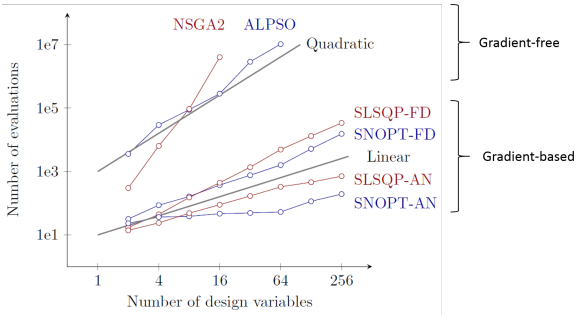

Fig. 2.30 Effect of number of design variables on number of function evaluations for different optimizers [112] (AN: Analytic, FD: Finite Difference)

- Computational cost
- Finding the global optimum
- Continuous, discrete, mixed variable?
- Are my functions differentiable?

2.5.2 Common Gradient-Free Methods

The idea behind gradient-free optimization is to use only function values. The defining characteristic of gradient-free optimizers is that they do not need to compute derivatives of the objective function nor constraints with respect to the design variables. This makes them suitable for problems with a non-smooth or noisy objective functions. The termination of gradient-free optimization, which is a pseudo optimality condition since there are no optimality condition in such methods, is generally the lack of improvement or reaching the maximum number of iterations [177]. Gradient-free optimizers can be subdivided into local, “hill-climbing” methods and global, evolutionary or statistical, methods [45].

Direct search methods consist of ordering relationships in the design space like x_1 is better than x_2 if $f(x_1) < f(x_2)$ in the case of a minimization problem [107, 177]. The coordinate search method evaluates the current design variable value in all the directions of the design space with respect to the step size of the search. It then chooses the best direction and increases the design variable value of one

step size. If a step in each direction does not give a better objective function value then the step size is reduced and the process continues until objective function variation are smaller than the tolerance.

Nelder-Mead is similar to direct search methods as it reduces the search space through the iterations. It is in some cases referred to as downhill simplex method. It relies on the modification at each iteration of a simplex composed of n+1 points for n design variables using six main operations: order, reflection, expansion, contraction and shrink [172]. It permits the optimization of non-smooth and derivative-free objective functions as it is a gradient-free method. It has shown limitations for problems with a large number of design variables and is not adapted for constrained optimization. Constrained optimization by linear approximation (COBYLA) is an iterative method for derivative-free constrained optimization [188]. The method maintains and updates linear approximations to both the objective function and to each constraint. The approximations are based on values computed at the vertices of a well-formed simplex. Each iteration solves a linear programming problem where the step size decreases as the method progresses toward a constrained optimum and stops when it is sufficiently small.

Bayesian optimization is a gradient-free optimization approach that finds its application in the optimization of costly and noisy objective functions [169]. It is based on the construction of a surrogate model of the costly objective function while quantifying its uncertainty using a Bayesian learning technique [169]. However, its utilization is often limited to problems that contains a limited number of design variables (typically below 20) [24]. The acquisition function of the surrogate model enables to determine where to sample by evaluating the expected improvement, which represents a trade-off between promising and uncertain areas [8]. The interest of such global optimization approach has been outlined for high-dimensional constrained problems such as wing aerodynamic optimization based on both Kriging and Mixture of Experts surrogate models [17].

Metaheuristics are another type of gradient-free methods and are often inspired by natural phenomena [244], for example, simulated annealing optimization. Furthermore, it contributed to the development of evolutionary algorithms. Biological evolution influenced greatly the development of genetic algorithms. Genetic algorithms are much more efficient than random methods like Monte-Carlo but they also result in a large number of function evaluations. Some genetic algorithms offer the possibility to consider multiple objectives and mixed variables [48]. The ethology domain is very similar to particle swarm algorithms. Evolutionary strategies such as Covariance Matrix Adaptation Evolution Strategy (CMA-ES) [99] are used for non-linear continuous problems. In opposition to simplex methods, they are stochastic methods which avoid combinatorial explosion for finding the global optimum. Figure 2.31 shows the evolution of objective function value when solving the Rosenbrock function [202] with different gradient-free optimizers. It enables to assess first how many iterations each optimizer requires and also compare how the search covers the design space. However, the search path cannot be clearly outlined as it would require two many paths but could be achieved if a single optimizer was plotted.

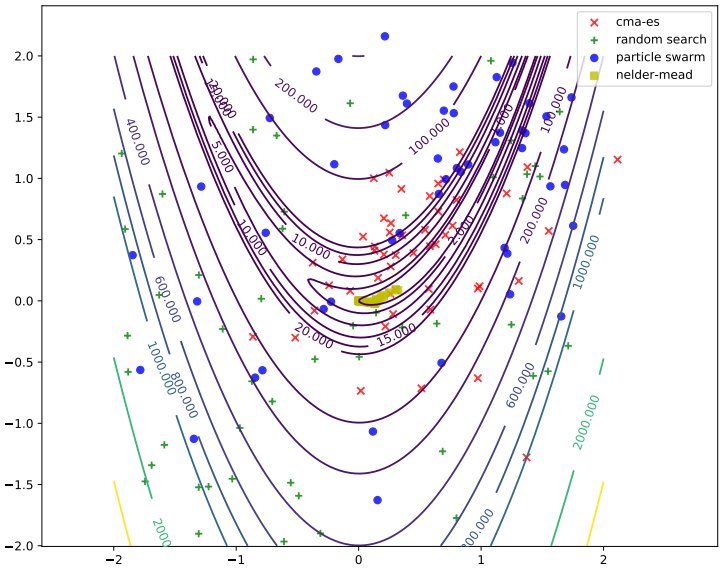

Fig. 2.31 Search evolution when minimizing the Rosenbrock function for different gradient-free methods

Figure 2.31 shows that the Neldear-Mead requires less design space exploration and has a faster convergence for this problem. However, the particle swarm and CMA-ES methods have a more efficient search than the random search.

Despite that metaheuristics methods offer the possibility to not worry about derivatives, dealing with constraints can be quite tricky. Constraint handling can be implemented using different techniques such as the penalty function [177]. In addition, they lead to a large number of function evaluations and thus important computational cost.

2.5.3 Common Gradient-Based Methods

For problem composed of a large numbers of variables, gradient-based methods are generally the most efficient. The idea behind gradient-based optimization is that it used gradient of objective (and constraints) with respect to design variables. The gradient of an objective function corresponds to a n-rows vector composed of each partial derivative of the objective function with respect to each of the n design variables.

$$\nabla f(x) = \begin{bmatrix} \frac{\partial f}{\partial x_1} \\ \frac{\partial f}{\partial x_2} \\ \vdots \\ \frac{\partial f}{\partial x_n} \end{bmatrix} \tag{2.7}$$

If the partial derivatives that are part of the gradient are continuous then it is possible to express the Hessian matrix:

$$H(x) = \begin{bmatrix} \frac{\partial^2 f}{\partial^2 x_1} & \cdots & \frac{\partial^2 f}{\partial^2 x_n} \\ \frac{\partial^2 f}{\partial x_2 \partial x_1} & \cdots & \frac{\partial^2 f}{\partial x_2 \partial x_n} \\ \vdots & & \\ \frac{\partial^2 f}{\partial x_n \partial x_1} & \cdots & \frac{\partial^2 f}{\partial^2 x_n^2} \end{bmatrix} \tag{2.8}$$

The necessary conditions for local minimum x^* when employing gradient-based methods are [145]:

- $\|\nabla f(x)\| = 0$
- $H(x^*)$ is positive semi-definite

Different gradient-based methods for solving unconstrained optimization problems have been proposed during the last century [156]. The steepest descent method is the most simple method that uses the gradient of the objective function with respect to the vector of design variables. In the case of smooth quadratic function it guarantees a convergence but it will generally take a large number of iterations. Newton's method uses the second-order Taylor series expansion which enhances its convergence rate. Quasi-Newton methods like Broyden-Fletcher-Goldfarb-Shanno (BFGS) use only first-order derivative information but estimates numerically the Hessian through the iterations [173]. Figure 2.32 shows benchmark results of different unconstrained gradient-based methods.

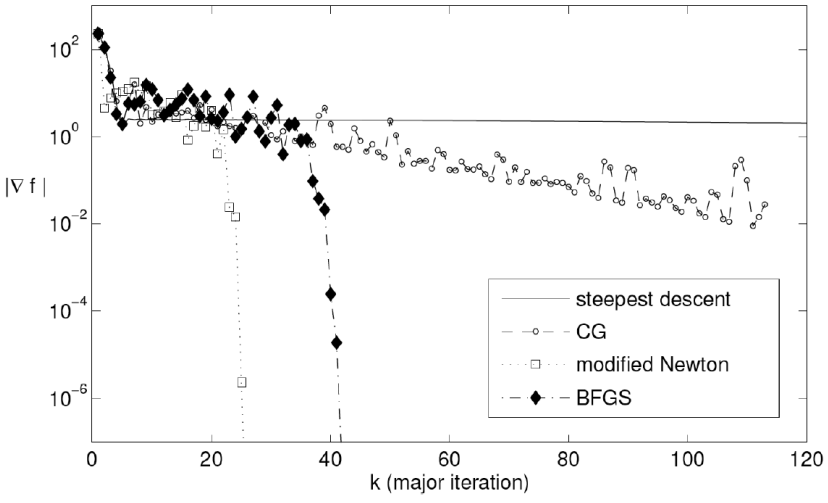

Fig. 2.32 Comparison of convergence rates for the Rosenbrock function [156]

The use of gradient-based methods also exist for constrained optimization problems. Karush-Kuhn-Tucker (KKT) are first-order optimality conditions for constrained problems that use the Lagrangian multiplier method [145, 134]. Research investigations in gradient-based optimization have led to the

implementation of efficient numerical methods for gradient-based constrained optimization such as Sequential Least Square Quadratic Programming (SLSQP) [131] or Sparse Nonlinear OPTimizer (SNOPT) [85].

2.5.4 Derivatives Computation

As described previously, gradient-based methods require the computation of function derivatives. Different methods for obtaining derivatives can be used depending on the properties of the given function.

Partial Derivatives

Partial derivatives are used to express derivatives of system model elements with respect to design variable. The most common method to obtain partial derivatives in a numerical computation environment is Finite Difference (FD) as its implementation is easy. Besides, its accuracy can in some cases be limiting and requires smooth functions to be efficient. Their implementation uses in most case forward difference as in Equation 2.9.

$$f'(x) = \frac{f(x+h) - f(x)}{h} + \mathcal{O}(h) \tag{2.9}$$

This is a first order approximation of Taylor series expansion which leads to a truncation error $\mathcal{O}(h)$. Decreasing the step size enables to minimize truncation error until the step size becomes so small that the substraction error becomes the main source of error [159]. Furthermore, decreasing the step size, as it remains fixed and is not adaptative, results in higher computational cost. The substraction error is directly linked to the precision of floating numbers of the computational environment. If the step size becomes really small with regard to digit precision the substraction $f(x+h) - f(x)$ becomes equal to zero.

Complex step (CS) derivative approximation is another option to compute derivatives of a multidisciplinary system [159]. It utilizes complex variables to compute the real function derivatives. It is a very accurate method with a reasonable computational cost [155]. Nevertheless, in many numerical computational environments some mathematical functions do not allow to pass them complex number as parameters. Additionally, as it requires the source code of the function it is not applicable to black box functions. Equation 2.10 shows how to complex step derivative approximation is computed.

$$f'(x) = \frac{\mathrm{Im}[f(x+ih)])}{h} + \mathcal{O}\left(h^2\right) \tag{2.10}$$

The main difference between Equation 2.9 and 2.10, despite the use of complex numbers, is that the complex step does not use substraction. This means that the complex step method has no substraction error. Hence, the only error is truncation which can be decreased by reducing step size to a reasonable computational cost. It is the fundamental advantage of complex step in comparison to finite difference. Figure 2.33 shows some benchmarking results that compare both methods.

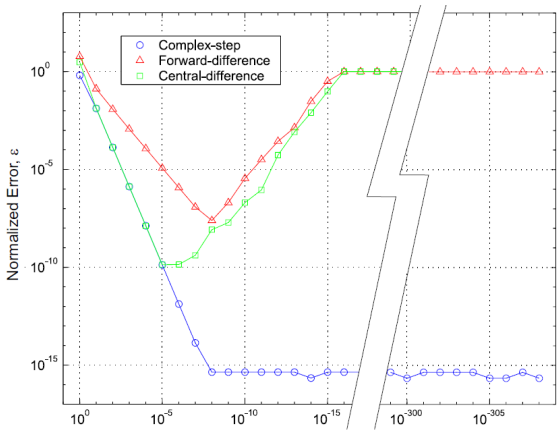

Fig. 2.33 Relative error in the sensitivity estimates given by the finite-difference and the complex step methods using the analytic result [159]

Symbolic Differentiation (SD) can be applied for explicit functions and can be obtained manually or using symbolic computation softwares such as Maple, Matlab, Mathematica and Python (Sympy).

Figure 2.30 shows that analytical derivatives (Automatic differentiation (AD), SD) are more effective than numerical methods like FD especially for problems composed of a large number of design variables.

Once that the individual function or discipline derivatives are obtained the challenge is to determine the total system derivative in order to have the gradient of objective and constraints with respect to system design variables.

Total System Derivatives

The total system derivatives correspond to what the optimizer requires that is the gradient of the functions (contraints and objective) with respect to the design variables. The challenge is that in between the design variables and the functions there are multiple model components. Thus, total derivatives cannot be determined straight away. Total system derivatives can be obtained by analyzing design code described by successive algebraic analysis functions, with the help of a symbolic solver compute the derivative of a given variable with respect to another. The attempts to use such approach are inefficient when the algebraic analysis function are hard to differentiate or when the system is composed of a large number of analysis functions. The chain rule is also an option to compute total derivatives [112].

The Unifying Chain Rule is a matrix equation formulation for expressing the relationship between partial derivatives and total system derivatives using linearization [157]. Such formulation enables to express the Unified Derivatives Equations. They enable to compute the total derivatives of a system of non-linear equations by solving a linear system of equations in the forward (direct) (Equation 2.11) or reverse (adjoint) (Equation 2.12) form.

$$\left[\frac{\partial \mathscr{C}}{\partial v}\right]\left[\frac{dv}{dc}\right] = I \tag{2.11}$$

$$\left[\frac{\partial \mathscr{C}}{\partial v}\right]^T\left[\frac{dv}{dc}\right]^T = I \tag{2.12}$$

Where v is the vector of all the outputs of each component, c is the vector of the component residual values, C is the vector of the component residual functions, $\left[\frac{\partial \mathscr{C}}{\partial v}\right]$ is a matrix composed of all partial derivatives (known) and $\left[\frac{dv}{dc}\right]$ the total system derivatives of v with respect to c (unknown) as shown in Figure 2.34. Since the partial derivatives are known, thus $\left[\frac{\partial \mathscr{C}}{\partial v}\right]$, then the both forms of the Unified Derivatives Equation can be solved linearly. The computational cost of solving of the Unified Derivatives Equations is proportional to the number of design variables in the forward form and proportional to the number of objectives and constraints in the reverse form. Thus, if you have less design variables than objectives and constraints then the most efficient form is the forward form. When there are more design variables than objectives and constraints, the selected form should be the reverse form.

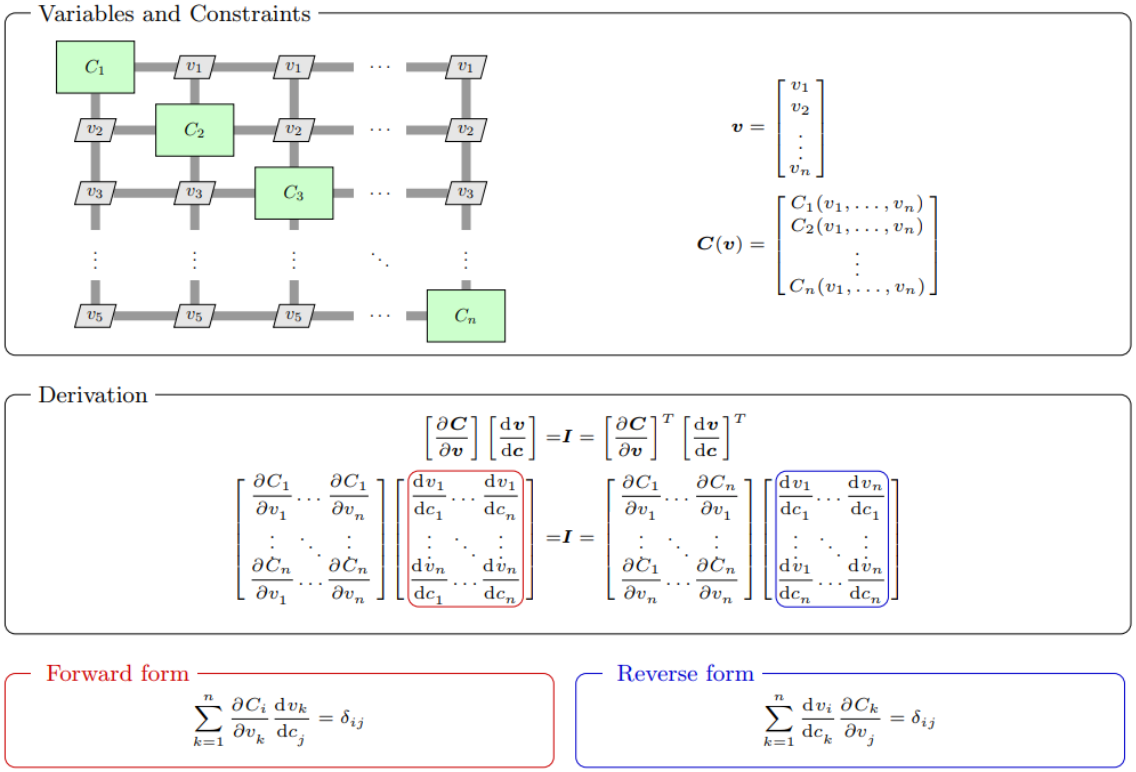

Fig. 2.34 Equations for computing total derivatives in a general system of equations [157]

Monolithic differentiation methods assume the system to be a black box where partial derivatives of components are not available. Both Finite Difference and Complex Step are examples of such

methods which compute the derivatives of functions (objectives and constraints) with respect to design variables.

Automatic Differentiation (AD) has to have access the source code to analyze each line and compute the partial derivatives using symbolic differentiation. It uses forward or back substitution to compute total derivatives [92]. Open-source frameworks enable to implement easily AD and use them for gradient-based optimization problems [146]. Despite the effortless implementation of AD, features like array indexing remain still uncovered.

Analytic differentiation methods are the most efficient but require detailed knowledge of the model. Discrete methods allow coupled analytic methods such as direct or adjoint form [157]. In an implicit form both can be derived as described in Figure 2.35.

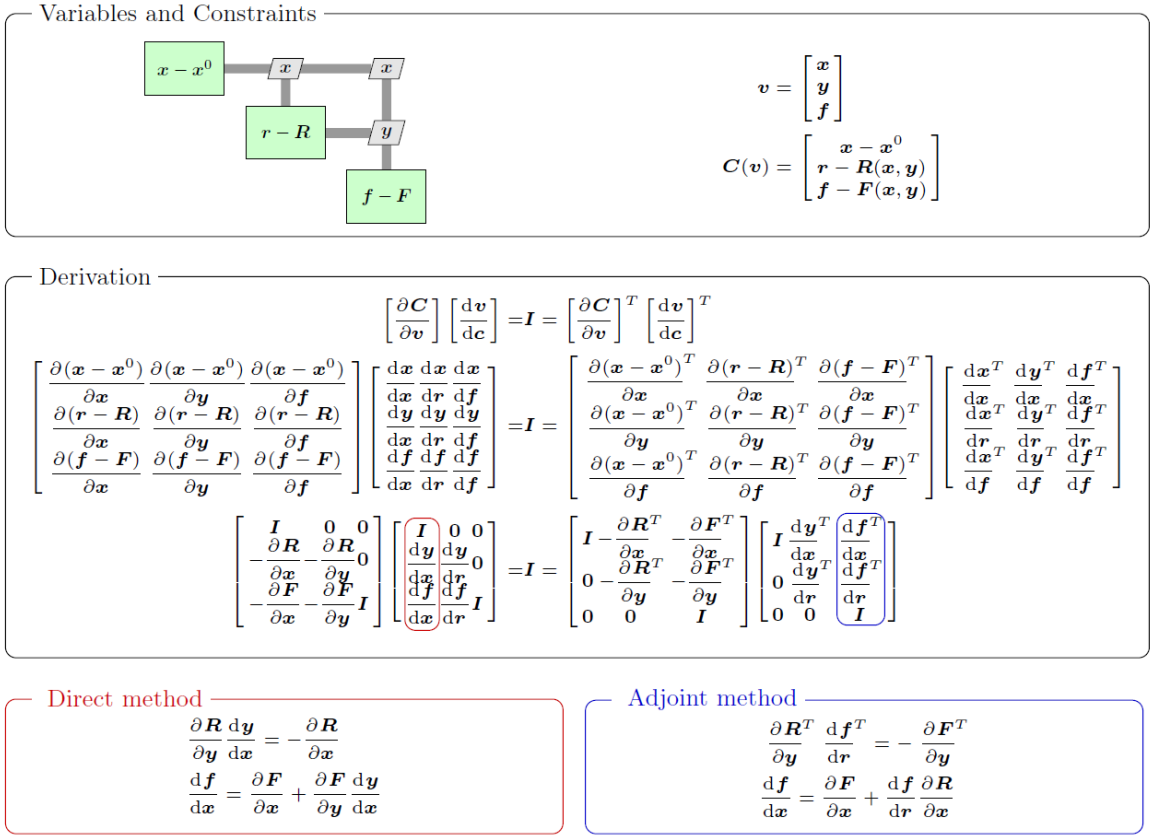

Fig. 2.35 Derivation of the analytic methods for direct and adjoint froms [157]

Unified Derivatives Equations (UDE) is an efficient method to obtain total system derivatives while mixing the different differentiation methods [157]. Such method is used in the modular analysis and unified derivatives (MAUD) computational architecture developped by Hwang and Martins [112, 113]. This computational architecture provides the computational core algorithms to the open-source MDAO framework openMDAO [89].

2.5.5 Multidisciplinary System Design Optimization

Many mechatronic systems are multidisciplinary. They are also referred to as coupled systems. Many other engineering systems use multidisciplinary design optimization (MDO) methods in order to achieve sucessful system designs [186, 80]. If the multidisciplinary couplings are ignored, then the resulting designs will be inconsistent. Therefore, the system analysis has to be achieved in a tightly coupled manner. Numerical methods are able to achieve multidisciplinary system analysis and optimization but the first step is to decompose and coordinate the problem in the most efficient way [7]. As shown in Figure 2.36, the way the system model is implemented can have a significant effect on the number of couplings. In design and sizing activities emphasis is placed on rapid computational results. Thus, it is prefered to avoid a high number of couplings in the system model.

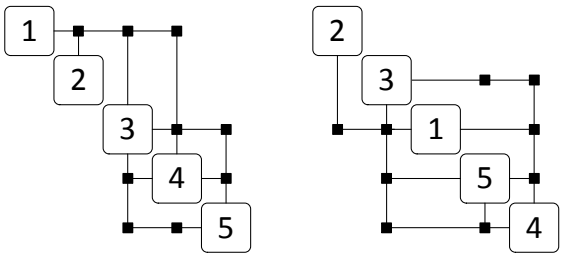

Fig. 2.36 Sub-systems modules with minimized feedback (left) and random (right) ordering (adapted from [20])

Different strategies can be chosen to deal with multidisciplinary couplings during system analysis and optimization. Two main approaches are used: solver based or optimizer based. The first uses numerical solvers in order to solve the multidisciplinary couplings. The second relies on the optimizer by reformulating the design optimization problem to solve multidisciplinary couplings. Sequential optimization does not achieve multidisciplinary analysis and results in not finding to the true optimum of the system.

The most common monolithic architectures used in MDO are All At Once (AAO), also referred to as Simultaneous Analysis and Design (SAND), Individual Discipline Feasible (IDF) and MultiDisciplinary Feasible (MDF) [158]. Monolithic formulations are described in more details in the following chapter.

Distributed architectures enable to use simultaneously different optimizers for multidisciplinary optimization. These can be used when disciplines are heterogeneous and their analysis difficult. Martins and Lambe provided a survey of MDO architectures where the distributed formulations were Concurrent Subspace Optimization (CSO), Collaborative Optimization (CO) illustrated in Figure 2.37, Bilevel Integrated System Synthesis (BLISS) and Analytical Target Cascading (ATC). Differences between them come from differences in the implementation of optimizers, discipline analysis, consistency design variables and constraints.

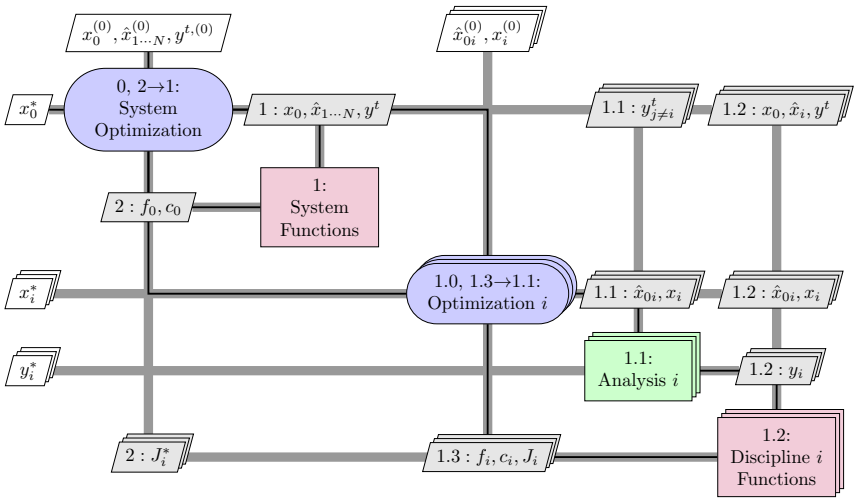

Fig. 2.37 XDSM diagram for the CO architecture [158]

In engineering design optimization, emphasis is placed on obtaining quickly feasible and close to optimal solutions. Comparisons in terms of computational cost were made for different type of MDO formulations as shown in Table 2.1 [90]. The tests were ran for solving the Sellar Problem which is an analytic coupled problem due to the interdependency of disciplines computing respectively y_1 and y_2 [212]:

$$\begin{aligned} &\text{minimize} && x_1^2 + z_2 + y_1 + e^{-y_2} \\ &\text{with respect to} && z_1, z_2, x_1 \\ &\text{subject to} && \frac{y_1}{3.16} - 1 \geq 0 \qquad 1 - \frac{y_2}{24} \geq 0 \quad -10 \geq z_1 \leq 10 \quad 0 \geq z_2 \leq 10 \quad 0 \geq x_1 \leq 10 \end{aligned} \tag{2.13}$$

Where $y_1 = z_1^2 + x_1 + z_2 - 0.2y_2$ and $y_2 = \sqrt{(}y_1 + z_1 + z_2$.

Table 2.1 Function evaluation counts for all architectures solving the Sellar Problem [90]

	Discipline 1	Discipline 2
IDF	60	50
MDF	222	216
CO	5647	8252
BLISS	3344	3130
BLISS-2000	818	108

These results show clearly the advantage of using monolithic architectures (when possible). Indeed, the total function evaluations are much greater for BLISS or CO than for IDF and MDF. As mechatronic systems remain reasonably complex, the rest of the thesis will include only monolithic formulations.

The development of frameworks for multidisciplinary system design optimization of engineering systems [56, 89, 147, 205] have been achieved in different engineering design domains. The establishment of holistic approaches for the design of complex engineering systems is a real need for today companies as development time, cost and quality objectives become more and more challenging.

2.6 Conclusion

Embedded mechatronic system design is core part of the aerospace engineering problem solving. It has medium number of disciplines and requires all types of model fidelity. Multidisciplinary couplings are done in the mechatronic layer which leads to different nature of couplings. The design of mechatronics systems have many challenges. Reliability expectations of embedded applications constrain significantly the design of these critical systems. The multi-level and multi-engineering specializations aspects lead to the challenging management of heterogeneous engineering teams and design tools. In addition, these complex systems involve multiple physics and show a large range of scale in their components size and the time constants of involved physical phenomenas. Many mechatronic systems are a coupled system, and thus they require specific design approaches. Their design is also a challenge in terms of knowledge management since their design involves different fields of expertise and engineering teams.

Model-based Design techniques are a promising answer to these engineering design challenges. Existing tools provide efficient methods for requirements engineering, functional and organic architecture definition. Different standards define mathematical fundation to conduct system reliability analysis. System sizing is generally achieved by one expert who masters system trade-off with respect to engineering specializations. Some co-simulation or distributed engineering tools provide computational workflows that can achieve sizing analysis and optimization but they induce high computational cost. Engineering specializations for model-based design tools are numerous and cover all the fields of engineering. They can drive high fidelity simulations of component performances. System virtual prototyping softwares are a great alternative to assess rapidly system performances and support the validation process. Functional Mock-up Units offer the possiblity to be used in different simulation tools or scientific computing environments such as Python. Surrogate modelling methods are an interesting alternative to reduce models and use them in applications requesting a high number of function evaluations such as numerical Design of Experiments or optimization.

The complexity of embedded mechatronic systems makes a systemic approach mandatory. Many different system representations are possible, the N2 chart is very pertinent for multidisciplinary systems. The decomposition of a system is intricate, it depends strongly on the type of application. Mechatronic system are commonly decomposed in two main layers: system and component. Nonethe-less, design is an iterative process between both of these layers. The coordination of engineering design can be achieved by using graph and tearing algorithms. System analysis can be performed in environments that enable the connection of dataflows between different engineering legacy tools. Algebraic computation environments are sufficient when elementary models have been reduced to

algebraic expressions. Once system analysis is performed many visualization tools are interesting for engineering design. Scatter plot, scatter matrix and parallel coordinates enable the visualization of large data sets and design by shopping techniques.

What this introduction reveals about design optimization is that the most effective optimization is achieved by combining gradient-based optimizers with monolithic formulations. Nevertheless, this combination requires the availability of partial derivatives and the computation of system total derivatives. For that analytical derivatives such as symbolic differentiation and the MAUD architecture for total derivative computation are interesting alternatives. To handle multi-modal functions gradient-based methods can be combined with multi-start features. Uncertainty and robust optimization [183] have not been investigated in this state of the art but are important topics in engineering design.

In this thesis, emphasis is placed on computational time as the main objective is to permit rapid decision making during preliminary sizing process. The biggest challenge remains to better utilize different engineering specialization knowledge during system design. The development and utilization of engineering design tools have been outlined for the different steps of the design process. System design optimization tools can bring significant outcomes for system performance and collaborative engineering design [205]. The objective of this thesis is to develop a similar tool for rapid sizing and design of actuation system in the Safran company context. The positioning of this sizing tool among other design tools is given Figure 2.38.

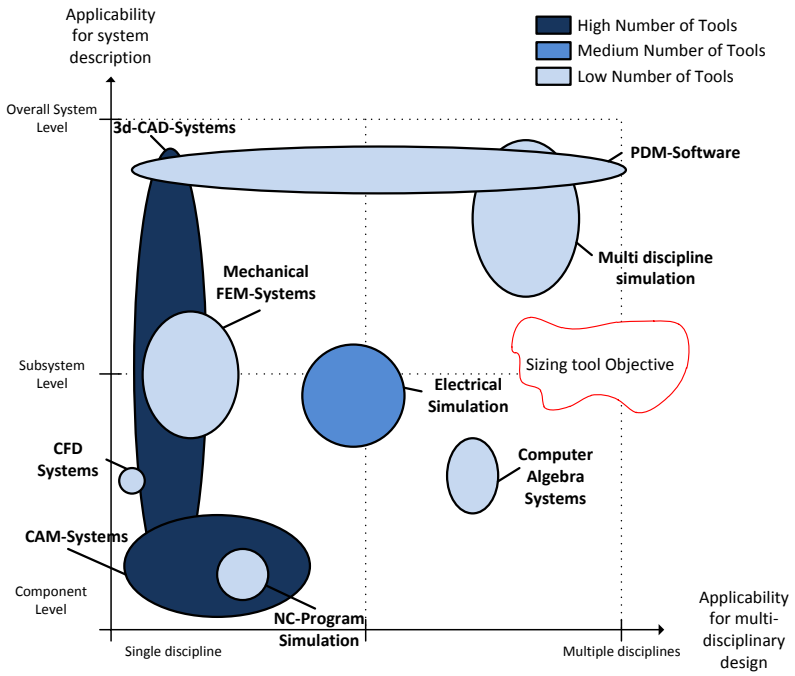

Fig. 2.38 Existing design tools classification and objective sizing tool location (adapted from [101])

The following sections of this manuscript aim to describe a methodology that would include such sizing tool and its application to aerospace actuation systems.

Chapter 3

The Normalized Variable Hybrid Formulation and Graph-Based Approach for Efficient MSDO

3.1 Introduction

Many engineering systems involve multiple disciplines and sub-systems. Similar to other products and domains, mechatronic systems are composed of interdependent sub-systems and components. Dealing with the interdependencies is a fundamental and intricate aspect of engineering. These interdependencies have to be solved in a tightly coupled manner during system design to avoid non-compliant designs. The multi-physical, multi-level and multi-scale aspects of mechatronic systems increase the sophistication of these interdependencies and therefore overall system design. It involves multiple engineering specializations such as systems engineering, electrical engineering, machine design engineering, control engineering and mechanical engineering. Furthermore, when these systems are embedded and integrated in harsh environments, requirements in terms of reliability, mass objective, geometric integration and thermal management become even more challenging. A rigorously coordinated effort is needed during the design process in order to deal with heterogeneous numerical design tools and human aspects of the engineering teams. To handle component interdependencies, system design requires iterations, commonly achieved through human interactions. The overall result is a significant amount of costly iterations that does not necessary achieve an optimum.

The main objective of methods developed in this thesis is to achieve complex system optimization. In order to handle high complexity of design optimization problems, Multidisciplinary Design Optimization formulations are used to define the optimization problem. It is sought to develop a formulation that suits our needs within the following bounds:

- Integrate various types of models that include multidisciplinary couplings
- Enhance analysis and optimization computation time
- Enhance reusability

This chapter examines the fulfilment of these three main needs.

The formulation of complex system design optimization problems leads to typical issues for designers to handle:

- Orientation and ordering of models
- Over-constrained and under-constrained singularities
- Multidisciplinary couplings

Orientation of models is problem dependant but model generally have fixed causality. The ordering of models corresponds to determining a computational sequence that provide output values with respect to given inputs. This is achieved graphically using standard representation like N2 diagram [122] or the Extended Design Structure Matrix (XDSM) notation proposed by Lambe and Martins [135]. Ordering can also be automatically determined using graph-based methods [179].

Over-constrained and under-constrained singularities can appear due to human errors during the model implementation. As the model get more and more complex, the risk of singularity apparitions increases. These singularities are in some cases intrinsic to the design problem and have to be solved numerically by reformulating the design problem by choosing alternative design variables and/or constraints [195].

In this chapter, these two issues are considered but emphasis is placed on the third issue: multidisciplinary couplings. Multidisciplinary couplings that commonly occur in the engineering systems design process. They are handled using numerical techniques that use either solvers or optimizers. Here, we focus on the detection and resolution through problem reformulation.

The resolution of these three typical issues common to MDO applications will be integrated in a design and sizing methodology presented in the next chapter.

3.2 MSDO Formulations Definition

3.2.1 An Electro-Mechanical Actuator Design Problem

The case study presented here is a simplified optimization problem that illustrates the multidisciplinary design of a mechatronic device. The low number of analysis functions required to represent the problem enables to present concisely and test the resolution of it using different MSDO formulations. Examples with a larger number of analysis functions will be described in the following chapters. MSDO formulations are also referred to as Multidisciplinary Design Analysis and Optimization (MDAO) or Multidisciplinary Design Optimization (MDO) architectures. The system is an electro-mechanical actuator designed for dynamic applications such as an Individual Blade Control (IBC) [127] or Thrust Vector Control (TVC) [35]. Despite the simplicity in terms of number of analysis functions, the design of an electro-mechanical actuator for TVC aerospace application is still a challenging topic. Figure 3.1 shows that for launchers electro-hydraulic actuators are preferred because of the high dynamic and high loading conditions.

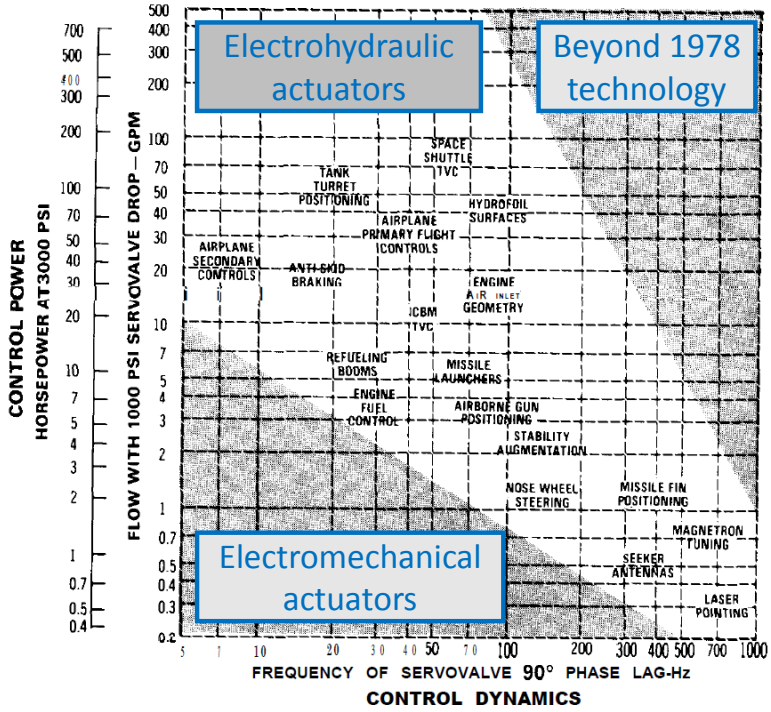

Fig. 3.1 Spectrum of Servoactuation Aerospace Applications in 1978 [160]

Nevertheless, the use of electro-mechanical actuators (EMAs) has been a success on small launchers [221]. However, such applications are on the technological limit frontier of such systems. For some requirements there might be no existing solution because of these technological constraints. Hence, the numerical resolution of the sizing problem for TVC electro-mechanical actuators is challenging.

The EMA is composed of a ball screw, a spur gear set and a brushless motor as shown in Figure 3.2. The maximum external load acting on the actuator and the maximum acceleration and speed of the actuator have been extracted from the mission profile. Since the application is high dynamic, the effect of motor inertial acceleration has to be considered when choosing the motor torque performances. The sizing problem is expressed using only algebraic analysis functions. For more complex design problems where numerical simulations are necessary it is possible to reduce them to algebraic functions using surrogate modelling of lumped parameter (0D-1D) models [31] or Finite Element Method (3D) models [209].

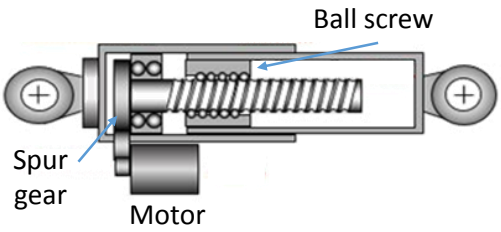

Fig. 3.2 High dynamic EMA architecture

The EMA sizing problem is represented by the following equations:

$$T_{em} = J_{mot} \cdot A_{max} \frac{N_{red}}{p} + F_{ema} \frac{p}{N_{red}} \tag{3.1}$$

$$J_{mot} = J_{mot_{ref}} \cdot \left(\frac{T_{em}}{T_{em_{ref}}} \right)^{\frac{5}{3.5}} \tag{3.2}$$

$$\Omega_{mot} = \Omega_{mot_{ref}} \cdot \left(\frac{T_{em}}{T_{em_{ref}}} \right)^{-\frac{1}{3.5}} \tag{3.3}$$

$$\Omega_{mot} \geq V_{max} \cdot \frac{N_{red}}{p} \tag{3.4}$$

$$M_{mot} = M_{mot_{ref}} \cdot \left(\frac{T_{em}}{T_{em_{ref}}} \right)^{\frac{3}{3.5}} \tag{3.5}$$

Where T_{em} is the motor electromagnetic torque, J_{mot} is the motor inertia, A_{max} is the maximum actuator acceleration, N_{red} is the reducer reduction ratio, p is the screw pitch, V_{max} is the maximum

velocity of the actuator, Ω_{mot} the maximum mechanical speed of the motor and M_{mot} its mass. The motor sizing scaling laws are based on a reference motor where T_{ref}, J_{ref}, W_{ref}, M_{ref} are respectively its electromagnetic torque, inertia, maximal mechanical rotational speed and mass [31]. Motor torque Equation (3.1), motor inertia Equation (3.2) are two coupled disciplines of the sizing problem whereas motor speed Equation (3.3), motor speed constraint Equation (3.4) and motor mass objective Equation (3.5) are ordinary analysis functions. The motor torque (3.1) and motor inertia Equation (3.2) are coupled through motor electromagnetic torque T_{em} and motor inertia J_{mot}. The high-level design problem consists of minimizing the motor mass M_{mot}, with respect to reduction ratio N_{red}, subject to motor speed constraint Equation (3.4).

The optimization problem formulation is the following:

$$\begin{aligned} &\text{minimize} && M_{mot} \\ &\text{with respect to} && N_{red} \\ &\text{subject to} && V_{max} \cdot \frac{N_{red}}{p} - \Omega_{mot} \leq 0 \end{aligned} \tag{3.6}$$

The optimization problem, and the multidisciplinary coupling, are represented in Figure 3.3 using the XDSM diagram formalism.

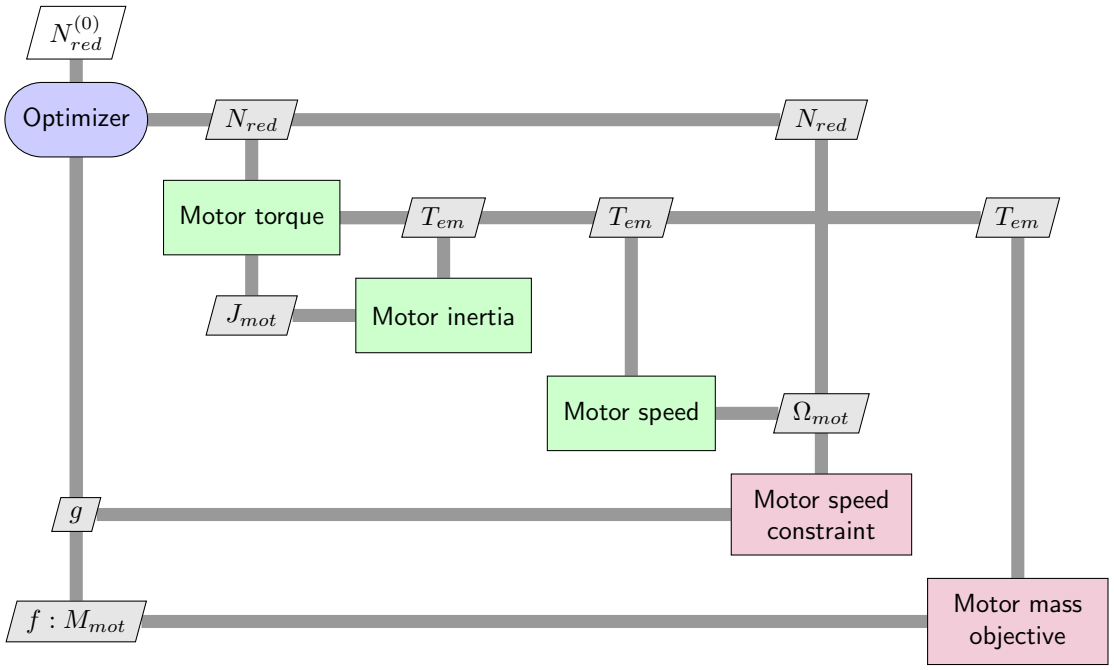

Fig. 3.3 XDSM diagram for the EMA design problem

Additionally, the consistency of the coupling variables T_{em} and J_{mot} between disciplines Equation (3.1) and Equation (3.2) must be verified. For that, the optimization problem can be solved using

different MDO strategies. Each of the strategies are described and represented using the XDSM notation where the mathematical notation is given in 3.1.

Table 3.1 Mathematical notation for MDO problem data (adapted from [136]).

Symbol	Definition
x	Vector of design variables
$x^{(0)}$	Vector of design variables initial values
y^t	Vector of coupling variable targets
$y^{t,(0)}$	Vector of coupling variable targets initial values
y	Vector of coupling variable responses
f	Objective
g	Vector of design constraints
g_c	Vector of consistency constraints

The benchmark of the different System Design Optimization formulations is achieved using open-MDAO. This can be used as a standard a platform for benchmarking MDAO formulations developed by NASA [90]. Analysis functions are implemented using an explicit form. The benchmarking purpose is to evaluate the performance of each formulation to allow design optimization and for design exploration.

3.2.2 The MultiDisciplinary Feasible (MDF) Formulation

The representation of the MDF strategy for the EMA design problem is given in Figure 3.4. It consists of a single design variable, the gear reduction ratio, and a single constraint, the maximum motor speed. The consistency of the coupling between motor torque Equation (3.1) and motor inertia Equation (3.2) disciplines is achieved by using a system analyzer. The system analyzer determines the values of coupling variables that match their respective analysis result. Since system analysis is performed for every optimization iteration, couplings variables remain consistent and independent of the optimizer's behaviour. Here the first computed discipline is the motor torque that requires an estimation of the motor inertia computed by the subsequent discipline. In such architecture the decomposition of circular dependencies can be achieved by using Gauss-Seidel or Jacobi iterative methods [158]. Gauss-Seidel uses a decomposition into lower and strictly upper triangular elements, whereas the Jacobi method decomposes the linear system into a diagonal element and a corresponding remainder.

The coupling can also be solved by gradient-based solvers like Newton-Raphson. In that case, a linear solver is required to compute coupled derivatives. Gauss-Seidel or Jacobi methods can be used to obtain coupled derivatives. Another option is to use a non-iterative direct linear solver. It uses the system Jacobian to compute the coupled derivatives using lower-upper (LU) decomposition, which is possible for any non-singular square matrix [32]. The coupled derivatives are also required to compute total system derivatives when using gradient-based optimizers. All these solvers are

implemented within the openMDAO framework. Here, a Direct linear solver and a Newton non-linear solver performs the multidisciplinary analysis.

The MDF formulation enables us to use no additional design variables or consistency constraints and delivers a consistent design even if the optimizer fails to find a feasible solution and reaches the maximum iteration limit. In addition, MDF eases the incorporation of legacy analysis tools which are often very effective to converge within a particular type of physical discipline. The advantages of system analysis have to be kept in perspective since such approaches rely on the system analyzer effectiveness. Indeed, the non-convergence of the analyzer results in non-consistent designs despite that in some cases convergence is achieved. Furthermore, strongly coupled disciplines lead to important number of analyzer iterations and hence a costly system analyses.

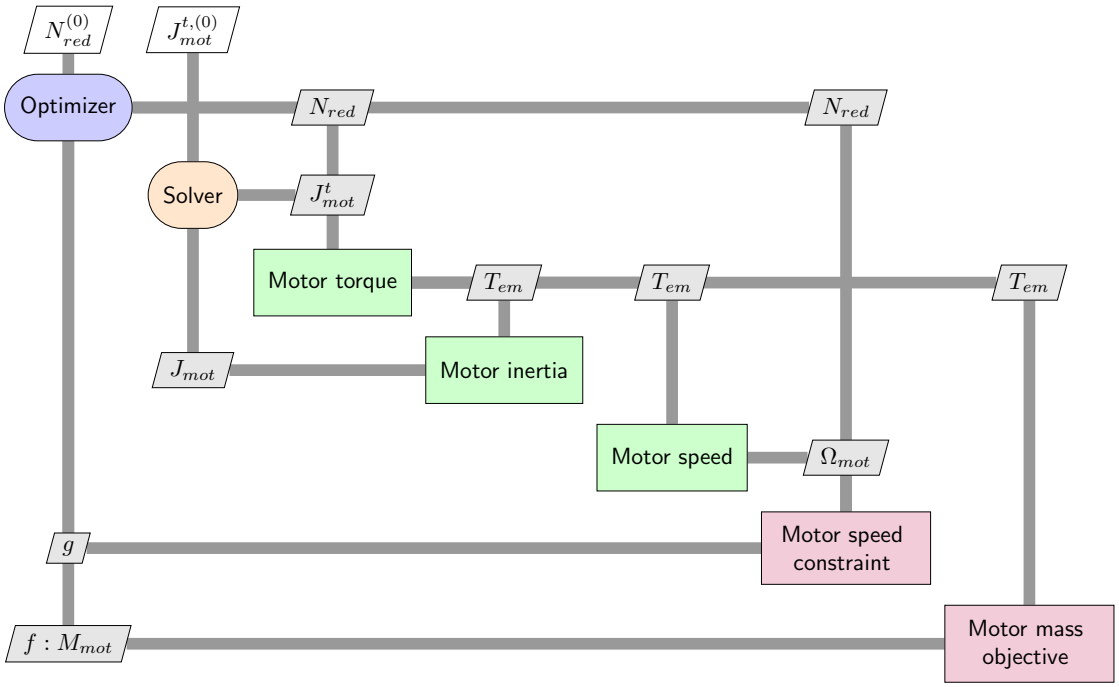

Fig. 3.4 XDSM diagram for MDF formulation of the EMA design problem

3.2.3 The Individual Disciplinary Feasible (IDF) Formulation

As for MDF, IDF uses a single optimizer but an analyzer for each individual discipline is employed. As shown in Figure 3.5, in this formulation it is the optimizer that coordinates the interactions between the disciplines analyses. The optimizer chooses values for both design and coupling variables. In order to ensure consistency between coupling variables, additional design variables T_{em}, J_{mot} and auxiliary equality constraints are added. Here, the optimizer chooses a value for the motor inertia of (3.1) and verifies that it is equal to the motor inertia obtained by Equation (3.2). Similarly, it chooses a value for the motor torque of Equation (3.2) and then verifies that it is equal to the motor torque

obtained by Equation (3.1). The IDF approach enables us to put aside the intricate concerns of system analyzer effectiveness, but has notable shortcomings. Equality constraints can introduce numerical solutions difficulties [228] and provide feasibility only at solution, rather than at each iteration [5]. Furthermore, setting bounds on the couplings variables is in some cases not straightforward and can introduce a large dimension of the coupling variables. Large dimension of design variables has a significant effect on the efficiency of the optimization. If the optimization process is interrupted, the design corresponding to the last iteration may be not consistent or feasible whereas MDF guarantees the consistency between coupling variables if the system analyzer is effective.

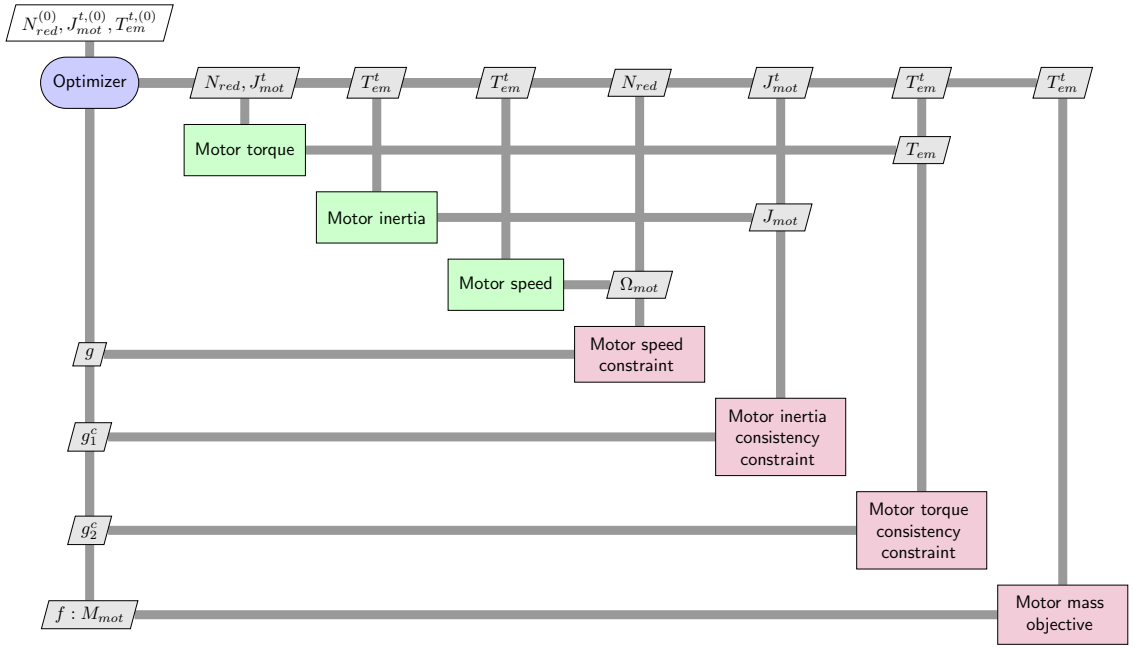

Fig. 3.5 XDSM diagram for IDF formulation of the EMA design problem

3.2.4 The Hybrid Formulation

Balling and Sobieski proposed a hybrid formulation to handle coupled variables consistency [15]. This architecture is similar to IDF except that, as illustrated in Figure 3.6, the feedforward consistency relationship is achieved by computing analysis functions in a sequence, and the feedback consistency relationship remains achieved by an auxiliary equality constraint and an additional design variable J_{mot}^{t}. This approach has the same advantages and drawbacks as the IDF approach but it enables to remove for the case study one equality constraint and one design variable.

3.2.5 The Normalized Variable Hybrid (NVH) Formulation

The success of attempts to use numerical optimization for design depends strongly on how well the design problem has been formulated. Reysset and Budinger [195] propose to reformulate a

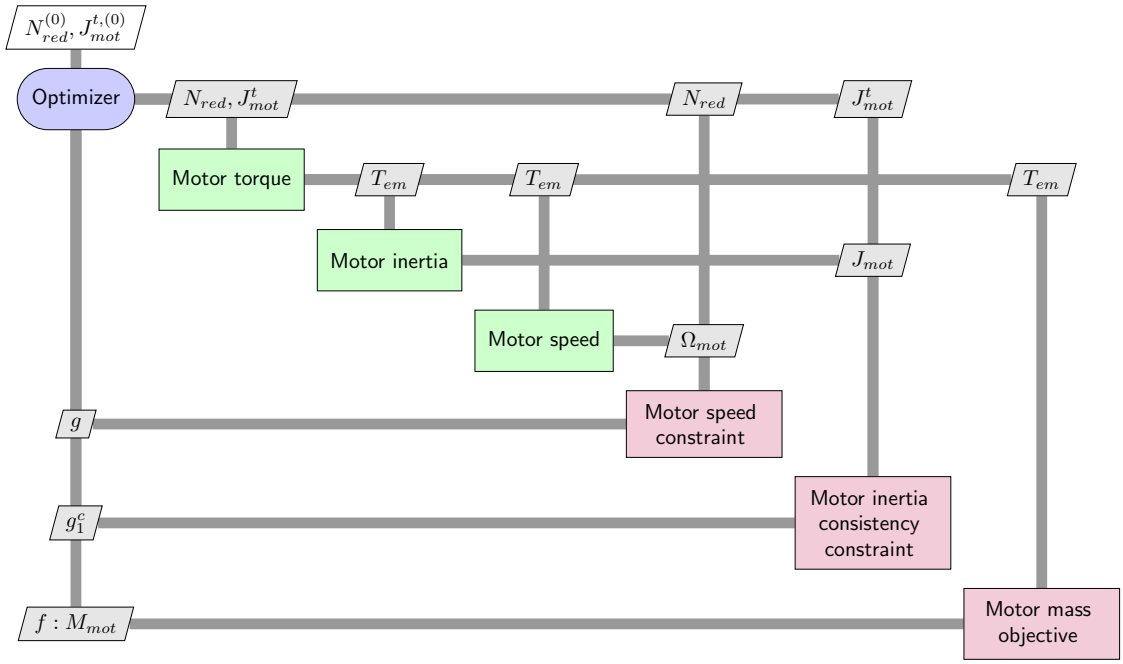

Fig. 3.6 XDSM diagram for Hybrid formulation of the EMA design problem

multidisciplinary design problem with a view in order to get the best from numerical optimization. This formulation was underlined through a case study but was never benchmarked and compared to other formulations. The NVH formulation, represented in Figure 3.7, similarly proposes a Hybrid approach to consider feed-forward consistency relationship by computing analysis functions in a set sequence. In addition, the feedback consistency relationship is achieved by introducing a normalized design variable and a single inequality constraint. Removing the equality constraint reduces the risk of numerical solutions difficulties. Furthermore, the reduction of the new design variable dimension ([1.0-10.0] for most design problems) improves the numerical solution accuracy and the ability to achieve convergence. The difficulty is that this approach requires a reformulation effort. The process is described in Section 3.4.4. Discipline Equation (3.1) is reformulated as in Equation (3.7), where the normalized design variable is introduced in order to (in this case) oversize the chosen electromagnetic torque. Furthermore, the additional consistency inequality Equation (3.8) is added to the design problem to verify (in this case) that the chosen electromagnetic torque is sufficient to face the inertial acceleration and the equivalent EMA external load.

$$T_{em} = k_{os} \cdot F_{ema} \cdot \frac{p}{N_{red}} \tag{3.7}$$

$$T_{em} \geq J_{mot} \cdot A_{max} \frac{N_{red}}{p} + F_{ema} \frac{p}{N_{red}} \tag{3.8}$$

The optimization problem becomes:

$$\begin{aligned} &\text{minimize} && M_{mot} \\ &\text{with respect to} && N_{red}, k_{os} \\ &\text{subject to} && V_{max} \cdot \frac{N_{red}}{p} - \Omega_{mot} \leq 0 \\ & && J_{mot} \cdot A_{max} \frac{N_{red}}{p} + F_{ema} \frac{p}{N_{red}} - T_{em} \leq 0 \end{aligned} \tag{3.9}$$

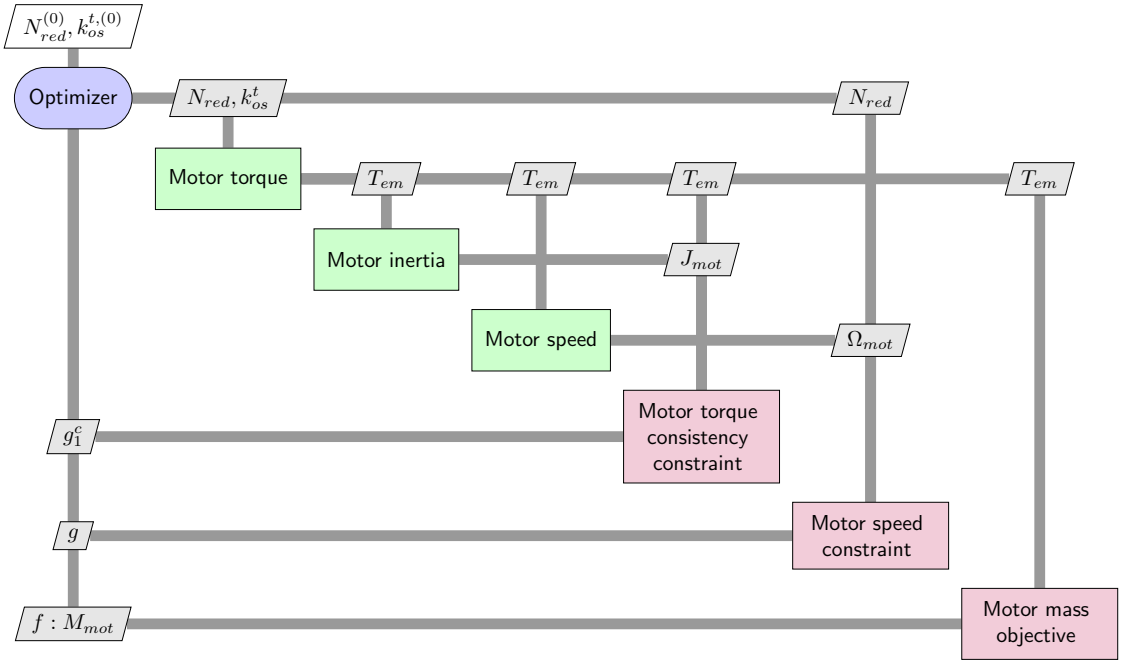

Fig. 3.7 XDSM diagram for NVH formulation of the EMA design problem

Table 3.2 summarizes the different formulations characteristics.

Table 3.2 Formulations characteristics for the EMA design problem.

Formulation	Solver type	Number of design variables	Number of equality constraints	Number of inequality constraints
MDF	Solver	1	0	1
IDF	Optimizer	3	2	1
Hybrid	Optimizer	2	1	1
NVH	Optimizer	2	0	2

The NVH formulation does not use any equality constraint and only one inequality constraint. It uses one consistency design variables that has a smaller dimension (in terms of bounds width) when

compared to IDF or Hybrid approaches. The following section presents some benchmarking results that assess performances of each formulation.

3.3 Formulations Benchmarking

3.3.1 Optimization Test Results

A Sequential Least Squares Programming (SLSQP) [131] gradient based optimizer is used, and analytic derivatives (symbolic differentiation) are provided for each disciplines and functions. The tolerance was set to 10^{-8}. The bounds of the additional design variables that enable coupling consistency are the same for the IDF and Hybrid formulations . The bounds of the global design variables are the same for all formulations. The initial values of variables are the same for each formulation.

As underlined by Gray al. [90], there are multiple ways to measure the effectiveness of MSDO formulations. In order to standardize the evaluation of these formulations, it is chosen to use the same MDAO platform, openMDAO, using the criteria suggested by Gray al. [90] :

1. Proximity to known solution
2. Total function evaluations
3. Convergence characteristics

Proximity to Known Solution

The values given in Table 3.3 show the absolute difference between the known optimum and the optimization results for each formulation. MDF, IDF and NVH converge to the known optimum within the 10^{-8} tolerance. However, the Hybrid formulation fails to be as effective as the other formulation because of its lack of degrees of freedom to satisfy the equality constraint due to the suppression of one additional variable.

Table 3.3 Absolute error from known optimum for all formulations solving the EMA design problem.

	Objective
Optimum	7.60547035
	Δ Objective
MDF	0.00000000
IDF	0.00000000
Hybrid	0.00048962
NVH	0.00000000

Total Function Evaluations

The data given in Table 3.4 shows that the NVH formulation needs the fewest function evaluations to convergence, followed by IDF, Hybrid and MDF. The MDF formulation is greatly penalized by the system analyzer function evaluations.

Table 3.4 Number of function evaluations and derivative evaluations for all formulations solving the EMA design problem.

	Number of function evaluations	Number of derivative evaluations
MDF	97	5
IDF	22	11
Hybrid	28	8
NVH	5	5

The number of function and derivative evaluations gives an indication about the computational cost of each formulation. By removing an additional design variable and an additional equality constraint the Hybrid approach seems to be more effective than the IDF approach. However, the results show that not only this formulation is more costly in terms of function evaluation, it also fails to converge to the known optimum. Besides, the fact to transform an equality constraint into to an inequality and to reduce the dimension of the additional design variable is very efficient as shows the NVH results.

Convergence Characteristics

Convergence characteristics are given in Figure 3.8. The MDF and NVH formulations enable the optimizer to converge rapidly. IDF is penalized by the dimension of the couplings variables especially the motor inertia which is typically between $1.0 \cdot 10^{-4}$ and $1.0 \cdot 10^{-6}$ $kg.m^2$ for the power required in this application depending if the motor is high torque or high speed. The same effect of motor inertia dimension can be noticed for the Hybrid formulation.

It is important to underline that the choice of the feedforward discipline in the Hybrid formulation influences the effectiveness of the optimization especially when the dimension of the coupling variables are different.

3.3.2 Design of Experiments (DOE) Test Results

A Latin Hypercube Sampling (LHS) Design of Experiments is accomplished for F_{ema}, A_{max}, p and N_{red}. The design space is defined by +/- 10% the previous design input values, with the number of samples set to 50. For MDF the consistency is achieved using the same system analyzer as previously, and for IDF, Hybrid and NVH approaches the consistency is achieved by the optimizer using the same

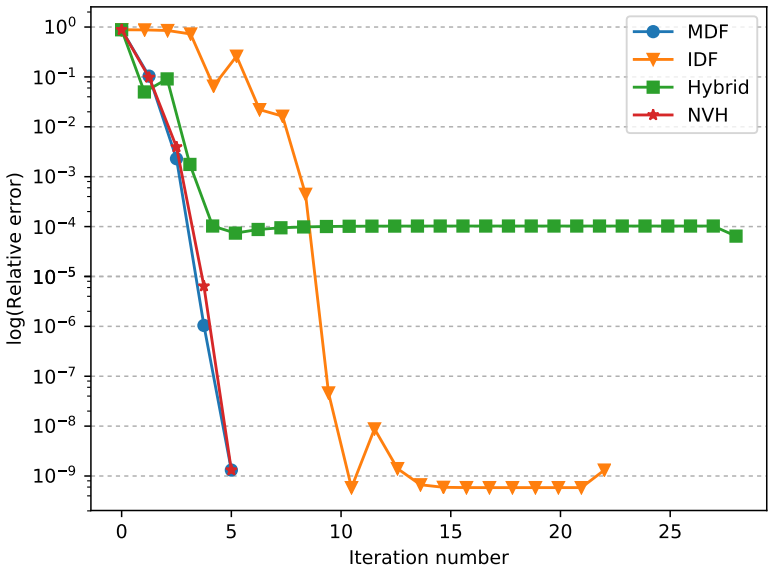

Fig. 3.8 Relative error vs iteration number for all formulations running the EMA design

configuration as the optimization test. These formulations require us to define an objective for the optimizer to solve the consistencies, which is not the primary purpose of design exploration. Defining the wrong objective can lead to inconsistent designs during the exploration, particularly for the NVH architecture.

The suboptimization problem using the NVH formulation is:

$$\begin{aligned} &\text{minimize} && M_{mot} \\ &\text{with respect to} && k_{os} \\ &\text{subject to} && J_{mot} \cdot A_{max} \frac{N_{red}}{p} + F_{ema} \frac{p}{N_{red}} - T_{em} \leq 0 \end{aligned} \tag{3.10}$$

The Design of Experiments is run on top of this suboptimization problem as shown in Figure 3.9.

Success of Solving the Consistency of Coupling Variables

This part evaluates the success of solving the consistency of the coupling variables for each formulation. Where as IDF and NVH succeed in solving the system coupling for each sample, MDF fails due to numerical difficulties. The system analyzer for some samples tries to converge the couplings by using negative electromagnetic torque which make Equation 3.2 singular. Therefore, Equation 3.2 has to be reformulated into Equation 3.11 by introducing the absolute function to make sure that the electromagnetic torque remains positive.

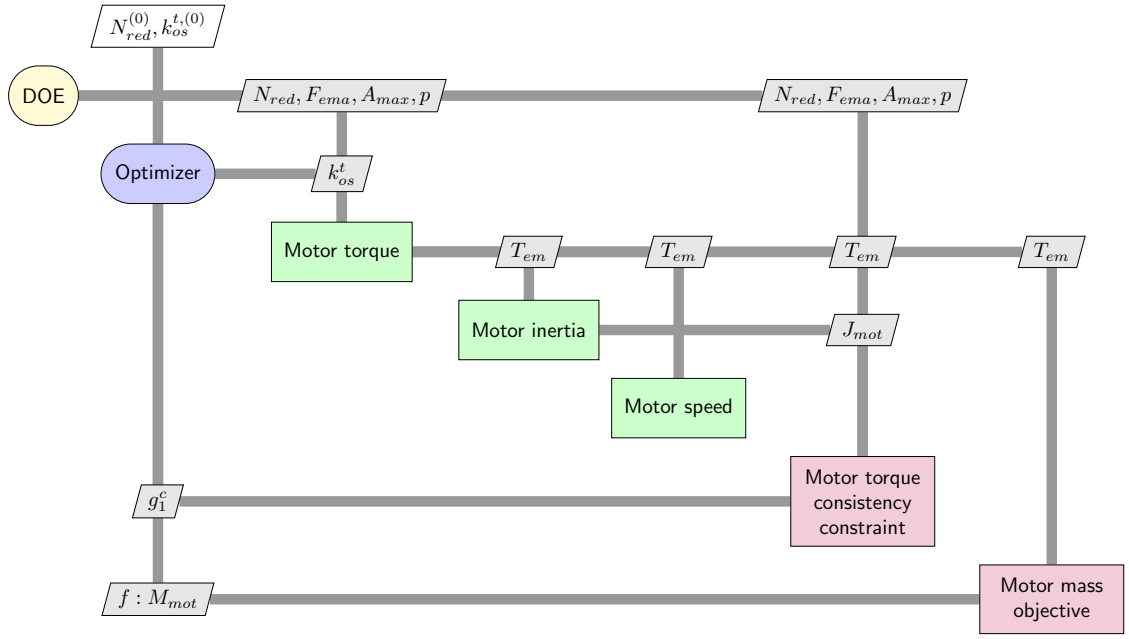

Fig. 3.9 XDSM diagram for NVH formulation of the EMA design exploration problem

$$J_{mot} = J_{mot_{ref}} \cdot \left(\frac{| T_{em} |}{T_{em_{ref}}} \right)^{\frac{5}{3.5}} \tag{3.11}$$

After this manipulation the system analysis is successful for each sample. If a Krylov linear solver is used instead of the Direct solver some samples are not consistent as shown in Table 3.5. The Hybrid formulation optimization convergences to a solution but the coupling variables are inconsistent with regard to the fixed tolerance for some 65 % of the samples. This is due to the lack of degrees of freedom when compared to IDF approach.

Table 3.5 Percentage of success in solving coupling variables consistency for all the formulations exploring the EMA design space.

	% of success
MDF (Krylov)	15 %
MDF (Direct Solver)	100 %
IDF	100 %
Hybrid	65 %
NVH	100 %

MDF is very effective once analysis functions are defined properly and good choices of solvers are made. The other formulations might be more costly but do not require any tuning or manipulation of the models for DOE purposes.

Total Function Evaluations

Table 3.6 shows that the most costly formulation is the IDF regarding mean and maximum number of function evaluations. MDF is the formulation that achieves the fewest derivative evaluations. The NVH formulation is the less costly in terms of mean and maximum number of functions.

Table 3.6 Mean, max., min. number of function evaluations and derivative evaluations for all formulations exploring the EMA design space.

	[mean - max. - min.] Number of function evaluations	[mean - max. - min.] Number of derivative evaluations
MDF	[9.8 - 20 - 6]	[3.45 - 9 - 2]
IDF	[30.95 - 141 - 4]	[9 - 41 - 4]
Hybrid	[11.15 - 28 - 4]	[4.23 - 5 - 3]
NVH	[5.25 - 14 - 3]	[4.05 - 5 - 3]

3.3.3 Robustness to Scale Changes

The system design is achieved for a set of requirements. Many products are used for different scales and therefore different values in requirements. For instance, a same family of actuators can contain actuators that move load on a relative scale from $1\times$ to $5\times$. A sizing code should be able to deliver the optimal sizing at any of the loads on the scale. Therefore, we run the same DOE test as previously but for an EMA load three times greater. The success percentage of each MSDO formulation is given in Table 3.7.

Table 3.7 The success percentage in solving coupling variable consistency for all the formulations at a new load requirement.

	% of success
MDF (Direct Solver)	15 %
IDF	60 %
Hybrid	45 %
NVH	100 %

Increasing the load requirement increased the stiffness of the coupling. This leads to a decrease of successful designs for all the formulations except the NVH formulation. The bounds of consistency variables for IDF and Hybrid were adapted to the new scale. The tolerance of MDF solvers were increased but led to the same results. The NVH formulation by introducing the normalized variable and the way it is used is more robust to scale changes. This is an important evaluation criterion as in actuation system design load requirements vary with the load type or the aircraft size. For reusability

and robustness to scale changes of the sizing code the NVH formulation is an interesting choice but requires important manipulation of analysis functions, design variables and constraints within the sizing problem. Furthermore, it is an intrusive approach as it requires the modification of the disciplinary models. Hence, it is not applicable to problems where models are not available such as Black-box optimization.

3.3.4 Outcome and Needs for Automated MSDO Formulation

The formulation of MSDO problems can get tricky as the number of variables, analysis functions and constraints increase. As seen previously, the implementation of a multidisciplinary strategy is not straightforward and requires a manipulation of these design variables, analysis function and constraint. These manipulations lead to high-time consumption for designers when facing new large-scale MSDO problems. Research has proven the limits of human brain when processing a large number of information [167]. Thus, there is a need for assisting designer when formulating MSDO problems which have not yet been investigated. Additionally, singularity problems can appear during the formulation process intrinsic to the design problem or due to designer human errors. Graph methods and symbolic manipulations that enable to detect design problem singularities as well as automating the NVH formulation are presented in the following section of this chapter.

3.4 Graph-Based Methods to Assist MSDO Problem Formulation

3.4.1 Previous Work

Gathering knowledge to build a sizing code through the association of algebraic functions can results in solvability problems and non-efficient multidisciplinary analysis or optimization. The decomposition and coordination of the design problem is a complex task even for monolithic architectures. Friedman was one of the first to propose a constraint theory in engineering design [77]. Elmqvist and Otter introduced the principle of tearing methods for systems of differential and algebraic equations [68]. Bunus proposed several graph-based algorithms to debug equation-based modelling languages [33]. Reysset gave a methodology to formulate design problems composed of algebraic analysis functions [195]. Allison proposed a technique for optimal partitioning and coordination for distributed optimization problems [7]. Changes in requirements or integration environment as well as the mechatronic product power architecture lead to various design problem formulations. Formulations are, in many cases, not straightforward as the disciplines, design variables and design constraints are numerous in large scale design problems. Debugging the sizing code to remove over-constrained, under-constrained singularities or algebraic loops by adding/removing variables/disciplines or reordering discipline analysis can be complex and time consuming. For these reasons, it is proposed a graph-based approach that assists designers when formulating a MSDO problem. This graph-based approach is implemented in the Python programming language and is build on top of the NetworkX graph library [95] and the

Sympy symbolic computation library [224]. To illustrate the different situations, the EMA design case will be modified.

3.4.2 Definitions

Bipartite Undirected Graph

The high dynamic EMA design problem can be represented by a bipartite graph where on the left (top nodes) we have the analysis function that permit estimation of the unknown variables as well as constraints on the right (bottom nodes), as in Figure 3.10.

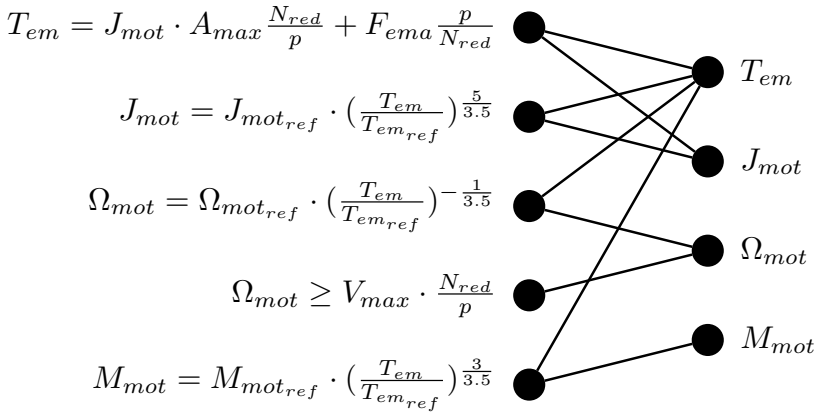

Fig. 3.10 Bipartite undirected graph of the EMA design problem

Bipartite Matching

The perfect matching of a bipartite graph representing a system of analysis functions signifies that the system is structurally well constrained. The most computationally efficient matching algorithm is the Hopcroft and Karp matching algorithm [108] and is the one used here. It is important to underline that the result of a maximal matching is not unique. In this method, design constraints are also part of the bipartite graph but are removed when computing the maximum matching. Figure 3.11 shows one resulting matching of the EMA design problem where matched edges are represented by double lines.

Bipartite Directed Graph

As the number of analysis functions and couplings increase, the detection of solvability issues becomes more intricate. Manually detecting, solving singularities and implementing a strategy for dealing with multidisciplinary couplings can become time consuming. To determine which analysis functions should be associated to which unknown, Algorithm 1 is used.

Applying Step 1 and 2 leads to the graph given in Figure 3.11. Applying Step 3 leads to the graph given in Figure 3.12.

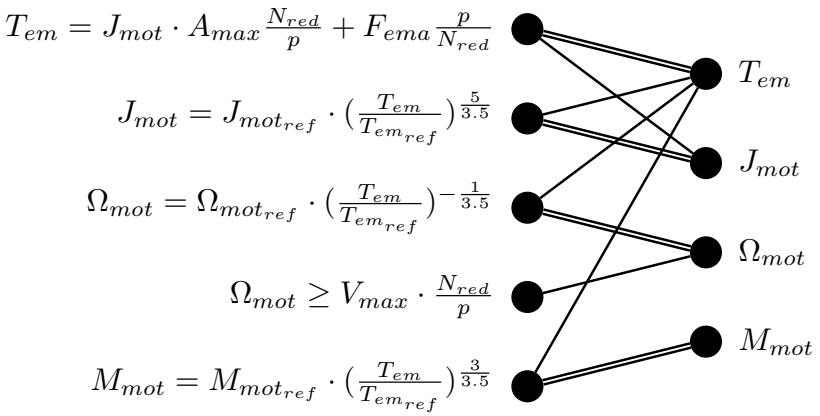

Fig. 3.11 Bipartite matched graph of the EMA design problem

Algorithm 1 Matching and Directing

1: Remove constraint nodes and associated edges for the undirected graph
2: Get matched edges by computing the maximum matching of the new undirected graph
3: Orientate edges of the original undirected graph from analysis functions to unknowns for matched edges
4: Orientate edges of the original undirected graph from unknowns to analysis functions and constraints for unmatched edges

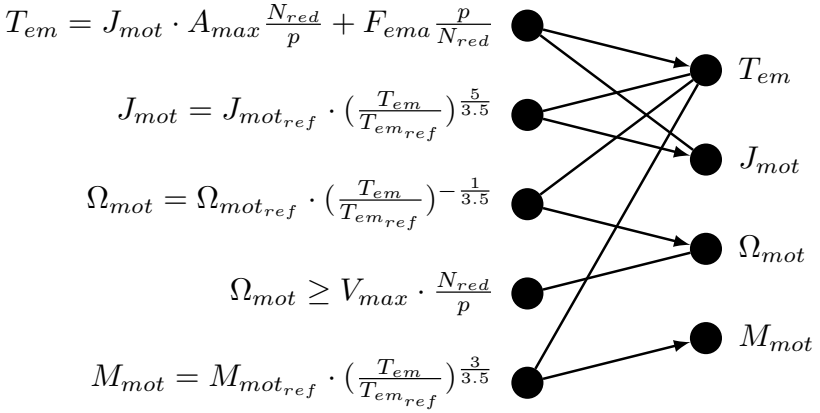

Fig. 3.12 Bipartite graph of the EMA design problem after applying Step 3 of Algorithm 1

Finally applying Step 4 leads to the graph given in Figure 3.13.

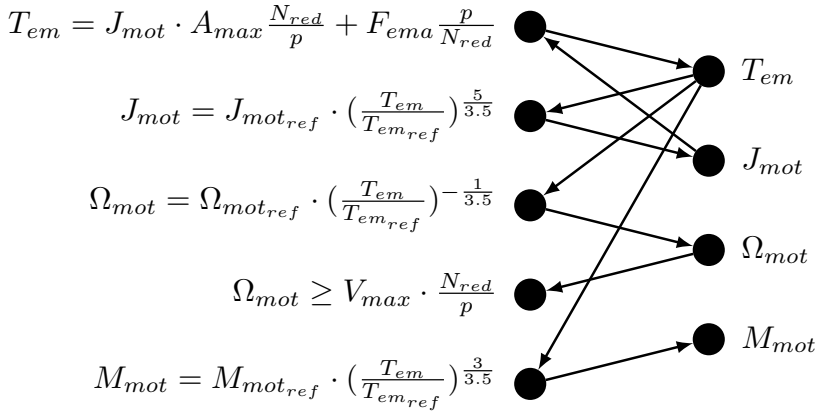

Fig. 3.13 Bipartite graph of the EMA design problem after applying Step 4 of Algorithm 1

Therefore, Figure 3.14 is the result of applying the previous algorithm to the initial undirected graph representing the EMA design problem. The intrinsic cycle of the design problem is highlighted in black, this way the designer can easily visualize which analysis functions and which unknown variables are involved. The detection method of the cycle will be described in Section 3.4.4.

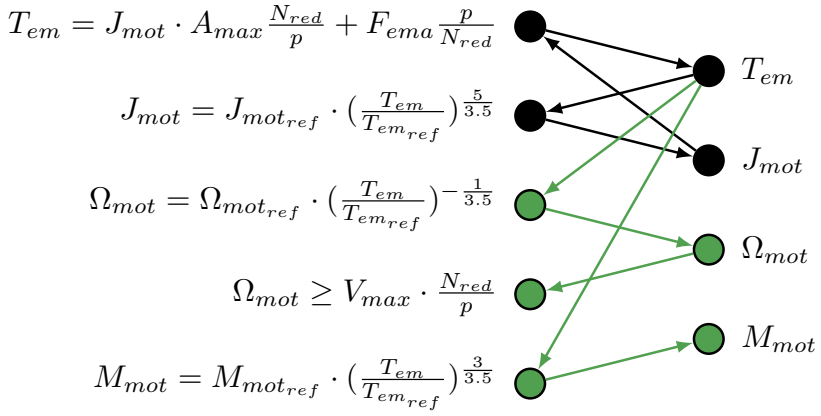

Fig. 3.14 Bipartite directed graph of the EMA design problem with cycle (black)

3.4.3 Over-Constraint and Under-Constraint Singularities

A design problem can be structurally inconsistent. Such problems are in many cases due to a formulation error of the designer. The following steps show how singularities and the subsequent subgraphs are detected.

Algorithm 2 Detection of over-constraint and under-constraint singularities

1: Remove constraint nodes and associated edges for the undirected graph
2: Get matched edges by computing the maximum matching of the new undirected graph
3: Transform matched edges of the original undirected graph into bidirectional edges
4: Orientate edges of the original undirected graph from unknowns to analysis functions and constraints for unmatched edges
5: Find the unmatched analysis function nodes, all the descendants of these nodes are part of the over-constrained subgraph (red nodes and edges)
6: Find the unmatched unknown variable nodes, all the ancestors of these nodes are part of the under-constrained subgraph (blue nodes and edges)

If another analysis functions that is added to compute the motor speed for instance, the design problem becomes over-constrained as shown in Figure 3.15. This can typically be an error of the designer but over-constrained singularities can also be intrinsic to the design problem [195].

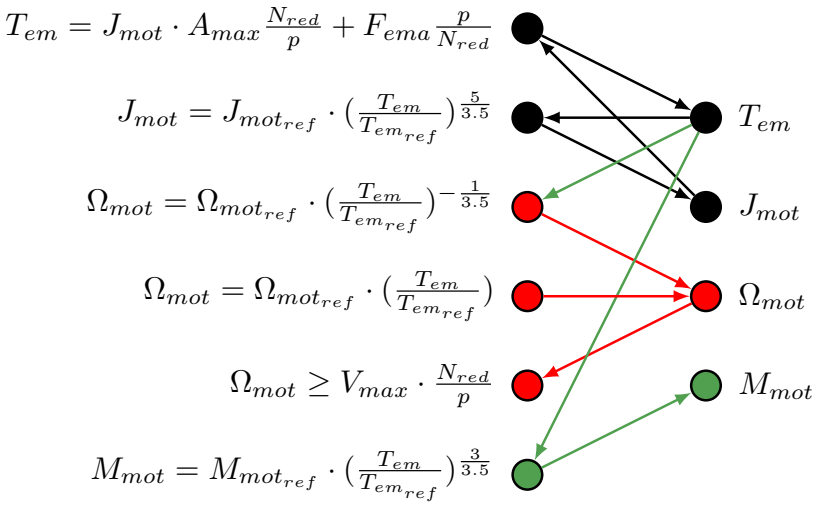

Fig. 3.15 Bipartite directed graph of the EMA design problem with a cycle (black) and an over-constrained (red) subgraph

In a similar manner, if the motor inertia is not estimated by an analysis function, and remains an unknown then the design problem becomes under-constrained as shown in Figure 3.16.

The bipartite graph representation enables to easily notice the singular nodes. In Figure 3.15, the singular node is the motor speed Ω_{mot} and in Figure 3.16 it is the motor inertia J_{mot}.

3.4.4 The Design Loop Problem

Design loops can come from a human error when formulating the design problem. They have in this case to be solved manually by the designer. In the case where the system involves multidisciplinary couplings design loops can appear between analysis functions. They have to be taken care of by the

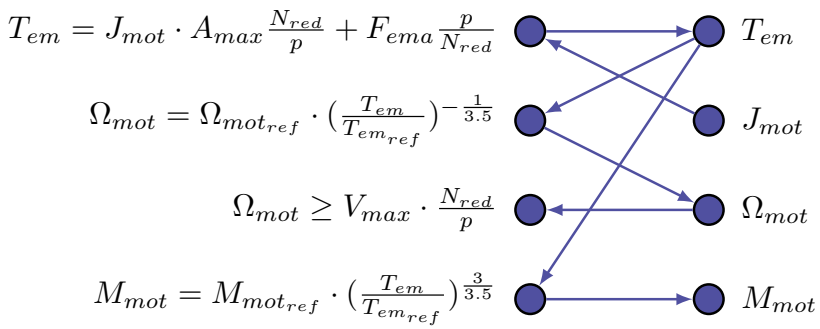

Fig. 3.16 Bipartite directed graph of the EMA design problem with an under-constrained (blue) subgraph

designer to avoid inconsistent designs. The Tarjan algorithm enables us to detect strongly connected components (SCC) in a graph [227]. Therefore, in this case the design cycle can be detected and highlighted as shown in Figure 3.14. In addition, the developed method proposes to the designer to either let him deal with the cycle manually or try to solve the cycle using symbolic resolution or assist the implementation of the NVH formulation introduced in Section 3.2.5. If the symbolic resolution is possible then no additional design variables or constraints have to be added to the design problem which is an useful advantage. For the EMA design case, the Sympy symbolic solver fails to solve [224]. The following algorithm shows the detection and solving of design loops using the NVH formulation.

Algorithm 3 Detection and highlighting of strongly connected components

1: Apply Algorithm 1 to the undirected graph
2: Get strongly connected components using the Tarjan algorithm
3: Highlight in black color the analysis function nodes and unknown variables nodes that are strongly connected components and the edges that connect them

Algorithm 4 Automation of the NVH formulation

1: Choose the unknown variable and analysis function in which the chosen variable will be replaced with the normalized variable
2: Remove the chosen variable and introduce the normalized variable in a copy of the chosen analysis function
3: Reformulate the analysis function if necessary and choose adapted bounds for the normalized variable (default: [1-10])
4: Transform the chosen analysis function into an inequality
5: Replace directed edges by undirected edges
6: Apply Algorithm 1 to the new undirected graph

The removal and replacement steps can vary depending on the design problem. In the case of the electro-mechanical actuator, if the chosen variable is J_{mot} and the chosen analysis function is

$T_{em} = J_{mot} \cdot A_{max} \frac{N_{red}}{p} + F_{ema} \frac{p}{N_{red}}$, then a straightforward reformulation would be to fix J_{mot} to zero, which under-sizes the motor, and multiply what remains of the analysis function by the "over-sizing" normalized variable k_{os} that varies between 1 and 10:

$$\begin{aligned} T_{em} &= k_{os} f\left(J_{mot} = 0, A_{max}, N_{red}, p, F_{ema}\right) \\ J_{mot} &= g\left(J_{mot_{ref}}, T_{em}, T_{em_{ref}}\right) \\ T_{em} &\geq f\left(J_{mot}, A_{max}, N_{red}, p, F_{ema}\right) \end{aligned} \tag{3.12}$$

In the case of an electrical motor design, a coupling appears between the electrical resistance R_{mot} and the temperature Θ_{mot} computation. R_{mot} is used to compute Joule losses which themselves are used for the computation of Θ_{mot}. However, the electrical resistance of the motor R_{mot} is temperature dependant. A strategy would be to fix Θ_{mot} for the maximum temperature acceptable by windings $\Theta_{mot_{max}}$, which over-sizes the motor, and multiply by a "under-sizing" normalized variable k_{us} that varies between 0.1 and 1:

$$\begin{aligned} R_{mot} &= k_{us} h\left(\Theta_{mot} = \Theta_{mot_{max}}, d_{mot}\right) \\ \Theta_{mot} &= u\left(R_{mot}, d_{mot}, T_{em}\right) \\ R_{mot} &\geq h\left(\Theta_{mot}, d_{mot}\right) \end{aligned} \tag{3.13}$$

Figure 3.17 illustrates the resulting graph once Algorithm 3 and Algorithm 4 are applied to the EMA design problem undirected graph.

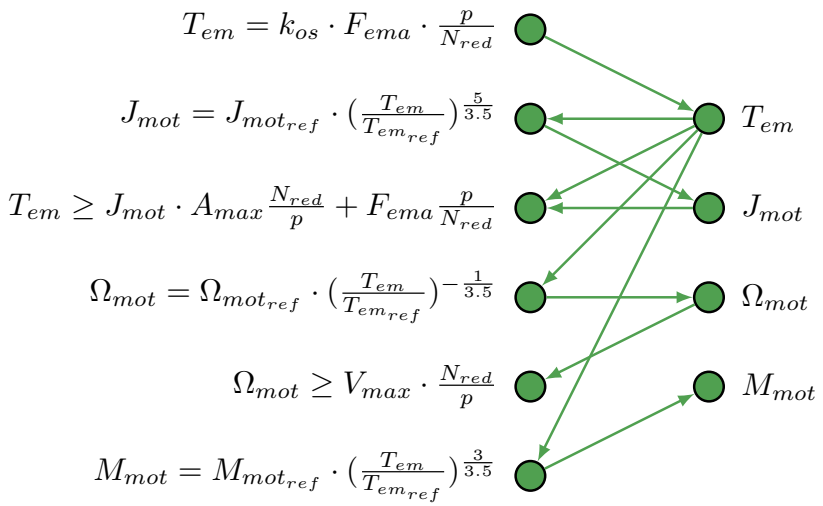

Fig. 3.17 Bipartite directed graph of the EMA design problem with NVH formulation

3.4.5 Matching and Ordering

It is chosen to implement algebraic analysis functions with an explicit form. This means that the analysis function is in a form such that the matched unknown variable can be written explicitly

with respect to the independent variables. As it is proposed in the Modelica programming language [37, 79], the algebraic analysis functions used are acausal and can be expressed with different explicit manners depending on the inputs/outputs configuration that the designer has chosen for the design problem. The matching and ordering is the final step in the problem formulation. It consists of, once singularities have been removed, reorienting analysis function with matched unknowns using symbolic manipulation. Then using a shortest path algorithm with no weighted edges to determine the best computational sequence. The Algorithm 5 illustrates how the matching and ordering methods is implemented in terms of graph theory and symbolic manipulation.

Algorithm 5 Matching and ordering of analysis functions

1: Apply Algorithm 1 to undirected graph
2: Reorient the analysis functions to respect the new directed graph using the symbolic manipulation of Sympy
3: Reorder the equations to respect the new directed graph using the symbolic manipulation of Sympy

3.5 Graph-Based Approach Summary and Implementation

3.5.1 Approach Summary

The proposed approach can be illustrated using a high-level flow chart that correspond to the aggregation of the previously outlined methods as show in Figure 3.18.

The graph-based approach encompasses a system of equations and inequalities that represent a sizing model. It permits the analysis of the model and checks whether it contains singularities or multidisciplinary couplings. If singularities or multidisciplinary couplings are detected, they are then outlined using a bipartite graph and a color code is assigned to distinguish them. Over-constrained and under-constrained singularities have to be handled manually by the designer. However, the utilization of the bipartite graph is a significant help since it underlines which equations and unknowns are involved. Multidisciplinary couplings can be solved manually or using a symbolic solver. A third option is to implement the NVH formulation by introducing an additional consistency design variable and inequality constraint as well as reformulating the model. Once these singularities and design loops are handled, other algorithms and symbolic computation orientate the equation in an explicit form and order them to provide a computational sequence that can be realized in any suitable numerical computation environment.

The advantages of this approach are an easier reuse of analysis functions and a lightened computational cost of global analysis. Furthermore, it enables a faster formulation of a sizing model for designer especially when a large number of analysis functions are involved. The proposed graph approach to condition MSDO problems has also been tested for large scale design problems that are presented in the remaining chapters. The approach can be extended to design problems where analysis functions have fixed causalities and cannot be re-oriented for specific design needs.

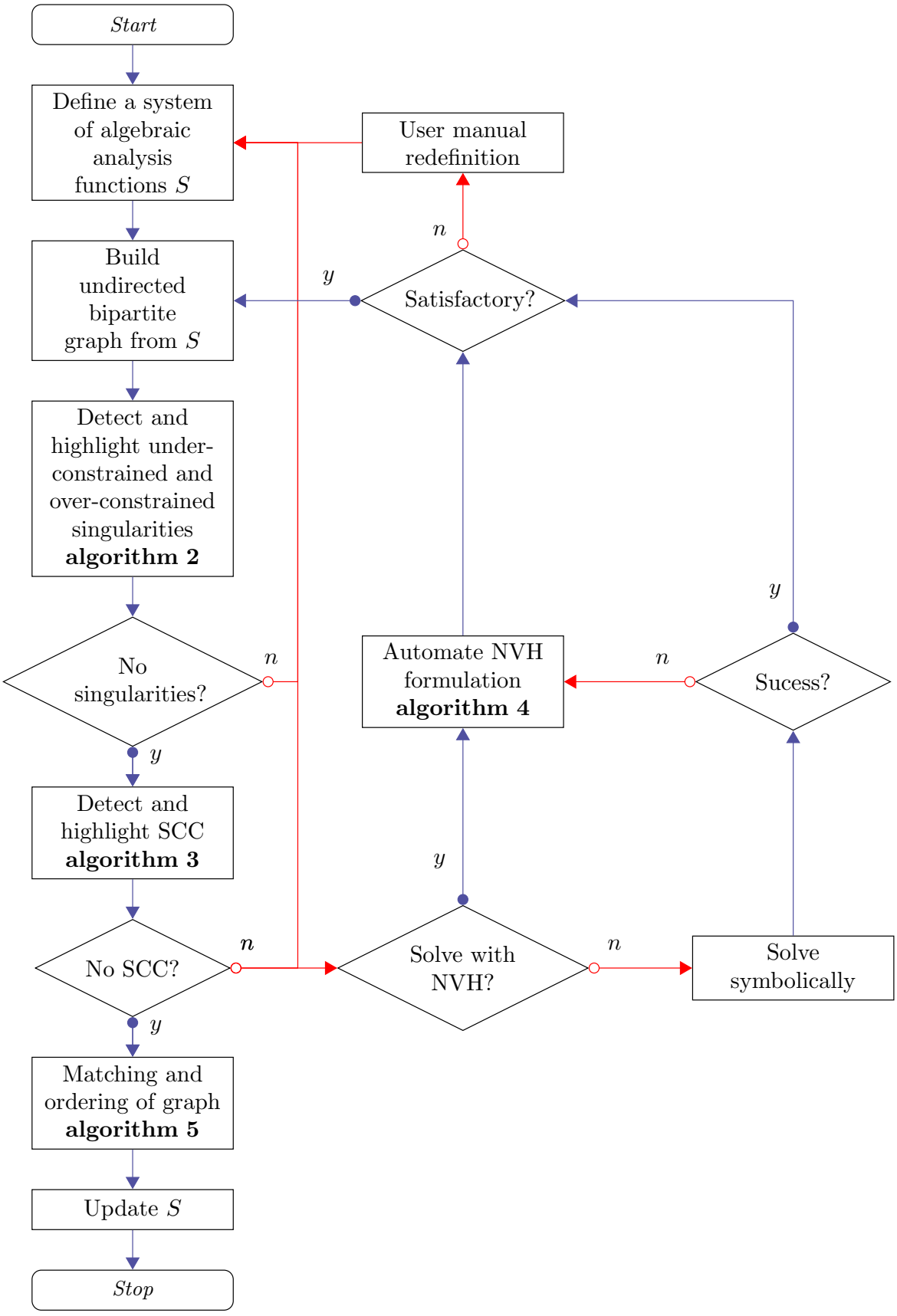

Fig. 3.18 A High-Level flow chart representing the global approach

3.5.2 Implementation

The presented graph-based approach has been implemented in a sizing framework that will be outlined in the next chapter. This implementation has been achieved to enable the usage of such features in an industrial context.

The framework enables the user to enter equations and inequalities and detect automatically the parameters involved in this system. In order to specify his design needs in terms of input and output variables, the user must choose among five types of parameters. These types will be described in more details in the next chapter. To understand how the graph-based approach is implemented the only information necessary is that *Input*, *Fixed* and *Consistency* parameter types means that they are inputs of the model. Conversely, *Guess* and *Output* parameter types means that they are outputs of the model and have to be computed using equations and inputs.

To illustrate the implementation, the previous of high dynamic EMA is used. Table 3.8 presents the parameters and their type for the original model of the EMA.

Table 3.8 High Dynamic EMA model implementation parameters

Parameter	Type	Description
A_{max}	*Fixed*	Maximum acceleration at actuator level
F_{ema}	*Fixed*	Maximum force at actuator level
J_{mot}	*Guess*	Motor inertia
$J_{mot_{ref}}$	*Fixed*	Reference motor inertia
M_{mot}	*Output*	Motor mass
$M_{mot_{ref}}$	*Fixed*	Reference motor mass
N_{red}	*Input*	Reduction ratio
p	*Fixed*	Screw pitch
T_{em}	*Guess*	Motor electromagnetic torque
$T_{em_{ref}}$	*Fixed*	Reference motor electromagnetic torque
V_{max}	*Fixed*	Maximum speed at actuator level
Ω_{mot}	*Guess*	Motor maximum speed
$\Omega_{mot_{ref}}$	*Fixed*	Reference motor maximum speed

This table can be implemented in the sizing framework as shown in Figure 3.19.

Now that the model is implemented, the user can run the process previously described. The results are summarized in Figure 3.18. This leads to a bipartite graph that represents the equations and the unknowns that have been user specified as illustrated in Figure 3.20.

The multidisciplinary coupling is outlined in black edges and a pop-up window asks the user to choose an option to handle this design loop. To outline the detection of over-constraint singularity, the motor inertia is changed from *Guess* to *Fixed*. This leads an over-constrained subgraph that is highlighted in red color as well as the equations involved. See Figure 3.21.

Similarly, an over-constraint singularity is introduced by removing the equation that computes the motor inertia which leads to the visualization shown in Figure 3.22.

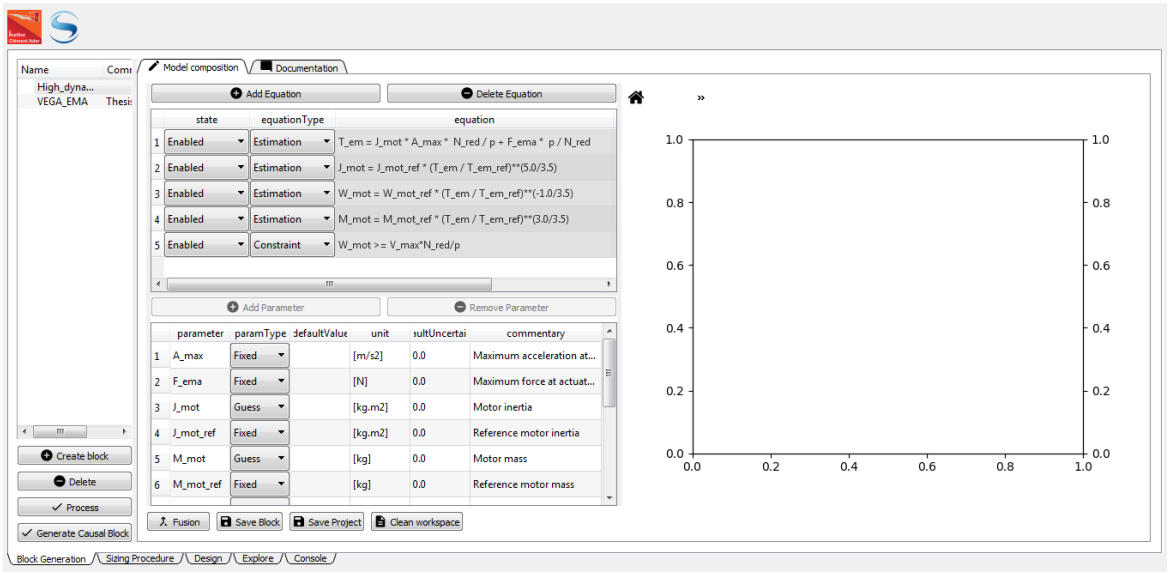

Fig. 3.19 Original high dynamic EMA model implementation

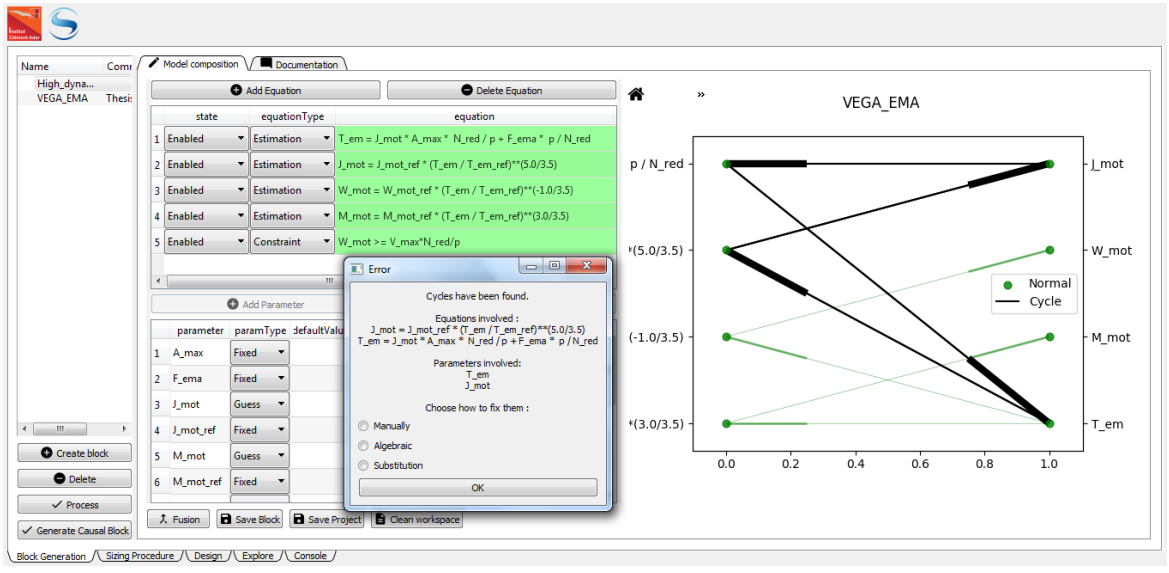

Fig. 3.20 Original high dynamic EMA model implementation with bipartite graph

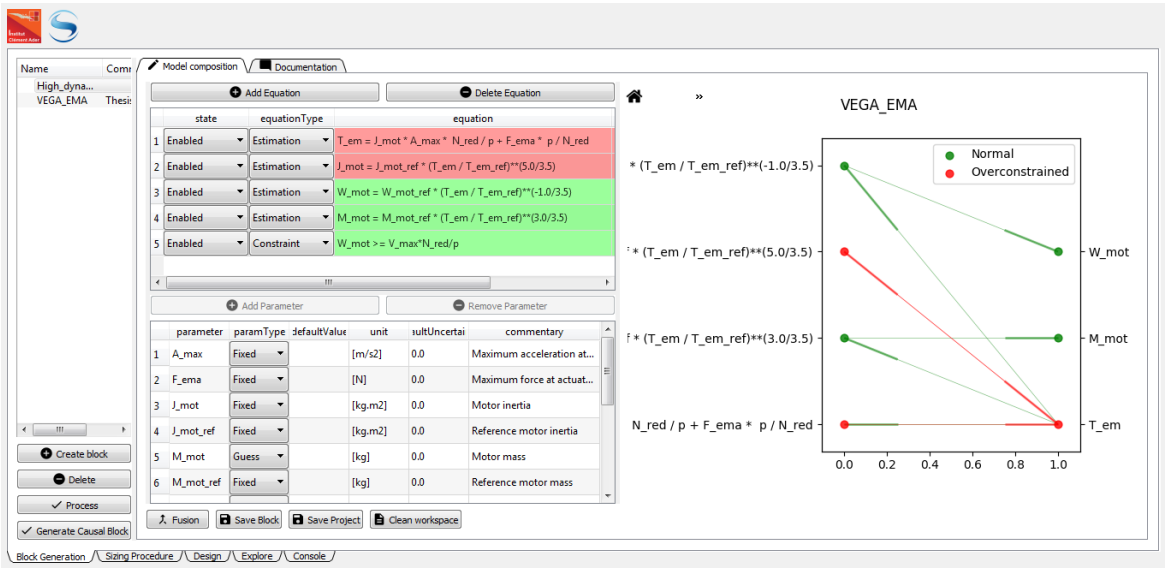

Fig. 3.21 Introduction of a over-constraint singularity in the high dynamic EMA model implementation

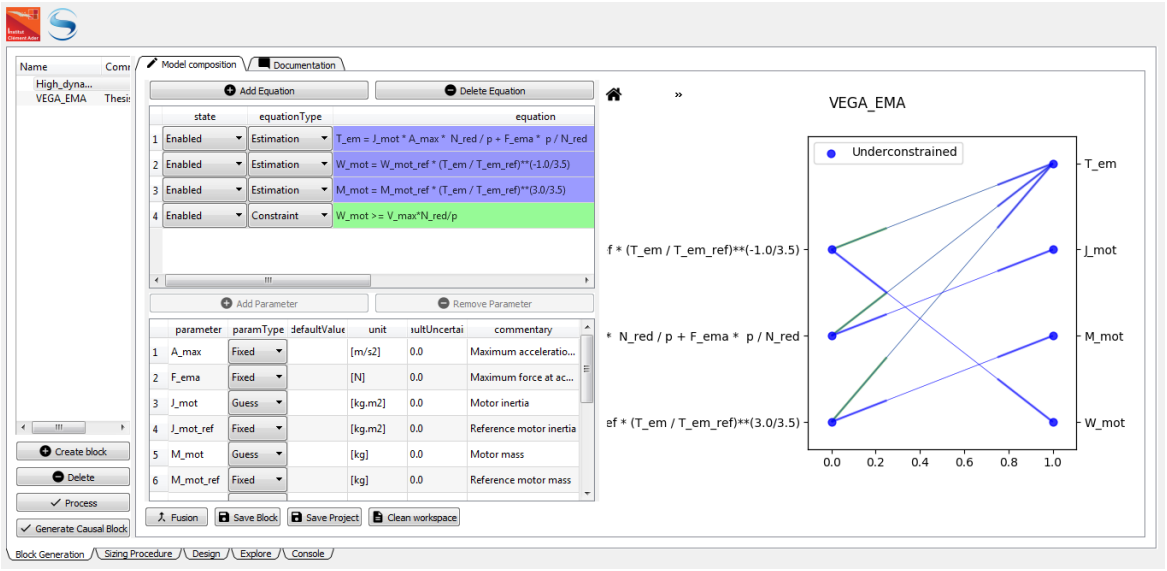

Fig. 3.22 Introduction of a under-constraint singularity in the high dynamic EMA model implementation

Finally, if the NVH formulation is chosen by the user to solve the multidisciplinary coupling this leads to a solvable system highlighted by only green nodes and edges as shown in Figure 3.23.

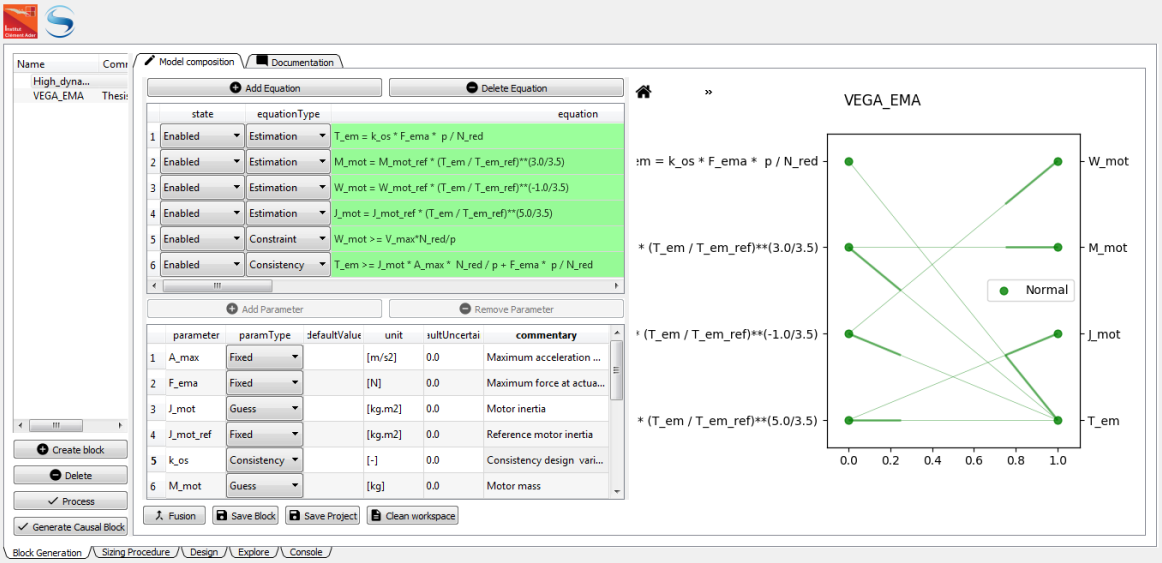

Fig. 3.23 Post-process high dynamic EMA model implementation

A consistency variable k_{os} and a consistency inequality constraint $T_{em} \geq J_{mot} \cdot A_{max} \frac{N_{red}}{p} + F_{ema} \frac{p}{N_{red}}$ have been added to the system. The details of parameter types configuration after the implementation of the NVH formulation are outlined in Table 3.9.

Table 3.9 Post-process high dynamic EMA model implementation parameters

Parameter	Type	Description
A_{max}	*Fixed*	Maximum acceleration at actuator level
F_{ema}	*Fixed*	Maximum force at actuator level
J_{mot}	*Guess*	Motor inertia
$J_{mot_{ref}}$	*Fixed*	Reference motor inertia
k_{os}	*Consistency*	Consistency variable
M_{mot}	*Output*	Motor mass
$M_{mot_{ref}}$	*Fixed*	Reference motor mass
N_{red}	*Input*	Reduction ratio
p	*Fixed*	Screw pitch
T_{em}	*Guess*	Motor electromagnetic torque
$T_{em_{ref}}$	*Fixed*	Reference motor electromagnetic torque
V_{max}	*Fixed*	Maximum speed at actuator level
Ω_{mot}	*Guess*	Motor maximum speed
$\Omega_{mot_{ref}}$	*Fixed*	Reference motor maximum speed

3.6 Conclusion

This chapter outlined the different common monolithic MDO strategies. Their performances for optimization purposes in terms of absolute error, total function evaluations and convergence are similar to what can be found in the literature. However, for DOE purposes these common formulations show limitations. In addition, their robustness to scale change is not suited for sizing optimization problems where the design inputs can change scale from an application to another (flight control, landing gear, electrical thrust reverser...). Moreover, loads are in most applications proportional to the aircraft size. Hence, in order to reuse a sizing code for different applications or for different aircraft sizes, its robustness to scale change can not be neglected. The proposed NVH formulation benchmark results make it the most suitable strategy for mechatronic products that involve algebraic analysis functions and different design inputs scales. In addition, it enables a better reuse/capitalization of sizing models during architectures trade-off studies.

The work reported in this chapter is a significant advancement in methods for the application of MSDO for embedded mechatronic systems sizing. A new formulation well suited for design problems composed of algebraic analysis functions has been described and benchmarked. Robustness to scale change has been proposed as a new multidisciplinary analysis benchmark criteria. The NVH formulation is a convenient formulation for most of designers as the additional consistency design variables have easily scalable bounds. Furthermore the normalized variable values after running optimizations give an idea of how tight the couplings are and what the main design drivers are. The NVH remains an intrusive approach as the disciplinary models have to be modified. This makes it not suited to Black-box optimization. However, in the case of sizing problems defined by algebraic models it remains an interesting alternatives to other monolythic formulations.

Finally, a theoretic graph approach used for helping designers deal with problem formulation singularities. The key finding is that to industrialize the use of MSDO an effort is needed when composing the different engineering specializations. If not, empirical design methods with large amounts of design iterations will be preferred and optimal solutions will never be reached. Transforming engineering specialization models into algebraic analysis functions is an interesting topic for surrogate modelling activities as analyses increase in sophistication and design data becomes more and more heterogeneous. Additionally, the use of algebraic analysis function enables symbolic computation of analytic derivatives which are very efficient for gradient based optimization. Optimization and exploration time are an important criteria in an industrial context where the main objective is rapid decision making during design activities especially in early bid and proposal phases.

Chapter 4

Knowledge-Based Multidisciplinary Sizing and Optimization of Mechatronic Systems

4.1 Introduction

Successful mechatronic system development requires the consideration of multiple engineering disciplines and assessment of tradeoffs among conflicting objectives in preliminary design phases. The difficulty to achieve this is the lack of detailed design information in these early design phases. A possible remedy for this challenge is knowledge-based engineering. The purpose of this chapter is to propose a knowledge-based methodology applicable to electro-mechanical actuation system and more generally embedded mechatronic systems. A methodology is defined by a process, methods and tools [101]. These elements will be outlined through a case study.

Many methodologies for similar purposes have been developed. Roos proposed a methodology for the multidisciplinary design of control system design and system performances [200]. G2ELab have developed the Cades Framework [55] which enable automatic differentiation of electrical system models for rapid gradient-based optimization. Malmquist outlined the use of frequency solver in rapid design of mechatronic systems with consideration for control [147]. Hammadi proposed a multi-agent approach to achieve optimization through co-simulation of different analysis software [97]. A framework for more complex systems like aircraft have been developed to integrate engineering specializations (domain experts) knowledge during conceptual design [205]. The integration of these knowledges was done using surrogate modelling techniques that provide low computational cost models. Friedl developed a parametric design optimization framework based on analytic model to provide non-experts the possibility to make system level assessment with respect to parameter changes [76]. Reul proposed to use the All-At-Once formulation combined with a interior point algorithm for optimization which also generates sensitivity analysis results to help further decision making [193]. Rahimi provides a framework for preliminary design optimization with features like model library and differential algebraic equations handling [192]. Research in Multidisciplinary Design

Optimization (MDO) is driven by the aircraft design needs where multiple research projects aim to industrialize MDO [83, 42]. These projects are resulting in methods and tools with emphasis placed on collaborative and high-fidelity aspects which are provided by distributed high-fidelity analysis tools and a MDO platform that achieves the coordination and overall optimization [137].

A methodology is a collection of related processes, methods and tools [154, 70] where:

- a process is a logical sequence of tasks performed to achieve a particular objective ("WHATs").
- a method consists of techniques for performing a task ("HOWs").
- a tool is an instrument that, when applied to a particular method, can enhance the efficiency of the task (supports the "HOWs").

The motivation of this chapter is to describe the steps, their associated methods and tools related to the developed design and sizing methodology. The process is decomposed in different successive steps. First, requirements, design drivers and sizing scenarios of the system are defined in order to take into account the needs and constraints of each stakeholder. The elementary computational model must be generated by domain experts to represent the sizing scenarios and the required parameters. Once elementary models are available, they are assembled into reusable component sizing models. Component sizing model are then used to build a system sizing model. Finally, the system sizing model generated can be used jointly with numerical optimization and multidisciplinary analysis to determine design alternatives with optimal performances.

To illustrate these steps and the associated methods and tools, a design case study is achieved using these methods and the framework that has been developed. The design case is a more detailed design of the thrust vector control electro-mechanical actuator introduced in the previous chapter.

The studied actuation system is the electrical thrust vector control system for the VEGA launcher [221] a small european space launcher.

The trajectory control of the launcher first stage is achieved by an actuation system composed of two electro-mechanical actuators, described in Figure 4.1, lithium-ion batteries and a power control unit (PCU) [221].

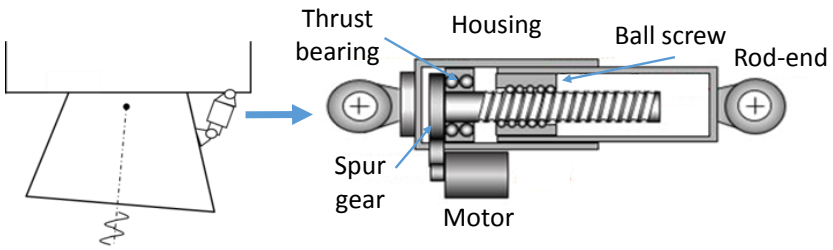

Fig. 4.1 Thrust vector control electro-mechanical actuator integration and architecture

Here, a focus is made on the design of electro-mechanical actuators with higher fidelity and more details than the one studied in Chapter 3.

4.2 Requirements, Design Drivers and Sizing Scenarios Definition

One of the most critical phase of the Generic Product Development Process is the Concept Development phase as important decisions are made [101]. This part outlines what are the important design knowledge that stakeholders must exchange for sizing and design purposes in order to avoid misunderstandings or the discovery of missing information later in the design process. This is why emphasis is placed decomposing knowledge into capitalized and reusable elements that can be reused in later projects.

For this purpose, it is chosen to distinguish three types of knowledge: requirements, design drivers and sizing scenarios. An illustration of their interactions is given in Figure 4.2 in addition to a detailed definition in the following parts of this section.

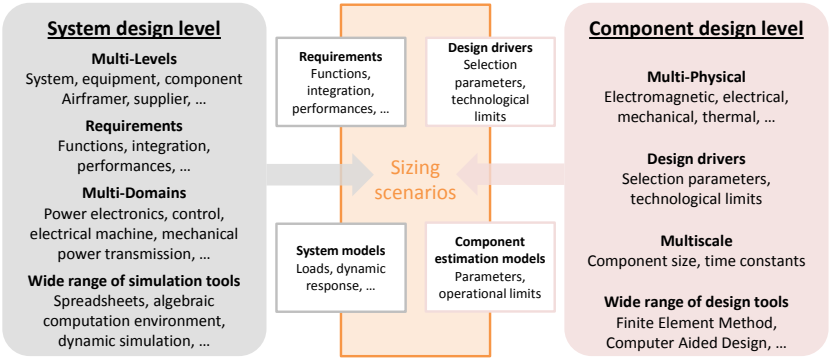

Fig. 4.2 Systemic design approach through requirements and design drivers

4.2.1 Requirements, Functions and Operational Modes

System-Level Design begins with the definition of functional requirements [101]. They outline what functions need to be done to accomplish the objectives of the system as a sub-system or a product. Here, the main function is to control the position of the nozzle subject to aerodynamic loads. Generally performance requirements are also provided to define how well the system needs to perform the functions (maximum acceleration and speed of the nozzle). Design solution definition process is then used to translate high-level requirements, functional requirements and performances requirements into a design solution. In this study, an electrical actuation system is used to control the nozzle position. The first step in this process is to define alternative design solutions by exploring different candidate hardware and software architectures for the mechatronic system. Another alternative could have been an hydraulic actuation system. Then each alternative design solution must be analysed

in order to select the best among them. To analyse and select a design solution, a sizing process is necessary to evaluate the necessary physical characteristics of the equipment and its components (mass, geometric integration, cost...). This can be achieved using numerical methods like system analysis and optimization. Mechatronic systems have several operational (take-off, cruise...) and failure modes (power loss, jamming...). They have to be taken into account during the sizing process to avoid non-compliant designs. Besides, a mechatronic system is defined by a physical or power architecture where various components are interfaced. Therefore, their design must consider the potential interactions and couplings between the components. These coupling can become more complex because components come from several domains such as electronic (power control unit), electrical (electrical motor) and mechanical (ball screw, spur gear, rod ends, housing and thrust bearings) domains and therefore solicit different engineering teams (power electronics, machine design, mechanical design...). Furthermore, the physical laws that govern the components behaviour belong to different physical disciplines like electromagnetics (electromagnetic torque, iron losses...) , electricity (Joule losses), structural mechanics (vibrations) or heat transfer (component temperatures) for instance. In some applications different physics are coupled like between fluid dynamics and structural mechanics (wind turbine blade design) or electromagnetics and heat transfer (electrical machine design). Additionally, time constants and geometric elements of the different physics show a large panel of scales (size: micro-controller chip vs actuator housing or time constant: power electronics switching period vs actuator thermal time constant).

Thus, mechatronic system are complex multi-domain, multi-physical and multiscale systems composed of numerous interdependent components. The sizing process of such system has to be accomplished with a systemic approach in order to partition the sizing problem into lighter, more manageable sizing tasks. Regarding the previous complexities, a solution for implementing a systemic approach is to partition system sizing into two layers of knowledge: a system layer and a component layer. The following sub-parts aim to outline the different knowledge used in each layer and how to coordinate them for generating sizing scenarios.

4.2.2 Component Design Drivers

The knowledge used to size components at a preliminary design stage is generally their main design drivers. Component design drivers define the selection parameters (e.g. reducer reduction ratio, motor diameter) and the technological limits of a given component (e.g. tooth bending stress, winding hot spot temperature). If these design drivers are neglected or non-accurately quantified during the sizing process of the equipment, then risks that problems occur during subsequent design steps are increased such as tooth rupture or motor winding short-circuit. For evaluating selection parameters and technological limits, physical characteristics have to be evaluated. To estimate these needed characteristics, a set of multidisciplinary and multi-scale models is necessary obtain through different modelling techniques. For instance, distributed parameters models are used for local level such as Finite Element Method (FEM) for motor electromagnetic torque and Computational Fluid Dynamics

(CFD) to compute aerodynamic loads on the nozzle. They also enable to characterize complex phenomena such as mechanical contact stress or 3D heat exchanges at local level considering components geometry. In this case study, the main component design drivers considered are motor maximum speed and electromagnetic torque, mechanical components max force and housing resonance stress.

4.2.3 System Design Drivers

System design drivers are generally operational modes (take-off, cruise), performances (bandwidth, maximum static load) and integration criteria (maximum length) that the system must accomplish or respect. These sizing criteria depend strongly on the environment, interfaces with other systems (attachments stiffness) and the interaction between components (heat transfer). They can be evaluated using numerical methods through modelling and simulation. Different types of models are available for representing the knowledge of the system layer like lumped parameters models such as 0-Dimension (0D), 1-Dimension (1D), Ordinary Differential Equation (ODE), Algebraic Differential Equation (ADE) and state machine for instance. For example, the maximum torque that the actuation shall deliver can be computed by simulating and analyzing the mission profile. Effect of component characteristics (motor inertia) on the system dynamic behaviour (maximum torque) and the coupling between components can then be quantified (torque/speed). For instance, it can be necessary to model and simulate the power consumption of electro-mechanical actuators with direct and inverse efficiencies of the mechanical transmission to avoid over-sizing the required torque or penalizing the thermal performances. In this case study, the main system design driver considered is actuator maximum acceleration and speed.

A System Breakdown Structure (Figure 4.3) combined with an influence diagram [60] principle is achieved in order to outline the system architecture and design drivers using the Graphviz library [67].

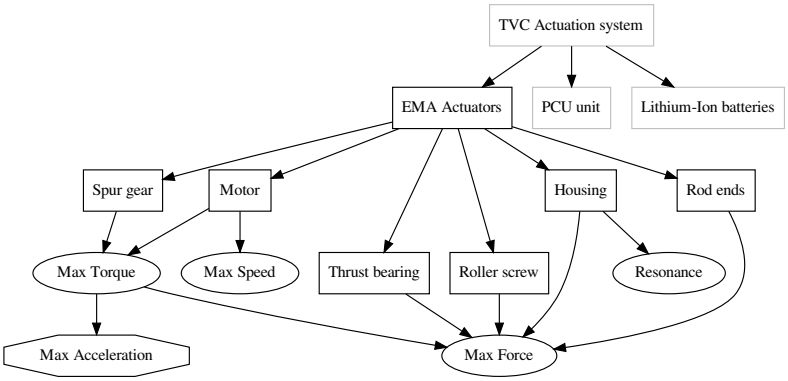

Fig. 4.3 System Breakdown Structure of electro-mechanical actuators with component design drivers (oval), system design drivers (octagone)

4.2.4 Sizing Scenarios

In order to achieve a sizing and design using a systemic approach it is necessary to consider simultaneously component layer and system layer knowledge. It is possible for this purpose to establish what is referred to in this thesis as sizing scenarios. A sizing scenario represents a behaviour of the system that has an impact on one or more of the design drivers. Considering the thrust vector control example, the dynamic displacement of the actuator mission profile has an effect on maximum acceleration, speed and torque that the actuator shall perform. Sizing scenarios have to be modelled in order to evaluate design drivers of the system and its components with respect to parameters. Parameters can be design input variables (reduction ratio...), fixed parameters (security factors...) or computed by estimation models (motor inertia...) and/or other sizing scenarios.

An example of sizing scenario is the winding temperature of a motor which is a technological limit. It can be evaluated considering the motor thermal resistances (component layer) and the current flowing through the winding (system layer). Besides, an example of a system sizing scenario is the stability criteria of an actuator for instance. It can be evaluated considering the different masses and stiffness inside the system (component layer) and how the mechanical power flows through the system (system layer). The system sizing model corresponds to an assembly of all sizing scenario models and the upstream models for parameter computation and is discussed later parts of this chapter.

Figure 4.4 represents a breakdown of the thrust vector control actuation system where sizing scenarios are included. The sizing scenarios considered for this case study are dynamic displacement, maximum static displacement and vibrations.

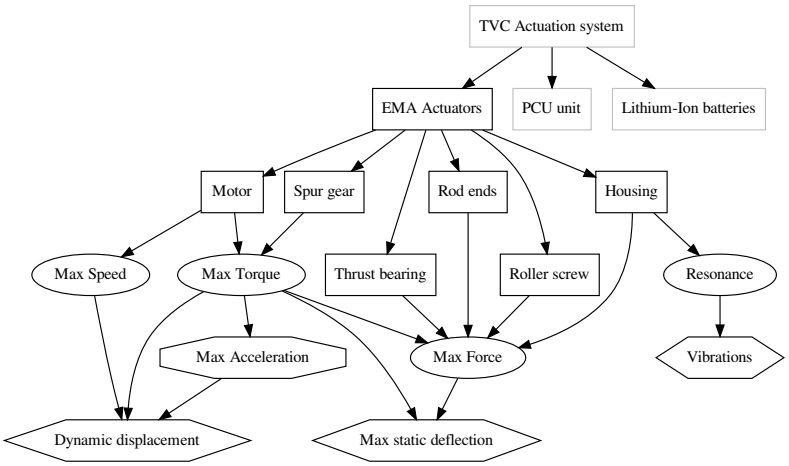

Fig. 4.4 System Breakdown Structure of electro-mechanical actuators with component design drivers (oval), system design drivers (octagone) and sizing scenarios (hexagone)

This representation provides a convenient and synthetic view of system architecture, design drivers and sizing scenarios. This way modelling needs linked to the sizing scenarios can be discussed and organized for the rest of the development process and future developments.

Therefore, this first step enables to outline the design considerations and the associated modelling needs by interactive knowledge and expertise exchanges of stakeholders. The next step is to determine what modelling techniques are relevant to represent this knowledge.

4.3 Elementary Computational Model Generation

As seen in the state of the art of engineering design approaches, mechatronic sizing knowledge is available in different forms, modelled and analyzed using different engineering specialization legacy tools. Additionally, as mentioned in previous parts, emphasis is placed on computational cost to enable rapid decision making during the sizing process.

The challenge of sizing knowledge composition is therefore to enable heterogeneous knowledge to be assembled and computed in an computationally efficient manner. This is why the sizing knowledge is decomposed into a system layer and a component layer that are supported by respective model types and analysis tools as illustrated in figure 4.5.

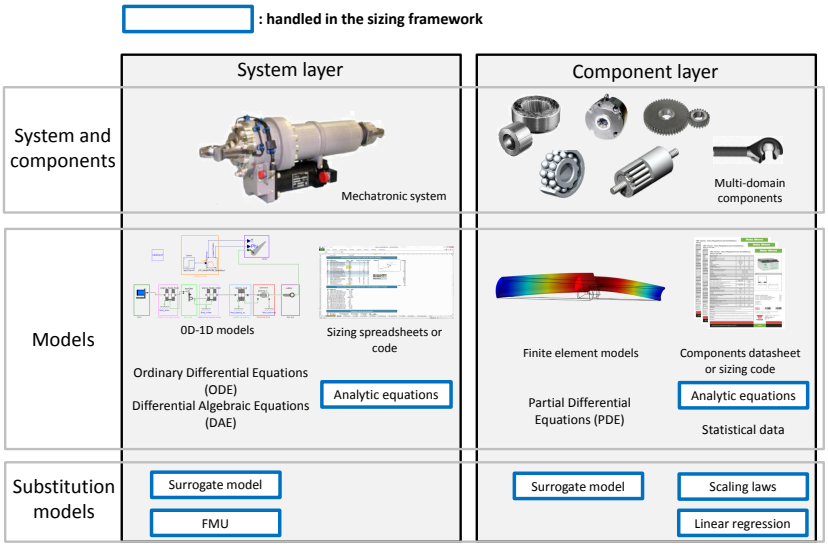

Fig. 4.5 System layer and component layer knowledge and associated models (adapted from [195])

In this methodology, it is chosen to use algebraic modelling to enable rapid analysis and increase reusability. Thanks to surrogate modelling and other substitution techniques, algebraic models can be used to represent both layers. In addition, it enables rapid optimization by having access to symbolic derivatives for gradient-based optimization. We present here different methods for obtaining algebraic sizing models in an engineering design context.

4.3.1 Analytic Analysis Functions

Analytic analysis functions or equations are obtained by derivation of the laws of physics and in some cases generated using experimental results. For the present case study several analytic analysis functions are used. The attachment positions of the actuator are considered as design variables. It is possible to utilize two parameters d_1 and d_2 to define and tune the electro-mechanical actuator positioning as shown in Figure 4.6.

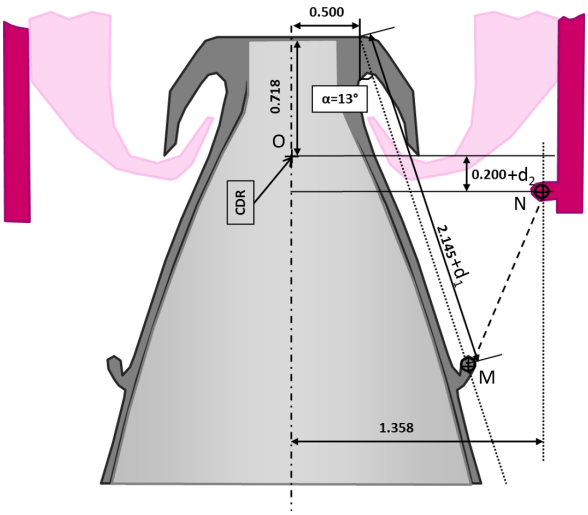

Fig. 4.6 Actuator attachments positioning and parametrization

The first analytic functions compute the equivalent lever arm and the actuator length. The link between the torque T on the nozzle and the force F of the actuator can be computed with the following cross product:

$$\vec{T} = \vec{OM} \times \vec{F} = \vec{OM} \times \frac{\vec{NM}}{\left|\vec{NM}\right|} \cdot F \tag{4.1}$$

Hence, the equivalent lever arm can be computed with the following equation:

$$L_{arm} = \left| \vec{OM} \times \frac{\vec{NM}}{\left|\vec{NM}\right|} \right| \tag{4.2}$$

and the torque is computed with the simple equation:

$$T = L_{arm}.F \tag{4.3}$$

We obtain Equations 4.4 for the actuator length L_{act} and 4.5 for the lever arm L_{arm} using symbolic computation.

$$L_{act} = \left((0.2248 \cdot d_1 - 0.3757)^2 + (-0.9744 \cdot d_1 + d_2 - 1.172)^2 \right)^{0.5} \tag{4.4}$$

$$L_{arm} = ((-(-0.9744d_1 - 1.372) \cdot (0.2248 \cdot d_1 - 0.3757) \cdot ((0.2248 \cdot d_1 - 0.3757)^2 + (-0.9744 \cdot d_1 + d_2 - 1.172)^2)^{-0.5} + (0.2248 \cdot d_1 + 0.9823) \cdot ((0.2248 \cdot d_1 - 0.3757)^2 + (-0.9744 \cdot d_1 + d_2 - 1.172)^2)^{-0.5} \cdot (-0.9744 \cdot d_1 + d_2 - 1.172))^2)^{0.5} \quad (4.5)$$

The actuator stroke S_{act} is computed with respect to the nozzle stroke Θ_{noz} and the lever arm:

$$S_{act} = \Theta_{noz} \cdot L_{arm} \quad (4.6)$$

Similarly, we express maximum actuator speed $V_{max_{act}} = \Omega_{max_{noz}} \cdot L_{arm}$ and max load $F_{max_{act}} = \frac{T_{dyn_{noz}}}{L_{arm}}$ where $\Omega_{max_{noz}}$ is the maximum speed of the nozzle and $T_{dyn_{noz}}$ its dynamic torque.

4.3.2 Algebraic Analysis Functions Based on Reference Components Data

A more empirical approach to obtain algebraic analysis functions is to use data based on existing design. This approach is widely used in gear design to assess design factors (pitting, geometric...) based on existing successful designs [66]. Here, two of these approaches are considered in order to build algebraic analysis functions for component parameters estimation models: scaling laws and data regression of catalogue datasheets.

Industrial catalogues of several mechatronic devices are available online. These are used to select the proper device to be integrated in the system under development. The datasheets available can also be used to build models that predict the component performances (torque, speed...) with respect to integration parameter (diameter, length, mass...) or the other way round (integration parameter w.r.t performances) [27].

The tremendous advantage of both approaches is that they enable to use detailed design knowledge using data from off the shelf components with very simple mathematical expressions.

Figure 4.7 gives some datasheets of Parker's brushless motors [98] which are used for this case study.

	Reference	TorqueStall	TorquePeak	Jmotor	ThermalTime	Diameter	Length	Mass	SpeedNominal	TorqueNominal	PowerNominal
3	NX210EAP	1.0	3.4	0.000038	350.0	0.0565	0.120	1.3	733.038286	0.50	370
4	NX310EAP	2.0	6.6	0.000079	1200.0	0.0710	0.147	2.1	502.654825	1.57	790
6	NX420EAP	4.0	13.4	0.000290	720.0	0.0915	0.175	3.8	492.182849	2.96	1460
10	NX620EAR	8.0	26.7	0.000960	1620.0	0.1210	0.181	7.0	471.238898	5.57	2620
15	NX820EAL	16.0	50.0	0.003200	2040.0	0.1580	0.200	13.0	649.262482	10.35	6720

Fig. 4.7 Parvex Brushless motors parameters (Parker)

The principles of scaling laws were outlined in Chapter 2. Here, we outlined the process to obtain the diameter of the motor with respect to nominal torque. The scaling law establishment supposes that the design of the electrical motor is achieved for constant maximum winding temperature as in [29].

The thermal resistance of an electrical motor R_{th} is a function of its exchange surface S and the convective and radiation heat exchange coefficient h:

$$R_{th} = \frac{1}{hS} \tag{4.7}$$

Hence, for a constant heat exchange coefficient and geometric similarity:

$$R_{th}^{*} = l^{*-2} \tag{4.8}$$

Where l is a dimension of the motor.

The electrical losses at low speeds at mainly the Joule losses in the windings:

$$P_J = RI^2 = \int \rho J^2 dV \tag{4.9}$$

Where R is the equivalent electrical resistance of the motor, I the equivalent current, ρ the volumic mass of the windings total volume V and J the current surface density inside the windings. ρ is assumed constant as the same winding material are used. Hence,

$$P_J^{*} = J^{*2} l^{*3} \tag{4.10}$$

The maximum temperature of windings at continuous torque can then be expressed:

$$\theta^{*} = P_J^{*} R_{th}^{*} = J^{*2} l^{*} \tag{4.11}$$

Since the maximum temperature shall remain the same, $\theta^{*} = 1$. Hence,

$$J^{*} = l^{*-\frac{1}{2}} \tag{4.12}$$

The continuous torque can then be obtained by integrating the Laplace force:

$$T_{nom}^{*} = J^{*} B^{*} l^{*4} \tag{4.13}$$

The magnetic field inside the air gap is constant, thus $B^{*} = 1$. Hence,

$$T_{nom}^{*} = l^{3.5} \tag{4.14}$$

Therefore, the diameter of the motor can be estimated with respect to its continuous torque and a reference motor design:

$$D = D_{ref} \cdot \left(\frac{T_{nom}}{T_{nom_{ref}}} \right)^{\frac{1}{3.5}} \tag{4.15}$$

The second approach based on reference components data is to use a linear regression approach. From the data of Figure 4.7, the log function is performed to pass in log scale to transform a non-linear problem (power law) into a linear problem. A simple linear regression is then performed on the

data (diameter [mm] with respect to nominal torque [N.m]). The result of the linear regression is transposed back ro real scale which leads to Equation 4.16.

$$D = 66T_{nom}^{0.33} \tag{4.16}$$

Figure 4.8 illustrates the result of both approaches for nominal torque inside the construction domain.

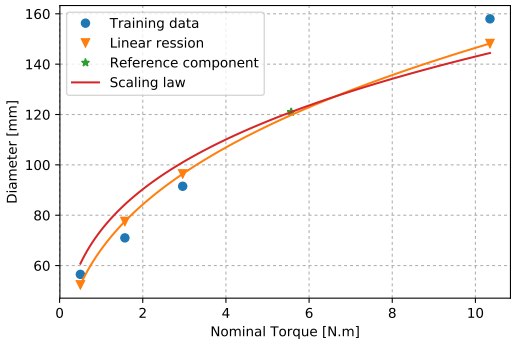

Fig. 4.8 Diameter vs Nominal Torque / Scaling law vs Linear regression

The same process will be achieved in the last chapter but assuming that the motor is sized for constant magnetic saturation because the electrical thrust reverser actuation system is very short and the thermal response is not a dominant criteria. Figure 4.8 outlines that the linear regression is more accurate that the scaling law. Accuracy can be furthermore increased by using more powerful regression methods like kriging [75]. Nevertheless, scaling laws have coefficients based on physical laws and require only one reference component which makes them more generic. However, like in many engineering design situations it is a compromise between accuracy and elaboration time. Scaling laws are more generic where as the linear regression has to be preferably performed for each new component data sets. The scaling law of Equation 4.15 is used for the thrust vector control case study.

In addition, data regression methods require to have "clean" data sets. For example, the datasheets of SKF thrust bearings show a relatively chaotic data set when plotting bearing diameter with respect to static axial load limit as shown in Figure 4.9.

This disparity is due to the fact that some bearings are designed more to handle radial load that axial loads. Performing directly a regression on this data set to obtain an estimation of the bearing diameter with respect to the axial load would be inaccurate. Hence, data filtering is necessary in order to prepare it for regression. Here, it is proposed to keep only the components representative of the problem considered. For this purpose, Pareto filtering is used where only dominant components are kept. A component dominates another if the first is not inferior to the second in all selected objectives. Here the objective is small diameter and high maximum static force. The Pareto filtering leads to a smaller and cleaner dataset given in Figure 4.10.

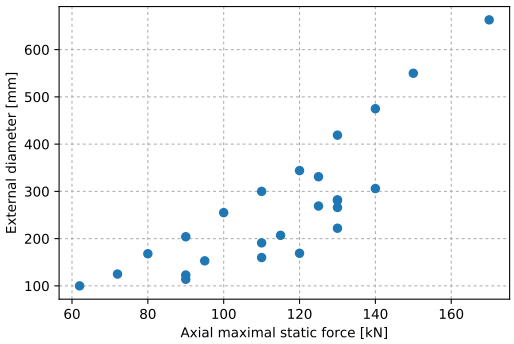

Fig. 4.9 Raw bearing data

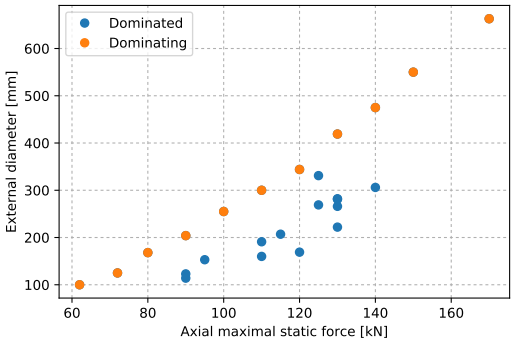

Fig. 4.10 Pareto filtering of bearing data

It is straightforward to see that after this filtering the data set containing the dominating design alternatives is more adapted for building an algebraic model using linear data regression. Therefore, model generation based on catalogue datasheets requires often some manipulation of the data set and thus more work effort.

4.3.3 Algebraic Analysis Functions Based on Finite Element Method Simulations Data

It is possible to determine algebraic analysis functions based on simulations data using surrogate modelling techniques. Here, we outline a surrogate modelling of Finite Element Method simulations methodology developed by Sanchez in his PhD thesis [207]. The methodology is applied here for the mechanical design of the actuator housing.

An actuator housing is subject to two categories of loads: mechanical stresses induced by the power transmission to the load (static) and the stress induced by vibrations (high frequency) [110]:

- Static load sizing generated by:
  - Tensile/compressive/buckling forces that are transmitted through the rod to the nut and the screw, then to the thrust bearing and finally to the housing. The high number of cycles generally requires the fatigue limits of materials to be taken into account
  - Shearing and bending stresses that are due to the masses of components and friction torques in spherical bearings or anchorage points
  - Torsion stresses induced by friction and reaction torques of motor / reducers / nut screw
- Dynamic stress sizing generated by:
  - Transverse vibrations due to the vibratory environment which can generate important mechanical bending stresses
  - Transient rotational, longitudinal and transverse loads (e.g. at end-stops)

The path of the various static or dynamic loads is represented for a generic actuator as shown in Figure 4.11.

In this part, we will focus on developing a model for a vibratory criterion. DO-160 document defines a set of test environments and test procedures for aircraft equipment [191]. Typical vibration tests are between 5 Hz and 2 kHz. The VEGA launcher thrust vector control electro-mechanical actuator has been specified and designed to sustain 22.5 g up to 200 Hz and 10 g between 200 and 2 kHz [84, 237]. Here, it is assumed that the design shall sustain a vibratory perturbation of 20 g from 5 Hz to 2 kHz. Therefore, a surrogate model that estimates the mechanical stress induced by vibrations is performed in order to achieve the preliminary sizing of the housing.

A Finite Element Method (FEM) modal and stress analysis is achieved using the COMSOL Multi-physics software [44]. The vibratory loading problem is analyzed using the following simplified geometry (Figure 4.12):

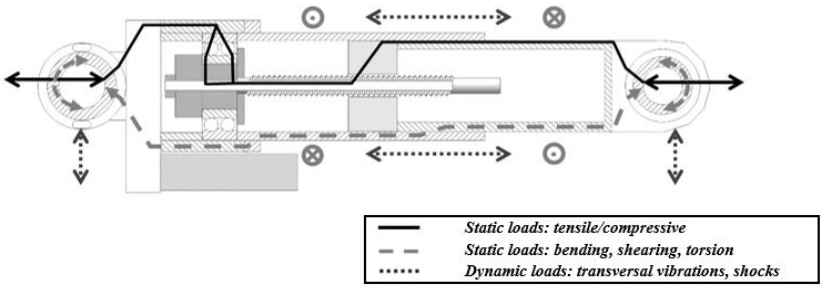

Fig. 4.11 Actuator attachments positioning and parametrization

- Two hollow cylinders for representing the housing
- One full cylinder to represent the ball screw nut

Some modelling assumptions are made:

- The effect of the screw mass at the nut level is neglected
- The mechanical links between different parts of the housing are perfect

The FEM modal and stress analysis is achieved to obtain:

- The resonance frequency f_r or the resonance angular frequency ω_r
- The maximum displacement U_0 of the modal form
- The corresponding maximum stress σ_0 (located on the smallest diameter hollow cylinder)

The maximum stress σ is assumed to be linear with respect to the maximum displacement U:

$$\sigma = k_\sigma \cdot U \tag{4.17}$$

Where $k_\sigma = \frac{\sigma_0}{U_0}$, σ_0 and U_0 are respectively the stress and the displacement for the first bending mode of a given housing design.

The parametrization of the problem is given in Figure 4.12.

The maximum displacement at resonance angular frequency can be approximated by the following relationship:

$$U = \frac{F}{C_{eq}.\omega_r} = \frac{Q_m.k_{acc}.M_{eq}.a}{K_{eq}} = \frac{k_{acc}.Q_m.a}{\omega_r^2} \tag{4.18}$$

Where a is the vibratory sinusoidal acceleration and Q_m the mechanical quality factor (Q factor), M_{eq} the equivalent mass where kinetic energy is stored, C_{eq} and K_{eq} are respectively the equivalent damping and stiffness of the housing.

The equivalent force F of acceleration effect can be evaluated thanks to equivalent work:

$$F \cdot U = \iiint_V u(x,t)a(t)\rho \, dv \tag{4.19}$$

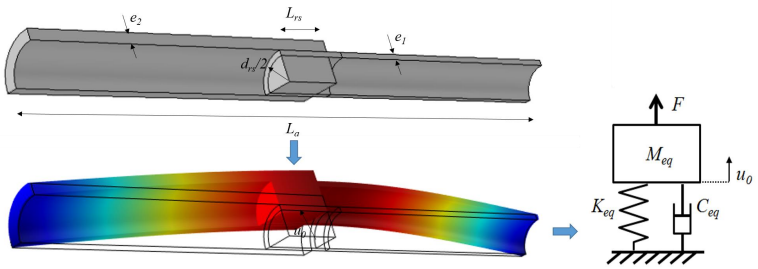

Fig. 4.12 Parametrization of the FEM analysis of the housing

Thus,

$$F(t) = M_{acc}.a(t) \tag{4.20}$$

Where $M_{acc} = \frac{\iiint_V u(x,t)\rho\, dv}{U}$.

The mass subject to the acceleration (M_{acc}) is not that as the one expressing the kinetic energy (M_{eq}):

$$M_{eq} = \frac{\iiint_V u(x,t)^2 a(t)}{U^2} \tag{4.21}$$

In Equation 4.18: $k_{acc} = \frac{M_{acc}}{M_{eq}}$

Now that the modelling problem has been parameterized, a dimensional analysis is achieved. The utilization of Buckingham theorem and dimensional analysis enables to reduce to number of variables that define the physical problem [26].

In the case of the housing design, the link between stress and displacement is function of:

$$\frac{\sigma}{U} = k_\sigma = f\left(E, d_{rs}, L_a, e_1, e_2, L_{rs}\right) \tag{4.22}$$

Where E is the Young modulus of the material, d_{rs} the nut diameter, L_a the length of the housing at full stroke, e_1 and e_2 the hollow cylinders thicknesses and L_{rs} the nut length. Which can be rewritten with the following dimensionless numbers:

$$\pi_{\sigma_U} = \frac{\sigma.d}{U.E} = f\left(\frac{L_a}{d_{rs}}, \frac{e_1}{d_{rs}}, \frac{e_2}{d_{rs}}, \frac{L_{rs}}{d_{rs}}\right) \tag{4.23}$$

For the angular pulsation:

$$\omega_r = g\left(E, \rho, d_{rs}, L_a, e_1, e_2, L_{rs}\right) \tag{4.24}$$

Where ρ is the volumic mass of the material. Which can be rewritten with the following dimensionless numbers:

$$\pi_{\omega_r} = \omega_r \cdot \sqrt{\rho/E} \cdot d_{rs} = g\left(\frac{L_a}{d_{rs}}, \frac{e_1}{d_{rs}}, \frac{e_2}{d_{rs}}, \frac{L_{rs}}{d_{rs}}\right) \tag{4.25}$$

The mechanical stress generated at the resonance frequency under a vibratory load is obtained using Equation 4.23 and Equation 4.25:

$$\sigma = k_\sigma.U = k_\sigma.\frac{Q_m.a}{\omega_r^2} = \frac{E \cdot Q_m \cdot a.d_{rs}^2 \cdot \rho}{d_{rs} \cdot E} \frac{f\left(\frac{L_a}{d_{rs}}, \frac{e_1}{d_{rs}}, \frac{e_2}{d_{rs}}, \frac{L_{rs}}{d_{rs}}\right)}{g\left(\frac{L_a}{d_{rs}}, \frac{e_1}{d_{rs}}, \frac{e_2}{d_{rs}}, \frac{L_{rs}}{d_{rs}}\right)^2} \tag{4.26}$$

Hence,

$$\pi_0 = \frac{\sigma}{Q_m a d \rho} = h\left(\frac{L_a}{d_{rs}}, \frac{e_1}{d_{rs}}, \frac{e_2}{d_{rs}}, \frac{L_{rs}}{d_{rs}}\right) \tag{4.27}$$

The expression of the stress is thus a function of four aspect ratios. The aspect ratio $\frac{L_{rs}}{d_{rs}}$ is assumed constant because of geometric similarity of ball screw components. The objective now is to determine the function h using simulation results and data regression.

To generate the data a design of experiment (DOE) using the Latin Hypercube Sampling (LHS) method is achieved for the four variables involved d_{rs}, e_1, e_2 and L_a. FEM simulations are executed for each sample of the DoE and the variable of interest π_0 is retrieved from the simulations results.

The variable of interest can be approximated here with a linear regression (Response Surface Model or RSM) with a development taken into account order 1 (main effect), interactions and order 2 effects which would give the following form:

$$\pi_0 = a_0 + \sum a_i \pi_i + \sum a_{ij} \pi_i \pi_j + \sum a_{ii} \pi_i^2 \tag{4.28}$$

A *log* transformation is performed on variables which provides the form:

$$log(\pi_0) = a_0 + \sum a_i log(\pi_i) + \sum a_{ij} log(\pi_i) log(\pi_j) + \sum a_{ii} log(\pi_i)^2 \tag{4.29}$$

which can be rewritten as:

$$\pi_0 = 10^{a_0} \prod_{i=1}^{n} \pi_i^{\,a_i + a_{ii} log(\pi_i) + \sum_{j=i+1}^{n} a_{ij} log\left(\pi_j\right)} \tag{4.30}$$

This variable power law form enables to deal with large variation range of dependant and independent variables outside the construction domain [209, 207].

$$
\begin{aligned}
\log(\pi_0) = 124\log\left(\frac{L_a}{d_{rs}}\right) + \\
\frac{2}{23}\log\left(\frac{L_a}{d_{rs}}\right)\cdot\log\left(\frac{e_1}{d_{rs}}\right) + \\
\frac{31}{421}\log\left(\frac{L_a}{d_{rs}}\right)\cdot\log\left(\frac{e_2}{d_{rs}}\right) + \\
\frac{713}{812}\log\left(\frac{L_a}{d_{rs}}\right) + \frac{125}{892}\log\left(\frac{e_1}{d_{rs}}\right)^2 - \\
\frac{194}{911}\log\left(\frac{e_1}{d_{rs}}\right)\cdot\log\left(\frac{e_2}{d_{rs}}\right) - \\
\frac{231}{391}\log\left(\frac{e_1}{d_{rs}}\right) + \frac{13}{48}\log\left(\frac{e_2}{d_{rs}}\right)^2 + \\
\frac{704}{875}\log\left(\frac{e_2}{d_{rs}}\right) + \frac{290}{231}
\end{aligned}
\tag{4.31}
$$

Figure 4.13 shows the prediction test results using the π_0 surrogate model. The input data set for testing is split with regard to the training data set to avoid over-fitting [116].

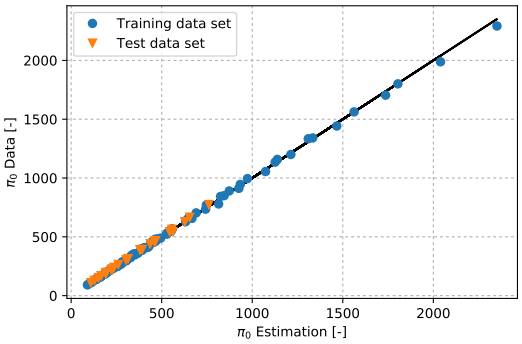

Fig. 4.13 π_0 surrogate model validation

4.3.4 Algebraic Analysis Functions Based on Time Domain Simulations Data

Similarly to surrogates models of Finite Element Methods simulations, surrogate models can be used for lumped parameter time domains simulations. The surrogate modelling requires a DOE that is used to drive the simulations. To increase the speed of the DOE driven simulation, Functional Mock-up Units [219] are used. They are fifteen times faster that using a Dymola dymosim in some examples. Then simulation can be fitted using data regression techniques like response surface model or kriging [239]. This way a low computational cost and manipulable model can be generated. In the case of the Thrust Vector Control electro-mechanical actuator, this method can be used to assess the maximum load generated by the shock that occurs at firing [35, 84]. Without a lumped parameter model this

would be intricate as they are several stiffness in the system and that a force feedback that acts as an artificial damping is used. An example of utilization of this technique is presented for the Electrical Thrust Reverser Actuation System example in chapter 6.

4.4 Decomposition and Coordination of the Sizing Code

From now on, the steps of the methodology are supported by a framework called BOA (Bind your models, Optimize your system, Accelerate your design). The systemic approach previously presented has influenced the architecture of the framework. It does not enable the generation of algebraic analysis functions with the different outlined methods. However, it enables to implement any type of algebraic analysis functions once they are generated outside the framework. Then a global process permits the generation of a whole system model using these elementary functions and perform design optimization and design space exploration on it. This framework was developed using Python programming language. The computational core relies on key scientific computing packages like Scipy, Numpy, Sympy, NetworkX, pyDOE and OpenMDAO. The following steps outline the features and philosophy of this sizing framework. The user interface was implemented using PyQt5. Decomposition and coordination steps provide efficient methods for managing engineering design knowledge and elementary models to build a total system model.

4.4.1 Decomposition

The wide spectrum of engineering design knowledge has been previously outlined. This part proposes an approach to decompose this knowledge to provide collaboration, reusability, capitalization and rapid implementation of system model.

By engineering specialization

Two levels of knowledge are considered: component level and system level. The component level is considered to be a level where elementary algebraic functions are assembled into reasonably complex groups and use acausal modelling. This way these groups of models are more manageable and more reusable as users deal with a limited number of elements [167]. The groups are then saved in a model library dedicated to component level.

In the framework the component level corresponds to the *Block Generation* tab as shown in Figure 4.14. A group, also referred to as "block", has a simple documentation which can contain a reference to a document and that is attached to the block throughout the process.

When an algebraic analysis function is added, parameters are automatically identified using Sympy [224] and added to the parameters. These blocks can then be sent to the system level in a causal form.

The system level modelling is where the component level blocks are assembled to form the total system model. The previous features are also available except acausal modelling. In the framework the

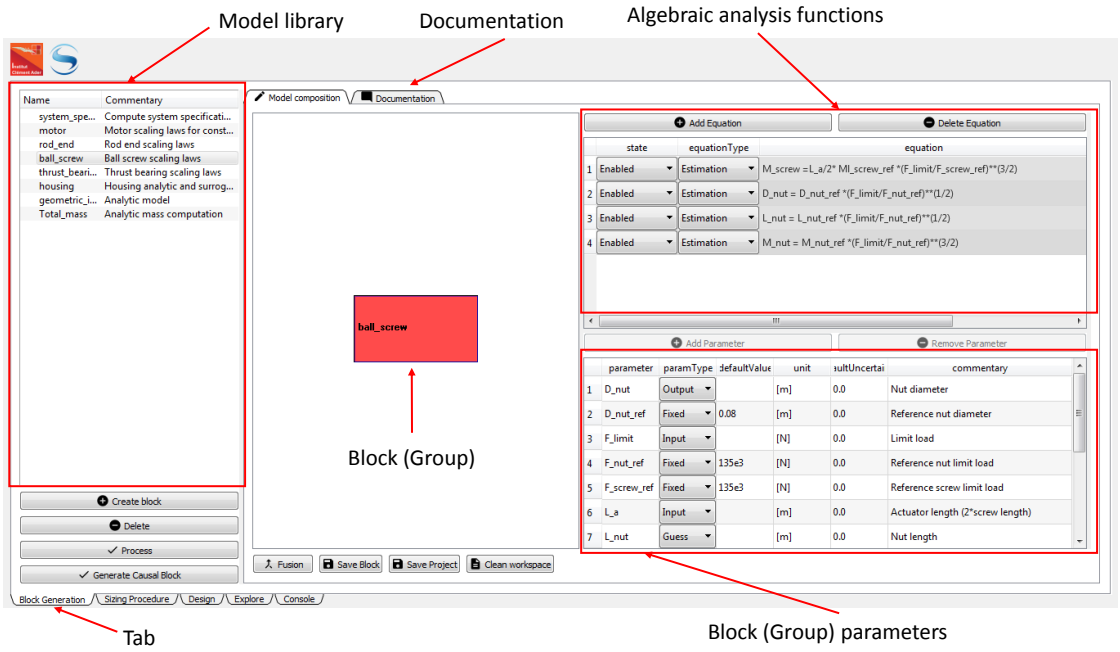

Fig. 4.14 *Block Generation* tab for component level modelling

component level corresponds to the *Sizing Procedure* tab. The assembly is achieved using graphical links that defines how the parameters of two blocks are connected as illustrated in Figure 4.15.

By Analysis Function and Parameter Type

Analysis functions are all algebraic but they can be typed by the user in order to better define the sizing problem and enhance coordination. They can be typed as:

- *Estimation*: Used for component parameter estimation models (e.g motor inertia)
- *Scenario*: Used for sizing scenario models (e.g motor speed required)
- Constraint: Used for constraints (algebraic inequality) (e.g motor maximum speed)
- *Consistency*: Used for consistency constraints (multidisciplinary couplings) during system analysis, optimization and Design of Experiments (e.g dynamic torque + torque due to aerodynamic loads)

During the implementation of the models emphasis is placed on extracting relevant knowledge of engineering specialization experts and system architects. Thus, additional information can be provided for parameters. The user can define a default value especially for constant (fixed) parameters. Units can also be defined and a commentary can be added to give further information concerning

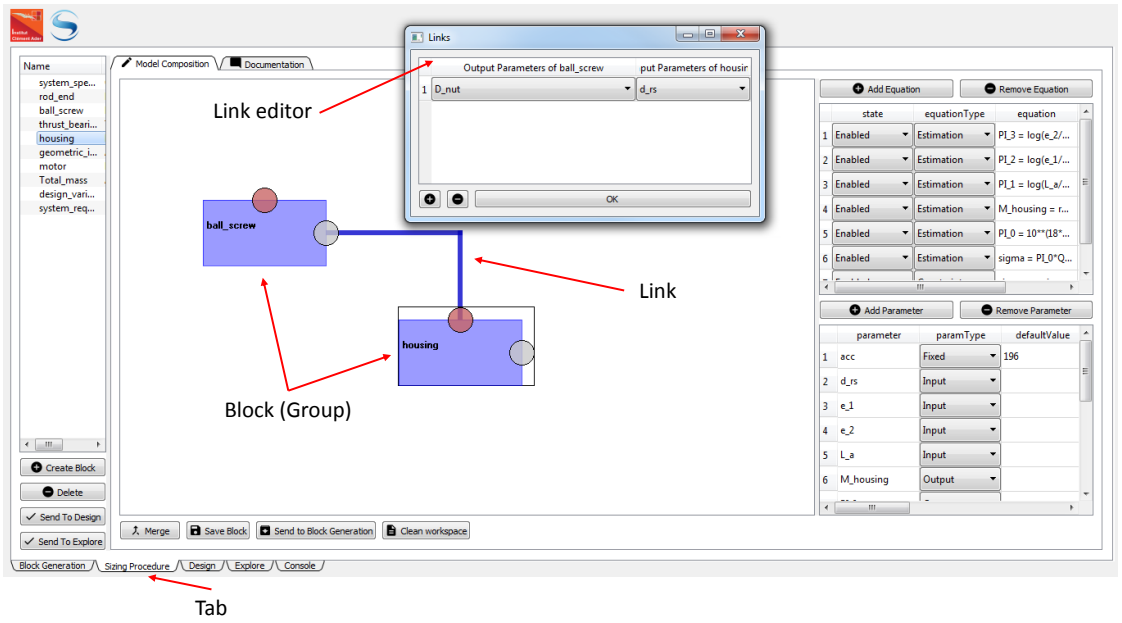

Fig. 4.15 *Sizing Procedure* tab for system level modelling

the parameter. Finally, the engineering specialization expert can give a value of uncertainty on a parameter.

Figure 4.16 shows how these features are implemented in the framework.

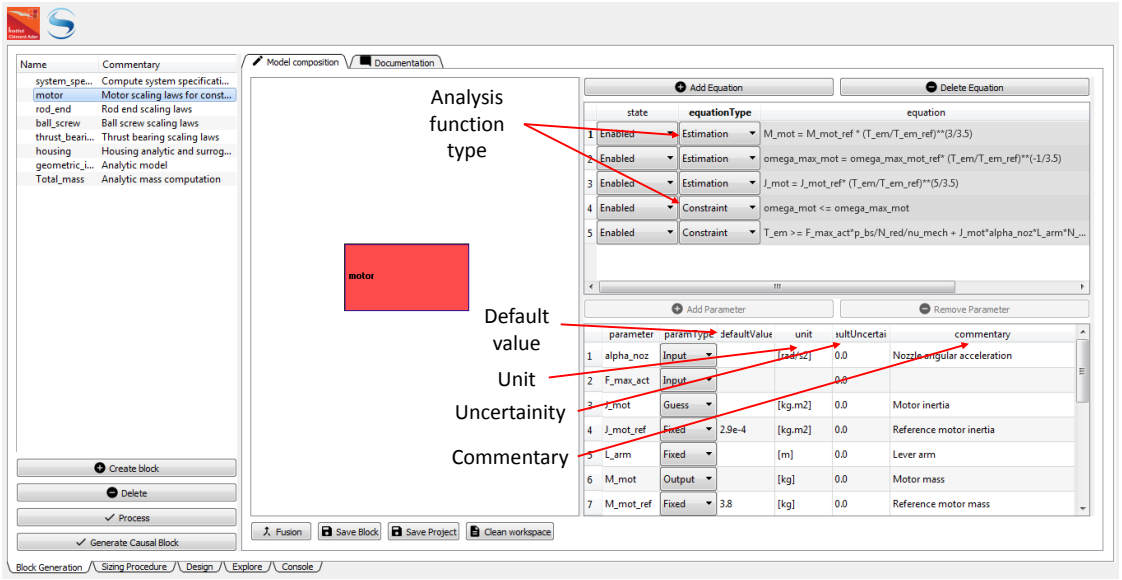

Fig. 4.16 Decomposition of engineering design knowledge

Sub-systems Handling

Some systems can become very complex and the system sizing model can as well. To deal with system sizing model complexity it is possible to build sub-system sizing models to reduce the number of elements of the model. The Dymola [226] and OpenModelica software encourage users to build a sub-system as soon as the system elements do not fit in the default grid. It has been proven that the mean number of elements the brain can handle is seven [167]. Hence, the framework offers in the Sizing Procedure environment the possibility to build sub-systems by merging blocks together. The difficulty here is to define what are the variables of the sub-system available at the higher level. For that an hierarchical decomposition used in system engineering approaches is implemented. Before merging to blocks the user has to define a requirement block which contains the inputs variables of the sub-system and an output block which contains the output variables of the sub-system. This enables to avoid risky manipulations that can generate singularities in the sub-system model. If the sub-system has to be changed the user can ask the author of the sub-system model to achieve a modification. The concept of sub-system where all mechanical transmission models (thrust bearing, ball screw and rod-end) are merged into one common model is illustrated in Figure 4.17.

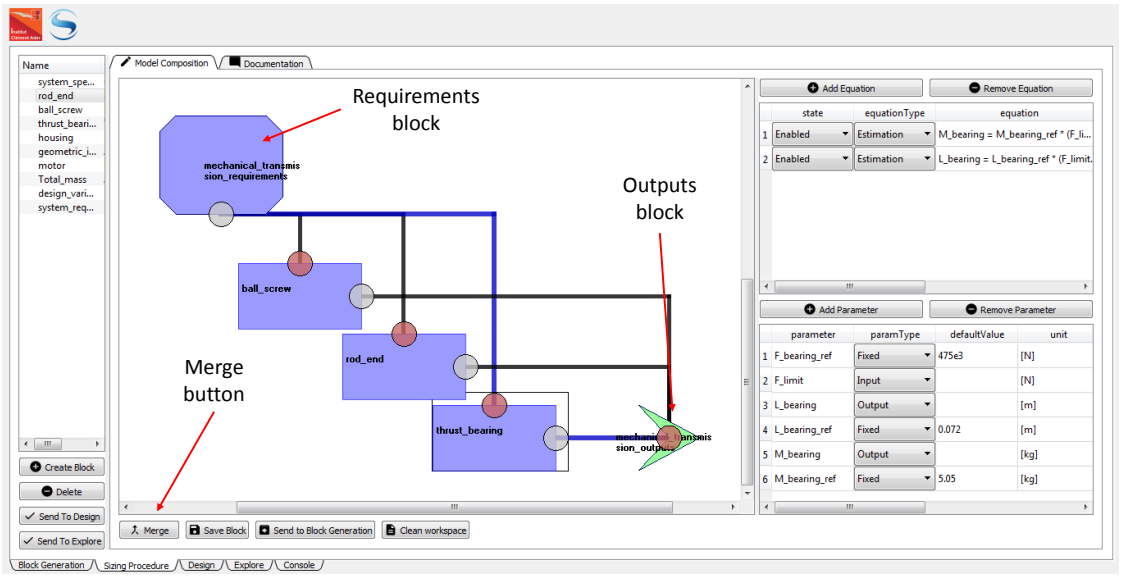

Fig. 4.17 sub-system generation through hierarchical decomposition

The decomposition of the sizing problem has been outlined in this part. The other challenge of the sizing problem definition is the coordination of the models.

4.4.2 Coordination

The decomposition enables to partition a large sizing problem into elementary acausal models more manageable and more reusable models. This increase the complexity of the coordination task for the

design engineer. A set of methods are then needed to enable to perform coordination in a intuitive manner.

Chapter 3 outlined typical issues that occur when defining a system model. These singularities are due to over-constrained or under-constrained situations or the presence of algebraic loops in the system model.

Solution at Component Level

To provide the acausal modelling features of blocks from the *Block Generation* environment parameters have to be typed to define how they can be manipulated. Here is the list of parameter types implemented:

- *Input*: The parameter is an input variable of the block which is needed outside the block, and thus can be connected to an output variable of another block (e.g required actuator speed, maximum aerodynamic load...)
- *Fixed*: The parameter is a constant parameter with a value defined in the block (e.g reference motor inertia...)
- *Guess*: The parameter is a variable computed with respect to an analysis function which is not available outside the block (e.g motor inertia...)
- *Output*: The parameter is a variable computed with respect to an analysis function which is available outside the block, and thus can be connected to an input variable of another block (e.g motor mass...)
- *Consistency*: The parameter is a design variable used for multidisciplinary coupling consistency during system analysis, optimization and Design of Experiments (e.g over-sizing factor...)

The user can choose different parameter type configurations to meet the engineering design needs. The graph-based process presented in Chapter 3 is implemented in the framework. It can be applied to detect singularities and solve algebraic loops at component level. It then re-orient and re-order the equations to meet the parameter type configurations that fulfils the needs of the user (if possible). The bipartite graph is connected to the system of equations which enables to help the user to solve singularity issues by highlighting the algebraic analysis functions and parameters involved as shown in Figure 4.18.

Once the acausal blocks meet the inputs and outputs needs and that they do not contain any singularity issues they can be processed as causal blocks to the *Sizing Procedure* environment.

Solution at System Level

The *Sizing Procedure* environment enables to build the system model. It is where the causal block are assembled to form a complete model. The main coordination issue at this level is the introduction of

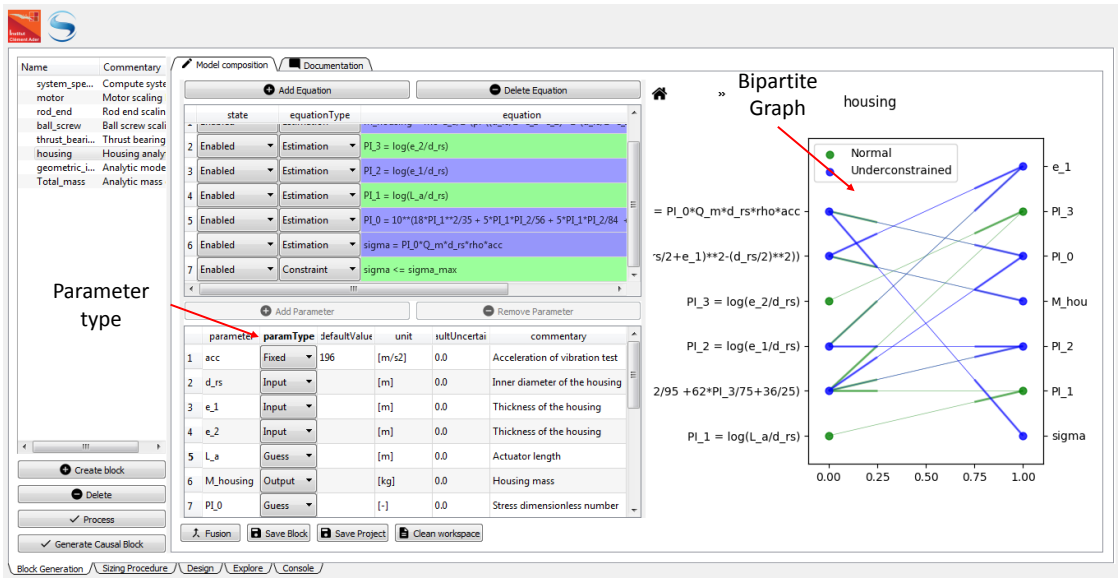

Fig. 4.18 Component level coordination using graph-based methods

system level multidisciplinary couplings because other singularities have been solved at component level. To enable efficient coordination during the sizing procedure definition the N2 diagram formalism is used [122]. The system model and optimization problem formulation can be achieved by creating and connecting different kind of blocks:

- *Causal block*: They are blocks that contain the algebraic analysis functions i.e equations and inequalities (e.g motor sizing model). They come from the *Block Generation* environment but can also be created and modified in the *Sizing Procedure* environment.
- *Input block*: They are blocks that contain only fixed parameters that can be connected to inputs of other blocks (e.g system specifications).
- *Output block*: They are blocks that contain variables of a sub-system that can be connected to inputs of other blocks.
- *Design variable block*: They are blocks that contain design variable parameters. They have additional fields when compared to other parameter: initial value, minimum value and maximum value (e.g reduction ratio).
- *Constraint block*: It is a block that contains only inequalities and can only receive incoming information. (e.g motor speed)
- *Objective block*: It is a block that contains the parameter that corresponds to the objective function (e.g total mass of the actuator). It has to be connected to the interest variable of another block.

Figure 4.19 gives the sizing procedure for the thrust vector control actuator using the BOA framework.

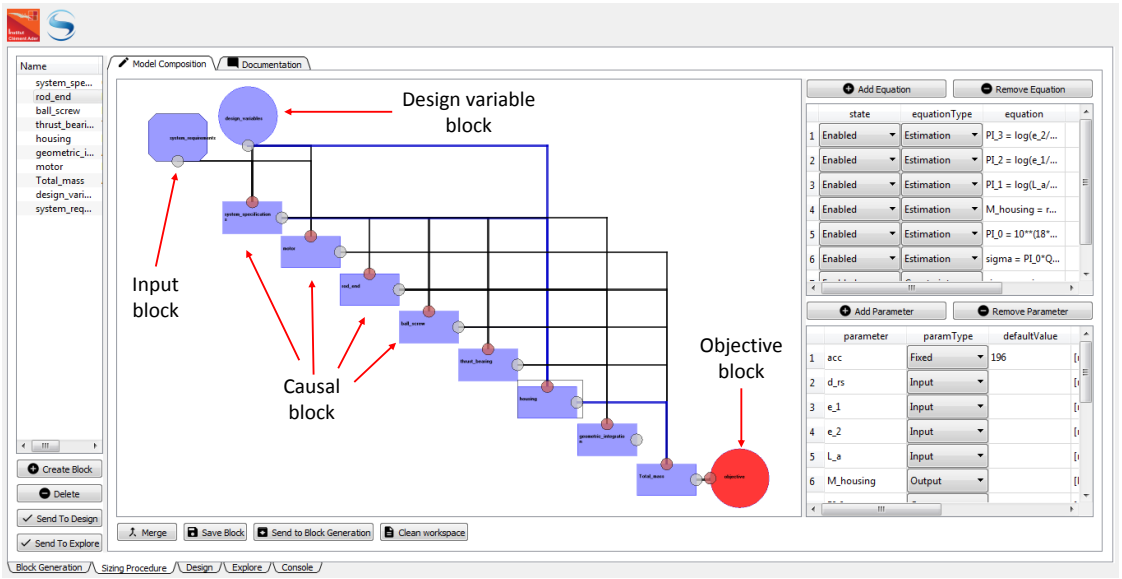

Fig. 4.19 Sizing procedure of thrust vector control actuator

The N2 diagram enables to detect rapidly the system level multidisciplinary couplings and visualize the dependence between blocks. In addition, the user can modify the parameter type to fit his design needs. The modified block can be sent back to the Block Generation environment to check if singularities have been generated by the modifications. The framework enables only single objective optimization, thus only a single objective block must be implemented. The sizing procedure that correspond to the assembly of all the block defining the sizing optimization problem can be saved into a sizing project. This enhance knowledge capitalization and reusability during the sizing process.

The sizing and optimization model has been built to enable efficient system analysis. Indeed, the model are low computational cost (algebraic) and singularity problems have been solved using the singularity analysis tool described in Section 3.5.2. This enables to avoid costly solver calls during system analysis. Furthermore, algebraic analysis function are expressed explicitly and are ordered as an optimal computational sequence. At the end of this step the sizing optimization problem is defined and can now be sent to the Design Optimization environment.

4.5 Design Optimization and Exploration

The *Design* tab proposes a computational core and user interface well suited for rapid sizing optimization and decision making. Finally, *Exploration* tab provides methods and visualization tools for design space exploration. The computational core is implemented using the openMDAO open-source framework developed by NASA [89].

4.5.1 Analysis and Optimization of the System Sizing Model

This part of the framework enables to achieve design analysis as well as design optimization. Choices have been made on the methods used to fit best the main objective of the framework rapid sizing and decision making.

Normalized Variable Hybrid Formulation

The generated sizing and optimization model of the thrust vector control is outlined in Figure 4.20 using the XDSM formalism [136]. All the models used can be found in Appendix A.

In the BOA framework, the MultiDisciplinary Feasible formulation (MDF) is not implemented. The user can build any monolithic formulation that does not include a multidisciplinary analysis solver (Individual Discipline Feasible, All At Once, Hybrid ...). However, the Normalized Variable Hybrid formulation (Chapter 3) is prioritized and automatized due to its robustness to scale changes in typical sizing problems. The multidisciplinary coupling of the case study is between the motor electromagnetic torque analysis function (Equation 4.32) and (Equation 4.33) the motor inertia analysis function that both need/compute the electromagnetic torque T_{em} and motor inertia J_{mot}.

$$T_{em} = F_{max_{act}} \frac{p_{bs}}{N_{red}\eta_{mech}} + J_{mot}\alpha_{noz}L_{arm}\frac{N_{red}}{p_{bs}} \tag{4.32}$$

Where $F_{max_{act}}$ is the maximum load applied to the actuator, p_{bs} the ball screw pitch, N_{red} the spur gear reduction ratio, η_{mech} the mechanical transmission efficiency, J_{mot} the motor inertia, α_{noz} the maximum angular acceleration of the nozzle and L_{arm} the lever arm length.

$$J_{mot} = J_{mot_{ref}} \left(\frac{T_{em}}{T_{em_{ref}}} \right)^{\frac{5}{3.5}} \tag{4.33}$$

Where $J_{mot_{ref}}$ and $T_{em_{ref}}$ are respectively the inertia and the nominal electromagnetic torque of the reference motor used by the scaling law.

The Normalized Variable Hybrid is implemented using a normalized variable k_{os} which corresponds to an over-sizing factor of the electromagnetic torque in Equation 4.34 and removing the motor inertia J_{mot} following the method described in Chapter 3.

$$T_{em} = k_{os}F_{max_{act}} \frac{p_{bs}}{N_{red}\eta_{mech}} \tag{4.34}$$

An additional consistency constraint (Equation 4.35) is used to check that the previously chosen electromagnetic torque is sufficient for the inertial torque and the load.

$$T_{em} \geq F_{max_{act}} \frac{p_{bs}}{N_{red}\eta_{mech}} + J_{mot}\alpha_{noz}L_{arm}\frac{N_{red}}{p_{bs}} \tag{4.35}$$

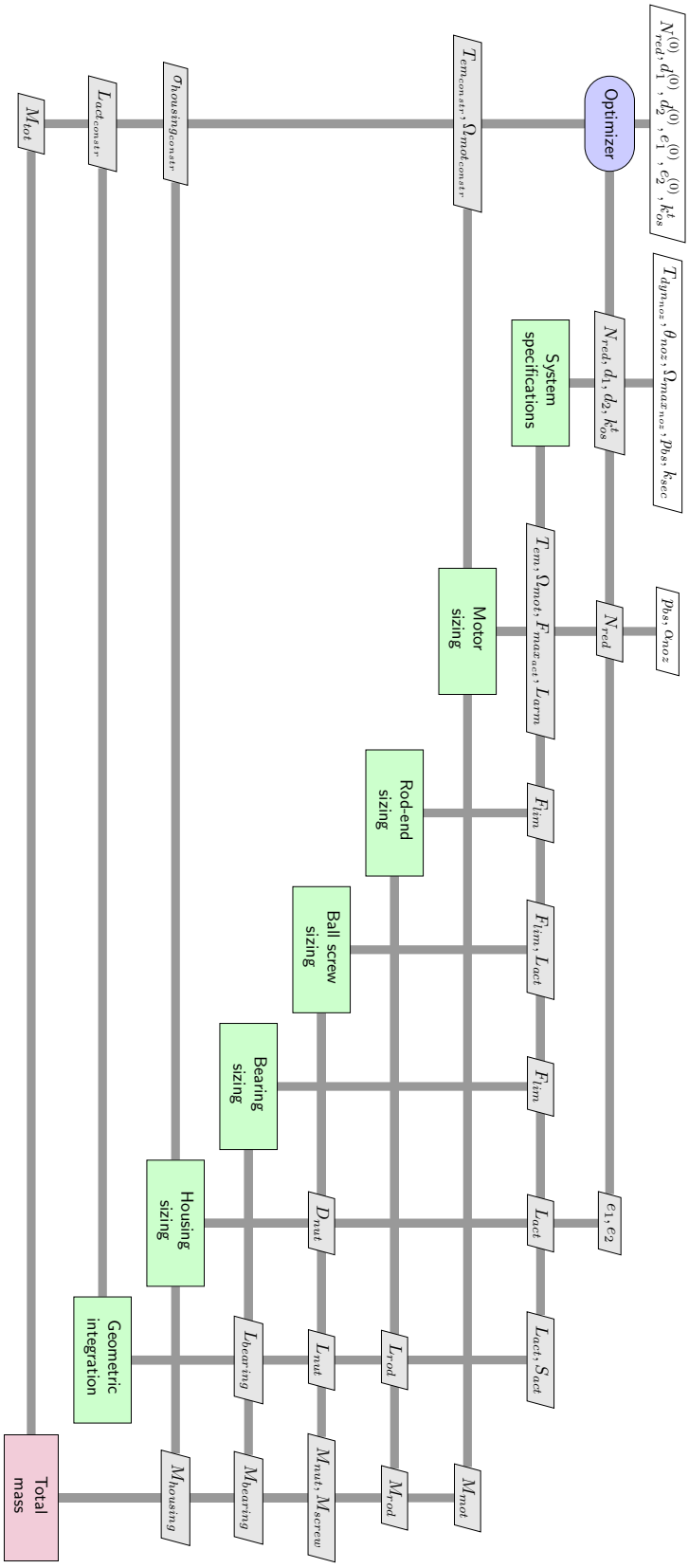

Fig. 4.20 XDSM diagram of the thrust vector control electro-mechanical actuator optimization

Gradient-Based Optimization with Analytic Derivatives

Two optimization algorithms are implemented. A local gradient-based optimizer SLSQP enables rapid optimization (seconds to minutes). A global genetic optimizer NSGAII enables a global search but with higher computation times (minutes to tens of minutes). The framework has a multi-start feature which can be combined with the SLSQP local optimizer to enhance chances of finding the global optimum when facing multimodal problems. The use of the gradient-based optimizer is preferable since it has the smallest computational cost and enables the optimization of large design spaces intrinsic to conceptual and preliminary sizing.

For system model elements, symbolic differentiation is used for computing derivatives thanks to the Sympy package [224]. The system model total derivatives are computed using the Unified Derivatives Equations implemented in openMDAO [157, 113].

Parametrization and Visualization

The parametrization and visualization is achieved using a format similar to spreadsheets. The spreadsheet is decomposed in several parts:

- Inputs: This part corresponds to the parameters defined in the input blocks of the Sizing Procedure environment. They can be modified by the user.
- Design variables: This part corresponds to the parameters of the design variables blocks. The user can modify their initial value, minimum value and maximum value. Once an optimization or analysis is performed the constraints can be highlighted using different colors: green for feasible, orange for boundary and red for unfeasible (failed optimization). This way the designer can identify constraining requirements and component technologies.
- Constraints: This part corresponds to the parameters of the constraints defined in the causal blocks. The user has to go back to Sizing Procedure to modify them. This choice was made to avoid too easy changes of engineering specialization knowledge by high-level users and thus efficient but incorrect design solutions. Similarly to design variables, constraints can be highlighted using colors with respect to their value regarding the bounds.
- Objective: This part contains the parameter of the objective block. It enables to rapidly visualize the analysis of optimization results.
- System model parameters: This part corresponds to all the causal blocks and their respective parameters. They are easily foldable this way the designer can easily browse through all the variables and parameters that characterize the system model.

These implementation choices are shown in Figure 4.21.

A normalization process is achieved on both design variables and constraints as their scale can be high (Mechanical stress, motor winding current density...) and some small (housing thickness, motor yoke thickness...) when operating with International System of Units.

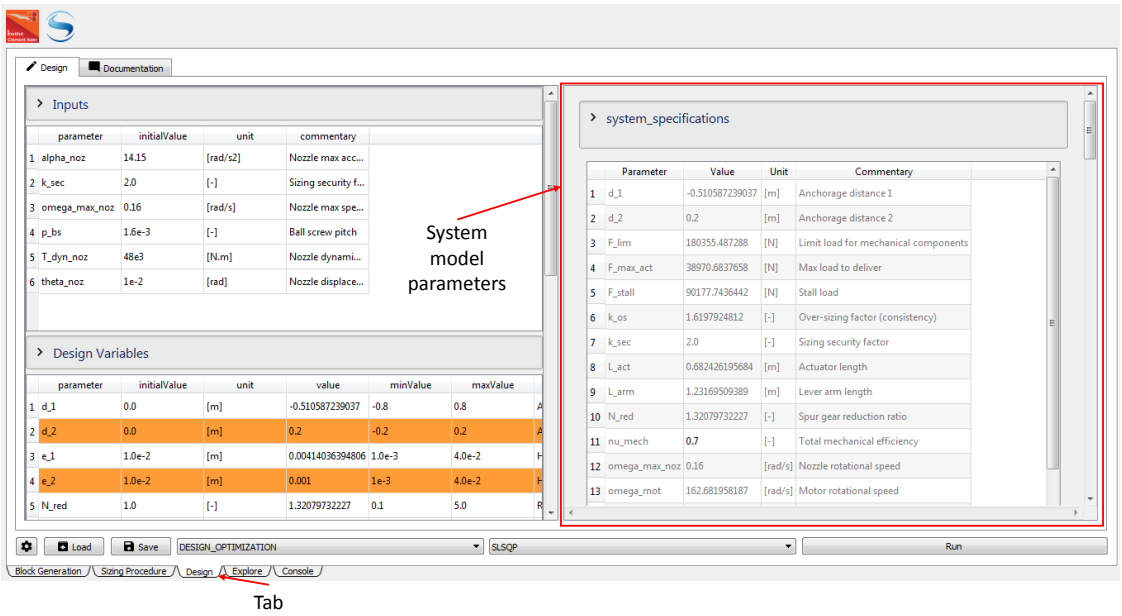

Fig. 4.21 environment of the framework

4.5.2 Design Space Exploration of the System Sizing Model

Mechatronic system preliminary sizing allows large design space and design alternatives as well as in some cases unusual form factors. It is very interesting during engineering design to provide optimization and exploration capabilities. Some design engineers might prefer design space exploration instead of optimization because they have a better hand on the design alternatives. Furthermore, design space visualization tools are very interesting for decision making [223]. Effect of changes of requirements on performances can be investigated as well as effects of technology alternatives.

Design of Experiments of Multidisciplinary Systems

Running a Design of Experiments (DOE) of multidisciplinary systems is an intricate task. The Design of Experiments is greatly dependant of the system analysis effectiveness. Chapter 3 outlined that for some monolithic formulations except MDF, system analysis requires a sub-optimization problem to be implemented even though it is for Design of Experiments purposes. Ignoring this leads to inconsistent system analysis and therefore most of the Design of Experiments result in unfeasible solution as consistency is one of the feasibility conditions in multidisciplinary analysis and optimization [7].

It is chosen to use only the Normalized Variable Hybrid formulation due to its significant robustness which is even more put to the test during large design space exploration. This requires to type the consistency design variables and constraints during parameter definition in the Block Generation and Sizing Procedure formulation. This way the sub-optimization problem is defined and multidisciplinary couplings are solved by the optimizers.

The sampling method used is a Latin Hypercube Sampling (LHS) with normal distribution [114]. The formulation of the Design of Experiments problem for the case study is illustrated in Figure 4.22. The variables (factors) of the DOE are e_1,e_2,d_1,d_2 and N_{red}. The consistency design variable is k_{os} and the consistency constraint given in Equation 4.35.

A post treatment in necessary to check that the optimization was successful. This is achieved by checking that the optimization result is feasible by inspecting the multidisciplinary couplings values. The remaining design alternatives are therefore all consistent.

Design Space Visualization

Once the Design of Experiments task is achieved the results corresponding to the entire design alternatives can be analyzed. As often the number of samples is high for design space exploration, the challenge is to analyze a large number of design alternatives which include a large number of system parameters. The state of the art of engineering design approaches outlined in Chapter 2 has proposed different visualization charts used in engineering design. As the number of system parameters is large, we chose to implement the parallel coordinates plot as shown in Figure 4.23.

The *Exploration* environment provides the possibility to filter the large number of parameters and brush the large number of samples by acting on parameter bounds. The filtering is achieved by selecting the parameters in the list of system parameters. The brushing can be achieved either directly on the parallel coordinates plot or by entering the parameter bounds directly in the corresponding cells.

The framework also gives the possibility to export the exploration results before or after brushing. The export can be done in '.txt' with tab separators or '.csv' with coma separators. This way the results can be analyzed in other tools like Trade Space Visualizer [223] which offers more features that the BOA framework.

4.5.3 Design and Exploration Models Exportation and Co-Simulation

Both *Design* environment and *Exploration* environment models can be saved as respectively a design project or an exploration project in a dedicated model library. This provide the possibility to capitalize knowledge and increase reusability of sizing tasks. The saving of these models is made using serialization. As the framework is entirely running under python, the choice made was to used Python Object Serialization using dill package [62]. Not only this feature enables to save/open projects it provides the possibility to run the design project or the exploration project in an external python program. Compiling projects as executables or as a C program resulted in respectively large files as all the necessary libraries were also compiled and a significant amount of programming skills to wrap some python code into C or Cython. Safavi used Windows COM (Component Object Model) objects for interfacing analysis tools but this limits the usage to Windows operating systems [205]. For these reasons, Python Object Serialization was preferred even if the python environment that will run the project model will have to install the package dependencies of the framework necessary to run them.

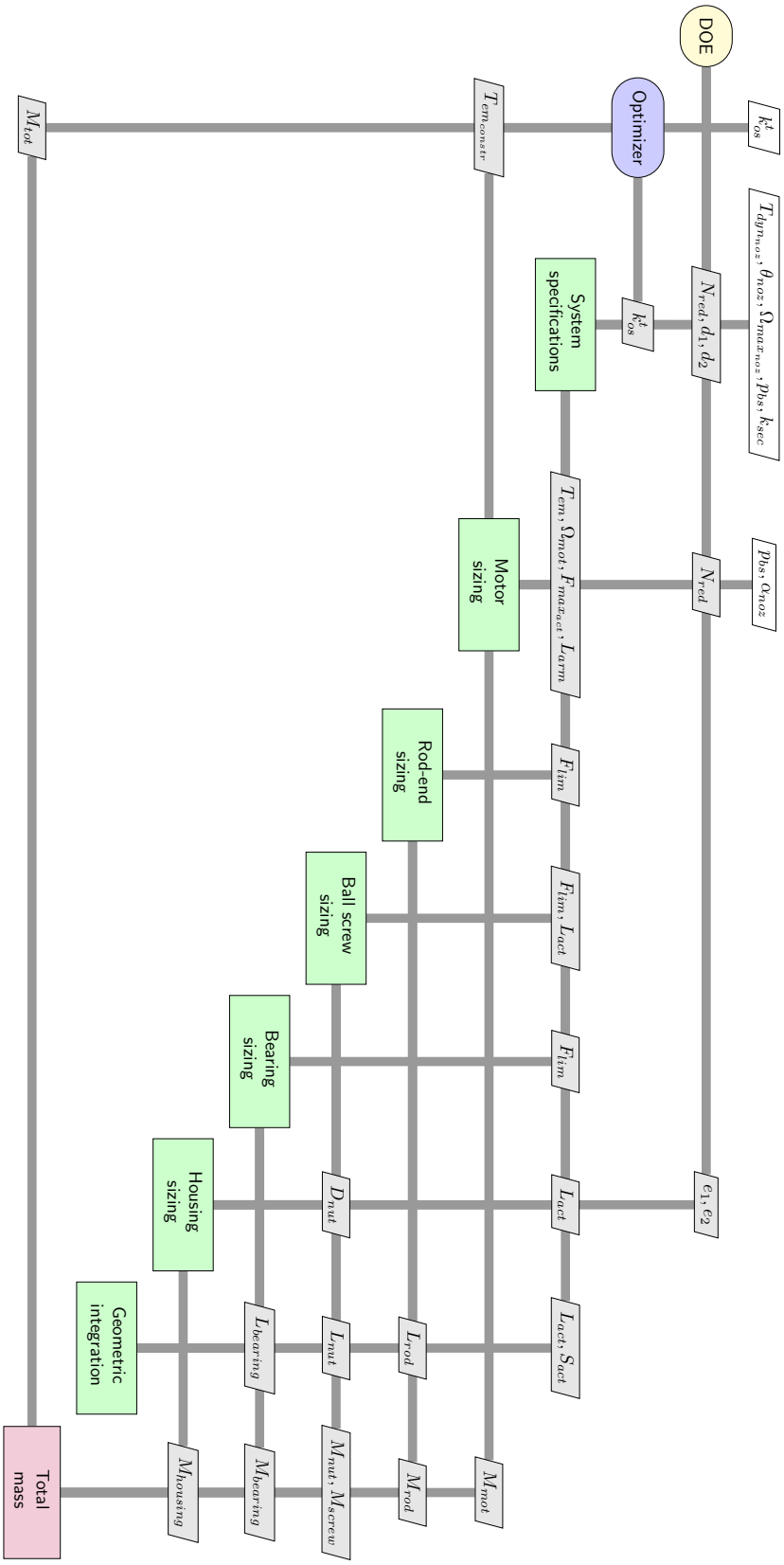

Fig. 4.22 XDSM diagram of the thrust vector control electro-mechanical actuator DOE

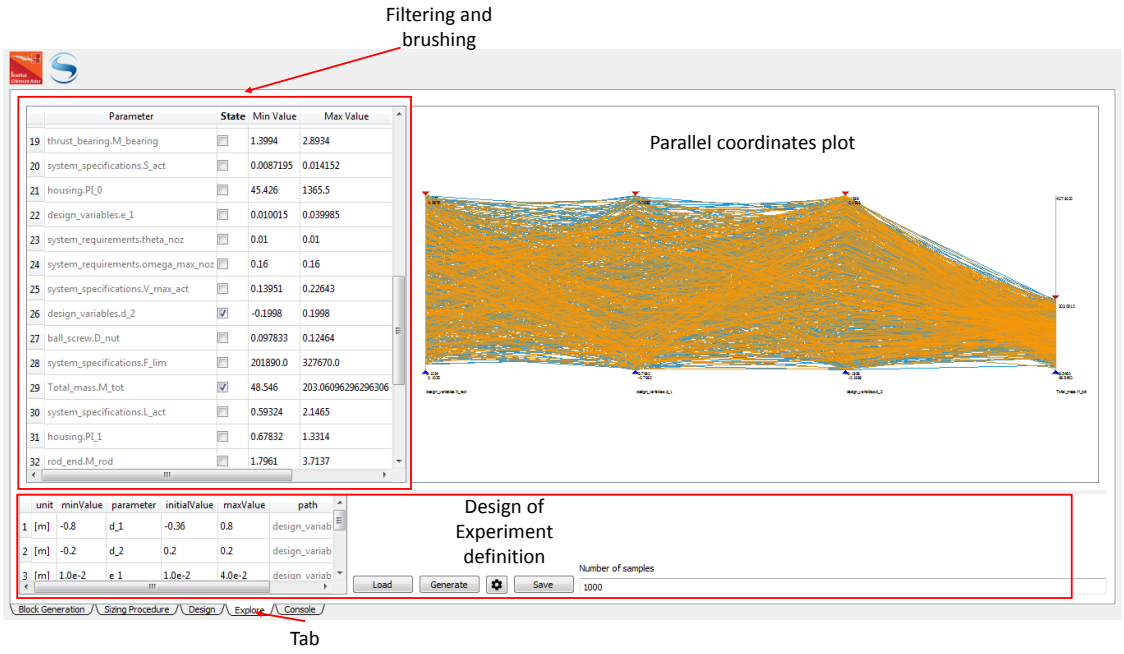

Fig. 4.23 *Exploration* environment of the framework

Models exported from the framework can be executed either to perform an analysis, an optimization or a DOE. This provides significant insights for engineering design activities. It enables to use a complex sizing model that assembles different engineering specializations into a system sizing code by exploiting scientific methods through a process. This low computational cost sizing code can be used as a sub-system sizing code in a larger sizing problem. In the case study for instance, the actuator sizing code, provided by the supplier, can be used by the system integrator during nozzle design and integration where anchorage positioning could have been a design variable. This can be achieved in co-simulation environments like ModelCenter [148] or iSight [235] that enable the integration of python scripts in global computational workflows.

In the scope of this thesis, the export and simulation of these sizing codes have been used to run analysis and optimization for different purposes. They have been used to run some DOE on top of optimization to build response surface models that represented the optimization model results. Furthermore, they have been used inside larger optimization problems that included more complex model handling like Functional Mock-up Units (FMU). One example was the sizing optimization of an aileron linear electro-mechanical actuator subject to thermal response over an entire flight profile [54]. The thermal response of the actuator with respect to the mission profile was performed by a FMU generated in Dymola [226]. The parameter of the simulation were computed in the optimization model (motor conduction resistance, reduction ratio...) and maximum temperatures of the thermal responses from the FMU were handled as constraints of the optimization problem as shown in Figure 4.24.

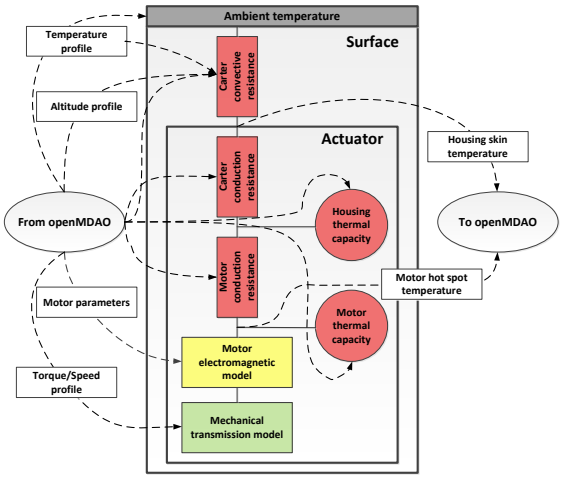

Fig. 4.24 Interaction between optimization model and FMU model [54]

4.5.4 Results of Thrust Vector Control Electro-Mechanical Actuator Sizing

A summary of the Thrust Vector Control electro-mechanical actuator sizing problem is given in Appendix A. The design optimization problem is the following.

$$\begin{aligned}
&\text{minimize} && M_{tot} \\
&\text{with respect to} && N_{red}, d_1, d_2, e_1, e_2, k_{os} \\
&\text{subject to} && \Omega_{mot} - \Omega_{mot_{max}} \leq 0 \\
& && S_{act} + L_{nut} + L_{bearing} + 2L_{rod} - L_{act} \leq 0 \\
& && \sigma - \sigma_{max} \leq 0 \\
& && F_{max_{act}} \frac{p_{bs}}{N_{red}\eta_{mech}} + J_{mot}\alpha_{noz}L_{arm}\frac{N_{red}}{p_{bs}} - T_{em} \leq 0
\end{aligned} \tag{4.36}$$

The objective is to minimize the overall mass of the electro-mechanical actuator with respect to the positioning of the anchorage using d_1 and d_2, the reduction ratio of the spur gear N_{red}, the housing thicknesses e_1 and e_2 and an over-sizing factor k_{os} for solving the multidisciplinary coupling explained in Section 4.5.1. The optimization is subject to four constraints: the maximal speed of the brushless motor, the mechanical axial clearance, the maximum housing stress and a consistency constraint.

The optimization is achieved using the gradient-based optimizers SLSQP. The typical runtime is $2.1s$ ($2min58s$ with NSGAII a gradient-free optimizer). The variables d_2 and e_2 are respectively on their maximum and minimum bound. The active constraints are the housing stress and the actuator torque consistency constraint.

The first optimization showed that the over-sizing factor was higher than one (typically 2) meaning that the inertial torque was dominating the torque due to the load applied on the nozzle. Thus, an investigation was made to assess the effect of the motor inertia on the overall design. For this purpose,

different optimizations were achieved for different reference motor inertia $J_{mot_{ref}}$ reduction factors (1.0 to 3.0). The optimization results for each reduction factor are given in Figure 4.25.

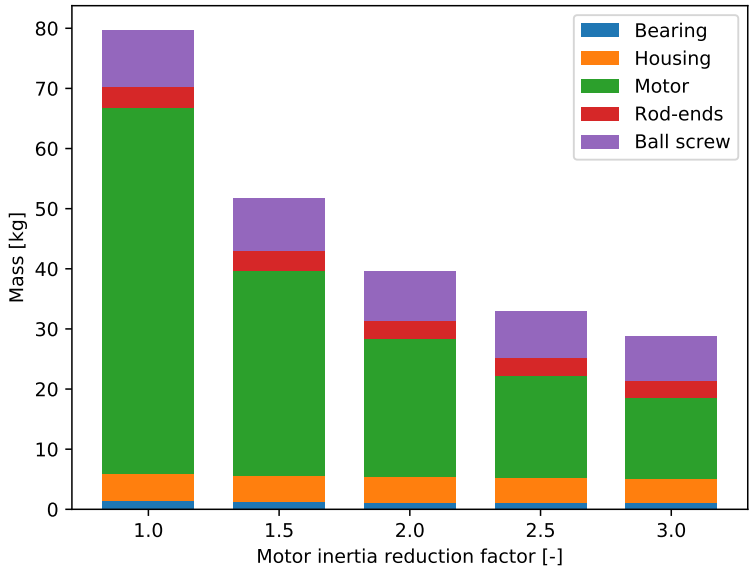

Fig. 4.25 Effect of motor inertia reduction on optimization results

The effect of motor inertia on the motor mass and the total mass is significant. Reducing the reference motor inertia by a factor 2 leads to an important decrease of the mass. Hence, emphasis must be placed on the motor detailed design and the reduction of the inertia by changing the motor technology or machining the rotor. A reduction factor on the inertia of 2 is achievable. Hence, from now on this reduction factor is considered in the calculations.

The actual VEGA TVC EMA's mass is $78kg$ [152]. The optimization results shows a different positioning configuration but the resulting mass for no inertia reduction is close to the existing actuator mass. Hence, it proves that the magnitudes of the actual results are coherent. Nevertheless, the reduction of the motor inertia could improve the overall mass of the actuator.

Now, requirements include fixed anchorage positioning and therefore a given lever arm value. The positioning of the anchorage has been made to have a reasonable lever arm which has a positive effect on the motor sizing has less torque is required. However, this leads to a longer actuator and thus a longer housing.

As seen in Section 4.3.3, adding length to the housing increase the stress generated at resonance frequency. Hence, the housing will have to be thicker and longer, hence heavier. Therefore, there is a compromise on the anchorage positioning and consequently the lever arm between adding mass to the motor and adding mass the housing (and screw since it is longer). To assess this compromise, two optimizations were achieved. One with fixed anchorage positioning and another were they are free (bounded). Figure 4.26 outlines the results of both optimizations.

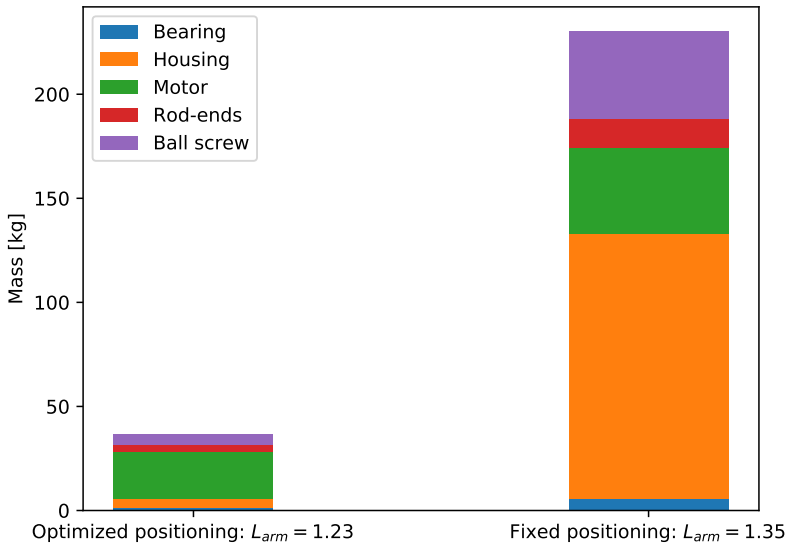

Fig. 4.26 Effect of anchorage positioning

The effect of anchorage positioning has a significant effect on the total mass of the actuator. Thanks to the optimizer, the optimal positioning of anchorage is determined which would have not been an easy task by hand as one might think that the largest lever arm is the best.

4.6 Methodology and Framework Implementation Summary

The previous sections have described in detail the concepts and implementation of the methodology developed in this thesis. In this section,a summary of the methodology is given and some assessments about the amount of work necessary for the implementation of the framework.

The first step in the methodology discussed methods and visual tools to define an architecture, design drivers and sizing scenarios. This way the sizing problem is summarized and modelling needs can be identified. This enables sizing knowledge capitalization that can be reused for future developments. The tools used for this step are databases and the Graphviz package.

The second step proposes to use only algebraic models in the sizing problem. This way acausal modelling can be used which enhances reusability of models. In addition, algebraic models are low computational cost and thus are well suited for analysis and optimization. For that, different methods for generating algebraic models using different types of models have been proposed. The tools used here are Python packages like Numpy, Scipy, pyDOE, and Scikit-Learn.

The third step consists of building component sizing model by assembling elementary algebraic models. Acausal modelling is used thanks to graph-based methods and symbolic computation. Furthermore, a model library and expertise information relevant for the sizing problem included

in the models such as uncertainty or assumptions. This step is supported by the Block Generation environment of the in-house BOA framework.

The fourth step assembled component sizing models into a causal system sizing model. This is achieved thanks to the N2 diagram formalism and hierarchical decomposition. System sizing models and projects can be saved in a library to permit reusability. This step is supported by the Sizing Procedure environment of the in-house BOA framework.

The fifth step proposes to achieve analysis and optimization of the system sizing model. For that, gradient-based method is preferred and used symbolic differentiation for elementary models derivatives. The formulation for multidisciplinary sizing models is the NVH. The optimization relies on the computational core of openMDAO [89]. A spreadsheet formalism is used to parameter the analysis and optimization and visualize results. The computational model can be exported as a Python Serialization Object to be used externally of BOA framework. This step is supported by the Design environment of the in-house BOA framework.

The sixth and last step enables to explore the design space by using Design of Experiments and multidisciplinary analysis. Results can be visualized and filtered using the parallel coordinates plot. As for the Design environment, the computational model can be exported. This step is supported by the Explore environment of the in-house BOA framework.

The summary of this design and sizing methodology is given in Table 4.1.

Table 4.1 Methodology summary

Process	Methods	Tools
Step 1: Requirements, design drivers and sizing scenarios definition	Design drivers & Sizing scenarios graph	Graphviz Database
Step 2: Elementary computational model generation	Scaling laws Datasheet regression FEM surrogate models Lumped parameter surrogate models	Numpy Scipy pyDOE + Scikit-Learn pyDOE + pyFMI + Scikit-Learn
Step 3: Elementary models assembly into reusable component sizing models	Acausal modelling Symbolic computing Graph algorithms Bipartite graph representation Model library	Block Generation environment (BOA)
Step 4: Component model assembly into a system sizing model	Causal modelling N2 diagram Hierarchical decomposition Model library Project library	Sizing Procedure environment (BOA)
Step 5: Analysis and optimization of the system sizing model	Multidisciplinary Design Optimization Gradient-based method Gradient-free method Symbolic differentiation NVH formulation Spreadsheet Project library Model export	Design environment (BOA)
Step 6: Design space exploration of the system sizing model	Multidisciplinary analysis Design of Experiments Parallel coordinates plot Project library Model export	Exploration environment (BOA)

The framework development required one and a half year of intensive work and a year of continuous improvements when achieving the case studies with it. The development can be decomposed by the different modules that form the framework given in Figure 4.27.

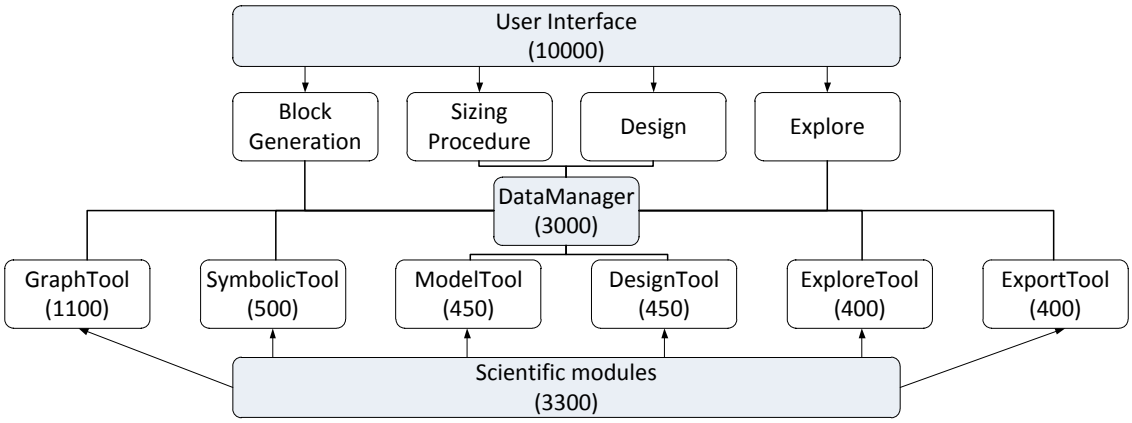

Fig. 4.27 Amount of work for the BOA framework implementation: number of code lines in parenthesis

The *User Interface* was a significant work amount, around some 10000 lines of codes (LoC), and was achieved mainly by internships within the laboratory. The *DataManager* module handled the structure of models and libraries and is the meeting point of all the others modules. It required around some 3000 LoC for it to be functional. The most important part that reflects the work of this thesis is the scientific modules (3300 LoC). The GraphTool is only used by the *BlockGeneration* environment was one of the most intricate work (1100 LoC). It was combined with the *SymbolicTool* module (500 LoC) in order to provide the acausal modelling capabilities. *SymbolicTool* module was also used to obtain the analytic derivatives used in the *Design* and *Explore* environments. *DesignTool* (450 LoC) and *ExploreTool* (400 LoC) were respectively used by the *Design* and *Explore* environments. Both also used the *ModelTool* (450 LoC) used to adapt our model structure to the openMDAO API. They also use the *ExportTool* (400 LoC) to generated Python Object models that can be used externally of the framework.

Nevertheless, the LoC indicator does not assess the amount of work required to decide and specify which features should be implemented and how they should be. The BOA framework started from a blank sheet and is at this date a optimized and tested sizing tool.

4.7 Conclusion

This chapter has outlined a design and sizing methodology for complex technological systems. This methodology was illustrated through a case study: a Thrust Vector Control electro-mechanical actuator.

Emphasis has been placed on knowledge capitalization and reusability as well as rapid decision making. Another objective was also to provide an environment which enables a collaborative work between engineering specializations experts during sizing.

An answer to these challenges was to propose a first essential step where different stakeholders can interact and structure their respective design constraints and needs. This way modelling needs for the sizing process are better defined. The choice to use algebraic models which can come from different types of models and tools enables to have lightweight and acausal reusable models that are stored in libraries. All models have an attached documentation that can refer to more detailed technical documents. Algebraic model enable to compute symbolically their partial derivatives used during system gradient-based optimization. The N2 diagram used in the Sizing Procedure environment provides a convenient way of constructing and visualizing the model structure. The framework enables to deal with large multidisciplinary systems by using hierarchical decomposition of models to maintain reasonably complex models. It is also capable of handling coupled systems by providing an quasi-automatic NVH formulation. Optimization and DOE driven analysis are achieved it most cases within seconds thanks to gradient-based algorithms, symbolic differentiation derivatives of model elements, the MAUD architecture of openMDAO, the low computational cost of algebraic models and the performances of the NVH formulation. The framework includes convenient parametrization and visualization user interfaces for design optimization and design space exploration.

The design and sizing methodology and framework outlined is this chapter will now be used for the sizing of typical aerospace actuation system applications. Chapter 5 deals with the design of an primary flight control actuation system with the particularity to integrate 3D model knowledge in the sizing. Chapter 6 concerns the design of a electrical thrust reverser actuation system with emphasis placed on integrating 0D-1D model knowledge in the system sizing model.

Chapter 5

Primary Flight Control Actuation System Design

5.1 Introduction

The primary flight control system provides the pitch, roll and yaw control of an aircraft. This system is one of the most critical system of an aircraft since the loss of control of the aircraft leads to a crash. As part of this system, the primary flight control actuation system is also a high criticality system. Hence, it shall be designed adequately. An extract of one certification basic requirement for aircraft system and equipment design is the following [72]:

"The aeroplane systems and associated components, considered separately and in relation to the other systems, must be designed so that

- Any catastrophic failure condition
    1. is extremely improbable; and
    2. does not results from a single failure; and
- Any hazardous failure condition is extremely remote; and
- Any major failure condition is remote."

Hence, no single failure of an actuation system component or equipment shall lead to a losses of the function. This is why each control surface is actuated by at least two parallel actuators with segregated power supplies. Fully Fly-by-Wire aircraft requires three independent power sources to be controllable at all time. Hence, three power sources is a reliability and certification requirement for civil aircraft. Some large aircraft like B747, A380, B787 and A350 use an additional power source which provides a redundancy beyond certification requirements. The Airbus A380 was the first commercial aircraft to integrate electrically supplied actuators: Electro-hydrostatic Actuators (EHA). The three hydraulic power sources cannot be all positioned under the cabin due to uncontained engine rotor failure which can chop the hydraulic pipe and cause a failure. Thus, it was necessary

to introduce an electrical power network that can be positioned above the passenger cabin whereas hydraulics are not permitted due to the harmful characteristic of hydraulic fluid. It was decided to use two hydraulic power sources and two electrical power sources for flight control actuation system as shown in Figure 5.1.

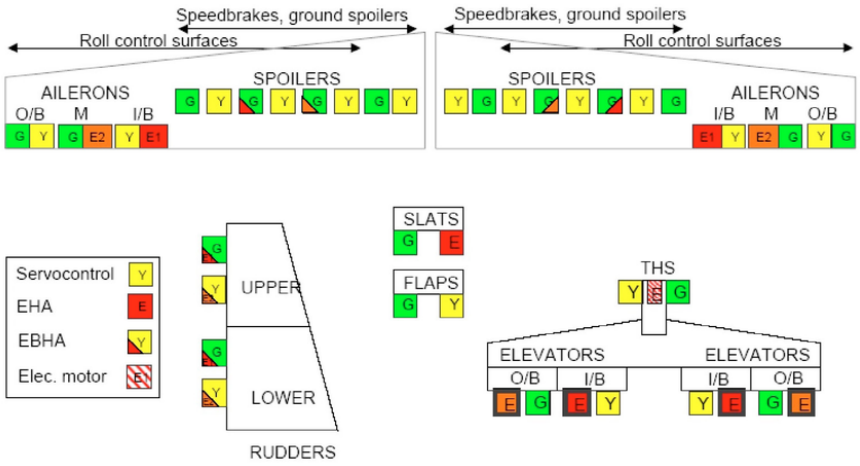

Fig. 5.1 Airbus A380 flight controls architecture [234]

Removing the third hydraulic network resulted in significant weight savings due to the largeness of such aircraft [234]. The aileron surface had to be split in three elementary surfaces as shown in Figure 5.1. This was due to wing deflection requirements but it consequently provided a higher reliability and more control degrees of freedom for passenger comfort and gust load alleviation [49, 50].

One main assumption made in this chapter is that the allocation of control surfaces are determined by the aircraft flight envelop requirements and are not part of the actuation system design. Nevertheless, the present study can be integrated within control surface allocation problems and find a more globally optimized solution at aircraft level [38, 57].

The main topology of flight control surface actuators is the linear topology. The linear topology choice was straightforward for conventional hydraulic systems due to the linear motion of hydraulic cylinders. This topology has been seen in many aerospace actuator developments. However, rotary topology are also investigated either electro-hydraulic [236] or electro-mechanical [53] technologies particularly for hinge moment surfaces.

This chapter is organized as follows. First, a review of fixed-wing aircraft primary flight control actuation system is presented. Then, standardized actuation system with control surface splitting and actuators architectures are proposed. Subsequently the assumptions and sizing process of the actuators is outlined. Sizing models for control surfaces and wing/surface attachments are also outlined. Finally, an optimal sizing of the complete actuation system is described and results are presented.

5.2 Review of Power-by-Wire Primary Flight Control Actuation System Design Drivers

This section focuses on the main design drivers of Power-by-Wire Primary Flight Control Actuation System (PFCAS) and associated actuator technologies. The considered primary flight control surface are ailerons, elevators and the rudder. The actuator technologies discussed are linear electro-hydrostatic actuators (EHA) and electro-mechanical actuators (EMA) as well as rotary electro-mechanical EMA.

5.2.1 Primary Flight Control Actuation System Level

Reliability requirements at primary flight control level lead to fail-safe control surfaces with the most low failure rate (typically 10^{-9}). Such reliability requirements lead to either parallel redundant actuators or duplex actuators. In order to provide Power-By-Wire to the actuators, aircraft using such technologies have at least one electric power supply and associated distribution systems. Recent aircraft developments use two hydraulic and two electric power supplies (the Airbus A380, A400M and A350) whereas lighter aircraft may use two hydraulic and one electrical power supply (the Gulfstream G650). The actual trend is the electrification of the flight control actuators. While Horizontal Stabilizers surfaces have been using redundant electro-mechanical actuators, primary flight control surfaces have only been using Power-By-Wire actuators in back-up especially due to the lifetime limitation of EHAs except some of the Boeing 787 spoilers. The first aircraft with a fully electrically supplied primary flight control actuation system is the Lockheed Martin F-35 as illustrated in Figure 5.2.

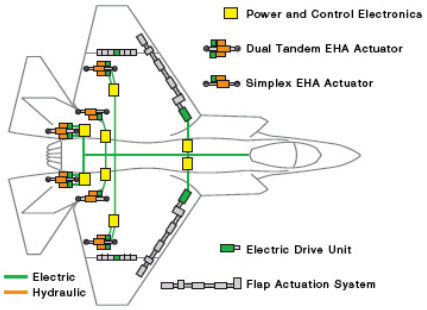

Fig. 5.2 The F-35 full Power-by-Wire architecture (MOOG)

The main objective for such implementation was to win maintenance cost and availability penalized by hydraulic actuator and network maintenance which are also key design drivers.

Generally, flight control structure tend to use composite alloys. One main design driver of the actuation system is to not damage the control surface structure or wing structure. Furthermore, a maximum skin temperature is specified for actuators in order to protect the environment surrounding composite structure from overheating since it is linked through heat conduction to actuators. In

addition, ailerons are closed to fuel tanks and require class H maximum temperature according to DO-160 [191].

The common architecture for primary flight control actuation systems is to have two actuators per surfaces with simplex electronics and electrical motor. At system level, another design driver is the total power consumption of the actuation system has an effect on the overall aircraft design like other non-propulsive airframe systems [213]. The power required by primary flight control actuation systems is mainly linked to the load because of the low speed levels needed. Hence, the power required is a function of the control surfaces hinge moment which are generally proportional to aircraft size and cruise speed, and the flight envelop. Aileron surfaces are particularly subject to high aerodynamic load during cruise. Hence, the nominal operating point remains close to peak power operating points when compared to other surfaces such as spoilers. Figure 5.3 shows that the load requirements for an Airbus A320 are close to a generic mission profile whereas the required speed is far from the general usage.

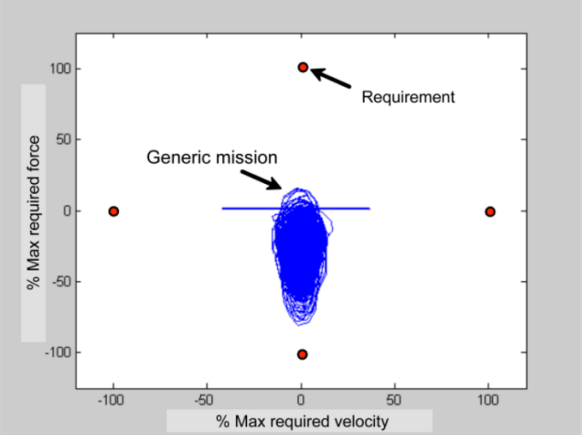

Fig. 5.3 Power requirements for an Airbus A320 aileron actuator [153]

The aileron behaviour is similar to the elevators and the rudder. They are almost permanently acting against aerodynamic loads with very small deflection due to high stability during cruise and the high effectiveness of control surfaces at high speeds [203].

Aerodynamic flutter can be a design driver for actuation systems. Flutter is due to a coupling phenomena between detachment of a wing swirling flow and the wing structural modes [81]. Control surfaces are particularly subject to this complex phenomena depending on the flight envelop. Solutions to the handling of flutter can be to either introduce weight balancing of the control surface (e.g blow horn on ATR 72) or to increase the strength of the structure so it can handle it. In general, it is preferred that the flutter is handled by the actuation system by providing passive damping by means of actuators. Active flutter control by means of the actuation system is also investigated [144]. The evident but important design driver for actuation systems with regard to flutter is that any elements of the system shall not be a generator of flutter.

One other main design driver of the primary flight control actuation system is that is has to fit in the allocated space of the aircraft. The space required by pin to pin linear actuator make rotary solution more convenient especially for hinge line surfaces [245]. For flaps, the actuation system requires to change the shape of the airframe especially due to the kinematic and usually far from the optimized aerodynamic shape. Similarly to other airframe systems, weight is a key design driver. Thus, emphasis is placed on weight reduction and leads to more and more challenging mass requirements for actuators and power electronics. The maintenance cost expectations are also increasing. Hence, actual specifications require maintenance free actuators.

5.2.2 Actuation Level

Reliability requirements for single failure lead to two simplex actuators in parallel per surfaces as one single actuator does not meet the minimum failure rate requirement of 10^{-9} for catastrophic failures. Duplex actuators are also used for instance in rotorcraft flight controls [43] and in F-35 stabilizer surface (Figure 5.2). Nevertheless, the main architecture for primary flight control surfaces actuators in a simplex topology with segregated power supplies.

The aircraft flight profile has an effect on the load and speed needs of control surfaces. The mission profile of an actuator is transformed into maximum load and continuous load specifications as well as maximum speed. Fatigue cycles can also be specified after analyzing the mission profile. The theoretic peak power consumption of the actuator is estimated and specified in order to avoid a re-design of the aircraft generators and power network. The specifications are key design drivers for actuators and have a direct effect on the design (architecture) and the sizing (mass, geometry).

The flutter phenomena requires to specify some actuator characteristics. The actuator shall have a maximum reflected inertia especially for electro-mechanical technologies where the motor inertia through the reduction stages leads to important reflected inertia values. Minimum values of actuator stiffness (when unactive) and dynamic stiffness (when operating in closed-loop) are also given. The stiffness and dynamic stiffness for hydraulic actuators can be challenging due to fluid compressibility which leads to a natural stiffness. Conversely, reflected inertia requirement will be challenging for electro-mechanical technologies. Maximum backlash requirements were also introduced for electro-mechanical devices as such characteristic can lead to low closed-loop performances and flutter. A minimum passive damping is also required to damp potential excitations of the rotating control surface and avoid oscillatory phenomenons that can generate flutter. However, this value should also be set to a maximum in order to ensure back-drivability of the actuator during maintenance operations. Back-drivability is also linked to the reflected inertia to be moved and the friction in the power chain.

Even if Fly-by-Wire ensures the control of surfaces deflection the control surface require a passive stroke limitation. This is provided by actuators by integrating mechanical end-stops. The actuator shall provide active load limitation as well as passive load limitation. Activate load limitation is mainly used to control the load of the structure due to aerodynamic loads. This is achieved by actuator control algorithms. Passive load limitation is used to avoid over-loads on the control surface and

the actuator due to a wind gust or a runaway during maintenance operations. This in particularly important for electro-mechanical actuators which have high kinetic energy stored in the motor inertia and low softness (high stiffness) and thus leads to a high equivalent load when impacting end-stops.

The losses generated by the actuator have to be dissipated in the confined environment allocated to them. This is particularly true for aileron, elevator and the rudder surfaces whereas spoilers for instance are in an open environment when operating (deployed) except when operating in droop. The thermal requirements are given by a maximum skin temperature and a thermal load profile. The thermal boundary condition is usually that the actuator is only cooled by natural heat convection in a fixed volume of air. These thermal requirements are really important because they directly impact the sizing of actuators. A too hard thermal requirements will lead to large actuators which do not fit in the allocated space whereas too soft requirements can lead to non-compliant thermal performances during flight test and the development of solutions for force convection cooling which penalize the aerodynamic performances of the aircraft as shown in Figure 5.4.

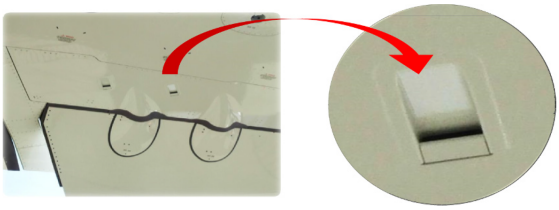

Fig. 5.4 Underwing scoops for actuator cooling (EHA of the Airbus A350 aileron) [152]

Other design drivers are the objective mass but especially the geometric integration constraints. Even if mechanical clearance is made between the rear spar of the wing and the forward spar of the control surface, linear Power-by-Wire actuators and their power electronics fit just in the allocated space [58, 152].

5.2.3 Summary and Discussions

A summary of the Primary Flight Control Actuation System level and actuation level main design drivers as well as their interaction is given in Figure 5.5.

As new aircraft concept tend toward thin and flexible wings, some forthcoming challenges for actuation systems appear. Thin wings can lead to a diminution to the space allocated to actuators. A miniaturization of them would require major technological breakthroughs. Despite that rotary on-hinge solutions seem more adapted for thin wing applications than classical linear topologies [232], the ratio between the hinge moment and the hinge line diameter can be in some cases too high. This can lead to the situation where no actual actuator technologies can match that ratio due the diameter of components, especially mechanical, for the required torque. For the considered diameter envelop and motor electromagnetic torque, other reduction stages have to be added to provide the required hinge moment. Adding these mechanical components in series increases the probability of

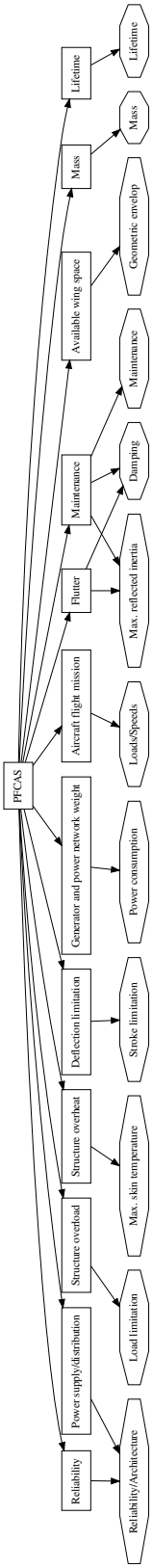

Fig. 5.5 PFCAS design drivers (rectangle) and actuation design drivers (octagon)

jamming and therefore the failure rate of the actuator. Figure 5.6 illustrates this remark for typical MTBF values of brushless motor, power electronics and mechanical gear stages.

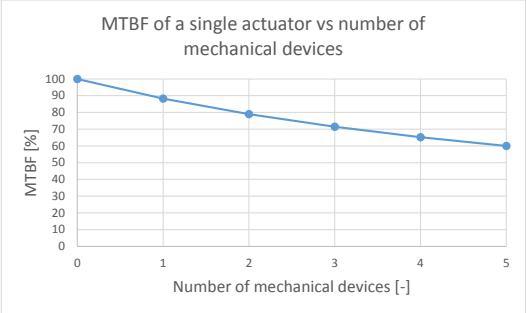

Fig. 5.6 Reliability analysis for different number of mechanical devices in the load path

Reducing the hinge diameter would limit the aerodynamic insights of a thin wing, however, reducing the length of control surfaces by splitting them into multiple elementary surface, as illustrated in Figure 5.7, can be a solution. Another option can be to change aircraft trajectories in order to reduce the performances of actuators [46] or a more drastric solution can be to reduce the flight envelop making the aircraft less manoeuvrable.

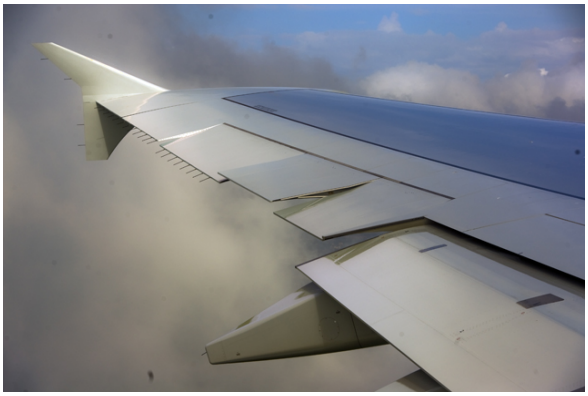

Fig. 5.7 Aileron control surface splitting on the Airbus A380 [2]

In addition, control surface splitting can lead to smaller inertia surfaces which would have less authority on the wing behaviour. Hence, investigations can be achieved to assess the wing behaviour subjected to free or damped small surfaces. Flexible wings can lead to active flutter requirements for actuation systems or a more tight calibration of damping and reflected inertia. Nevertheless, these flexible wings will also lead to re-think the allocation of control surfaces. Control surface positioning can also be considered during primary flight control actuation system trade offs [204]. However, for advanced concept with coupled aerostructural studies the trade-offs are more complex and require sophisticated simulation as outlined in Figure 5.8 [220].

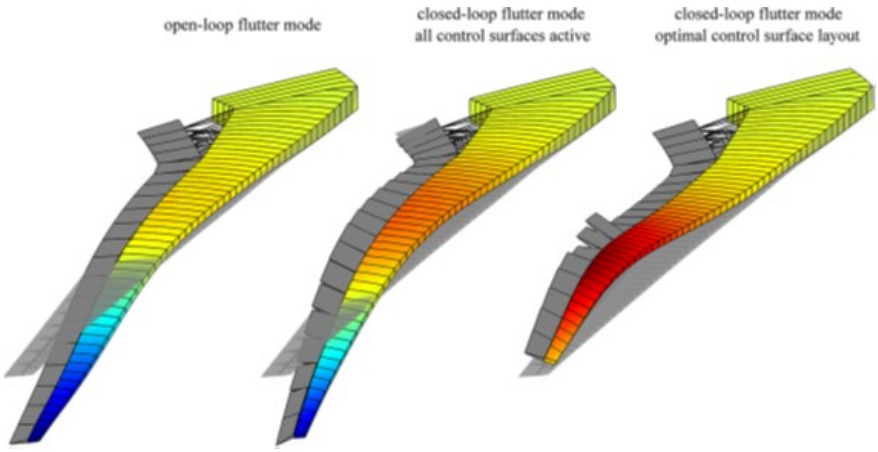

Fig. 5.8 Optimal Control Surface Layout for an Aeroservoelastic Wingbox [220]

Future investigation of novel wing and actuation concepts can use a more integrated design approach which can simultaneously assess the effects of structure, aerodynamics, control surface allocation and actuation on each other and on aircraft performances.

The question around which is best between electro-hydraulic technologies or electro-mechanical technologies for flight control actuation remains intricate and has no true answer at this date. However, clear advantages and drawbacks can be outlined for each technologies. As mentioned previously, EHAs will have a low reflected inertia and a low dynamic stiffness, conversely EMAs have a high reflected inertia and a high dynamic stiffness. The fact that the damping mode of hydraulic actuators operates on demand thanks to a bypass valve controlled by a solenoid ensures that the damping function of the actuator has no effect on its back-drivability conversely to EMAs. In addition, the electromagnetic torque of the motor is increased to compensate the equivalent viscous friction of damping. Furthermore, their low reflected inertia and low dry friction contribute as well to a reachable back-drivability. The high reflected inertia of EMAs can generate a high load when impacting end-stops due to the event of a runaway or a windgust. Therefore, passive load limitation devices like torque limiters much be added for such technologies in order to cancel the effect of such event and keep loads lower than the required hinge moment. This leads to large actuators and decreases the overall reliability by integrating additional components on the load path as mentioned previously. One other drawback of EMAs is the potential backlash which can lead to flutter. EHAs have very low efficiency mainly due to the internal leakage of pumps and additional iron losses in the hydraulic fret of the electro-pump. The thermal behaviour of both technologies is critical due to a non-effective cooling environment (natural convection). EHAs are interesting because the hydraulic fluid flowing through the airgap helps cooling the motor. However, for primary flight control surface the actuator mainly holds a load with no deflection. Hence, the electro-pump is permanently rotating in order to compensate the internal leakage of the pump leading to thermal runaways [152]. The lifetime of EMAs can be considered as higher than EHAs because of the lifetime limit of pump technologies as this date and this is one of the reasons why EHAs have not been utilized in the front-line yet.

Furthermore, autonomous EHAs are under investigations and operating EHAs are connected to the hydraulic network in order to refill them from time to time to compensate external leakage. EMAs on the other side seem more adapted to long life application since the only maintenance required is to change or refill the oil lubricant. Nevertheless, rotary solutions provide seals with do not translate relatively between parts and thus provide no external leakage and maintenance free solutions [245]. Furthermore, this enables to avoid the contamination of the oil lubricant and thus decrease the risks of jamming. The translational motion of linear actuator also engenders a "pumping" effect. This is due to the change of volume in the actuator during extension/retraction. The "pumping" leads to the introduction of air and thus humidity problems. However, the modelling of fatigue for rolling elements in electro-mechanical actuators remains a challenge especially for gear stages with no complete revolution. The event of jamming in EMAs is also a concern and test campaign shall prove their robustness. An option to handle such event is to accept it by splitting control surfaces, like ailerons for instance, and degrading the roll performances of an aircraft but not loosing the function [74].

At this date, no decision can be made on eliminating EHAs or EMAs for primary flight controls. Nevertheless in the future, an interesting configuration of flight control actuation system can be more two or three electrical networks supplying EHAs and EMAs integrated in parallel on surfaces and one hydraulic network supplying classical servo-hydraulic actuators.

One actual trend of aerospace actuation systems is standardization. Both actuator and power electronics may be developed with a modular approach [88]. Another trend can be to develop more integrated solutions. For instance electro-mechanical units and power electronics can be integrated in one same housing [232]. This can be extended to actuator and control surface development where control surfaces, which are often designed in fatigue, can sustain a peak load generated by an actuator runaway leading to the removal of addition passive load limitation devices. Furthermore, the control surface structure can be considered as a heat sink for the actuator and leading to more optimized motors, power electronics and actuators.

A more challenging but interesting concept of standardization can be to have one same actuator for aileron, elevator and the rudder control surfaces. This chapter proposes to use the developed methodology to investigate such a concept.

5.3 Proposed Primary Flight Control Actuation System

5.3.1 Actuation System

The studied actuation system is composed only of EMAs with segregated power supplies, 540V HVDC, for actuators of a same surface. Nevertheless, the design approach can be extended to configurations that mix both EHAs and EMAs. The studied control surfaces are ailerons, elevators and the rudder for an Airbus A320 like aircraft.

It is chosen to consider control surface splitting as a design freedom. Hence, the number of elementary surfaces for each primary flight control surface has to be determined. Control surface

splitting enables to decrease the hinge moment of a surface and thus the required actuator torque. This leads to actuator architecture with less gear stages. Small and low inertia elementary surfaces also enables these surfaces to have less authority on the wing behaviour when studying flutter. In addition, splitting control surfaces increases the reliability of flight control as the loss of one elementary surfaces does not lead to a loss of the total surface function. The elementary control surfaces are all actuated by two parallel EMAs in active/damping configuration. Furthermore, control surface splitting can lead to configurations where elementary control surfaces of ailerons, elevators and the rudder are actuated by one same pair of actuators.

However, splitting control surfaces conducts to some disadvantages. Some elements do not benefit of this load reduction such as attachments, power electronics modules and connectors. Hence, increasing the number of surfaces will increase the overall weight of these elements. Furthermore, increasing the number of actuators increases the number of command path from the Flight Control Computer (FCC), thus requests redesign considerations. In addition, it will also increase the number of operations during actuator maintenance. Finally, the structural design will require additional design and analysis when compared to a single surface.

The chosen integration configuration is to use rotary on-hinge EMAs. This enables to reduce chord wise mechanical clearance when compared to linear actuators and free some space for fuel tank. Rotary configuration provide a maintenance free lifetime and an enhanced reliability due to the lack of contamination of the lubricant. Furthermore, such integration topology seems to be the most optimized for hinge applications like aileron, elevator and the rudder. It is chosen to specify actuator to have one packaging for the power electronics and electro-mechanical unit as suggested by Todeschi and Salas in Figure 5.9.

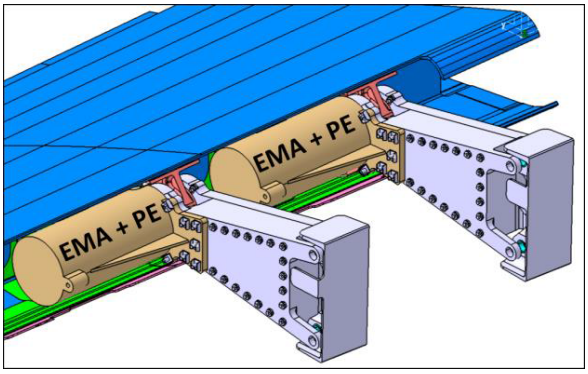

Fig. 5.9 Example of on-hinge rotary EMA for future thin wing application: EMA + Power Electronics (PE) in a same packaging [232]

Such integration concept leads to more compact solutions and less "open" electrical interfaces since the inverter, the motor and sensors are in the same housing. Another choice made was to fix the housing of the actuator to the wing whereas the actuator output is fixed to the control surface similarly to Figure 5.9.

5.3.2 Actuator Architecture

For the selected architecture, emphasis is placed on compactness and simplicity. The actuator is composed of an electro-mechanical power chain and an electronic chain as illustrated in Figure 5.10.

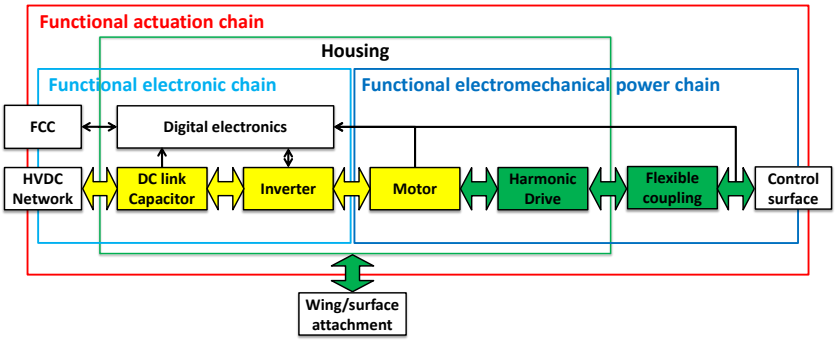

Fig. 5.10 Rotary EMA architecture

The electronic chain is composed of a DC link capacitor that limits the voltage ripple due to the switching the inverter transistors. The inverter drives the three-phase brushless motor with each bridge composed of a SiC MOSFET chip and a diode. Digital electronics are used for control, sensors, communication and monitoring but are not sized in this work. The digital electronic unit and the inverter are part of a single off the shelf power core module. Thus, geometry and mass are fixed. Nevertheless, operating temperatures must be checked during the sizing process as the load varies with the sizing of the electro-mechanical power chain and cooling part adapted. Besides, the capacitor is the only component that is sized.

The electro-mechanical power chain is composed of a permanent magnet synchronous motor which is chosen for its compactness and reliability. It converts the electrical power into rotational mechanical power. It is also composed of one gear stage, a Harmonic Drive, selected for its high reduction ratio, zero backlash and relatively low stiffness which can be used to absorb the kinetic energy of a runaway. A flexible coupling is also added in order to handle potential misalignment between the actuator and the hinge line and avoid hyper static assemblies which can degrade the lifetime of the actuator and the assembly. The EMAs is piloted in position with three cascade feedback loops: motor current, motor speed and actuator deflection. Active load control is also included in this control scheme by adding the load sensor information.

The actuator design is chosen to be more integrated. Hence, no runaway overload protection devices like spring, torsion bar or torque limiter are used. Thus, the overload generated by a runaway should be within the limit load of the control surface structure. Typically, on rotary actuators of this scale a runaway leads to 1.5 to 2.0 times greater peak torque than the operational peak torque requirement. Hence, the runaway event would probably not oversize the control surface structure as fatigue is more dominant than peak loads.

The housing is in the shape of a cylinder and has three main functions for the actuator: integrate the actuator components, transmit load between the electro-mechanical power chain and the wing assembly and act as heat sink to cool the electrical motor and the power electronics. The design and sizing of the control surface and the wing/surface attachment will be discussed in further sections of this chapter.

5.3.3 Design Drivers

Actuation System Design Drivers

This part outlines the design drivers at actuation system level. First, the ones not considered during sizing are given, then the ones which are included in the sizing problem are presented.

The reliability criterion for the actuator is covered by the selected architecture. The low number of components and the rotary configurations enable to obtain a compliant MTBF. The backlash requirement is necessary in order to prevent from flutter or non-compliant control performances. However, this is covered by the selected architecture where a single zero backlash gear stage is used. The damping requirement for an electro-mechanical actuator can be ensured by introducing a carefully selected amount of iron losses in the brushless motor [187]. This criterion is not included in the preliminary sizing of the motor and can be compensated by adding length to the motor during detailed design. The back-drivability design driver is not included in the sizing as it is dependent of the maximum damping and therefore can be achieved during detailed design. The dynamic stiffness and mechanical stiffness requirements for the actuator are covered by the fact that the EMA technology is chosen. Passive stroke limitation is achieved by integrating external mechanical end-stops to the actuator but is not included in the sizing problem as well as active load limitation. The maintenance and lifetime design drivers are also covered by the selected architecture as the rotary solution provide no maintenance operation for the lubricant. Nevertheless, the lifetime objective is used during sizing as mechanical components are sized in fatigue.

Overload protection due to a runaway event is a design driver which is considered during sizing. Despite that no specific devices are added, this design driver has an effect on the motor, the Harmonic Drive, the flexible coupling and the control surface. During the proposed sizing, emphasis is placed on thermal performances. Hence, maximum skin temperature design driver is considered during the sizing problem. Geometric integration is checked in the sizing process in order to provide actuator solution which can be integrated within the allocated space. The mass is an important design driver as it will be the quantity of interested to be minimized.

Component Design Drivers

This part outlines the design drivers of actuator components. It mixes selection parameters and technological limits of components that have to be considered to achieve a holistic sizing of the actuator.

The DC link capacitor provides a capacitive effect which limits the voltage ripple on the DC bus. Hence, the capacity value of the DC capacitor is one of its design drivers. Here, a film technology capacitor is used. The technological limit of such capacitor is its maximum hot spot temperature. A too high hot spot temperature can lead to a degradation of the insulation material. The temperature of the capacitor is determined by its thermal resistances and its losses which mostly are Joule losses. Therefore, depending on the application either the capacity value or the thermal behaviour determines the size of the capacitor.

One main design driver of the inverter is its switching frequency. The technological limit of a diode and the SiC MOSFET is their maximum temperature which is thus another design driver. The choice of switching frequency depends on the load to be driven and the thermal configuration as high switching frequency will lead to high commutation losses. The size of the diode and the SiC MOSFET chip has an effect on their electrical resistance and thus conduction losses. In addition, their size has an effect on their thermal resistances and therefore their thermal behaviour.

The main design driver of a brushless motor is its operating electromagnetic torque. This torque is either limited by the magnetic saturation of the iron core or the maximum winding temperature depending on the application. As primary flight controls actuators are operating during the entire flight which the duration is above thermal time constants of the actuator. Thus, the design driver of brushless motors in such application is their thermal behaviour. To determine the temperature, winding Joule losses and iron losses have to be determined. In addition, the equivalent conduction thermal resistance between the winding hot spot temperature and the external stator has to be determined to evaluate the winding temperature. Another technological limit of the brushless motor, and thus design driver, is its maximum mechanical speed. Furthermore, for high acceleration applications or applications involving runaway scenarios the motor inertia is an important design driver.

The main selection parameter of the Harmonic Drive, like other reducers, is its reduction ratio. Its peak torque or fatigue torque are as well design drivers as they determine its size. In addition, as the reducer is used to absorb the shock of a runaway, its stiffness is also a design driver for primary flight control actuators. The inertia of the harmonic driver has also an effect on the total reflected inertia and has therefore to be included as well.

The flexible coupling is here to deal with potential radial misalignment between actuator and hinge line as well as avoiding hyperstatic assembly. The main design driver of this component is its misalignment tolerance. The misalignment value enables to select a flexible coupling topology but does not depend on the sizing. Conversely, once the topology is chosen, the design drivers which determine the size of the flexible coupling are the peak torque or the fatigue torque depending on the application.

The housing design drivers are is thermal behaviour, its mechanical behaviour and the size of components to be integrated. The maximum skin temperature requirement leads to thermal analysis of the housing. Thus, the convection thermal resistance between the housing skin temperature and the wing skin temperature has to be determined. In addition, the housing is used as a heat sink for the power electronics and the brushless motor. The housing has also to sustain the mechanical loads

it is subject to. The vibratory environment of a very harsh in flight controls, hence it is chosen to size the housing for its maximum mechanical stress based on vibration analysis and not mechanical transmission. Therefore, both thermal behaviour and mechanical behaviour will determined influence the size of the housing.

5.3.4 Sizing Scenarios

The mission profile analysis enables to determine the maximum operating torque and speed requirements for the brushless motor as well as the equivalent fatigue torque for the flexible coupling and the Harmonic Drive. This torque and speed requirements enable to select these components size but the effect of other sizing scenarios on their size have also to be assessed.

Other sizing scenarios are the ones that estimate the components temperatures. Perfect thermal conduction is considered between the housing and the other components. Thermal grease is used for the power electronics and the glue between the motor stator and the housing guarantees heat conduction. The operating point considered is during cruise with maximum load and a relatively low speed. The maximum temperature of the capacitor is a function of its intrinsic thermal resistance, the housing thermal resistance and the Joule losses. The diode and the SiC MOSFET transistors temperatures are a function of their thermal resistances and the housing resistances and their commutation and conduction losses. The motor winding temperature is a function of its thermal conduction resistance, the housing thermal resistance and losses. The losses considered are Joule losses in the copper and the iron losses. The housing skin temperature is a function of its natural convection thermal resistance and the losses of the power electronics components and the motor.

The reflected inertia design driver leads to another sizing scenario. This scenarios is a function of the motor, Harmonic Drive inertia and reduction ratio. The contribution of the flexible coupling to the total reflected inertia is neglected.

Runaway generates a higher load than a wind gust. Hence, only the load generated by a runaway is determined and used in the sizing. The runaway scenario is a function of inertias, stiffness, motor speed and maximum electromagnetic torque. Hence, the choice of the reduction ratio also influences this scenario. Here, it is considered that the equivalent inertia involved is the sum of respective inertias of the motor and the Harmonic Drive. Only the reducer and flexible coupling stiffness are considered for the equivalent stiffness. The speed of a runaway at the actuator output is considered to be the maximum mechanical speed required by the mission profile for which the motor has been sized.

The vibratory specifications is a sizing scenario that provides inputs for the vibratory analysis of the housing. Another sizing scenario is geometric integration. It estimates the size of the overall actuator and verifies that in fits in the space given for a single actuator. Power electronics are considered to have a fixed sizes where as the housing, the flexible coupling, the reducer and the motor sizes are variables. The last considered sizing scenario is the system total mass estimation which will be dependent of the sizing results for the housing, the flexible coupling, the Harmonic Drive and the motor conversely to power electronics which have been selected.

5.3.5 Summary

A summary of the components design drivers, system design drivers and sizing scenarios considered for the actuator sizing is illustrated in Figure 5.11.

It is notable that different sizing scenarios have an effect on each other. The runaway sizing scenario seems to interact with many design drivers like mechanical stiffness and inertia. Furthermore, the reduction ratio has an effect on the motor torque, thus size, as well as the runaway and reflected inertia. In order to organize the system sizing model and achieve the overall sizing the BOA framework will be used.

5.4 Actuator Sizing

In order to decompose the total sizing problem, this section focuses on the actuator sizing.

5.4.1 Sizing Scenarios Models

Torque and Speed

The torque and speed required at each component has to be computed. For that the torque and speed values have to be computed at actuator level. These values are obtained by analyzing the mission profile. The maximum hinge moment is extracted from the mission profile. Since an on-hinge topology is chosen it is directly the required maximum torque. Similarly, the fatigue torque is extracted from the mission profile as one reduction stage is used. Nevertheless, since control surface splitting is considered the torque value has to be divided. The splitting is achieved so that the torque of elementary surfaces is equal. Hence, the elementary surface maximum torque T_{surf} can be expressed as:

$$T_{surf} = \frac{T_{surf_{tot}}}{N_{surf}} \tag{5.1}$$

Where $T_{surf_{tot}}$ and N_{surf} are respectively the hinge moment of the total surface and the number of elementary surfaces.

A security factor k_{sec} is considered for estimating the EMA maximum operating torque :

$$T_{EMA} = k_{sec} \cdot T_{surf} \tag{5.2}$$

An over-sizing factor k_{os} discussed later is introduced in order to obtain the required torque for mechanical component:

$$T_{EMA_{mech}} = k_{os} \cdot T_{EMA} \tag{5.3}$$

The speed sizing values are the maximum speed Ω_{max} of the mission profile and the equivalent speed used to compute the temperatures Ω_{mean}. Ω_{mean} is computed as follows:

$$\Omega_{mean} = \left(\frac{1}{t_f - t_0} \int \mid \Omega_{surf} \mid^{1.5} dt \right)^{\frac{1}{1.5}} \tag{5.4}$$

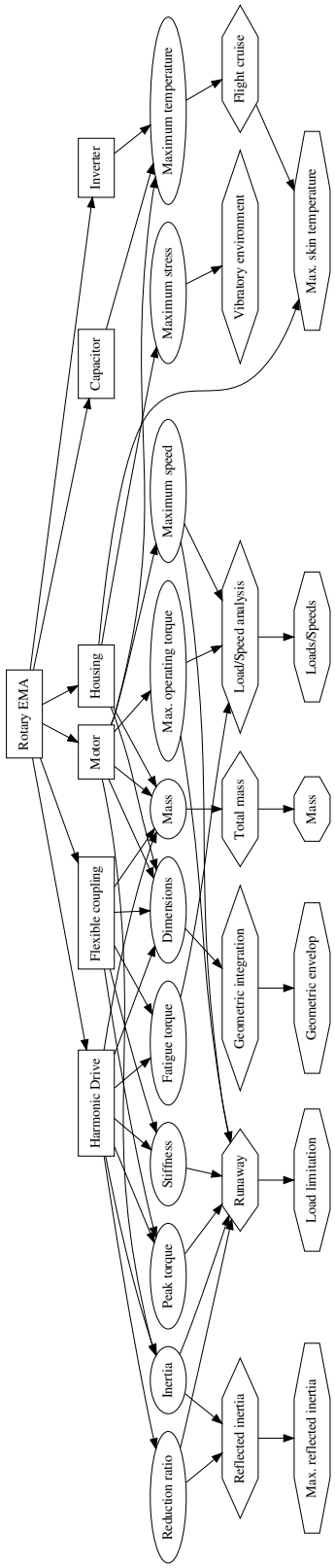

Fig. 5.11 PFCAS sizing problem component design drivers (oval), actuation system design drivers (octagon) and sizing scenarios (hexagon)

Where t_f and t_0 are respectively the final and initial time of the mission profile, and Ω_{surf} the instant rotational speed of the surface. The factor 1.5 is used since it is the exponent used for the electric pulsation, which is proportional to the speed, when estimating the motor iron losses using the Steinmetz model [207].

Once the torques and speeds are estimated at surface level, they are distributed at motor level:

$$T_{em} = \frac{T_{EMA}}{N_{red} \cdot \eta_{HD}} \tag{5.5}$$

Where T_{em} is the maximum electromagnetic torque of the motor, N_{red} and η_{HD} are respectively the reduction ratio and the efficiency of the Harmonic Drive. The maximum and mean speed of the motor are also derived:

$$\Omega_{mot} = \Omega_{max} \cdot N_{red} \tag{5.6}$$

$$\Omega_{mot,mean} = \Omega_{mean} \cdot N_{red} \tag{5.7}$$

Thermal Behaviour

The characterization of the thermal environment of aileron actuators may be difficult due to the sensitivity to uncertain internal airflow. Hence, a conservative approach is to consider that the actuator is cooled only by natural convection. The operating point chosen to compute the temperature of components is an intricate concern. A detailed study of the thermal behaviour of an aileron linear EMA has been achieved [54]. Three designs are achieved. Two use a linear steady state thermal model to evaluate the actuator temperatures. The first design is obtained for the temperatures corresponding to the maximum torque of the mission profile. The second design is obtained for the temperatures corresponding to the RMS torque of the mission profile. The third design is obtained for the temperatures evaluated using the dynamic model response to the entire flight profile presented previously. A validation of each design is achieved by running the dynamic model for each configuration. The thermal response for the three designs have been achieved for the same operating speed Ω_{mean}. Thermal simulation validation results are illustrated in Figure 5.12.

The first conclusion is that the most critical flight phase for the thermal behaviour of an EMA is during cruise when the loads are high and the heat transfer is less efficient due to low air density despite that the ambient temperature is very low. The optimal mass was obtained for the complete mission profile scenario and an increase of 10 % was obtained for maximum torque. However, the sizing achieved for the RMS torque operating point was not compliant with thermal constraints. In the present study, it is therefore chosen to use the maximum torque T_{surf} to compute temperatures even though it is not the optimum. More details of the work achieved in [54] can be found in Appendix B. The chosen operating point T_{surf} and Ω_{mean} enable to determine the losses in the different components.

As the surfaces studied operate during the entire flight, the steady state response is used to compute component temperatures. Hence, only the losses obtained for the operating point and the

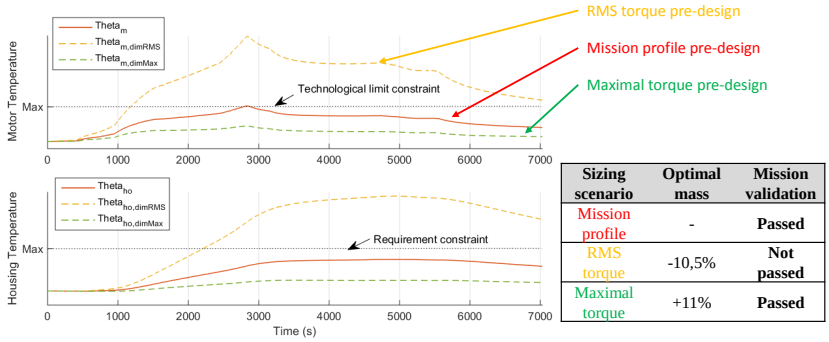

Sizing scenario	Optimal mass	Mission validation
Mission profile	-	**Passed**
RMS torque	-10,5%	**Not passed**
Maximal torque	+11%	**Passed**

Fig. 5.12 Thermal response of preliminary design over the entire mission

component thermal resistances are needed. These will be determined during the component estimation models description. The thermal losses in the Harmonic Drive are not considered during temperature estimation.

For example, the motor winding temperature is obtained as follows:

$$\Theta_{mot} = \Theta_{amb} + (R_{th_{conv}} + R_{th_{cd}}) \cdot P_{J_{mot}} + R_{th_{conv}} \cdot P_{ir_{mot}} \tag{5.8}$$

Where Θ_{amb} is the ambient temperature, $R_{th_{conv}}$ and $R_{th_{cd}}$ are respectively the natural convection thermal resistance between the housing temperature and the wing and the motor conduction thermal resistance between the winding and the stator skin. Finally, P_J and P_{ir} are respectively the Joule and iron losses of the brushless motor. The temperatures of the housing Θ_{skin}, diode Θ_{dio}, MOSFET Θ_{mos} and capacitor Θ_{capa} are obtained with a similar approach.

Reflected Inertia

The EMA shall have a maximum reflected inertia. This requirement strongly impacts the sizing of the motor as it depends on its inertia. It also influences the choice of Harmonic Drive as it depends on its reduction ratio and its inertia. This variable is expressed as follows:

$$J_{ref} = (J_{mot} + J_{HD}) \cdot N_{red}^2 \tag{5.9}$$

Where J_{mot} and J_{HD} are respectively the inertia of the motor and the Harmonic Drive. The flexible coupling inertia is neglected since it is positioned after the reduction ratio.

The maximum reflected inertia per surface is obtained by dividing the total surface inertia by the number of elementary surfaces.

Runaway

As mentioned previously, the runaway sizing scenario strongly impacts the electro-mechanical power chain design. Indeed, it generates the maximum stress on mechanical components (Harmonic Drive,

flexible coupling). It consists of the maximal torque capability of the EMA T_{EMA} and the inertial torque due kinetic energy stored in motor and Harmonic Drive inertias, at maximum motor speed capability Ω_{mot}, which is transformed into elastic energy in an equivalent torsional stiffness K_{eq} when impacting end stops. It is expressed as follows:

$$T_{RA} = \sqrt{K_{eq}\left(J_{mot} + J_{HD}\right)\Omega_{mot}^2} + T_{EMA} \tag{5.10}$$

The equivalent stiffness corresponds to Harmonic Drive stiffness K_{HD} and flexible coupling stiffness K_{FC} in series:

$$K_{eq} = \frac{K_{HD} \cdot K_{FC}}{K_{HD} + K_{FC}} \tag{5.11}$$

Vibration Analysis

The vibration analysis is used to size the housing. The stress due to vibration will be modelled by FEM and will be described in the housing estimation models section. Nevertheless, the boundary conditions are defined at system level by the DO-160 [191]. It is therefore chosen to evaluate simulations for a vibratory excitations of 20 g from 5 Hz to 2 kHz.

Geometric Integration and Mass

The geometric integration scenario verifies that the actuator fits diameter wise and length wise in the control surface. Therefore, the diameter and the length of the actuator have to be determined. The diameter is estimated as follows:

$$D_{act} = max(D_{mot}, D_{HD}, D_{FC}) + 2 \cdot e \tag{5.12}$$

Where D_{mot}, D_{HD} and D_{FC} are respectively the diameter of the motor, Harmonic Drive and flexible coupling, and e is the housing thickness.

The length of the actuator is obtained as follows:

$$L_{act} = L_{PE} + L_{mot} + L_{HD} + L_{FC} \tag{5.13}$$

Where L_{PE}, L_{mot}, L_{HD} and L_{FC} are respectively the height of the power electronics module (fixed), the length of the motor, Harmonic Drive and flexible coupling. The length-wise thickness of the housing is neglected and included in the integration margin discussed in Section 5.5.

The mass of the EMA is obtained by adding each component mass as follows:

$$M_{act} = M_{PE} + M_{mot} + M_{HD} + M_{FC} + M_H \tag{5.14}$$

Where M_{PE}, M_{mot}, M_{HD}, M_{FC} and M_H are respectively the mass of the power electronics module (fixed), motor, Harmonic Drive, flexible coupling and housing.

5.4.2 Estimation Models

Power Electronics

The power electronics components have fixed size. However, their thermal behaviour must be verified and can have an effect on the heat sink (housing) and electro-mechanical power chain sizing. To evaluate losses generated in MOSFETs, diodes and the capacitor, root mean square (RMS) and mean values of current passing through each component must be expressed. Here, RMS and mean values are expressed as a function of modulation index β [86]. Modulation index is computed with electrical properties of the motor and the operating point (torque and speed) and will be given in the motor models. We assume that the power factor $\cos(\varphi)$ of the electrical load is equal to 1.0 for the considered range of operating points. Conduction losses and switching losses are evaluated for the MOSFET using the following equations:

$$P_{cd_{mos}} = R_{d_{mos}} \frac{I_{peak}^2}{8} \left(1 + \frac{8}{3\pi}\beta\cos(\varphi)\right) \tag{5.15}$$

$$P_{sw_{mos}} = f_{sw}(E_{ON} + E_{OFF}) \frac{I_{peak}}{I_{peak_{ref}}} \frac{U_{DC}}{U_{DC_{ref}}} \tag{5.16}$$

Where $R_{d_{mos}}$ is the drain source resistance, f_{sw} is the switching frequency, I_{peak} is the peak current passing through one leg of the inverter and U_{DC} the DC bus voltage, E_{ON} and E_{OFF} the commutation energies, and $I_{peak_{ref}}$ and $U_{DC_{ref}}$ respectively the current and voltage for which the commutation energies have been measured.

Similarly the conduction and switching losses are expressed for the diode:

$$P_{cd_{dio}} = V_d \frac{I_{peak}}{2\pi} \left(1 - \frac{\pi}{4}\beta\cos(\varphi)\right) + R_{d_{dio}} \frac{I_{peak}^2}{8} \left(1 + \frac{8}{3\pi}\beta\cos(\varphi)\right) \tag{5.17}$$

$$P_{sw_{dio}} = \frac{1}{4} Q_{rr} \frac{I_{peak}}{I_{peak_{ref}}} \tag{5.18}$$

Where V_d, $R_{d_{dio}}$ and Q_{rr} are respectively .

Dielectric losses in the capacitor are neglected, only Joules losses generated by RMS current are considered. The RMS current in the DC bus capacitor can be expressed as follows [86]:

$$I_{capa_{RMS}} = I_{peak} \sqrt{\frac{\sqrt{3}\beta}{4\pi} + \left(\frac{\sqrt{3}\beta}{\pi} - \frac{9\beta^2}{16}\right) \cdot \cos(\varphi)} \tag{5.19}$$

The Joule losses generated by the capacitor are then estimated with respect to the RMS current and the resistance of the capacitor R_{capa}:

$$P_{J_{capa}} = R_{capa} \cdot I_{capa_{RMS}}^2 \tag{5.20}$$

Brushless Motor

The sizing model of the brushless motor used is based on the work of Sanchez [209, 207] who developed electromagnetic and thermal surrogate models based on FEM simulations illustrated in Figure 5.13.

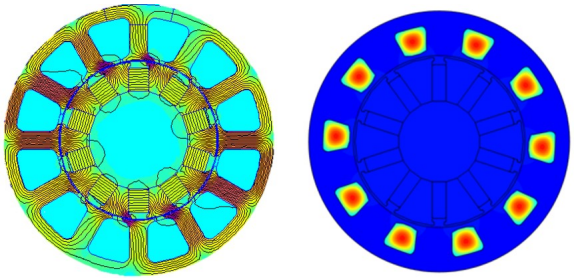

Fig. 5.13 Brushless motor electromagnetic (left) and thermal (right) FEM simulations [207]

A more detailed explanation of the following models can be found in Appendix B.

The linear electromagnetic torque of the motor $T_{em,l} = \frac{T_{em}}{L_{mot}}$ can be determined with the following dimensionless equation [207]:

$$\pi_0 = 1.72 \cdot 10^{-4} \cdot \pi_1^{1.142-0.262\log(\pi_1)+1.679\log(\pi_2)} \pi_2^{-2.256-0.721\log(\pi_2)+0.518log(\pi_2)log(\pi_1)} \tag{5.21}$$

Where $\pi_0 = \frac{T_{em,l}}{J_{cur}B_r D_{mot}^3}$ which represents the dimensionless linear torque, $\pi_1 = \frac{\mu_0 J_{cur} D_{mot}}{B_{sat}}$ which represents the magnetic saturation and $\pi_2 = \frac{e_y}{D_{mot}}$ which represents the quantity on iron the yoke and has a significant influence on the iron losses. With D_{mot} the stator outer diameter, e_y the yoke thickness, J_{cur} the current density in the windings, μ_0 the permeability of vacuum, B_r the induction of the magnet and B_{sat} the saturation value of the iron sheets.

Similarly, the conduction thermal resistance model between the stator skin temperature and the winding hot spot temperature is obtained using surrogate modelling and FEM simulations (Figure 5.13). The obtained surrogate model that represents the motor conduction thermal resistance is the following [209, 207]:

$$\pi_{cond} = 84.2 \cdot \pi_1^{-1.077+0.164\log(\pi_1)} \tag{5.22}$$

Where $\pi_{cond} = R_{th_{cond}} L_{mot} \lambda_{ir}$, $\pi_1 = \frac{D_{mot}}{e_N}$, and L_{mot} and D_{mot} are respectively the length and diameter of the motor, e_N is the Nomex insulation thickness, λ_{ir} is the thermal conductivity the iron.

In order to determine the thermal response of the actuator and motor, the motor losses have to be modelled. The losses considered here are the Joule losses and iron losses.

The Joule losses P_J in the motor are a function of the winding volume per slot pair V_w, current density J_{cur}, winding factor k_w, copper electrical resistivity σ_{cop} and the number of slots N_{slot}:

$$P_J = \frac{N_{slot}}{2} k_w \sigma_{cop} V_w J_{cur}^2 \tag{5.23}$$

The challenge to obtain an accurate Joule losses model is to have an accurate estimation of the winding volume. The winding volume per slot pair can be decomposed into the winding volume of the active part of the motor V_{slot} and the winding head V_{wh} as follows:

$$V_w = V_{slot} + V_{wh} = 2A_{slot}L_{mot} + 2\pi^2 \left(\frac{d_{tore}}{2}\right)^2 R_{tore} \tag{5.24}$$

Where A_{slot} is a single slot area, $d_{tore} = 2\sqrt{\frac{A_{slot}}{\pi}}$ the equivalent diameter of the winding head and $R_{tore} = 0.2877 \cdot D_{mot} \sin\left(\frac{\pi}{12}\right)$ the radius of the winding head from one slot to another.

Sanchez has also provided a surrogate model that estimates the slot area [207]:

$$\pi_{slot} = 2.31 \cdot 10^{-6} \cdot \pi_2^{-6.946-4.104\log(\pi_2)-0.833\log(\pi_2)^2} \tag{5.25}$$

Where $\pi_{slot} = \frac{A_{slot}}{D_{mot}^2}$ and $\pi_2 = \frac{e_y}{D_{mot}}$.

The second source of losses are the iron losses. The general expression of iron losses is the following:

$$P_{ir} = A \cdot V_{ir} \cdot B^2 \tag{5.26}$$

Where $A = k \cdot \delta_{p_{\frac{1}{50}}} \cdot \rho_{ir} \left(\frac{\Omega_{mot,mean} \cdot pp}{2\pi \cdot 50}\right)^{1.5}$, with k and $\delta_{p_{\frac{1}{50}}}$ loss factors measured for 50 Hz, ρ_{ir} the density of iron, $\Omega_{mot,mean}$ the operating speed of the motor for the temperature computation, pp the number of pole pair, and $B = B_y + B_t$, with B_y and B_t respectively the induction level in the yoke and the teeth.

A surrogate model for estimating the iron losses was also constructed [207]:

$$\pi_{P_{ir}} = 2.361 \cdot 10^{-2} \cdot \pi_1^{-0.498-0.0605\log(\pi_1)+0.496\log(\pi_1)^2} \cdot \pi_2^{-1.714-0.765\log(\pi_2)} \tag{5.27}$$

Where $\pi_{P_{ir}} = \frac{P_{ir}}{AL_{mot}D_{mot}^2 B_r}$, $\pi_1 = \frac{\mu_0 J_{cur} D_{mot}}{B_{sat}}$ and $\pi_2 = \frac{e_y}{D_{mot}}$.

The mechanical models of the brushless motor are also needed to evaluate mass, geometric integration, inertia and maximum mechanical speed.

The diameter of the motor D_{mot} is a design variable. Conversely, the motor length L_{mot} is obtained with respect to the required electromagnetic torque Tem and the linear electromagnetic torque $T_{em,l}$ obtained previously:

$$L_{mot} = \frac{T_{em}}{T_{em,l}} \tag{5.28}$$

The inertia is obtained as follows:

$$J_{mot} = J_{mot_{ref}} \left(\frac{L_{mot}}{L_{mot_{ref}}}\right) \cdot \left(\frac{D_{mot}}{D_{mot_{ref}}}\right)^4 \tag{5.29}$$

Where $J_{mot_{ref}}$, $L_{mot_{ref}}$ and $D_{mot_{ref}}$ are respectively the inertia, length and diameter of the reference motor. The diameter term $\frac{D_{mot}}{D_{mot_{ref}}}$ represent the effect of diameter on the rotor diameter.

The mass model is obtained using surrogate modelling:

$$M_{mot} = 5945.85 L_{mot} D_{mot}^2 e_y^{0.06654} \tag{5.30}$$

The motor maximum mechanical speed is obtained using a scaling law as follows:

$$\Omega_{mot_{max}} = \Omega_{mot_{max_{ref}}} \left(\frac{T_{em}}{T_{em_{ref}}} \right)^{-\frac{1}{3.5}} \tag{5.31}$$

Where $\Omega_{mot_{max_{ref}}}$ and $T_{em_{ref}}$ are respectively the maximum mechanical speed and electromagnetic torque of the reference motor.

The electrical model of the model is needed to evaluate the factor β used for the power electronics sizing.

The torque constant of the motor is derived using the DC bus voltage U_{DC} and the maximum operating speed of the motor Ω_{mot}.

$$K_e = \frac{U_{DC}}{2\Omega_{mot}} \tag{5.32}$$

The peak current can then be yielded:

$$I_{peak} = \frac{2}{3} \frac{T_{em}}{K_e} \tag{5.33}$$

The electrical resistance of one phase of the motor in obtained as follows:

$$R_{mot} = P_J \frac{2}{3} I_{peak}^2 \tag{5.34}$$

The electromotive force can also be derived for the operating point $\Omega_{mot,mean}$ used to compute the thermal response:

$$E = K_e \cdot \Omega_{mot,mean} \tag{5.35}$$

The effect of the inductor on the voltage when compared to the resistor is negligible. The phase voltage of the motor can then be obtained:

$$V = R_{mot} \cdot I_{peak} + E \tag{5.36}$$

Finally, the factor β is expressed as follows [86]:

$$\beta = 2 \cdot \frac{V}{U_{DC}} \tag{5.37}$$

Harmonic Drive

The Harmonic Drive is sized using algebraic models obtained through linear regression of catalogue datasheets as illustrated in Figure 5.14.

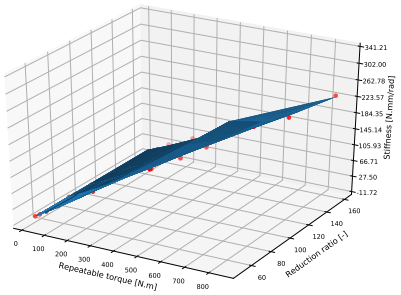

Fig. 5.14 Harmonic Drive stiffness linear regression with respect to repeatable torque and reduction ratio

The Harmonic Drive diameter D_{HD}, length L_{HD}, inertia J_{HD} , stiffness K_{HD} and mass M_{HD} are expressed with respect to the repeated peak torque T_{HD} and reduction ratio N_{red} as follows:

$$D_{HD} = 22.9 \cdot 10^{-3} T_{HD}^{0.31} N_{red}^{-0.12} \tag{5.38}$$

$$L_{HD} = 15.5 \cdot 10^{-3} T_{HD}^{0.275} N_{red}^{-0.141} \tag{5.39}$$

$$K_{HD} = 0.66 \cdot 10^{3} T_{HD}^{1.1} N_{red}^{-0.31} \tag{5.40}$$

$$J_{HD} = 3.8 \cdot 10^{-7} T_{HD}^{1.63} N_{red}^{-0.807} \tag{5.41}$$

$$M_{HD} = 2.55 \cdot 10^{-2} T_{HD}^{0.95} N_{red}^{-0.46} \tag{5.42}$$

Flexible Coupling

The flexible coupling topology is shown in Figure 5.15.

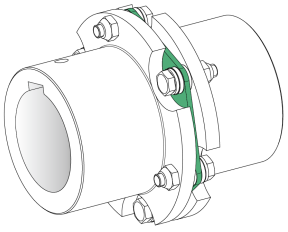

Fig. 5.15 Flexible coupling topology

Sizing models are based on scaling laws that assume that the flexible coupling is sized for constant mechanical stress. The diameter can then be estimated with respect to the required nominal (fatigue) torque T_{FC}, and reference component torque $T_{FC_{ref}}$ and diameter $D_{FC_{ref}}$:

$$D_{FC} = D_{FC_{ref}} \cdot \left(\frac{T_{FC}}{T_{FC_{ref}}} \right)^{\frac{1}{3}} \tag{5.43}$$

Similarly, the peak torque, length, stiffness and mass are determined:

$$T_{FC_{peak}} = T_{FC_{peak_{ref}}} \cdot \left(\frac{T_{FC}}{T_{FC_{ref}}} \right) \tag{5.44}$$

$$L_{FC} = L_{FC_{ref}} \cdot \left(\frac{T_{FC}}{T_{FC_{ref}}} \right)^{\frac{1}{3}} \tag{5.45}$$

$$K_{FC} = K_{FC_{ref}} \cdot \left(\frac{T_{FC}}{T_{FC_{ref}}} \right)^{\frac{1}{2}} \tag{5.46}$$

$$M_{FC} = M_{FC_{ref}} \cdot \left(\frac{T_{FC}}{T_{FC_{ref}}} \right) \tag{5.47}$$

Housing

The EMA housing acts as a heat sink and a mechanical link. It is assumed that the actuator is located in the wing with no airflow and only natural heat convection and radiation cools it. A surrogate model evaluates the thermal natural convection resistance between the EMA skin temperature and the wing skin temperature as a function of EMA geometry and losses. A detailed description of the model establishment can be found in [207] and examples of utilization can be found in [210, 53]. The integration and thermal configuration of the aileron rotary EMA is illustrated in Figure 5.16.

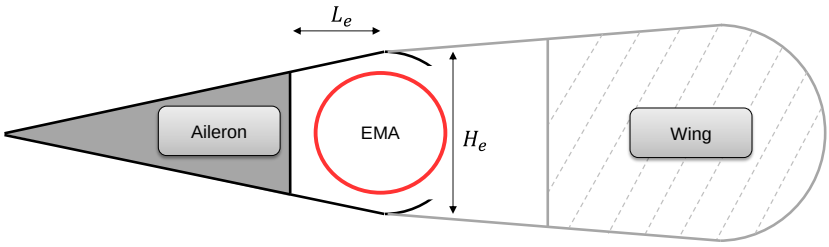

Fig. 5.16 Aileron rotary EMA integration and thermal configuration schematic

Some modelling assumptions are made:

- The heat transfer through the housing extremities is not considered. Hence, a 2D FEM model is used.
- Only natural convection cooling is assumed.

- Since the airframer requires that the structure cannot be used as a heat sink, the lateral wall of the model are considered adiabatic. The wing spar is far enough to consider that there is no confinement effect. Hence, it is considered as an open frontier.
- The upper and lower walls are the wing panels. The heat transfer at these surfaces level is modelled by a correlation law based for different air flow configurations on a NACA wing profile [241].
- The properties of air are assumed to be constant for the study, evaluated at the mean temperature and for cruise altitude.
- The size of the EMA integration environment is constant.
- The heat dissipated by the actuator is modelled by a volumic heat dissipated in the cylinder. Since natural heat convection is considered, the Grashof number will be used with respect to the heat flux density obtained for the exchange surface of the EMA and the total power to be dissipated.

The thermal resistance of the EMA housing $R_{th_{conv}}$ is a function of eleven physical quantities:

$$R_{th_{conv}} = f\left(L_{act}, \rho_{air}, C_{p_{air}}, \mu_{air}, \lambda_{air}, g\beta\delta\theta, h_1, h_2, L_e, H_e\right) \tag{5.48}$$

Where L_{act} is the actuator length, ρ_{air}, $C_{p_{air}}$, μ_{air} and λ_{air} are respectively the density, heat capacity, dynamic viscosity and thermal conductivity of the air, and $g\beta\delta\theta$ represents the Archimedes' force due to the temperature difference between the housing and the environment, and h_1 and h_2 are respectively the upper and lower wing panel convective heat transfer coefficients, and L_e and H_e geometric parameters of the environment.

The dimensional analysis and the Vaschy-Buckingham theorem enable us to reformulate Equation 5.48 in a dimensionless form:

$$\pi_{conv} = F\left(Gr_{L_{act}}, Pr, \pi_2, \pi_3, \pi_4, \pi_5\right) \tag{5.49}$$

Where $\pi_{conv} = \lambda_{air} L_{act} R_{th_{conv}}$, $Gr_{L_{act}} = \frac{\rho_{air}^2 g\beta\varphi_h L_{act}^4}{\lambda_{air}\mu_{air}^2}$ is the Grashof number defined for the dissipated heat flux density φ_h, $Pr = \frac{\mu_{air}\lambda_{air}}{C_p}$ the Prandtl number, $\pi_2 = \frac{L_e}{L_{act}}$ and $\pi_3 = \frac{H_e}{L_{act}}$ are the geometric ratios representing the actuator confinement, and $\pi_4 = \frac{h_1 L_e}{\lambda_{air}}$ and $\pi_5 = \frac{h_2 L_e}{\lambda_{air}}$ are dimensionless number that represent the thermal boundary conditions of the problem. The geometry of the environment is constant, thus L_e and H_e are constant. Therefore, π_4 and π_5 are considered constant. This enables us to reformulate Equation 5.49 with three dimensionless variables:

$$\pi_{conv} = F\left(Gr_{L_{act}}, Pr, \pi_2, \pi_3\right) \tag{5.50}$$

The surrogate model is then constructed based on FEM simulation results as illustrated in Figure 5.17.

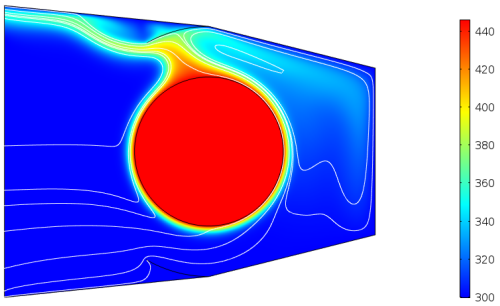

Fig. 5.17 Housing multi-physical FEM simulation

The regression of these results lead to the expression of the dimensionless variable representing the convective thermal resistance:

$$\pi_{conv} = 0.595\pi_1^{-0.00522}\pi_2^{-0.058}Gr_{L_{act}}^{-0.187} \tag{5.51}$$

The thermal resistance $R_{th_{conv}} = \frac{\pi_{conv}}{\lambda_{air}L_{act}}$ enables us to compute EMA skin, motor winding, capacitor, MOSFET and diode maximum temperatures using the different thermal conduction resistances and losses.

The EMA housing also acts as a mechanical link between the electro-mechanical power chain, power electronics and the wing/surface attachment. As vibrations are very important [110] for aerospace embedded actuators, a simplified sizing model is developed for the preliminary design of the rotary actuator housing under vibratory loads. The same approach is used for the linear EMA in Chapter 4. For this purpose, surrogate modelling techniques and dimensional analysis are used [209]. The vibratory loading problem is considered with the following simplified geometry: hollow cylinders for the housing, a full cylinder for the flexible coupling, reducer and motor, clamped boundary condition on one side. The effect of the reported weight of the actuator is neglected. The cylinder representing the flexible coupling, the Harmonic Drive and the motor is modeled using a low Young's modulus (1/10 of steel) to not increase the structure stiffness. A FEM modal analysis (Figure 5.18) is achieved and enables us to obtain: the resonance frequency, the modal form and finally the maximum stress for a given acceleration load.

The use of the Buckingham Theorem and dimensional analysis enables to reduce the number of variables to express a physical problem. For our example, after analysis of maximal stress, displacement and resonance frequency, the maximum stress σ at resonance frequency under a vibratory load can be expressed with the dimensionless following form:

$$\frac{\sigma}{Q_m a d \rho} = f\left(\frac{L_{act}}{d}, \frac{e}{d}\right) \tag{5.52}$$

Where a is the acceleration of vibration, ρ the volumic mass, d the components diameter (housing inner diameter), L_{act} the actuator length and e the housing thickness.

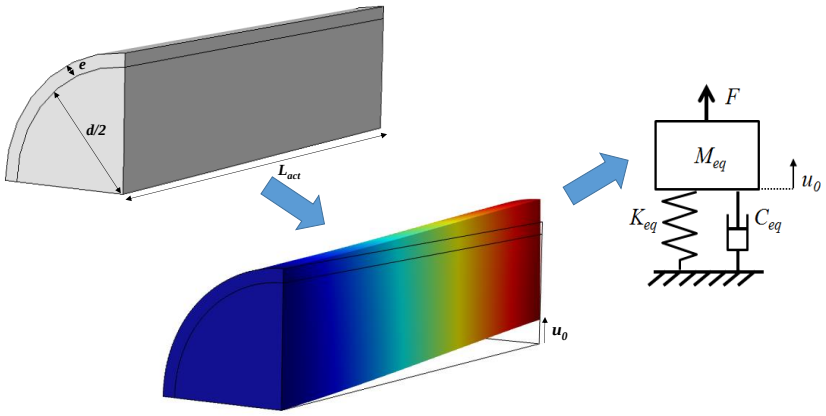

Fig. 5.18 Housing modal analysis

The global expression of the dimensionless number expressing the stress is thus only function of two aspect ratios. The function f will be approximated thanks a surrogate model after a numerical design of experiments [100]. The complete process yields:

$$\frac{\sigma}{Q_m a d \rho} = 2.75 \left(\frac{L_{act}}{d}\right)^{1.73} \left(\frac{e}{d}\right)^{-0.72} \tag{5.53}$$

Equation 5.53 shows that the maximum stress of the housing σ increases with the length L_{act} and decreases with the thickness e.

5.4.3 Actuator Sizing Model

As the rotary topology is chosen, the sizing problem is similar to an optimal motor and gearhead selection [201]. However, due to particular sizing scenarios like maximum skin temperature, maximum reflected inertia and resistance to runaway, the sizing problem is more intricate. An illustration of the integration and the components that must be sized (except ball bearings) is given in Figure 5.19.

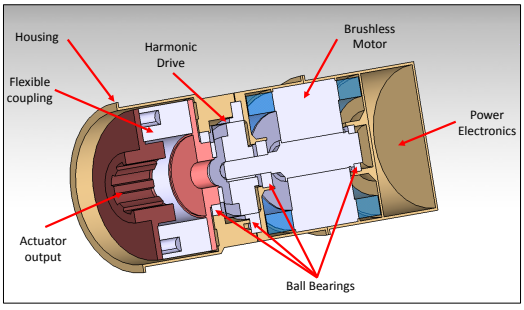

Fig. 5.19 Cut view of the actuator

The rotary EMA sizing model is implemented by associating the previously given sizing scenario and component estimation models. All the present models are algebraic and thus can be implemented in the BOA framework. The system sizing model contains a multidisciplinary coupling. The coupling is due to the runaway scenario. The mechanical components are selected on the $T_{EMA_{mech}}$ torque, nevertheless they must also sustain the torque generated by a runaway T_{RA}. However, the torque generated by the runaway is a function of the stiffness and inertia of the components. In order to make the system consistent $T_{EMA_{mech}}$ shall be greater than T_{RA}. $T_{EMA_{mech}}$ is initially smaller than T_{RA}, thus an over-sizing factor k_{os} is introduced in Equation 5.3 and is configured as a design variable. This technique is the application of the NVH formulation outlined in Chapter 3. The architecture of the actuator sizing model is illustrated in Figure 5.20.

The actuator sizing model is presented as an optimization problem which will be extended in the next section. The problem is the following:

$$
\begin{array}{ll}
\text{minimize} & M_{tot} \\
\text{with respect to} & N_{red}, D_{mot}, e_y, J_{cur}, N_{surf}, e_H, k_{os} \\
\text{subject to} & \Omega_{mot} - \Omega_{mot_{max}} \leq 0 \\
& T_{RA} - T_{EMA_{mech}} \leq 0 \\
& J_{ref} - J_{ref_{max}} \leq 0 \\
& \Delta V - \Delta V_{max} \leq 0 \\
& \sigma - \sigma_{max} \leq 0 \\
& \Theta_{skin} - \Theta_{skin_{max}} \leq 0 \\
& \Theta_{mot} - \Theta_{mot_{max}} \leq 0 \\
& \Theta_{dio} - \Theta_{dio_{max}} \leq 0 \\
& \Theta_{mos} - \Theta_{mos_{max}} \leq 0 \\
& \Theta_{capa} - \Theta_{capa_{max}} \leq 0 \\
& L_{act} - L_{max} \leq 0 \\
& D_{act} - D_{max} \leq 0
\end{array}
\tag{5.54}
$$

5.5 Control Surface Sizing and Actuator Integration

5.5.1 Integration

The case study of this chapter is the preliminary sizing of a primary flight control actuation system composed of multiple integrated actuators and control surfaces. This section focuses on the design of the integrated actuators and aileron control surface. An illustration of the system to be sized is given in Figure 5.21. The previously described actuator has now to be integrated in the control surface hinge line. The housing of the actuator is chosen to be fixed to the wing whereas the output of the actuator is fixed to the control surface. The linkage between the control surface and the wing is chosen to be a

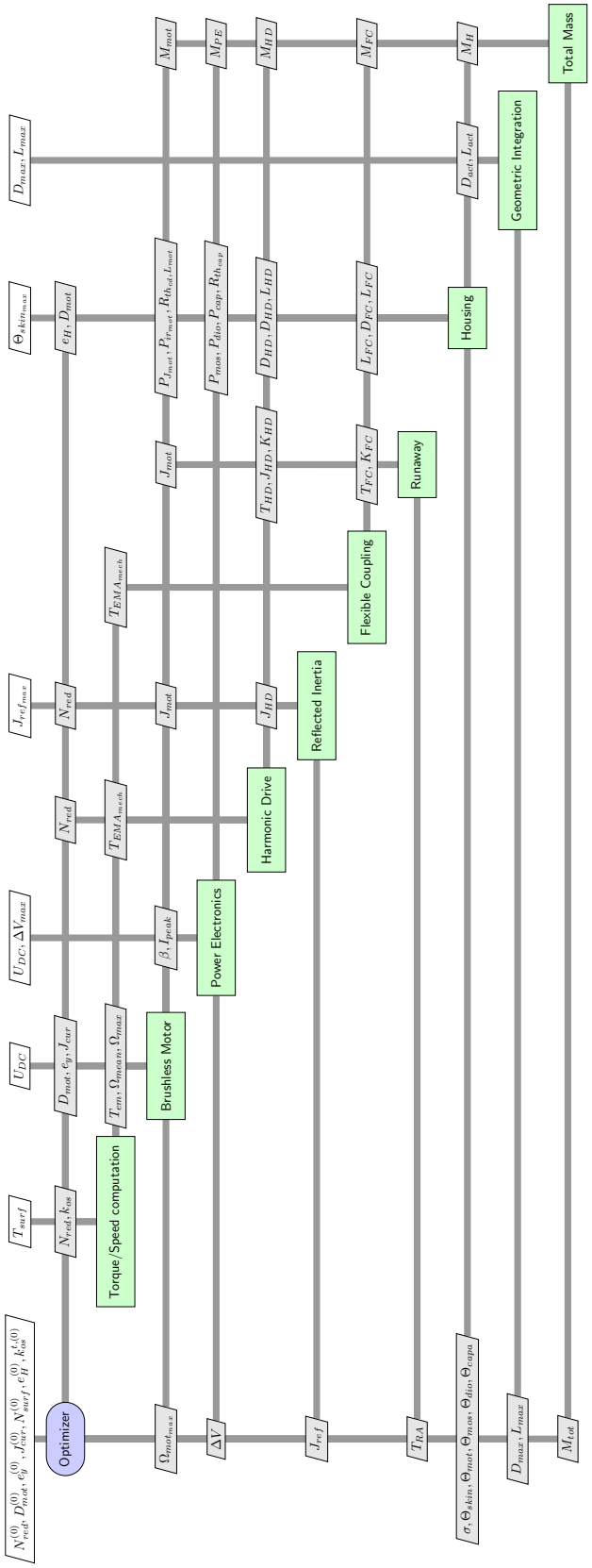

Fig. 5.20 XDSM diagram of the actuator sizing optimization problem

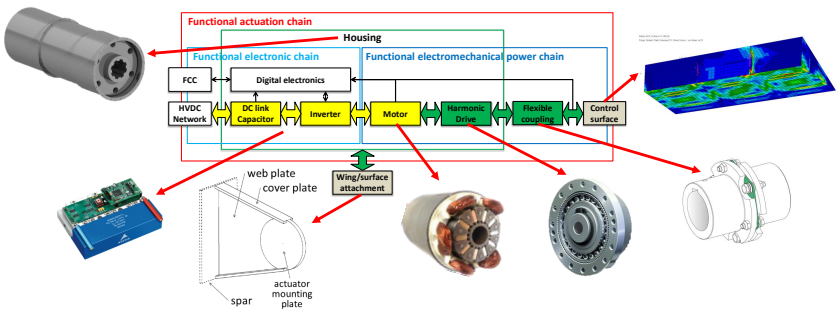

Fig. 5.21 Architecture of the system to be sized

pivot. A hyperstatic assembly between the actuator and the control surface is avoided by using the flexible coupling at actuator output level. However, this leads to have a male shaft which plugs into the actuator conversely to classical solutions. Nevertheless, this assembly enables an easy mounting of the actuator and avoids high stresses that could affect the lifetime of the mechanical components. The integration solution is illustrated in Figure 5.22.

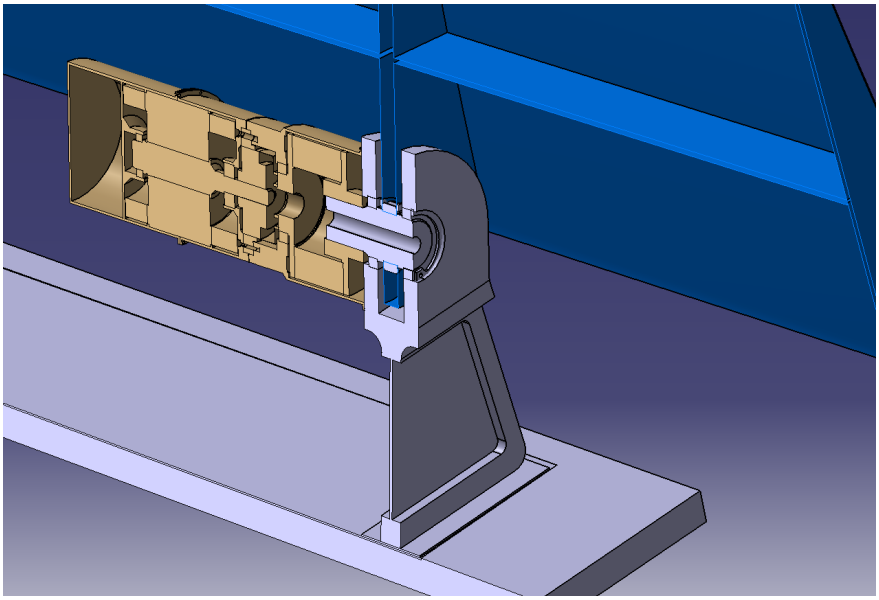

Fig. 5.22 Actuator on-hinge integration with housing fixed to the wing

Some geometric integration requirements are chosen. The space between the actuator and the wing spar shall be more than 1.5 times the actuator diameter for mounting and unmounting. The actuator diameter shall be less than 90 % of the surface hinge diameter. The length-wise geometric integration requirement will be described during the modelling part.

5.5.2 Control Surface Sizing

The control surface structure, as a beam along the hinge line, withstands torsional moment due to aerodynamic forces. Figure 5.23 shows an aileron subjected to aerodynamic forces and actuator torque. The 3-split design maximum torsional moment is 3 times smaller. The theoretical gain in mass offered by splitting a control surface in k elementary surfaces would be a k-factor, if maximum torsion stress was the only sizing criterion as illustrated in Figure 5.23.

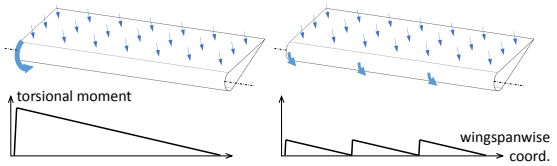

Fig. 5.23 Effect of control surface splitting on structure torsional moments

A finite element study was carried out to assess the actual gain. For each $k = 1...6$, the original aileron was split in k elementary ailerons of equal hinge moment; then a structural optimization was performed for each elementary aileron:

- Objective: minimize overall structural mass.
- With respect to design variables: thickness of each part: spars, ribs, upper and lower surfaces, spar caps, rib caps.
- Subject to constraints: Von Mises and buckling stress is lower than fatigue strength chosen as (30) MPa for aluminum alloy with a security factor of 2, thicknesses remain above manufacturing minimum value chosen as 1.5 mm for the spar caps, 1 mm for the rib caps, 0.5 mm for the other parts.

Each model featured, two spars, two outer “secondary” ribs and two inner “main” ribs, fitted with rigid elements (Nastran RBE2) in a 25 mm radius zone around the hinge line to avoid unrealistic stress concentrations. The master nodes consist of respectively a ball joint boundary condition that accounts for a pivot-type linkage and a ball joint condition with zero rotation around the hinge line, that accounts for the combination of a pivot junction and the actuator action. The model considers uniform 2850 Pa pressure on the lower surface as the effect of aerodynamic loads.

A preliminary buckling study led us to change the minimum thickness of the front spar to 1.25 mm. Figure 5.24 shows Von Mises stresses on an elementary control surface model after optimization.

The set of computations yielded the mass of every elementary control surface for each configuration, hence the mass of the set of elementary control surfaces for each configuration, as shown in Figure 5.25.

The gap between the theoretical mass and the FEM optimization results shows that the theoretical approach is too optimistic and a more detailed design that incorporates buckling and other effects

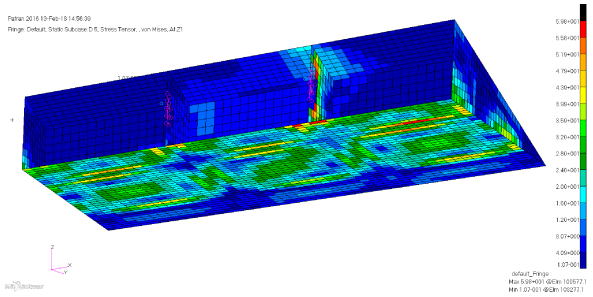

Fig. 5.24 Control surface FEM structural optimization result for one of five elementary surfaces

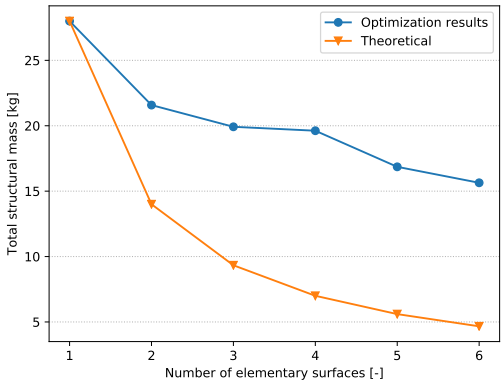

Fig. 5.25 Effect of number of surfaces on total control surface structural mass

is needed. Therefore, the FEM results are fitted with linear regression to consider the effect of the number of surfaces number of surfaces N_{surf} on control surface structural mass M_{surf}.

5.5.3 Wing/Control Surface Attachment Sizing

Each control surface is usually linked to the wing rear spar by at least two cantilever attachments. Splitting the control surface increases the number of attachments. The effect on total structural mass is taken into account.

Conventional designs feature enough space between the spar and the aileron chord-wise to fit the linear actuators. Using rotary actuators located on the hinge line of the aileron frees that space. The only requirement considered for choosing the cantilever length is that the rotary actuator has to be assembled to its final location through that space, so the distance from the spar to the hinge line has to be at least 1.5 times the actuator outer diameter. This study assumes that the wing structure is designed accordingly, which is beneficial as it allows more space for fuel inside the wing box.

The optimization procedure requires the attachment mass to be assessed. Figure 5.26 shows the geometry and the adjustable dimensional parameters.

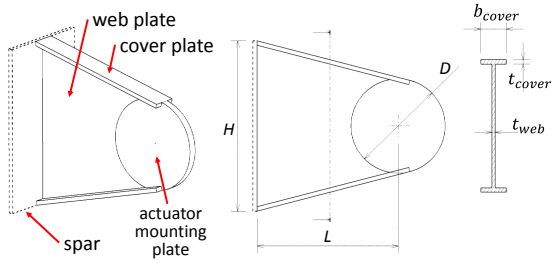

Fig. 5.26 Wing/Control surface attachment parameters

The list of considered sizing criteria consists of resistance as the control surface is subjected to vertical aerodynamic forces, and vibratory requirements. The resistance criteria leads to the assessment of the strength of the cover plates and the buckling of the web plate. The vibratory requirements lead to the assessment of the natural frequency of the mounted control surface has to be above 125 Hz.

For each of those, an analytical expression is developed. The maximum stress in the cover plates is calculated near the spar and near the actuator using beam theory. The quadratic moment of inertia of this section is:

$$I = \frac{b_{cover}D^3 - (b_{cover} - t_{web}) \cdot (D - 2t_{cover})^3}{12} \tag{5.55}$$

The bending stress is then computed:

$$\sigma_{bend} = \frac{F \cdot \left(L + \frac{D}{2}\right)}{2I} \tag{5.56}$$

Where $F = \frac{T_{EMA_{mech}}}{2L}$ since the torque is distributed to both attachment for one surface.

The allowable shear stress is assessed using formula for infinitely long rectangular plate:

$$\tau_{allow} = 5.34 \cdot \frac{\pi^2 \cdot E}{1-\nu} \cdot \frac{t_{web}}{L - \frac{D}{2}} \tag{5.57}$$

Where E is the Young's modulus of the material, ν the Poisson coefficient. For the considered geometric configuration, the shear stress is much lower that the admissible stress of the material and thus is not implemented in the sizing model.

Two natural modes are considered: lateral (i.e. horizontal) and vertical translation of the control surface. The moving mass M is the sum of the elementary aileron structural mass and the mass of two actuators. The lateral stiffness is expressed as follows:

$$K_{lat} = 2 \cdot K_{cp} = 2 \cdot \frac{3 \cdot E \cdot I_{cp}}{2 \cdot L_{cp}^3} \tag{5.58}$$

Where k_{cp} is the lateral stiffness due to only one cover plate, $I_{cp} = t_{cp} \cdot b \frac{3}{12}$ the quadratic moment of the cover plate. Finally the corresponding natural frequency in Hz is:

$$f_{lat} = \frac{1}{2\pi} \sqrt{\frac{K_{lat}}{M}} \tag{5.59}$$

In addition, vertical stiffness of attachment is assessed considering bending and shearing of the attachment as a beam.

5.5.4 System Sizing Model

The sizing model of the integrated actuator and control surface is an extension of the actuator sizing model.

The length-wise geometric integration constraint has to be modelled. Control surface splitting has an effect on the length of the surface, thus the EMA length. As control surfaces are split for equal torque the length of elementary surfaces is not the same. Hence, the most short control surface is taken. The length space for the actuator L_{max} also considers the space taken by two attachments and a 50 % margin on the sum of both actuator length:

$$L_{max} = \frac{L_{surf_{min}} - 2b_{cover}}{2.5} \tag{5.60}$$

Where $L_{surf_{min}}$ is obtained with respect to $L_{surf_{tot}}$ the total surface length, N_{surf} the number of elementary surfaces and the equal hinge moment configuration.

Once important choice made during the more integrated design approach concerns the runaway scenario. It has been chosen to use no torque limitation device and use only the stiffness is the mechanical transmission to absorb the shock. Nevertheless, the torque generated by that shock is higher than the operating torque. Thus, the attachment is sized for the torque $T_{EMA_{mech}}$ as achieved in Equation 5.56.

The sizing model used for the integrated actuator and aileron control surface is the extension of the actuator sizing model (Figure 5.20). The sizing scenario and estimation models that concern the actuator integration, control surface and attachment sizing are therefore added. The architecture of the model is shown in Figure 5.27.

The sizing problem is formulated as the following optimization problem:

$$
\begin{aligned}
&\text{minimize} && M_{tot} \\
&\text{with respect to} && N_{red}, D_{mot}, e_y, J_{cur}, N_{surf}, e_H, k_{os}, b_{cover}, t_{web} \\
&\text{subject to} && \Omega_{mot} - \Omega_{mot_{max}} \leq 0 \\
& && T_{RA} - T_{EMA_{mech}} \leq 0 \\
& && J_{ref} - J_{ref_{max}} \leq 0 \\
& && \Delta V - \Delta V_{max} \leq 0 \\
& && \sigma - \sigma_{max} \leq 0 \\
& && f_{max} - f_{lat} \leq 0 \\
& && f_{max} - f_{ver} \leq 0 \\
& && \sigma_{shear} - \sigma_{shear_{max}} \leq 0 \\
& && \sigma_{bend} - \sigma_{bend_{max}} \leq 0 \\
& && \Theta_{skin} - \Theta_{skin_{max}} \leq 0 \\
& && \Theta_{mot} - \Theta_{mot_{max}} \leq 0 \\
& && \Theta_{dio} - \Theta_{dio_{max}} \leq 0 \\
& && \Theta_{mos} - \Theta_{mos_{max}} \leq 0 \\
& && \Theta_{capa} - \Theta_{capa_{max}} \leq 0 \\
& && L_{act} - L_{max} \leq 0 \\
& && D_{act} - D_{max} \leq 0
\end{aligned}
\tag{5.61}
$$

5.6 Primary Flight Control Actuation System Optimization

5.6.1 Optimization and Exploration

All the present models are algebraic and thus can be implemented in the BOA framework.

In the previous sections, a rotary EMA sizing model and an integrated actuator and aileron control surface have been outlined. The integrated actuator and control surface sizing model enables us to determine the sizing of the actuator, wing/surface attachment and aileron control surface with respect to the number of elements into which the total control surface is split. In this section, the sizing model is extended to the complete primary flight control surface that includes ailerons, elevators and rudder.

The analysis of the different surface actuator requirements for the considered aircraft is achieved. The analysis shows that the aileron surface has the greatest linear hinge moment. This means that

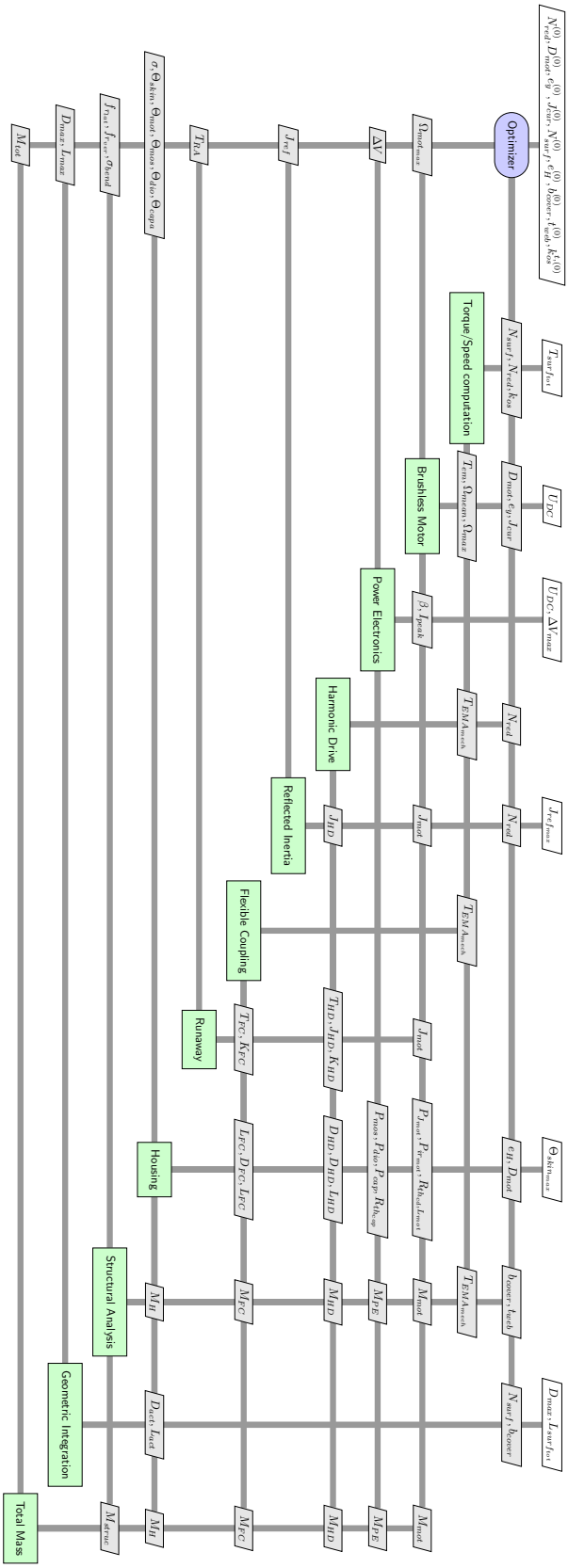

Fig. 5.27 XDSM diagram of the integrated actuator and aileron control surface optimization problem

ratio between the hinge moment and the length of the surface is the most important when compared to the elevator and the rudder. Hence, the aileron surface is the most constraining for the actuator linear torque. In addition, the hinge diameter of the aileron is also the most constraining for actuators. Hence, for any aileron control surface splitting configuration that has an actuator sizing that meets the requirements, a control surface splitting configuration for elevators and the rudder exist where the same actuator can be used.

Therefore, the primary flight control actuation system preliminary sizing study can be reduced to the study of an aileron sizing. However, a more detailed study should be achieved for the structural analysis and thermal analysis of the elevators and the rudder.

The sizing problem is composed only of algebraic models and is therefore implemented in the BOA framework. The sizing problem involves 104 analysis functions in total. It consists of the previously presented integrated actuator and aileron control surface sizing model. The optimization problem is composed of 9 design variables and 16 constraints. Thus, the model is solved using the adjoint method in the BOA framework. Hence, total system derivatives are obtained using the MAUD architecture [113] and partial derivatives are obtained using symbolic differentiation. The gradient-based optimizer SLSQP is used to solve the problem.

5.6.2 Results

The optimization leads to a configuration where the aileron control surface is split in 6 elementary surfaces. Then a design exploration is achieved by running several optimizations for different number of elementary surfaces. The typical runtime for each optimization is 4.4s (7min42s with NSGAII a gradient-free optimizer). The active constraints are housing stress, the housing skin temperature and the attachments bending natural frequency. The Harmonic Drive reduction ratio is at its maximum value despite the runaway scenario.

The results of this exploration are illustrated in Figure 5.28.

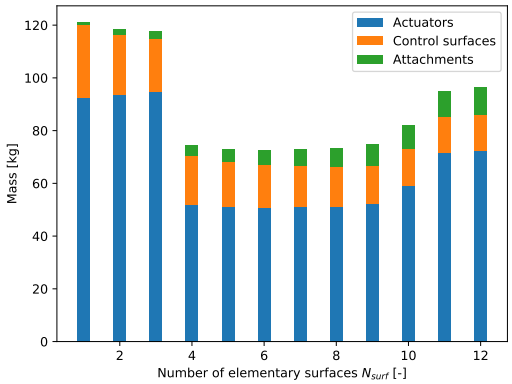

Fig. 5.28 Effect of number of surfaces on optimal overall system mass

For configurations with 1, 2, 3, 11 and 12 individual surfaces the design is unfeasible for the chosen EMA architecture and thermal environment assumptions. For configurations 1, 2 and 3 the thermal constraints lead to large diameter EMA which do not fit in the allocated space. For configurations 11 and 12, the maximum length is unachievable because of a too important splitting. It is important to note that a large number of surfaces penalizes maintenance cost as the number of actuators to unmount/mount are greater. In addition, the "dead mass" like electrical connectors and mechanical interfaces increase as well with the number of elementary surfaces. In the feasible domain, the effect of the number of surfaces on the total actuator mass is not significant. Hence, an interesting configuration could be to split an aileron in 4 or 5 elementary surfaces in order to limit the disadvantages.

The ratio between the actuator mass and structural mass is high partially due to very pessimistic thermal assumptions. Hence, it is chosen to investigate the effect of the natural convection thermal resistance of the housing on the design. This is achieved for the 5 surfaces configuration and mass are normalized for the nominal value of thermal resistance. It consists of the cylinder housing presented previously with no duct. It is proposed to reduce the housing thermal resistance by a factor which ranges from 1 to 4. The resulting overall mass are given in Figure 5.29.

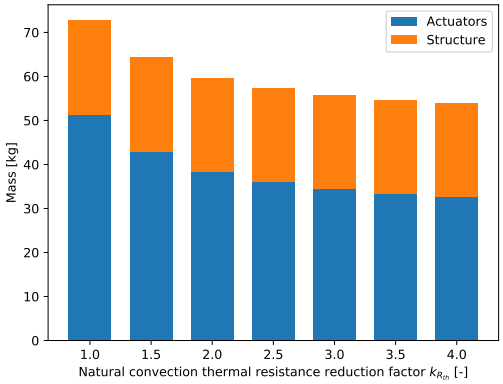

Fig. 5.29 Effect of reducing the housing thermal resistance on optimal overall system mass

Results show a significant positive effect of decreasing thermal resistance value on the total actuators mass and therefore the system mass. The effect slows down when the motor hot spot temperature constraint becomes active and conductive limit is reached. To further optimize the actuator, ducts or other cooling systems can be added.

Decreasing this thermal resistance value can lead to interesting performances and characteristics of EMAs. This can be done by studying more deeply thermal boundary conditions of EMA as natural convection is a confined space is very pessimistic as in reality EMA exchange by thermal conduction with the structure. Furthermore, cooling technologies or highly conductive insulations for the motor winding can lead to significant insights for flight control EMA technologies. Nevertheless, a further studies should include a distinction between permanent torque and maximal torque during sizing

of actuators should be done especially for surfaces different than aileron. The dynamic thermal optimization presented in Appendix B could be used for this purpose.

Another direction for increasing the proposed actuator competitiveness is mechanical integration. As shown in Figure 5.30, an important share of a single actuator mass is the flexible coupling.

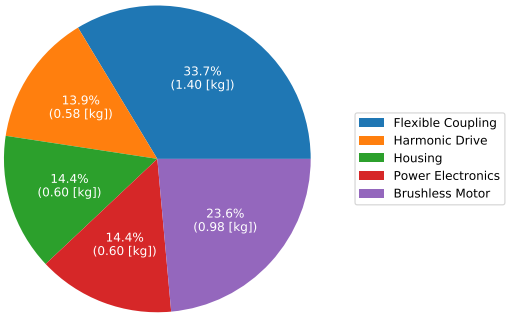

Fig. 5.30 Single EMA mass breakdown for five surfaces configuration

The flexible coupling was introduced in order to avoid an hyperstatic assembly and deal with potential radial misalignment. Thus, improving the mechanical integration between the control surface, the attachment and the actuator could lead to smaller misalignment values or innovative assembly concepts, hence a potential mass reduction.

5.6.3 Summary and Discussions

A primary flight control actuation system architecture and EMA architecture have been proposed. At the system level, the concept of control surface splitting enables to decrease the hinge moment of a surface and thus the required actuator torque. This leads to actuator architecture with less gear stages and thus compact solution. Small and low inertia elementary surfaces also enables these surfaces to have less authority on the wing behaviour and certainly flutter. At flight control and aircraft level control surface splitting increases reliability as it is intrinsically redundant. In addition it provides a higher control freedom. For example, on the Airbus A380 aileron and rudder control surface splitting enabled better passenger comfort and structural loading. The chosen integration configuration is to use rotary on-hinge EMAs. This enables to reduce chord wise mechanical clearance when compared to linear actuators and free some space for fuel tank. Furthermore, if an elementary surface is jammed, the other surfaces can potentially act in order alleviate the load on the jammed surface.

At the actuator level, the EMA technology is more environmentally friendly due to the removal of the hydraulic fluid. The rotary configuration provides a maintenance free solution and an enhanced reliability due to the lack of contamination of the lubricant. Such integration concept leads to more compact solutions and less "open" electrical interfaces since the inverter, the motor and sensors are in the same housing. The actuator design is chosen to be more integrated. Hence, no runaway

overload protection devices like spring, torsion bar or torque limiter are used which increases the compactness of the EMA. The selected actuator architecture is also back-lash free. In addition, the actuator, wing/surface attachment and control surface assembly is not hyperstatic which reduces the risk of failure and increases the overall lifetime.

The most significant finding of the conceptual sizing is that a solution exists where the same actuator can be used for ailerons, elevators and the rudder if the surfaces are split correctly. This solution could lead to lower maintenance and development costs. An illustration of the concept is given in Figure 5.31.

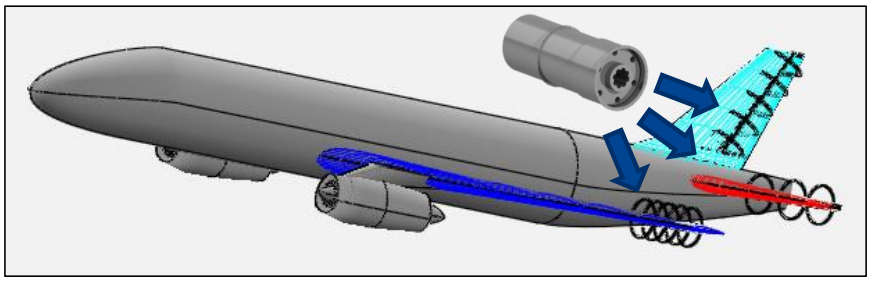

Fig. 5.31 Aileron, elevator and the rudder control surface splitting configuration visualization using OpenVSP [96]

However, the proposed concept has some limitations especially in terms of actuator mass. An indirect comparison to classical Servo-Hydraulic Actuators show that the overall mass of actuators for a five surfaces configurations is almost three times heavier as shown in Table 5.1.

Table 5.1 Comparison between overall actuator mass, structural mass and total mass of a conventional single aileron and split aileron configuration.

Concept	Overall Actuator Mass [kg]	Structural Mass [kg]	Total Mass [kg]
Conventional single surface with SHAs	13.2	28.0	41.2
Split surface with EMAs	51.2	21.5	72.7
Split surface with EMAs with improved cooling	38.7	21.3	60.0
Split surface with EMAs with improved cooling and without flexible coupling	24.7	21.3	46.0

However, Table 5.1 also outlines that with improved actuator cooling and no flexible coupling, the overall EMA mass becomes competitive. Hence, emphasis shall be placed on the thermal integration

and mechanical integration for the next generation of PbW actuators. In addition, the splitting of control surfaces leads to a structural mass gain which induces a total mass close to the conventional aileron. If the mass penalization of the hydraulic network is considered, the proposed concept can surpass the conventional configuration. Furthermore, the use of hydraulically powered actuators for the split control surface concept seems not convincing due to the additional hydraulic pipes when compared to electrical harnesses. Therefore, PbW actuators can compete with conventional SHAs during aircraft power system trade-offs with the principle of splitting the control surfaces.

The comparison between hydraulically powered and electrically powered actuator is delicate. The efficiency and power management of hydraulic solution is catastrophic whereas the actuator mass is interesting. Conversely, the electric solution is catastrophic in terms of mass whereas as the efficiency and energy management are better. Therefore, the comparison should be achieved at aircraft level with considerations for actuators, power distribution and power generation.

5.7 Conclusion

The work reported in this chapter is a significant advancement in primary flight control actuation system concepts. A compact and easy integration rotary EMA has been designed and presented. This case study has shown how to integrate component detailed design knowledge during the system preliminary sizing process. For this purpose, the methodology presented in Chapter 4 was used.

The state of the art of primary flight control actuation system needs and design drivers has been presented. An architecture of integrated actuator and split control surface has been proposed. A compact rotary EMA architecture has also been proposed. The design drivers and sizing scenarios of such solution have been outlined. A detailed sizing model was achieved for the actuator with emphasis placed on sizing scenarios such as thermal behaviour and runaway. For that, surrogate models of FEM models were used to evaluate the thermal resistances, motor losses and housing vibratory stress. The sizing model was then extended to wing/surface attachment and the control surface. This enabled to achieve a complete sizing of an integrated actuator and aileron control surface. The torque density and diameter confinement of an aileron enabled us to investigate the concept of control surface splitting at actuation system level.

Effects of aileron control surface splitting on overall mass of an integrated actuators and control surfaces have been studied. The main benefits come from structural components like control surface and actuator housing. Impact of thermal environment and number of elementary surfaces on overall mass were given. The concept of standardized multi-surface rotary on hinge EMA has been proposed.

The interface between airframer flight control actuation system integrator and actuator supplier are commonly through requirements. Insights can probably outcome by investigating the effect of requirements on an integrated actuator and control surface configuration has the example presented here. Furthermore, actuator integrators and suppliers must place emphasis on providing accurate thermal configuration and models between them. Indeed, as shown the thermal configuration has a significant

effect on the actuator size and mass. Furthermore, a more accurate value of the misalignment can significantly reduce the size of the flexible coupling and thus the EMA.

Instead of enduring control surface splitting as a requirement due to wing bending design driver why not see it as an opportunity for more integrated and standardized actuation systems. Control surface actuation standardization through control surface splitting can then be extended to aircraft programs developed in parallel and can have the same elementary actuators. Probably that fully electrically power electro-mechanical actuators will be introduced on commercial aircraft after thousands of flight hours on Unmanned Aerial Vehicule (UAV) and sophisticated health monitoring functions. Nevertheless, this study has also shown that with such sizing tool, better integration trade-off studies can be achieved by integrator and suppliers in the early design phases.

Future work should include for the motor sizing the surface damping requirement. In addition, more specific thermal and structural models for elevators and the rudder are needed. Finally, a detailed aero-elastic study should be achieved in order to investigate the effect of control surface splitting on the flutter phenomena.

Chapter 6

Electrical Thrust Reverser Actuation System Design

6.1 Introduction

At landing, fixed wing aircraft need a braking system in order to decelerate from landing speed to taxiing speed within the runway distance. Aircraft braking systems include:

- Aircraft disc brakes located on landing gears, used to brake the wheels when they are touching the ground.
- Airbrakes located on upper side of wings, they are dedicated flight control surfaces used to increase drag and decrease lift.
- Thrust Reversers, they allow to use engines thrust to be used to slow the aircraft.

This chapter focuses on Thrust Reversers and particularly the system that actuates them. The Thrust Reverser System is part of ATA 78 Engine Exhaust and Thrust Reverser. Thrust reversal, also called reverse thrust, is the temporary diversion of an aircraft engine's thrust so that it is directed forward, rather than backward. Reverse thrust acts against the forward motion of the aircraft, providing deceleration. The utilization of Thrust Reversers enables to increase tyres and brakes sustainability and decrease landing distance by 25% on a dry runway and 50% or a wet or icy runway. The need for thrust reversal is particularly important for emergency braking capability in event of Aborted Take Off (ATO) on icy runways when wheel brakes are not efficient. Hence, thrust reversers and their actuation system perform a critical function for the aircraft. Thrust reversers have to handle around some 60% of engine total thrust capacity which correspond to the thrust in reverse. There are three main types of thrust reversers on jet engines which all are a movable part of the nacelle that surrounds the engine core.

The target thrust reverser (Figure 6.1) uses a pair of "bucket" type doors to reverse the hot gas stream. For forward thrust, these doors form the propelling nozzle of the engine. Two reverser buckets

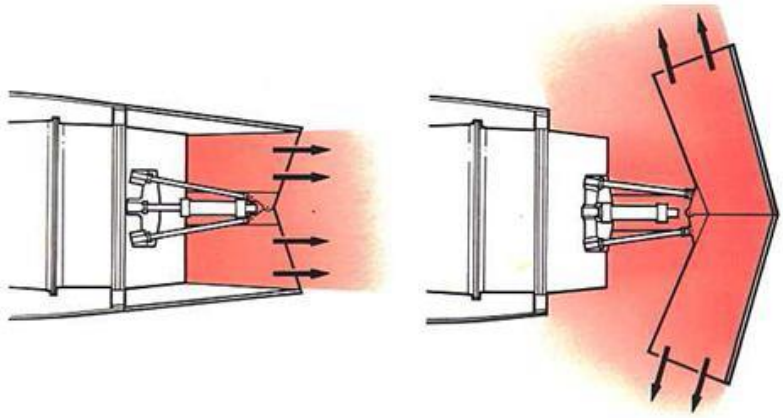

Fig. 6.1 "Bucket" type thrust reverser [214]

are hinged so when deployed they block the rearward flow of the exhaust and redirect it frontwards. This type of reverser is visible at the rear of the engine during deployment.

The "clam-shell" thrust reverser (Figure 6.2), or cascade system, are another alternative. When activated, the doors rotate to open the ducts and close the normal exit, causing the thrust to be directed forward. The cascade thrust reverser is commonly used on turbofan engines. On turbojet engines, this system would be less effective than the target system, as the cascade system only makes use of the fan airflow and does not affect the main engine core, which continues to produce forward thrust.

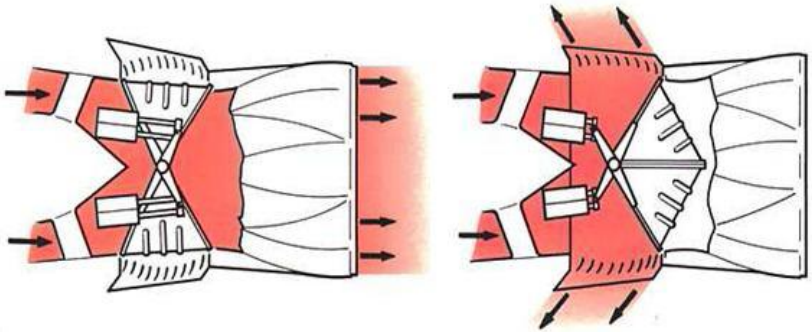

Fig. 6.2 "Clam-shell" type thrust reverser [214]

In addition to these two types which are used on turbojet and low-bypass turbofan engines, the "cold stream" type (Figure 6.3) of thrust reverser is found on some high-bypass turbofan engines. Doors located in the bypass duct are used to redirect the air that is accelerated by the engine's fan section but does not pass through the combustion chamber (called bypass air) such that it provides reverse thrust. During normal operation, the reverse thrust vanes are blocked. Once the deploy order is

received, the system folds the doors to block the cold stream heading towards the nozzle and redirect this airflow to the cascade vanes.

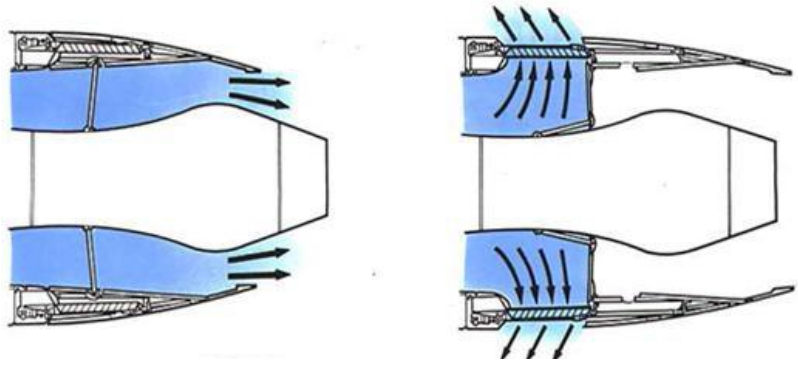

Fig. 6.3 "Cold stream" type thrust reverser [214]

Here we focus on the "cold stream" type thrust reverser that is actuated by an Electrical Thrust Reverser Actuation System (ETRAS). The thrust reverser are generally installed on the inboard position nacelles. The Thrust Reverser structure has one (O-duct) or two (C-duct or D-duct) translating cowls also referred to as transcowls. In forward thrust configuration the translating cowl is in the forward, stowed position, covering the cascade vanes. The blocker doors are are housed in the inner acoustic panel of the translating cowl in stowed position. In reverse thrust, the translating cowl moves backwards to uncover the cascade vanes and grids, while the blocker doors and rods rotate inward to block the fan flow duct as shown in Figure 6.4. The reverse thrust is obtained by forward redirection of the engine fan flow. The grids handle a portion of the aerodynamic loads and thus decreases the loads on the actuators and the transcowl.

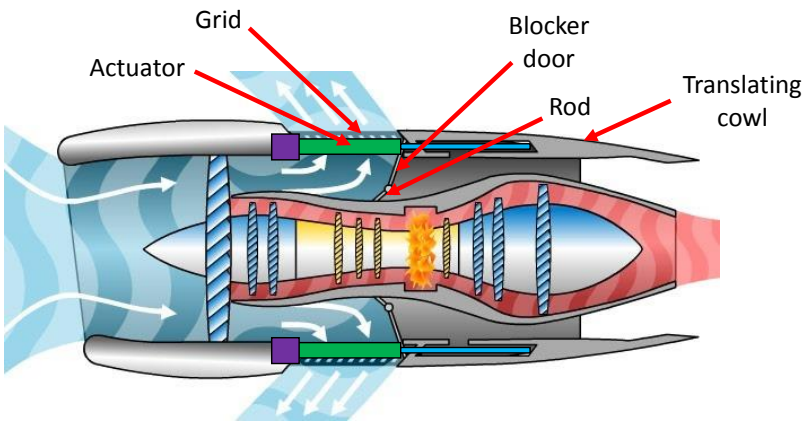

Fig. 6.4 Cold stream thrust reverser architecture (adapted from [190])

This chapter presents the design and sizing of the ETRAS of a cold stream type thrust reverser system. We focus here on determining the best suited mission profiles since they have a strong effect on the sizing and that some components like the electrical motor are on their technological limit due to the electrical supply (current/voltage) and what is requested by the trajectories. For that, the chapter in decomposed in two main parts that optimize the system design. In the first part, a system sizing model is developed with emphasis placed on the component sizing but with a surrogate model for the mission profile scenarios. Conversely in the second part, emphasis is placed on the trajectory model but a simplified system sizing model is used.

6.2 Architecture, Design Drivers and Sizing scenarios

Thrust Reverser Actuation System (TRAS) use pneumatic technology in some applications. Nevertheless, the predominant choice to initiate and control the motion of the reverser is linear hydraulic actuation [176]. These actuators in combination with a number of valves, position sensors, and locking devices constitute the TRAS. However, electrically power TRAS also referred to as ETRAS have been developed for recent aircraft developments such as the Airbus A380 and A350 as well as the COMAC C919. The ETRAS enables better maintainability and easier integration than hydraulically powered TRAS. The ETRAS is supplied by the AC voltage network of the aircraft. It has to deploy and stow the engine nacelle transcowl(s) during landing.

6.2.1 Architecture

Tertiary Locking System (TLS) and Primary Locking Systems (PLS) are installed to guarantee that the thrust reverser will not deploy during flight. At landing, the Thrust Reverser deployment order is sent by the pilot using the Throttle Lever to the Electronic Engine Controller (EEC) and other systems of the aircraft. The EEC sends a stow/deploy order to the Thrust Reverser Controller Unit (TRCU). The TLS unlocking is ordered by the aircraft. Once the deploy order is received by the TRCU and that the TLS is unlocked the ETRAS unlocks the PLS, unlocks the electromagnetic brake and actuators are actuated by controlling the electrical motor which is also referred to as Power Drive Unit (PDU). Mechanical power is transmitted from the electrical motor to the actuators through flexible shafts also referred to as flexshafts. They also guarantee position synchronization between the actuators. An overview of Thrust Reverser and ETRAS components is given in Figure 6.5.

The ETRAS enables to control deployment and stow of the nacelle thrust reverser subjected to aerodynamic loads. The ETRAS includes an electrical power chain and an electro-mechanical power chain. The electrical power chain main components are an Autotransformer Rectifier Unit (ATRU), an inverter, a braking resistor and a housing. The electro-mechanical power chain main components are a brushless motor, flexshafts and linear actuators. This architecture is illustrated in Figure 6.6.

The ATRU includes an autotransformer, two rectifiers and two interphase inductors. An actuator includes a bevel gear, a thrust bearing (TB), a ball screw and its tube (housing). The ATRU transforms the aircraft AC supply voltage into a DC voltage and enables a low Total Harmonic Distortion (THD).

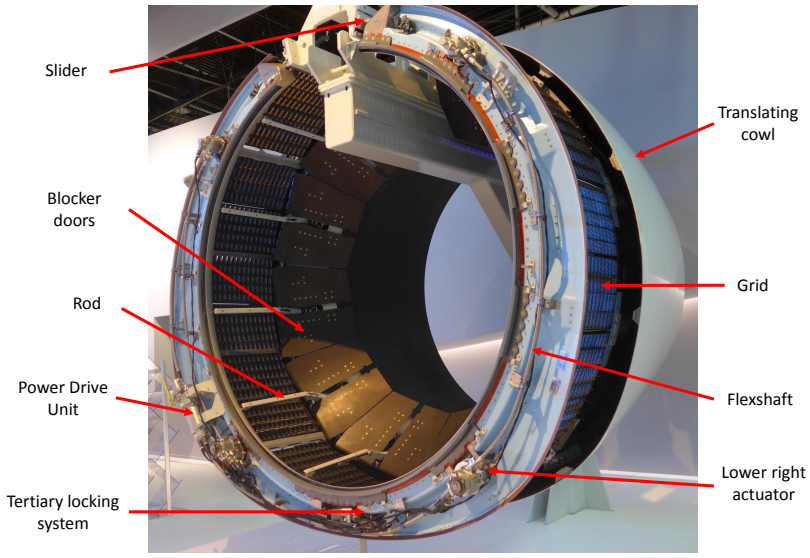

Fig. 6.5 ETRAS and TRAS integration on a nacelle

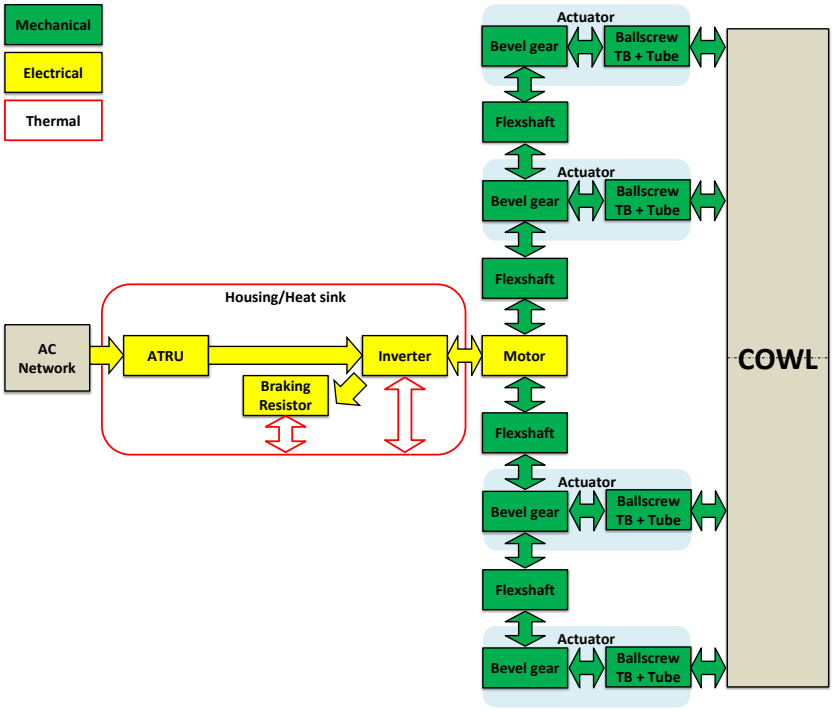

Fig. 6.6 ETRAS power architecture

The inverter drives the electrical motor by transforming the DC voltage into an AC voltage. The motor transforms the electrical power into mechanical power. This mechanical power is then distributed to the four actuators using flexshafts. For each actuator, the bevel gear reduces the speed and increases the torque transmitted to the ball screw. The ball screw then transforms this mechanical rotational power into a translational mechanical power. The power is transmitted through the nut and the tube to the transcowl. The thrust bearings handles the axial load transmitted to the structure through a gimbal. When the power is regenerative, the braking resistor is engaged to dissipated the energy into heat stored in the housing heat capacity.

We focus here on the sizing of components that have a significant effect on the total mass of the system. Hence, the sizing of the system includes the autotransformer, the housing which acts as a heat sink for the braking resistor and inverter, the motor, flexshafts and actuators.

6.2.2 Design Drivers

System

The system design drivers considered are the requirements such as fail-safe design, performances and integration constraints like maximum components temperatures. The components that are fixed to the nacelle structure shall not exceed a given temperature. The Aborted Take Off (ATO) deploy and stow performances are specified as a maximum time to achieve full stroke and 80% of full stroke. Hence, position/speed mission profile for both sequences are considered as a system design driver. Furthermore, maximum impact speed on end-stops have to be included in the position/speed mission profile. The transcowl mass is also a design driver as it has an effect on the dynamic torque. Aerodynamic loads profile have also an effect on the system design and are given as function of the transcowl/actuator position. The fail-safe requirements leads to the analysis of the effect of component failures like ball screw jamming on the system behaviour.

Mechanical Components

The main design drivers of flexshafts are their maximum/fatigue torque and maximum speed which come from technological limits whereas rotational stiffness and inertia are parasitic characteristics. Stiffness and inertia can be considered as design drivers as both have an effect on the load generated by a jamming and the inertia the dynamic torque of the motor. In addition, a technological limit of flexshafts is their maximum speed, thus it must be considered during sizing. Bevel gears are selected on their reduction ratio and maximum/fatigue torque whereas inertia is a parasitic characteristic that has an effect on the sizing problem. Bevel gear design suggests to have a fixed aspect ratio between teeth face width and outside diameter (typically 0.3) [66]. The main stresses that drive their design is Hertz contact stress between teeth and tooth bending stress. Thrust bearings are selected using the maximum/fatigue axial force. Fatigue stress has to consider the number of revolutions during the entire life of the bearing and might lead in some application to an over-sizing of the selected bearing. The main design drivers of ball screws are their pitch, the maximum/fatigue axial force as well as

parameters such as inertia and axial stiffness. The main stress if typically Hertz contact stress of balls, hence the weight of the screw can be optimized by machining an inner diameter. However, stress generated by buckling has to be checked especially for ETRAS applications where strokes are relatively high. The buckling stress can be limited by integrating deflection limiters to avoid too much bending of the screw.

Electrical Components

The main design driver of the autotransformer, the braking resistor, the inverter and the housing is their maximum operating temperature. Since the ETRAS application is very short (typically a few seconds), only heat capacities of components act as heat sinks. The autotransformer is designed for constant magnetic saturation and not maximum winding temperature. However, the thermal behaviour is checked. Autotransformers and braking resistors are also selected on their peak power. The braking resistor resistance has also to be carefully adapted to DC bus voltage. In addition, the intrinsic heat conduction resistance of the braking resistor is relatively high. Hence, potting materials or other devices have to be used to enhance heat conduction between the braking resistor and the housing. The main design drivers of brushless motors for dynamic and transient applications are maximum torque, maximum speed, maximum temperature and inertia. The maximum electromagnetic torque is limited by the magnetic saturation of the core material. Nevertheless, the temperature of windings have to remain reasonable. Here, the motor uses only its heat capacity to handle the losses it generates and the related temperature increase.

6.2.3 Sizing Scenarios

From now on, the deploy direction is considered as positive in the sign convention.

ATO Deploy

The deploy sequence begins with an overstow where the transcowl is stowed to enable the unlocking of the PLS. This asks for very high torque as important frictions of seals are acting. Then the rest of the deploy sequence consist of moving from 0% to 80% of full stroke in 2 seconds and reaching 100 % in 3.5 seconds. During the deploy, the aerodynamic loads are position dependent as shown in Figure 6.7.

The deploy load profile shows that before reaching a certain position the aerodynamic loads act against the deploy motion and once reaching this position they tend the pull the transcowl towards full stroke. The reach of full stroke must be mastered to avoid too high impact speeds that would generate strong shocks and thus an over-sizing of mechanical components. Hence, the ETRAS has to brake the transcowl and regenerate energy. Furthermore, the load and speed specifications for the ETRAS depend on the position/speed profile chosen to perform full stroke, system total inertia, transcowl mass and mechanical efficiency. Mechanical efficiency is temperature dependent, as the ETRAS operates in motor and generator quadrant the ATO deploy must be decomposed in two temperature scenarios.

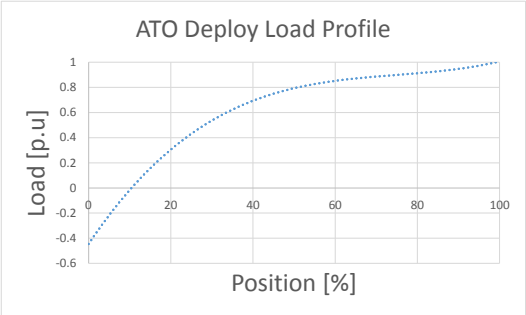

Fig. 6.7 ATO Deploy position dependent load profile shape

ATO deploy at cold temperatures (high friction in actuators and flexshafts). The low mechanical efficiency leads to significant power and energy for the motor, inverter and the autotransformer. ATO deploy at hot temperatures (low friction in actuators and flexshafts). The high mechanical efficiency leads to significant peak power and more energy to dissipate for the braking resistor. At full stroke actuators are on their end-stop and the reverse thrust generate only high axial load, no torque.

The ATO deploy sizing scenario can therefore be decomposed in four scenarios:

- A high torque scenario due to overstow (cold) phase.
- A cold deploy profile to reach 80 % of full stroke in 2 seconds and 100 % of stroke in 3.5 seconds subjected to position dependent aerodynamic loads. This requires a high power and energy demands in motor quadrant.
- A hot deploy profile to reach 80 % of full stroke in 2 seconds and 100 % of stroke in 3.5 seconds subjected to position dependent aerodynamic loads. This generates a high power and energy in generator quadrant.
- A full reverse load that generates a high axial load on actuators, no torque due to the presence of dog stops.

Normal Stow

The stow sequence begins at full stroke position and ends when the 0% of stroke is reached. The aerodynamic loads are position dependent as shown in Figure 6.8.

As for the ATO deploy, the position/speed profile chosen to perform full stroke, system total inertia, transcowl mass and mechanical efficiency have an effect on the power and energy required to perform a normal stow. Hence, the appropriate thermal condition for sizing the ETRAS is at cold temperatures when mechanical efficiency is very low. The components impacted by the stow scenario are the ATRU, the inverter, the heat sink and the motor.

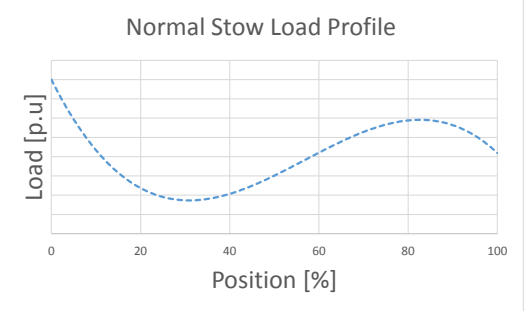

Fig. 6.8 Stow position dependent load profile shape

Without modelling and a priori no defined position/speed mission profile, it is not possible to assess wether the ATO deploy motor quadrant phase is more sizing in terms of peak power and energy than the normal stow.

Mechanical Components

The design of the ETRAS is subject to multiple scenarios. The sizing has to consider shock scenarios on the deploy and stow end-stops. The end-stops are achieved by dog-stop devices integrated on ball screws. Furthermore, loads in transit for normal operation and failure modes have to be taken into account for the mechanical components sizing.

Preliminary assessments can be done to outline the number of different scenarios to be covered. Let us consider three different normal mode load profiles: Normal Deploy (ND), Normal Stow (NS) and Aborted Take Off (ATO) deploy. Operating in normal mode leads to three different scenarios of shock on dog-stops. A failure case that has an effect on shock is the disconnection of one flexshaft or one actuator. Only one failure mode can occur at a time. As they do not have the same integration configuration this leads to eight other shock scenarios for components sizing. Hence, the design of the ETRAS shall consider $3 \times 1 + 3 \times 8 = 27$ shock scenarios. Furthermore, dog stops and ball screws have to hold the load generated by engine reverse thrust which leads to one additional scenario.

Load in transit have also to be taken into account. Normal operating mode leads to three loading cases (ND, NS, ATO). Some failure modes have an effect on the loads to which mechanical components are submitted. The considered failure modes are actuators (4) and flexshafts (4) jamming or disconnection, sliders (2) jamming. Hence, the design of the ETRAS shall consider $3 \times 1 + 3 \times 4 \times 2 + 3 \times 4 \times 2 + 3 \times 2 = 57$ load scenarios during transit.

The total number of sizing scenarios for mechanical component design is therefore $27 + 1 + 57 = 85$. This is a large number of scenarios even if not all of them were outlined here. It would not be efficient to integrate simultaneously all of them in one large system sizing model. Two options are possible to reduce the number of scenarios. The dominating scenarios are known by an expert or are clearly written in a technical document. Or the other option is to achieve a preliminary sizing without

considering any of the failure scenarios and obtain the component parameters. Then achieve a lumped parameter model that represent the behaviour of the system and its response in terms of loading to all the scenarios. An analysis can then be achieved to determine the dominating scenarios and integrate them in a more detailed sizing model.

In this chapter, the main sizing scenario considered for mechanical components sizing is the slider jamming. The modelling of the slider jamming scenario includes the aerodynamic loads, effect of kinetic energy stored in the rotating inertias and the motor torque when the jamming occurs.

Electrical Components

The main sizing scenario for electrical components is their maximum operating temperature. Peak power of the autotransformer, the braking resistor and the inverter correspond to the peak current if voltage is considered constant. Peak power is an image of how much amount of current can pass through them during an very short time. At preliminary level, it is chosen to select them for their peak power and check their maximum temperature due to energy losses they generate. Hence, their size depends on the amount of energy they have to sustain. The autotransformer is thermally isolated from the heat sink. Thus, it shall dissipate its energy losses in its own heat capacity. Whereas the braking resistor and inverter are thermally linked to the heat sink, the amount of energy to be dissipated permits the specification of the minimum mass of the housing dedicated to heat dissipation of these components. Two sizing scenarios are considered for the brushless motor: a maximum torque due to the overstow phase (static) and its maximum winding temperature.

6.2.4 Summary

This ETRAS case study is a preliminary design as not all the actual design drivers like vibrations or sizing scenarios like specific thermal cycles are considered. In addition, different power supply configurations can be taken into account as well as load and speed dependent frictions in the mechanical system. These will be considered in the section 6.6 during trajectory optimization. However, as shown in Figure 6.9, even at preliminary level the interdependencies of components through sizing scenarios remains relatively complex.

6.3 Sizing Scenarios Models

6.3.1 Deploy Mission Profile

The objective of the model developed for the deploy mission profile is to determine maximum powers and energies with respect to a speed order profile, transcowl mass, total system inertia and aerodynamic loads.

A speed order profile model has therefore to be established. This model shall determine the speed order profile over time with respect to stroke, deploy time and speed limitations. Trapezoidal speed profiles are commonly used to minimize the power for point to point applications. Hence, here it is

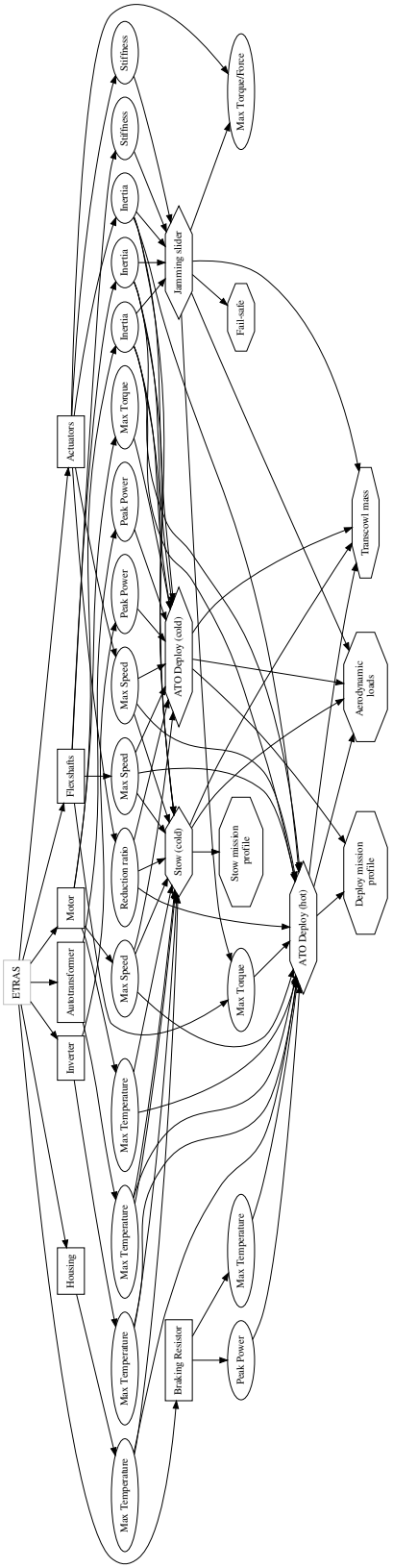

Fig. 6.9 ETRAS design drivers and sizing scenarios (non-exhaustive)

proposed to use a speed profile that contains constant acceleration/deceleration and constant speed phases. Emphasis is placed on building a model that requires a small number of input variables to be defined. Hence, the speed profile at actuator level illustrated in Figure 6.10 is proposed.

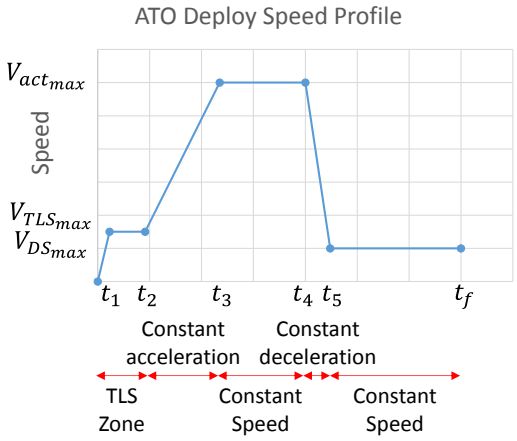

Fig. 6.10 ATO Deploy speed profile principle

This speed profile is parameterized with respect to maximum speed in TLS zone, distance of the TLS zone, maximum speed of the actuator, stroke, 80% of stroke, time to full stroke, time to 80% of full stroke, position uncertainty of actuators and maximum speed reaching end-stops. The only parameters chosen as a design variable during sizing is the maximum actuator speed. Detailed explanations of the speed profile are given in Appendix C.

To assess powers and energies with respect to the deploy mission profile a 0D-1D lumped parameter model is achieved using Dymola Software. It permits the computation of the power and energy during deploy with respect to the speed order profile, system total reflected inertia, transcowl mass and aerodynamic loads. The model uses the inverse simulation features of Modelica as shown in Figure 6.11. The speed order is imposed and the closed loop performances are supposed perfect using such approach. The model then estimates what power and energy are required to obtain such performances.

The two variables (degrees of freedom) considered for this deploy mission profile model are the maximum speed of actuators, that varies the speed order profile, and the total system reflected inertia which depends on the sizing result of the different components.

As mentioned previously, the deploy mission profile is particular because it involves a phase where the ETRAS is operating in the motor quadrant and a second phase where it operates in generator quadrant as illustrated in Figure 6.12. Hence, each phases size different components.

For component sizing, it is chosen to evaluate the motor quadrant peak power P_{mot} and total energy E_{mot}, and also the generator quadrant peak power P_{gen} and energy E_{gen}.

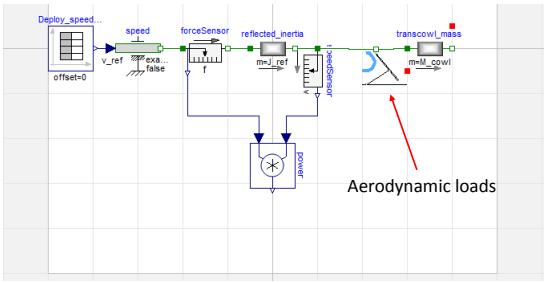

Fig. 6.11 ATO deploy mission profile model at transcowl level in Dymola

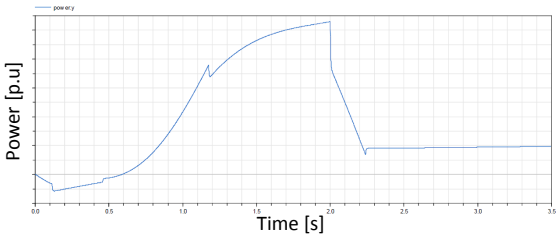

Fig. 6.12 Power response to ATO deploy profile for 300 [mm/s] actuator maximum speed

A sensitivity analysis is executed on the variables of interest with respect to maximum actuator speed $V_{act_{max}}$ and reflected inertia J_{ref}. An option would be to use a Sobol sensitivity analysis [206]. However, such method requires a very large number of samples. Futhermore, the SALIB open-source framework [105] provides only normalized sensitivities. Thus, it is not possible to assess the effect of parameters on the variable of interest only how it is distributed between them. It is well suited if it is known a priori of the sensitivity that all parameters chosen have a significant effect on the variable of interest which is not the case here. Thus, a Method of Morris is achieved using the SALib framework [105]. This method requires less samples (here 100 samples are used for two parameters) and it gives a non-normalized value of the mean elementary effect μ and the standard deviation of the elementary effect σ. Here, the obtained values are normalized with respect to the maximum value in the variable of interest results. The results of the sensitivity analysis, given in Figure 6.13, tell which parameters have to be considered for each variable of interest.

The results show that maximum actuator speed and reflected inertia have an effect on the peak power in motor quadrant. The maximum actuator speed is the only parameter that has an effect on the peak power in generator quadrant. However, they have a negligible effect on energies in both quadrant because the aerodynamic loads are most important than the inertial effect. In mean, effects are not significant (except for P_{gen}) but in standard deviation is relatively high and therefore has to be considered during sizing. Thus, surrogate models for peak power in generator quadrant and peak power in motor quadrant are achieved with respect to both actuator maximum speed and reflected inertia. A degree 3 polynomial response surface is used for P_{gen} and a degree 3 for P_{mot} as shown in Figure 6.14.

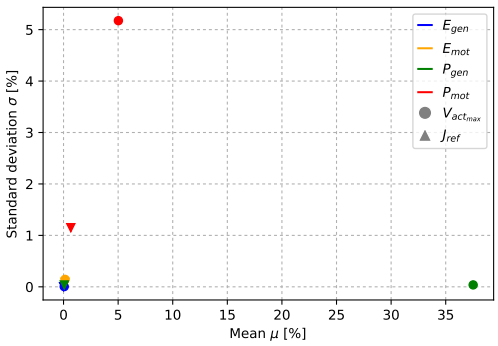

Fig. 6.13 Morris sensitivity analysis for ATO deploy for parameters $V_{act_{max}}$ and J_{ref}

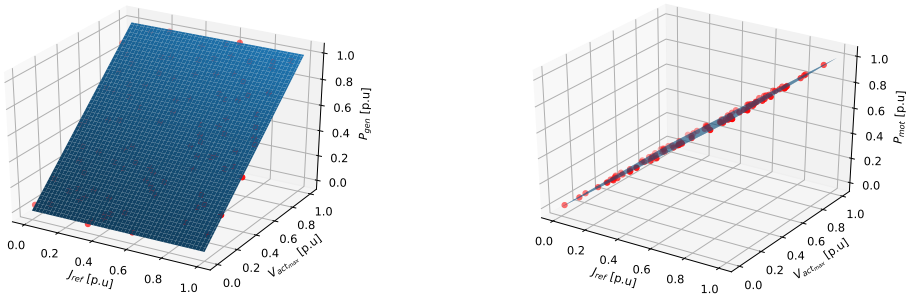

Fig. 6.14 Polynomial response surface for ATO deploy P_{gen} (left) and P_{mot} (right)

The negligible effect of J_{ref} on P_{gen} is confirmed on this figure. Hence, the surrogate for P_{gen} is achieved with respect to V_{max} only.

6.3.2 Stow Mission Profile

Similarly to the deploy model, the objective of the model developed for the stow mission profile is to determine maximum powers and energies with respect to a speed order profile, transcowl mass, total system inertia and aerodynamic loads. Figure 6.15 shows the trapezoidal speed profile used to achieve a full stroke stow in 3 seconds.

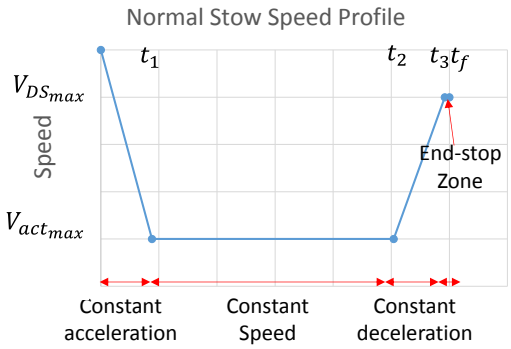

Fig. 6.15 Normal Stow speed profile principle

Details of the parametrization of the speed profile are given in Appendix C. As done for deploy, the stow mission profile is modelled using a lumped parameter model in Dymola (Figure 6.16) which differs only from deploy by its speed order profile and the aerodynamic loads model.

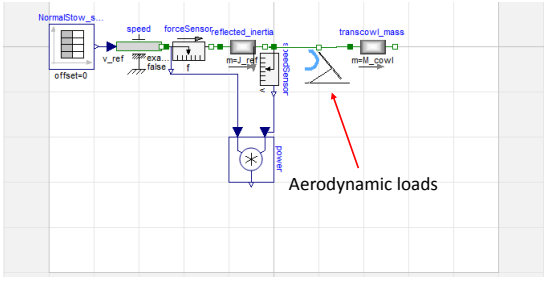

Fig. 6.16 Stow mission profile model at transcowl level in Dymola

Conversely to the deploy profile, during stow aerodynamic are always acting against the motion order. Hence, the ETRAS is operating in the motor quadrant as proves the power response shown in Figure 6.17. Hence, only motor quadrant peak power and energy are estimated here.

In order to verify what is the contribution of actuator maximum speed and reflected inertia on the peak power and energy response, a sensitivity analysis is achieved. The same analysis parameters and

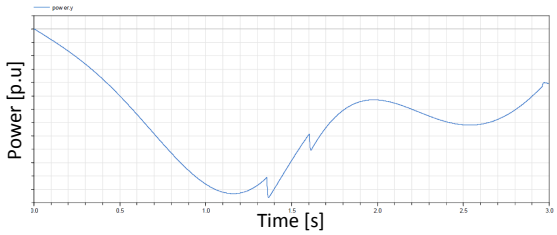

Fig. 6.17 Power response to stow profile for 300 [mm/s] actuator maximum speed

method than deploy mission profile are taken except maximum actuator speed bounds. The results of this analysis are outlined in Figure 6.18.

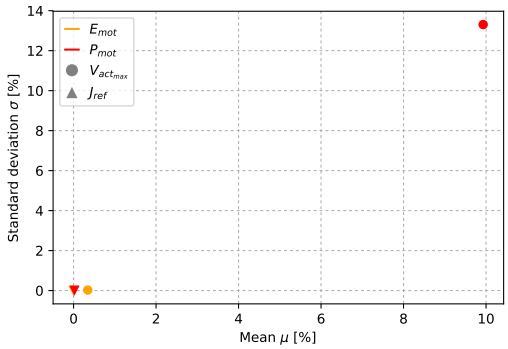

Fig. 6.18 Morris sensitivity analysis for stow for parameters $V_{act_{max}}$ and J_{ref}

The results show that maximum actuator speed and reflected inertia have an effect on the peak power in motor quadrant during stow. However, they have a negligible effect on energy in motor quadrant. Thus, a surrogate model for peak power in motor quadrant is achieved with respect to both actuator maximum speed and reflected inertia. A degree 3 polynomial response surface is used as shown in Figure 6.19.

6.3.3 Component temperatures

As mentioned previously, the ETRAS operates during a few seconds. Hence, the heat capacities drive the thermal behaviour when connected to relatively high thermal resistances.

If we consider a classical 2-body thermal model of a motor (winding w and iron ir) with two loss sources (Joule P_J and iron P_{ir}), with the thermal resistance ($R_{th,w}$) between winding and iron temperatures (Θ_w and Θ_{ir}) and the thermal resistance ($R_{th,ir}$) between iron and the skin temperatures (Θ_{ir} and Θ_{skin}), as illustrated in Figure 6.21, modelling and test results show that the thermal time constant are far more greater than the duration of the mission profiles.

Hence, the thermal resistances can be considered as infinite and thus open circuits for short time operations as illustrated in Figure 6.21.

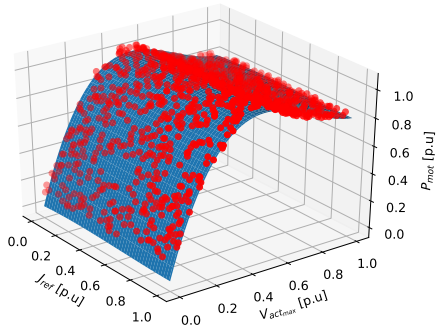

Fig. 6.19 Degree 3 polynomial response surface for stow P_{mot}

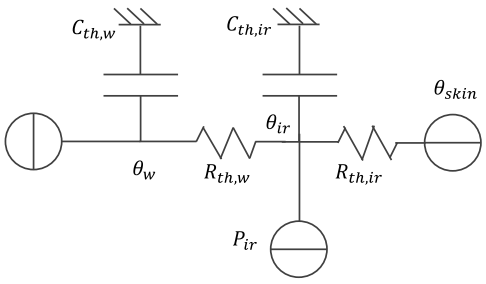

Fig. 6.20 2-body / 2-heat sources motor thermal model

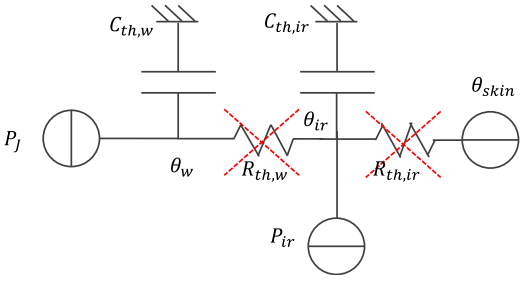

Fig. 6.21 Simplified motor thermal model

Typically for the autotransformer and the motor winding thermal model, only the winding heat capacity and the energy corresponding to the Joule losses are used to compute the maximum temperature. The braking resistor, inverter and housing temperatures are obtained by a simple thermal model that considers one same heat capacity (housing) and two heat sources (braking resistor and inverter).

Therefore, component temperatures Θ_{comp} can be obtained with respect to the available heat capacity C_{th} and the energy E to be dissipated as follows:

$$\Theta_{comp} = \Theta_{amb} + \frac{E}{C_{th}} \tag{6.1}$$

The energy to be dissipated are obtained for each component with respect to the energy at transcowl level and the different efficiencies involved in the power chain. As mentioned previously, the brushless motor and the autotransformer efficiencies are considered non-constant with the load and losses only come from the Joule losses. Such temperature estimation will be detailed in the estimation models of the motor.

6.3.4 Slider Jamming

The considered scenario that rules the sizing of mechanical components is a potential slider jamming. As the system shall be designed to be fail-safe, a single failure mode like slider jamming shall not engender the failure of a component and the system. Hence, such sizing scenario has to be represented in order to be included in the sizing model. Figure 6.22 illustrates the load path of a left slider jamming scenario. The aerodynamic loads pass through the Upper Right Actuator (URA), Lower Right Actuator (LRA), Lower Left Actuator (LLA) and the flexshafts to generate a compressive load on the Upper Left Actuator (ULA). It is assumed that one quarter of the aerodynamic loads are handled by the transcowl and the nacelle and the rest is handled by the actuator located near the jammed slider. The aerodynamic load chosen is the maximum load in transit of ATO deploy.

Furthermore, the motor torque generates an additional load on the ULA. The equivalent torque due to the shock of rotating inertias (mainly motor and flexshafts) is also considered.

The torque generated at actuator level is estimated as follows:

$$T_{jam} = \frac{3}{4} F_{aero} \frac{p_{bs}}{N_{red}} + T_{em} + \Omega_{mot} \sqrt{K_{eq} J_{eq}} \tag{6.2}$$

Where F_{aero} is the maximum aerodynamic load of the ATO deploy, T_{em} and Ω_{mot} are respectively the maximum torque and speed of the motor at jamming, J_{eq} the equivalent inertia (motor + flexshafts) and $K_{eq} = \frac{K_{fs_{mot}} \cdot K_{fs_{act}}}{K_{fs_{mot}} + K_{fs_{act}}}$ is the equivalent stiffness of the two left flexshafts in series.

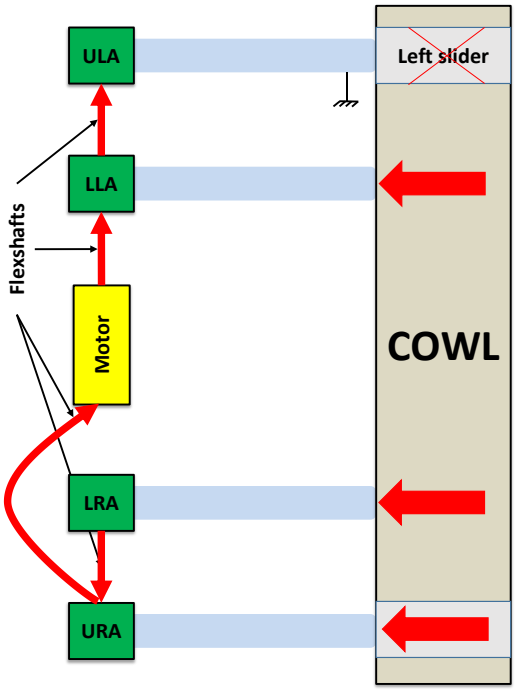

Fig. 6.22 Left slider jamming load case illustration

6.4 Estimation models

It this section, the following formalism is used to express the different scaling laws:

$$X^* = \frac{X}{X_{ref}} \tag{6.3}$$

Where X is the variable (unknown) of the component which is being sized and X_{ref} the parameter (known) of a reference component.

6.4.1 Brushless Motor

The motor is sized for constant magnetic saturation as the ETRAS operates during a very short time. Geometric similarity is assumed $D^*_{mot} = L^*_{mot}$ where D_{mot} is the motor diameter and L_{mot} its length.

The electromagnetic torque T_{em} of a brushless motor is obtained by multiplying the Laplace force F and r the distance between windings and the rotor axis:

$$T_{em} = F \cdot r = \int BJ_{cur} r dV \tag{6.4}$$

Where J_{cur} is the current density in slots, B the magnetic field generated by the magnets and dV an elementary volume of the machine.

As geometric similarity is assumed, the following scaling law can be derived [28]:

$$T^*_{em} = B^* J^*_{cur} D^{*4}_{mot} \tag{6.5}$$

The peak electromagnetic torque is limited by the magnetic saturation of the machine. The magnetic saturation is a function of the magnetic field generated by the permanent magnets and the current-induced magnetic field generated by the stator windings. A dimensionless number enables to express this magnetic saturation [209]:

$$\Pi_{em,sat} = \frac{B_{sat}}{J_{cur}\mu_0 D_{mot}} \tag{6.6}$$

Where B_{sat} is the magnetic saturation value of the ferromagnetic material of iron sheets and μ_0 its magnetic permeability.

As scaling laws assumed that the material remains constant $B^*_{sat} = 1$ and $\mu^*_0 = 1$. As it is chosen to size the motor on constant magnetic saturation, the saturation level of the machine has to remain constant. Hence, $\Pi^*_{em,sat} = 1$. These assumptions yield:

$$J^*_{cur} = D^{*-1}_{mot} \tag{6.7}$$

By combining Equation 6.7 and Equation 6.5 and assuming similar magnets, $B^* = 1$, we obtain:

$$D^*_{mot} = T^{*\frac{1}{3}}_{em} \tag{6.8}$$

Now that the motor size can be estimated with respect to the required peak torque the other motor parameters estimation models can be derived.

The motor mass estimation model is:

$$M^*_{mot} = D^{*3}_{mot} = T^*_{em} \tag{6.9}$$

Similarly its thermal capacity is obtained:

$$C^*_{th_{mot}} = D^{*3}_{mot} = T^*_{em} \tag{6.10}$$

Its inertia is computed as follows:

$$J^*_{mot} = D^{*5}_{mot} = T^{*\frac{5}{3}}_{em} \tag{6.11}$$

The mechanical speed of a motor is limited by the centrifugal forces acting on the permanent magnets. Hence, the following scaling law for estimating the maximum speed of the motor is used [28]:

$$\Omega^*_{mot_{max}} = D^{*-1}_{mot} = T^{*-\frac{1}{3}}_{em} \tag{6.12}$$

Power losses of a brushless motor can be decomposed into Joules losses and iron losses. Since magnetic saturation is considered, the modelling of iron losses is intricate and thus are not estimated

in this conceptual study. Furthermore, they remain relatively low when compared to Joule losses on this application. Hence, only Joule losses are taken into account in this preliminary study. For maximum torque they can be obtained as follows:

$$P^*_{J_{mot}} = J^{*2}_{cur} D^{*3}_{mot} = D^*_{mot} = T^{*\frac{1}{3}}_{em} \tag{6.13}$$

To obtain their value for intermediate torque and compute the motor winding temperature an α_J factor can be used.

For a short operating time, the temperature increase of a brushless motor is due to the Joule losses in the winding and is limited by the winding heat capacity:

$$\Theta_{mot} = \frac{E_{P_J}}{C_{th_{mot}}} \tag{6.14}$$

Where E_{P_J} is the energy of the Joule losses and $C_{th_{mot}}$ the heat capacity of the winding.

For a brushless motor the electromagnetic torque can be expresses as follows:

$$T_{em} = \frac{3}{2} \cdot k_e \cdot I_{max} \tag{6.15}$$

Where k_e is the torque constant and I_{max} is the max current of one phase. Deriving the previous equation to determine I_{max} yields:

$$I_{max} = \frac{2}{3} \cdot \frac{T_{em}}{k_e} \tag{6.16}$$

The Joule losses can be expressed for a three phase permanent magnet motor with respect to one phase winding resistance R_ψ and the current I_{max}:

$$P_{J_{mot}} = \frac{3}{2} R_\psi I^2_{max} = \frac{3}{2} R_\psi \left(\frac{2}{3} \cdot \frac{T_{em}}{k_e} \right)^2 \tag{6.17}$$

Which can be written with a factor α_J:

$$P_{J_{mot}} = \frac{2}{3} \frac{R_\psi}{k^2_e} \cdot T^2_{em} = \alpha_J \cdot T^2_{em} \tag{6.18}$$

The energy of the Joule losses can then be computed:

$$E_{P_J} = \int P_{J_{mot}}(t) \cdot dt = \alpha_J \cdot \int T_{em}(t)^2 \cdot dt \tag{6.19}$$

The factor α_J is linked to the size of the motor and can be estimated using a scaling law:

$$\alpha^*_J = \frac{P^*_{J_{mot}}}{T^{*2}_{em}} \tag{6.20}$$

Which can be expressed using the current density and the motor size:

$$\alpha_J^* = \frac{J_{cur}^{2*} \cdot D_{mot}^{*3}}{\left(J_{cur}^* \cdot D_{mot}^{*4}\right)^2} \tag{6.21}$$

Since the magnetic saturation is supposed constant $J_{cur}^* = D_{mot}^{*-1}$, which yields:

$$\alpha_J^* = \frac{D_{mot^*}}{D_{mot}^{*6}} = D_{mot}^{*-5} \tag{6.22}$$

Hence,

$$\alpha_J^* = D_{mot}^{*-5} = T_{em}^{*-\frac{5}{3}} \tag{6.23}$$

The Joule losses energy can be then estimated using the equivalent force at load level.

$$E_{P_J} = \alpha_J \cdot \int T_{em}(t)^2 \cdot dt = \frac{\alpha_J}{N_{red_{tot}}^2 \eta_{mech}^2} \cdot \cdot \int F(t)^2 \cdot dt \tag{6.24}$$

Where $N_{red_{tot}}$ is the total reduction ratio due to the bevel gear and the screw, η_{mech} the mechanical efficiency and $F(t)$ is the total force at transcowl level. $\int F(t)^2 \cdot dt$ is computed by analyzing the mission profile.

6.4.2 Autotransformer

The autotransformer is sized for constant magnetic saturation similarly as for the brushless motor. Hence, $J_{cur}^* = L_{at}^{*-1}$ where L_{at} is the length of the autotransformer and J_{cur} the current density in the windings.

The peak power of the autotransformer is obtained with assumed constant magnetic saturation:

$$P_{at}^* = U_{at}^* \cdot I_{at}^* = N_t^* B^* L_{ir_{at}}^{*2} \cdot \frac{J_{cur}^* L_{cop_{at}}^{*2}}{N_t^*} \tag{6.25}$$

Where U_{at} and I_{at} are respectively the equivalent DC output voltage and current of the ATRU, N_t is the number of winding turns, $L_{ir_{at}}$ the length of iron sheets, $L_{cop_{at}}$ the length of copper and B^* the magnetic field generated by the windings.

As geometric similarity is assumed, the copper and iron length increase similarly. Hence, $L_{ir_{at}}^* = L_{cop_{at}}^* = L_{at}^*$. In addition, as for the motor the magnetic field remains constant, $B^* = 1$. These assumptions lead to the following expression of the peak power:

$$P_{at}^* = B^* J_{cur}^* L_{at}^{*4} = L_{at}^{*3} \tag{6.26}$$

Hence, the length of the autotransformer can be obtained with respect to its peak power:

$$L_{at}^* = P_{at}^{*\frac{1}{3}} \tag{6.27}$$

The autotransformer mass estimation model is:

$$M_{at}^{*} = L_{at}^{*3} = P_{at}^{*} \tag{6.28}$$

Similarly its thermal capacity is obtained:

$$C_{th_{mot}}^{*} = L_{at}^{*3} = P_{at}^{*} \tag{6.29}$$

As for the motor, only the Joule losses are considered. The quantity of copper increases proportionally to the volume of the autotransformer. Hence,

$$P_{J_{at}}^{*} = J_{cur}^{*2} L_{at}^{*3} = L_{at}^{*} = P_{at}^{*\frac{1}{3}} \tag{6.30}$$

Conversely to the motor, the output voltage is considered constant. Hence, Joule losses can be estimated for a given power:

$$P_{J_{at}}(t) = \alpha_J \cdot P_{at}(t)^2 \tag{6.31}$$

Where α_J can be expressed as:

$$\alpha_J^{*} = \frac{P_{J_{at}}}{P_{at}^2} = L_{at}^{*-5} \tag{6.32}$$

6.4.3 Braking Resistor, Inverter and Heat Sink

The braking resistor resistance has to be adapted to the DC voltage U_{DC} and the peak generator voltage P_{gen}:

$$R_{bs} = \frac{U_{DC}^2}{P_{gen}} \tag{6.33}$$

The resistance is considered with constant thickness. Hence, only the printed circuit configuration can be used to change the resistance for a given resistor shape.

The peak power limit is proportional to the surface of the braking resistor:

$$P_{bs}^{*} = L_{bs}^{*2} \tag{6.34}$$

Where L_{bs} is length of the braking resistor.

The continuous power limit is not considered here due to the very short operating time.

The inverter is selected on its peak power, only its maximum operating temperature is evaluated. For that, it is assumed to have a constant efficiency.

The inverter and the braking resistor dissipate their energy losses through the heat sink. Hence, the heat sink is sized as an amount of aluminum mass with respect to the energy to be dissipated and the maximum operating temperatures of the inverter transistors and diodes as well as the braking resistor.

6.4.4 Flexshaft

The flexshafts are selected on their maximum torque and using scaling laws based on maximum shear stress. They are assimilated to cylinder shafts.

The shear stress σ_{fs} of a cylinder shaft is expressed as follows:

$$\sigma_{fs} = \frac{T_{fs}}{I_G} \cdot \frac{D_{fs}}{2} \tag{6.35}$$

Where T_{fs} is the peak torque applied to the flexshaft, I_G the area moment inertia of a solid cylinder and D_{fs} its diameter.

When transposing to scaling laws it yields:

$$\sigma^*_{fs} = \frac{T^*_{fs}}{I^*_G} \cdot D^*_{fs} = \frac{T^*_{fs}}{D^{*4}_{fs}} \cdot D^*_{fs} = \frac{T^*_{fs}}{D^{*3}_{fs}} \tag{6.36}$$

The mechanical properties remain the same and thus the level of stress shall remain similar $\sigma^*_{fs} = 1$. Hence, the diameter of the flexshaft can be obtained with respect to the required peak torque:

$$D^*_{fs} = T^{*\frac{1}{3}}_{fs} \tag{6.37}$$

The flexshaft mass is length dependant. The mass is obtained for the four flexshaft as they have different length.

$$M_{fs} = \left(\frac{D_{fs}}{D_{fs_{ref}}}\right)^2 \cdot M_{l_{ref}} L_{fs} = \left(\frac{T_{fs}}{T_{fs_{ref}}}\right)^{\frac{2}{3}} \cdot M_{l_{ref}} L_{fs} \tag{6.38}$$

Where $D_{fs_{ref}}$ and $M_{l_{ref}}$ are respectively the diameter and the linear mass of the reference flexshaft and L_{fs} the length of the flexshaft to be sized.

The linear softness $G_{l_{fs}}$ of the flexshaft is computed with respect to the area moment of inertia and the modulus of rigidity G of the material:

$$G^*_{l_{fs}} = \frac{1}{I^*_G \cdot G^*} \tag{6.39}$$

The material properties remain the same, hence $G^* = 1$. Thus,

$$G^*_{l_{fs}} = \frac{1}{I^*_G} = \frac{1}{D^{*4}_{fs}} \tag{6.40}$$

The torsional stiffness can then be derived:

$$K_{fs} = \left(\frac{D_{fs}}{D_{fs_{ref}}}\right)^4 \cdot \frac{1}{G_{l_{fs_{ref}}} \cdot L_{fs}} = \left(\frac{T_{fs}}{T_{fs_{ref}}}\right)^{\frac{4}{3}} \cdot \frac{1}{G_{l_{fs_{ref}}} \cdot L_{fs}} \tag{6.41}$$

The inertia is obtained by derivation of the diameter estimation:

$$J_{fs} = \left(\frac{D_{fs}}{D_{fs_{ref}}}\right)^4 \cdot L_{fs} = \left(\frac{T_{fs}}{T_{fs_{ref}}}\right)^{\frac{4}{3}} \cdot L_{fs} \tag{6.42}$$

6.4.5 Bevel gear

The bevel gear is sized for constant teeth Hertz pressure coefficient and selected on its peak torque.

The Hertz stress applied on a gear teeth can be expressed as follows [66]:

$$\sigma_H = C_k \sqrt{K C_d} \tag{6.43}$$

Where C_k is a geometric factor, C_d an overall de-rating factor and K the K-factor (pitting index). Geometric similarity is assumed, hence $C_k^* = 1$ and the reference bevel gear is sized for a previous ETRAS application, hence $C_d^* = 1$ and $K^* = 1$.

K-factor can be expressed with respect to the gear primitive diameter D_{bg} and teeth face width b, tangent force acting on the teeth F_t and its reduction ratio N_red:

$$K = \frac{F_t}{b \cdot D_{bg}} \cdot \frac{N_{red}+1}{N_{red}} \tag{6.44}$$

As the gear is selected on its peak torque T_{bg}, the K-factor can be re-written as follow:

$$K = \frac{2T_{bg}}{b \cdot D_{bg}^2} \cdot \frac{N_{red}+1}{N_{red}} \tag{6.45}$$

Transposing to scaling laws yields:

$$K^* = \frac{T_{bg}^*}{b^* \cdot D_{bg}^{*2}} \cdot \left(\frac{N_{red}+1}{N_{red}}\right)^* \tag{6.46}$$

A good practice in bevel gear design is to keep a fixed ratio between teeth face width and outer gear diameter (typically 0.3). Hence, $b^* = D_{bg}^*$. As the K-factor is kept constant $K^* = 1$, the diameter of the gear can be estimated:

$$D_{bg}^* = \left(T_{bg}^* \cdot \left(\frac{N_{red}+1}{N_{red}}\right)^*\right)^{\frac{1}{3}} \tag{6.47}$$

The mass of the gear can then be computed:

$$M_{bg}^* = D_{bg}^{*3} = T_{bg}^* \cdot \left(\frac{N_{red}+1}{N_{red}}\right)^* \tag{6.48}$$

6.4.6 Thrust Bearing

The thrust bearing is selected on its maximum axial load. The scaling laws are obtained for constant mechanical stress as done for the thrust bearing in Chapter 4.

Thrust bearing length is computed as follow:

$$L^*_{bearing} = F^{*\frac{1}{2}}_{bearing} \tag{6.49}$$

The estimation of the thrust bearing mass is then derived

$$M^*_{bearing} = L^{*3}_{bearing} = F^{*\frac{3}{2}}_{bearing} \tag{6.50}$$

6.4.7 Ball Screw

The ball screw is selected on its maximum axial load F_{bs}. The scaling laws are similar to the ones used for the Thrust Vector Control application studied in Chapter 4.

The nut mass is estimated as follows:

$$M^*_{nut} = F^{*\frac{3}{2}}_{bs} \tag{6.51}$$

The screw diameter can be expressed:

$$D^*_{screw} = F^{*\frac{1}{2}}_{bs} \tag{6.52}$$

The screw mass, which includes the tube, is obtained with respect to the axial load and the stroke S_{bs}:

$$M^*_{screw} = F^*_{bs} \cdot S^*_{bs} \tag{6.53}$$

However, because in the case of the ETRAS the ball screw stroke is relatively high, buckling load is computed:

$$F^*_{buck} = f^*_b \cdot D^{*4}_{screw} \cdot S^{*-2}_{bs} = D^{*4}_{screw} \cdot S^{*-2}_{bs} \tag{6.54}$$

Where f_b is a factor which depends on how the screw is mounted. The reference screw is mounted similarly, hence $f^*_b = 1$. Axial stiffness is also computed for the slider jamming scenario:

$$K^*_{screw} = F^*_{bs} \cdot S^{*-1}_{bs} \tag{6.55}$$

As well as the screw inertia:

$$J^*_{screw} = F^{*2}_{bs} \cdot S^*_{bs} \tag{6.56}$$

6.5 Actuation System Preliminary sizing

The objective of this section is to achieve and preliminary sizing of the ETRAS and obtain an optimal mass breakdown for the considered sizing scenarios, design variables and design constraints. This optimal mass breakdown will help fix mechanical components characteristics and enable a more detailed design of the electrical power chain in the next section.

6.5.1 Sizing Problem Definition

The sizing problem for the ETRAS consists of minimizing the overall mass of the system subject to the technological limits of components and system requirements. Some preliminary power and energy trades on the different mission profiles (ATO deploy cold and hot, stow cold) enable to better determine which mission profile impacts which design drivers.

The ATO deploy cold scenario, due to the overstow phase with very low efficiencies, leads to the low speed peak electromagnetic torque of the motor T_{em}. The ATO deploy hot scenario drives the thermal sizing of electrical components since the energies are important and moreover the ambient temperature is high: motor temperature Θ_{mot}, inverter temperature Θ_{inv}, ATRU temperature Θ_{ATRU}, braking resistor temperature Θ_{br} and housing temperature Θ_{hous}. It also impacts the peak power of the braking resistor and also generates the maximum jamming load as the mechanical efficiency is high. The stow cold scenario requires important power demand to the ATRU and the inverter. Hence, it enables to select these components. These interaction simplifications of electrical power chain components design drivers and sizing scenarios are outlined in Figure 6.23.

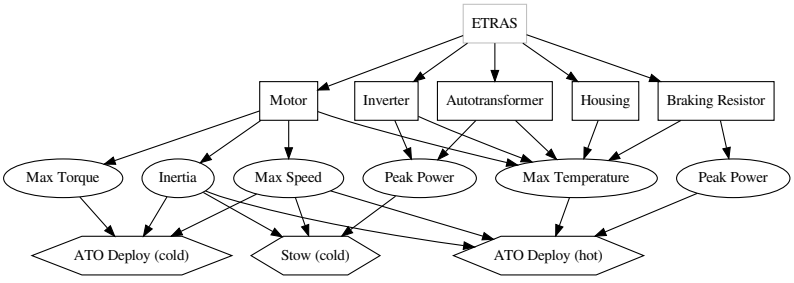

Fig. 6.23 Simplified interactions between design drivers and sizing scenarios of electrical components

6.5.2 System Analysis Model

The system analysis model is composed of a BOA causal block that analysis the mission profiles and distributes the sizing inputs the the other disciplines. The two variables are the maximum speed of the deploy profile $V_{max_{act,d}}$ and of the stow profile $V_{max_{act,s}}$. The autotransformer is selected on the maximum power in motor quadrant P_{mot} and an over-sizing coefficient $k_{os_{at}}$ is introduced to oversize it if the temperature constraint is no respected. Similarly the motor is selected on its maximum torque and is oversized thanks to $k_{os_{mot}}$. Conversely, the housing mass is directly estimated with respect to the inverter, the braking resistor and housing skin temperature by taking the most constraining configuration. The mission profile analysis gives the maximum torque and speed in order to size the mechanical components and the motor. Mechanical components load analysis enables to distribute the loads with respect to the reduction ratio. The total reflected inertia J_{tot} is computed and then used in the mission profile analysis.

The sizing problem includes one multidisciplinary coupling due to the slider jamming scenario. The inertias and stiffness of components are required to achieve jamming load analysis but are evaluated using components sizing models that require the value of this jamming load. Hence, this multidisciplinary coupling has to be solved to provide a consistent design solution.

The NVH monolithic formulation is used to solve it. It consists of adding a normalized design variable $k_{os_{jam}}$ and an inequality constraint for each coupling and the system total mass as an objective. In the present case, the coupling can be described by:

$$\begin{aligned} F_{jam_{slider}} &= f\left(M_{eq}, K_{eq}\right) \\ M_{eq} &= g\left(F_{jam_{slider}}\right) \\ K_{eq} &= h\left(F_{jam_{slider}}\right) \end{aligned} \tag{6.57}$$

Where $F_{jam_{slider}}$ is the load due to the jamming, M_{eq} the equivalent inertia at actuator level and K_{eq} the equivalent stiffness.

Is transformed into:

$$\begin{aligned} F_{jam_{slider}} &= k_{os_{jam}} \cdot F_{max} \\ J_{eq} &= g\left(F_{jam_{slider}}\right) \\ K_{eq} &= h\left(F_{jam_{slider}}\right) \\ F_{jam_{slider}} &\geq f\left(J_{eq}, K_{eq}\right) \end{aligned} \tag{6.58}$$

Where F_{max} is the maximum load of the profiles.

This formulation is the NVH presented previously which performs a low number of function evaluations. Nevertheless, the use of the inequality is only possible because decreasing the nominal torque $F_{jam_{slider}}$ decreases the total system mass and that is the optimization objective.

An outline of the system analysis model in given in Figure 6.24, in the form of a XDSM diagram [135].

6.5.3 Optimization Problem Formulation

The sizing optimization implemented minimizes the total mass of the ETRAS M_{tot} with respect to deploy and stow speed profile maximum speeds $V_{max_{act,d}}$, $V_{max_{act,s}}$, autotransformer and motor oversizing factors and the consistency variable slider jamming scenario $k_{os_{jam}}$. The constraints come from technological limits of components like maximum speed ($\Omega_{mot}, \Omega_{fs}$) and maximum temperature ($\Theta_{at}, \Theta_{mot}$). One consistency constraint introduced previously is used to solve the multidisciplinary coupling. The optimization problem formulation is the following:

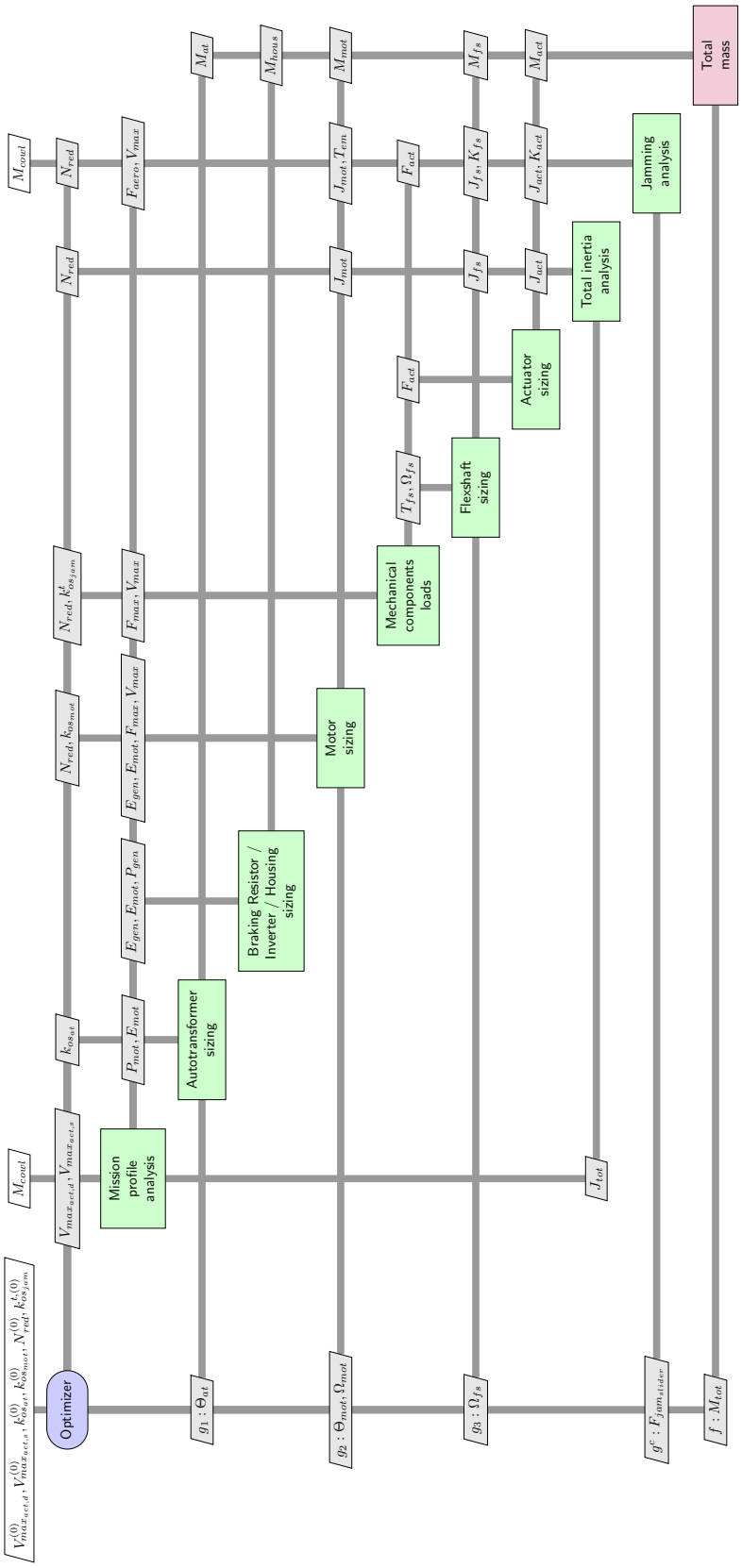

Fig. 6.24 XDSM diagram of the ETRAS preliminary sizing model

$$
\begin{aligned}
&\text{minimize} && M_{tot} \\
&\text{with respect to} && V_{max_{act,d}}, V_{max_{act,s}}, k_{os_{mot}}, k_{os_{at}}, N_{red}, k_{os_{jam}} \\
&\text{subject to} && \Omega_{mot} - \Omega_{mot_{max}} \leq 0 \\
& && \Omega_{fs} - \Omega_{fs_{max}} \leq 0 \\
& && F_{jam_s} - F_{nom_{mech}} \leq 0 \\
& && \Theta_{at} - \Theta_{at_{max}} \leq 0 \\
& && \Theta_{mot} - \Theta_{mot_{max}} \leq 0
\end{aligned}
\tag{6.59}
$$

6.5.4 Results

Performing this optimization provides the possibility to assess rapidly integration parameters such as mass and dimensions of the system in order to make system integration trade-offs. For example such sizing code can assess the effect of changes of requirements like deploy time on the total system mass. In addition, the effect of changes of technologies like motor inertia can be evaluated rapidly. In Figure 6.25, the effect of consideration of the slider jamming scenario is shown.

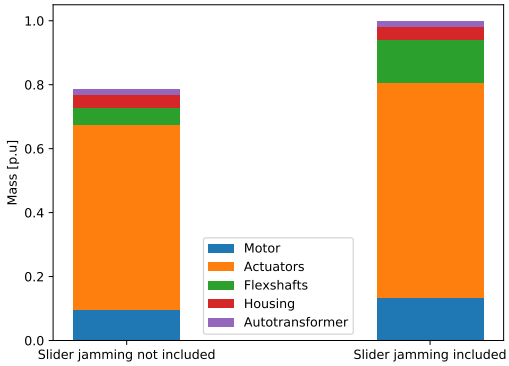

Fig. 6.25 Comparison of ETRAS preliminary sizing mass breakdown for no jamming and jamming

The jamming scenario strongly impacts the sizing of the electro-mechanical power chain. The choice of reduction ratio is directly impacted and thus the sizing of the motor and the mechanical components. In order to limit the effect of jamming, emphasis can be placed on designing a non-optimal motor is terms of torque density but with an optimized inertia. For different input configurations, the optimal mass tends toward the slowest deploy maximum speed. Changing the parameters and running analysis show that the mission profile and the associated trajectory have a significant effect on the result. Hence, more detailed trajectory model will be studied in the next part.

6.6 Preliminary Trajectory Optimization

The previous preliminary study has shown that the mission profile has a non-negligible impact on the power and energies required by the system. However, the preliminary approach which used one degree of freedom on the trapezoidal speed profile can be improved. To improve the mission profile analysis and optimization it is chosen in this section to investigate trajectory optimization and inverse simulation.

6.6.1 Description

The need of a thrust reverser system is to have an actuation system (ETRAS) which moves the transcowl from a stowed position to a fully deployed position within a certain amount of time. Here, only the ATO deploy is studied. Higher performances requirements for ETRAS ATO deploy to improve aircraft braking time, are considered:

- Time to 85% of full stroke shall be less than $2.0s$.
- Time to 100% of full stroke shall be less than $3.5s$.
- The deploy times shall be respected for the given aerodynamic load and ambient temperature.

The objective is to achieve a preliminary investigation on trajectories that minimizes the powers and/or energies at transcowl level as they are the inputs of the ETRAS sizing. The second step would be to determine the optimal trajectory that minimizes the overall size of the ETRAS by combining optimal trajectory and optimal sizing. Hence, the first study considers only the aerodynamic loads, the transcowl mass and the system total inertia. These values are fixed and the trajectory is the only variable. The maximum speed at transcowl level is limited. In addition, in the event of a motor control loss during the phase where the aerodynamic loads tend to deploy the transcowl, the ETRAS has to prevent from high shocks on the deploy end-stops. Thus, an electro-mechanical brake is engaged when such event is detected in order to brake the system and reduce the force generated by a shock to the specified level. However, the braking torque capacity and engagement time of such devices determine a speed limit with respect to position. This speed constraint will also be included in the optimal trajectory problem. The overstow phase and TLS zone phase are fixed and cannot be optimized. Therefore, they are not represented here. However, these two phases are considered by a time delay ($0.8s$) and a initial position and speed configuration. The initial position and initial speed conditions of the rest of the deploy phase considered here correspond respectively to the final position of the TLS zone and the maximum speed in the TLS zone.

6.6.2 Modelling

The overspeed limit is an envelop of position/speed configurations in which the ETRAS shall remain in order to be able to stop the motion, thanks to a braking device, despite the aerodynamic loads once

the motor control loss occurs. This protects the system from overloads due to high speed arrivals on mechanical end-stops. The benefits of friction in the mechanical power chain are not considered to be conservative. The study is achieved at transcowl level.

Once the motor control losses occurs the ETRAS is considered as a single mass $M_{ref_{tot}}$ submitted to aerodynamic loads F_{aero}. After the brake engagement time t_r the mass is submitted to aerodynamic loads which tend to open the transcowl and a constant braking force F_{brake}. The behaviour of the system to motor loss of control in different initial position and speed configurations in given in Figure 6.26.

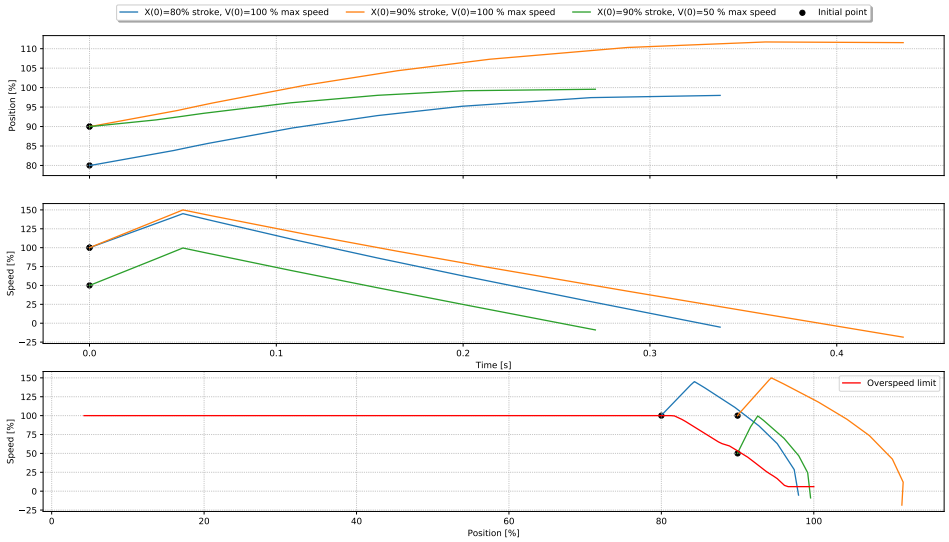

Fig. 6.26 Overspeed limit principle

It is shown that if the motor control loss occurs outside the overspeed limit envelop the ETRAS is not brought to the end-stop speed limit before reaching full stroke. The modelling and construction of this envelop is quite tricky due to the fact that the aerodynamic loads are position dependant and the braking starts with a delay. The system can be modelled by the following differential equation:

$$M_{ref_{tot}} \cdot \frac{\mathrm{d}^2 X(t)}{\mathrm{d}t^2} = F_{load}\left(X(t)\right) - F_{brake}\left(t - t_r\right) \tag{6.60}$$

The overspeed limit is determined by analyzing the system response in terms of braking distance for different position and speed initial conditions. Two difficulties have to be undertaken: the position dependant load and the delay of the speed brake (hybrid system). This has to be solved numerically. A detailed description of the overspeed profile and construction is given in Appendix C.

To model the trajectory, inverse simulation is used. The acceleration with respect to time is discretized into a vector A of N variables (in our case $N = 200$) as well as time. In some trajectory optimization ones may prefer to choose position or speed as variables [41]. As the acceleration is

requested to compute inertial loads, it has to be determined. Here, it is preferred to integration of state vectors that differentiation as it is numerically more accurate. The trajectory shape can be fully determined by this acceleration vector. This vector is used to determined the speed V by integrating the acceleration with respect to time and the initial speed is the maximum speed in TLS zone. Similarly, the position X is obtained by integrating the speed with respect to time and the initial position is the end of the TLS zone. The trajectory can be represented by the following equations:

$$V(t) = \int A(t) \cdot dt + V_{TLS_{max}} \tag{6.61}$$

$$X(t) = \int V(t) \cdot dt + X_{TLS} \tag{6.62}$$

The aerodynamic loads are position dependent. Now that the position with respect to time is known, the aerodynamic loads can be expressed with respect to time. The inertial load due to the acceleration of the system total inertia $M_{ref_{tot}}$ can also be expressed with respect to time since $A(t)$ is known. The total force required to moved the transcowl with respect to time can be expressed:

$$F_{tot}(t) = F_{load}(t) + M_{ref_{tot}} \cdot A(t) \tag{6.63}$$

Where $F_{load}(t) = h(X(t))$.

As $F_{tot}(t)$ and $V(t)$ are known the power required to move the transcowl can now be determined:

$$P(t) = F_{tot}(t) \cdot V(t) \tag{6.64}$$

The activity which is represented by the exchange of energy [69] during the deployment of the transcowl. This energy is expressed by integrating the absolute value of the power with respect to time:

$$E(t) = \int \mid P(t) \mid \cdot dt \tag{6.65}$$

The sign convention taken where the positive direction is the deploy direction leads to the following results:

- The negative power corresponds to the motor quadrant
- The positive power corresponds to the generator quadrant

6.6.3 Optimization Problem Formulation

The optimization relies on a inverse simulation model. Other trajectory optimization techniques use different approaches and generally formulate it as an optimal control problem by introducing non-linear state variables [104]. The purpose here is to use the different models that represent the trajectory and determine the acceleration vector which minimizes a given variable of interest subject to a set of constraints.

The only design variable for the optimization problem, as mentioned previously, is the acceleration of dimension N. The constraints are multiple. The first constraint is the speed constraint which is a

size N vector that combines the overall maximum speed at transcowl level and the maximum speed due to overspeed scenario. Two other constraints come from the position requirements. The trajectory has to pass through 85 % of stroke at a given time t_1 and 100 % of stroke by the end of the deploy sequence t_{deploy}.

Four different objectives are studied:

- The maximum power between generator power and motor power $max(P_{gen}, P_{mot})$
- The total activity energy E
- The maximum generator power P_{gen}
- The maximum motor power P_{mot}

Where $P_{mot} = \mid min\,(P(t)) \mid$ and $P_{gen} = max\,(P(t))$.

For the P_{mot} objective the optimization problem can be formulated as follows:

$$\begin{array}{lll} \text{minimize} & P_{mot} & 1 \\ \text{with respect to} & A(t) & N \\ \text{subject to} & V(X) - V_{max}(X) \leq 0 & N \\ & 0.85 \cdot stroke - X(t_1) \leq 0 & 1 \\ & stroke - X(t_{deploy}) \leq 0 & 1 \end{array} \tag{6.66}$$

The problem is represented in Figure 6.27 using the XDSM diagram formalism [135] for the maximum motor power objective P_{mot}.

The optimization problem is implemented using the open-source framework OpenMDAO [89]. The SLSQP gradient-based optimizer is used. Symbolic differentiation is used when possible, otherwise complex-step differentiation is performed. For components that achieved an interpolation, the differentiation method used is finite difference. As the number of design constraints in higher than the number of design variables, the MAUD architecture [113] is implemented in the adjoint form.

6.6.4 Results

Other energy quantities than the total activity E can be used as objectives. The energy in motor quadrant E_{mot} affects the ATRU, inverter and motor size. The energy in generator quadrant E_{gen} has an effect on the motor, inverter, braking resistor and housing. The quantity $\int F(t)^2 \cdot dt$ is the image of the motor Joule losses and has an effect on the motor size. Nevertheless, each of these quantities when chosen as the objective lead to the same trajectory as shown in Figure 6.28. Hence, only the trajectory for E as the objective will be compared to power objectives trajectories.

The trajectory optimization problem is solved for the four different objectives outlined previously. Figure 6.29 gives the different optimization results in terms of power and energy. It also shows that for the for different objectives the speed constraint is respected making the design feasible.

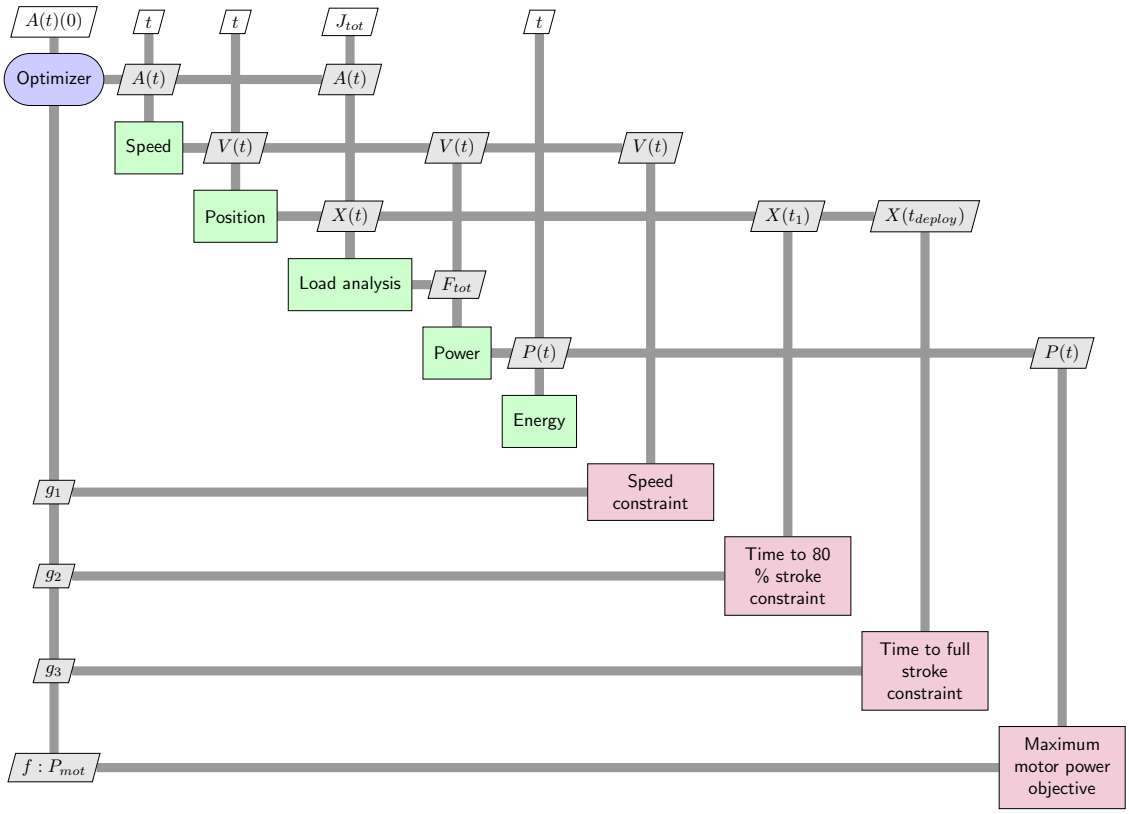

Fig. 6.27 XDSM diagram of the ETRAS trajectory optimization problem

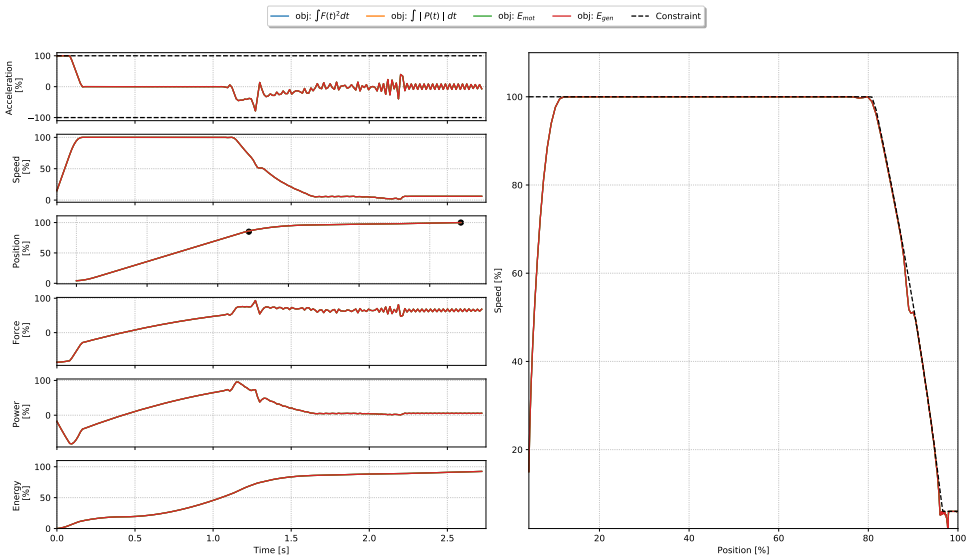

Fig. 6.28 Optimization results for different energy quantities objectives

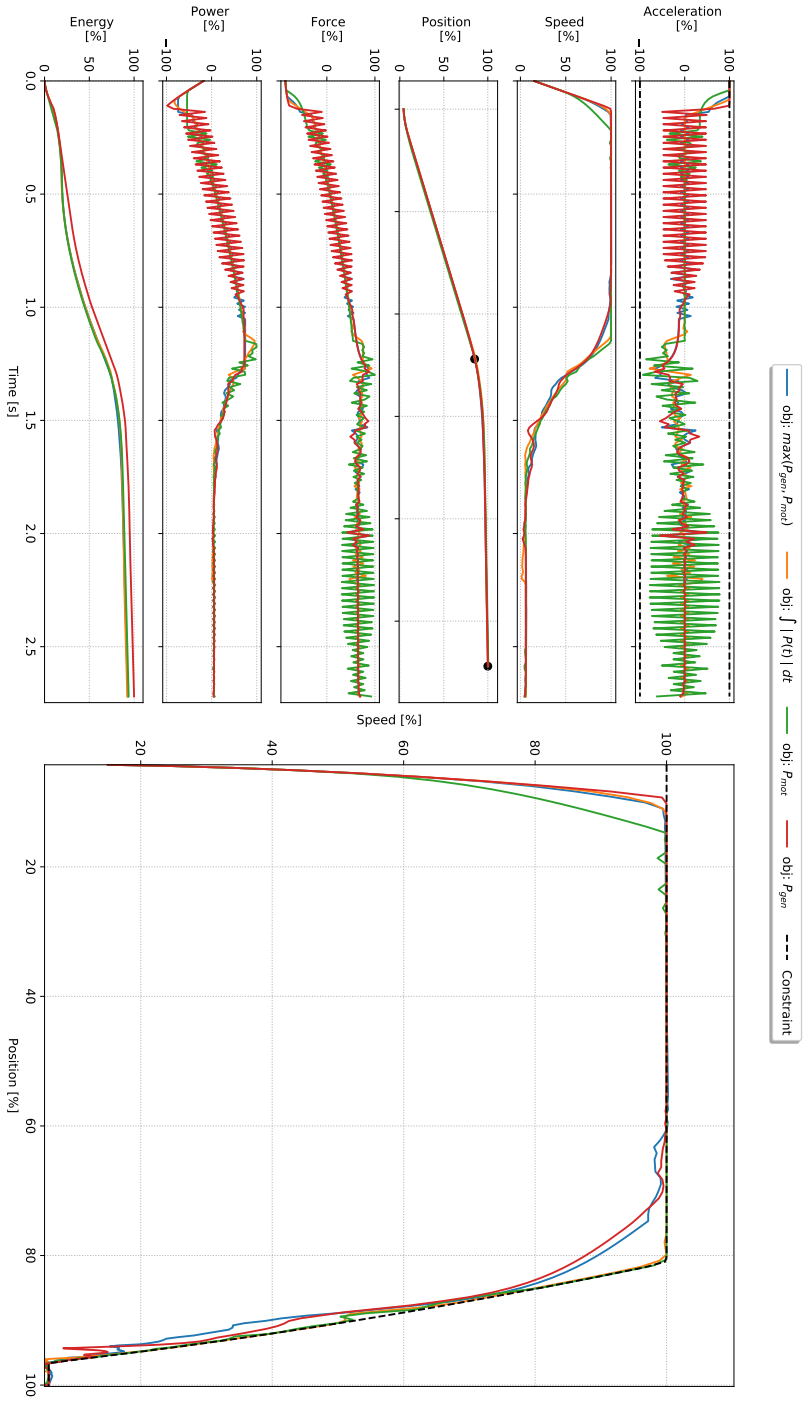

Fig. 6.29 Optimization results for different objectives

It is shown that the objective choice affects the trajectory choice. Force responses are almost identical for each solution. Hence, the power is directly the image of speed. Therefore, the minimizing the energies will enhance the motor, the housing and the ATRU size. Minimizing the motor power will decrease the inverter and ATRU sizes. Minimizing the generator power will decrease the inverter and braking resistor size. Results show that minimizing the motor power yields a gain of 50 % of motor power when compared to optimizing the generator power. Nevertheless, the time lost by decreasing the speed in the motor quadrant has to be caught up by increasing the speed and therefore the power by 25 % in the generator quadrant. Minimizing the maximum power between generator and motor yields a compromise by saving 25 % of generator power and motor power. Optimizing the total energy penalizes the maximum powers and does not provide significant insights on energy savings.

As the voltage is supposed constant, decreasing the motor power will decrease the current and therefore the sizing of the electronic devices involved in the ATRU. Furthermore, the motor power is directly the power supplied by the aircraft whereas the power lost in generator is handled by the ETRAS. Therefore, the most relevant choice of trajectory optimization objective will be the motor power. The number of winding turns is also a variable in order to adapt the motor torque constant to decrease voltage. However, increasing the number of turns increases the inductance and resistance.

6.6.5 Improving Trajectory Smoothness

The trajectories obtained for the previous objective and model lead to some oscillations on the acceleration design variables. This subsection investigates ways to improve this.

The oscillations seem to appear when the value of the design variable does not improve the objective value and does not affect the feasibility. Indeed, when minimizing the motor quadrant power P_{mot} almost no oscillations appear during that phase whereas in the generator quadrant high oscillations appear. Conversely, for P_{gen} no oscillations appear in the generator quadrant but only in the motor quadrant.

To affect the feasibility an additional constraint which limits the acceleration variation between two steps can be added. However, this constraint would be size N and would add more numerical complexity to the problem which is already difficult to solve. Hence, this option is not investigated. Another option is to change the model. The design variable can be the jerk (acceleration derivative) instead of the acceleration in order to benefit from the frequency filtering of integration. This filtering effect is notable on Figure 6.29 when comparing acceleration and speed vectors.

The last solution path would be to change the objective. For instance, choosing an objective for which oscillations increase its value can help. Thus, the choice of the root mean square value of the power as the objective is investigated.

Another, more complex, solution can be to choose an objective that mixes the different quantities of interest for the sizing which can be seen as an multi-objective optimization. Since a sizing code of the ETRAS has been previously developed, it can be used with a higher fidelity model of the mission profile to assess to effect of trajectory on the ETRAS size. As seen in the previous trajectory

optimization results, the speed constraint is tight and no lower maximum speed can provide the deploy time requirements. Hence, the jamming scenario that determines the size of mechanical components does not vary. Therefore, it is assumed that the trajectory has no impact on the mechanical components sizing. Nevertheless, the trajectory has an effect on powers and energies that have an effect on the electrical power chain components. An approach can be to export the sizing code from BOA and integrating in this trajectory optimization code. However, the approach chosen is to use a simplified model of the system sizing model.

The mission profile analysis component is removed and the different inputs of other component sizing are set into inputs. The objective here is to determine the effect of P_{mot}, P_{gen}, E_{mot} and E_{gen} on the ETRAS total mass. For that a full factorial DOE is achieved around (-20 % to 20 %) the previously obtained optimum for these four input variables. Then the samples are evaluated by running optimizations on BOA. The normalized total mass of the system is then expressed by:

$$M_{tot_{norm}} = \frac{\alpha_1}{P_{mot_{max}}} \cdot P_{mot} + \frac{\alpha_2}{P_{gen_{max}}} \cdot P_{gen} + \frac{\alpha_3}{E_{mot_{max}}} + \frac{\alpha_4}{E_{gen_{max}}} \cdot E_{gen} \tag{6.67}$$

Where $P_{mot_{max}}$, $P_{gen_{max}}$, $E_{mot_{max}}$ and $E_{gen_{max}}$ are the maximum values in the experiments. The values α_1, α_2, α_3, α_4 are the slopes of the linear regression on the $M_{tot_{norm}}$ experiments for each of the four inputs variables.

Figure 6.30 gives the resulting trajectories for the different proposed objectives and models in comparison to the previous P_{mot} objective choice.

The different solutions provide less oscillatory trajectories when compared to the original P_{mot}. The most efficient is minimizing the RMS value of the power. However, it does not provide the optimum motor quadrant peak power P_{mot} but the best P_{gen}. Changing the design variable for jerk improves oscillation but does find the optimal P_{mot} when compared to when varying the acceleration. The multi-objective approach is the solution that generates, relatively small, oscillations. As it mixes power and energies in the objective, its is the less performant to find to optimal P_{mot}. Nevertheless, α_1 could be tuned to find the compromise between aircraft consumption and ETRAS total mass.

6.7 Trajectory and Electrical Power Chain Sizing Optimization

6.7.1 Description

The preliminary sizes and characteristics of components have been obtained is the previous section. The objective now is to use trajectory optimization and motor control flux-weakening strategy and winding configuration to minimize the mass of the electrical power chain by minimizing the current used for the deploy sequence. For this purpose, the study focuses on the motor because it is on its technological limit due to voltage and current supply. At transcowl level, the system is modelled as previously. Now, friction due to mechanical components are considered non-constant and assessed for cold and hot ambient temperatures. The ball screws and the bevel gears generate load dependent friction through an efficiency value and a fixed dry friction. The friction due to flexshafts are

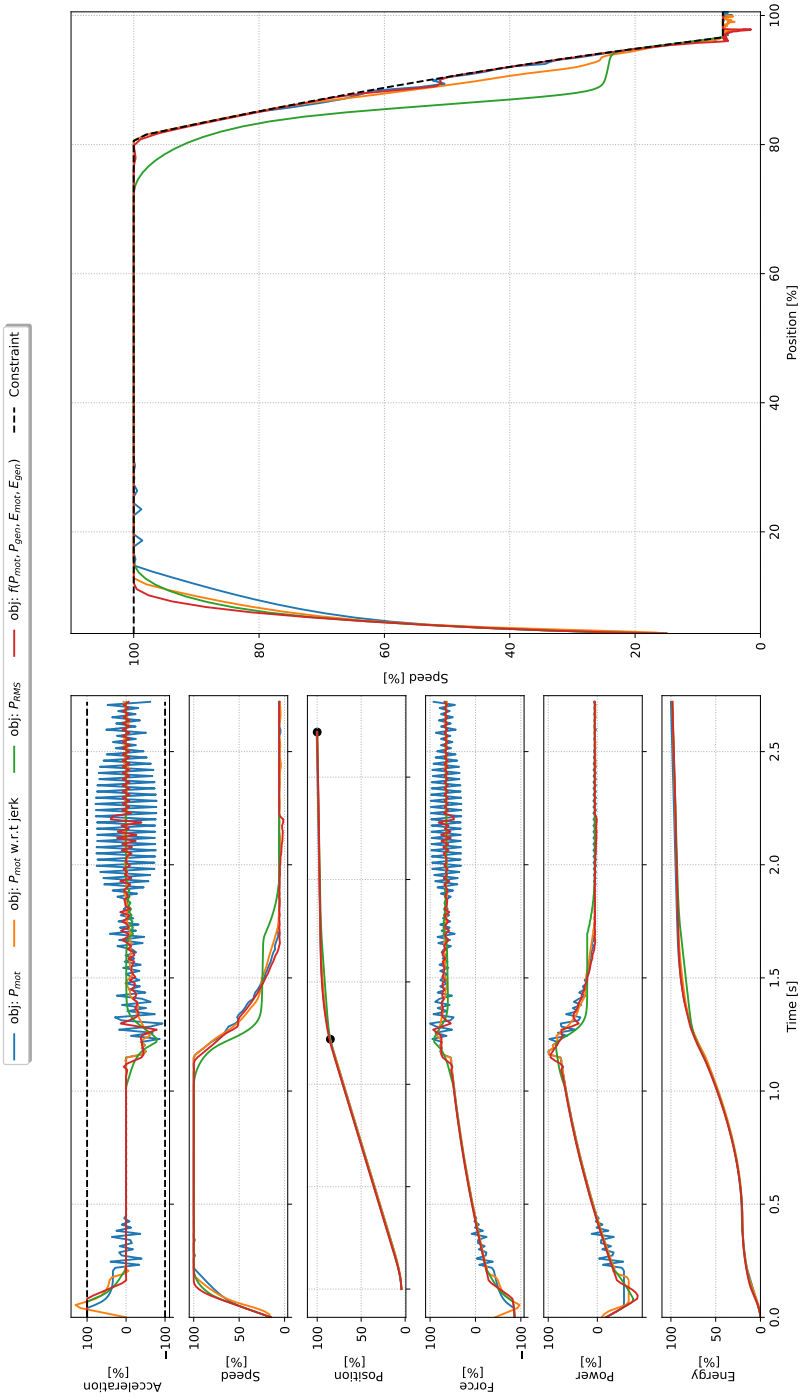

Fig. 6.30 Effect of objective on the trajectory smoothness

decomposed into dry friction, viscous friction and load dependent friction. Therefore, the mission profile has an effect on total frictions at motor level.

Two different voltage supply configurations are consider on the ATO deploy profile. When functioning in motor quadrant, the ETRAS is supplied by the aircraft. Hence, the voltage of the inverter is fixed to the minimum guaranteed by the aircraft and the efficiency of the ATRU. Conversely, in generator quadrant the DC voltage supply is chosen to be as high as the inverter and the braking resistor offers. This voltage is higher than in motor quadrant. It provides high torque at high speed capability during the braking phase. In addition, having enough torque during the braking phase is mandatory to avoid the risk that the aerodynamic loads cannot be controlled and continue accelerating the transcowl until end-stops are impacted. In the motor quadrant, too low torque will stop the transcowl because aerodynamic loads are acting against deployment. It will lead to a landing without thrust reversal but there are no risk to damage the ETRAS or the nacelle. In addition, the current is limited due to the technological choice of power electronics components.

In order to provide high torques at high speeds with limited voltage and current supply, a flux-weakening strategy is needed for controlling the motor. Furthermore, flux-weakening enables to maximize the motor torque for a given current and voltage when saliency is introduced by saturating the machine iron core [47]. The motor is saturated in order to exploit a maximum the magnetic properties of the iron core and therefore minimize the overall mass of the motor.

6.7.2 Modelling

The electrical behaviour of an electrical motor can be represented by a phasor diagram. Figure 6.31 gives a simplified representation of the electrical motor by neglecting the voltage drop due to its electrical resistance.

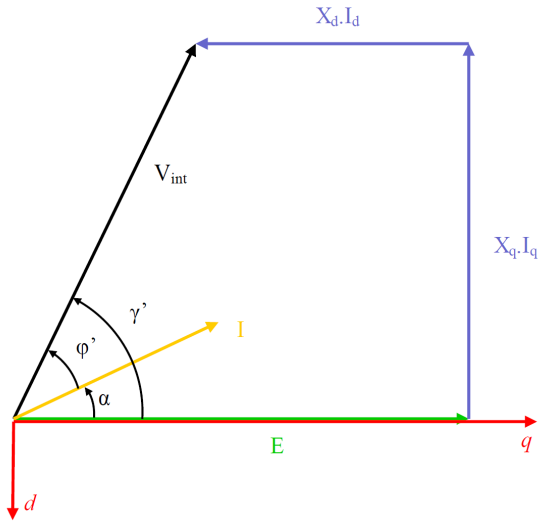

Fig. 6.31 Simplified phasor diagram for synchronous electrical machine [47]

V_{int} is the interphase voltage, X_q and X_d are the reactance due to the inductance L_q and L_q and E is the electromotive force (EMF). Here, the motor voltage V corresponds to phase to neutral voltage where $V = \frac{V_{int}}{\sqrt{3}}$

$$T_{em} = \frac{3}{2} \cdot \left(k_e I_{peak} \cos(\alpha) + (L_q - L_d) I_{peak}^2 \cos(\alpha) \sin(\alpha)\right) \tag{6.68}$$

Where k_e is the electromagnetic torque constant with $E = k_e \cdot \Omega_{mot}$ and I_{peak} the peak current.

$$V = \sqrt{\left(E - L_d \omega_e I_{peak} \sin(\alpha)\right)^2 + \left(L_q \omega_e I_{peak} \cos(\alpha)\right)^2} \tag{6.69}$$

Where $\omega_e = pp \cdot \Omega_{mot}$ with pp the number of pole pairs and Ω_{mot} the speed of the motor.

Generally, for a non-saturated machine with no saliency the maximum electromagnetic torque is obtained for $\alpha = 0$. However, for machines which have some saliency the maximum electromagnetic is not for $\alpha = 0$ as shown in Figure 6.32. Hence, flux-weakening enables to set the angle to the maximum torque.

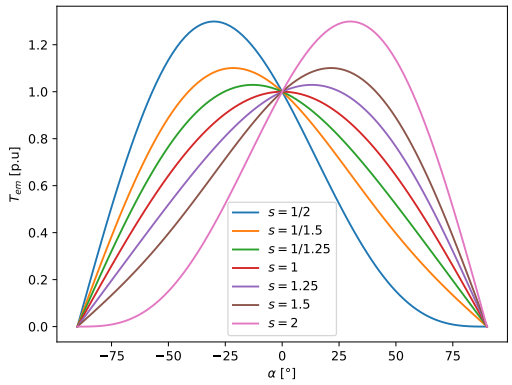

Fig. 6.32 Effect of saliency and angle α on electromagnetic torque

When machine with no saliency are saturated, some saliency can appear due to the saturation of zones close to the air gap. The saturation zones lead to a larger air gap in the zone which introduces changes in the inductance L_q and L_d. The saliency due to magnetic saturation does not increase the maximum torque capacity of the machine but just shifts to an angle different that zero. Hence, flux-weakening can also be used to maximize the electromagnetic torque of saturated machine. Figure 6.33 shows the effect of angle α for different levels of peak current and thus different levels of saturation. The torque and voltage are normalized and given for a fixed speed.

Therefore, the inductances L_q and L_d and the electromagnetic torque constant k_e are characterized by FEM simulations and enables to obtain an analytical expression of them with respect to the peak current I_{peak} for the chosen design. The main need for flux-weakening strategy in the ETRAS application is to provide torque at high speeds. The voltage is limited due to the high EMF E at high speeds. To increase the voltage limit the flux-weakening tunes the angle α to meet the voltage

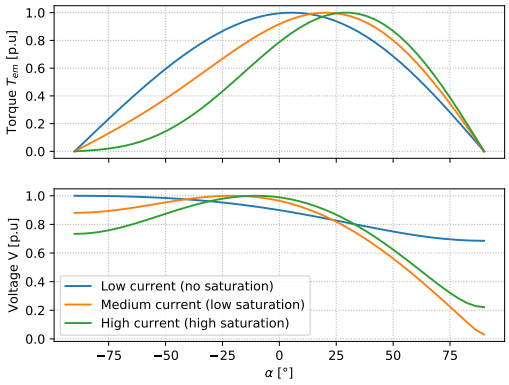

Fig. 6.33 Effect of angle α on electromagnetic torque and voltage for a saturated permanent magnet synchronous motor (PMSM)

objective. However, it decreases the torque capacity once a certain value of angle is reached. Hence, when using flux-weakening strategy, the speed of the motor is only limited by its mechanical behaviour and the electrical losses it can dissipate.

In order to decrease the voltage limit, the number of winding turns can be carefully decreased since it leads to higher current for the same torque. Thus, the number of winding turns is considered as a design variable. Nevertheless, it has an effect on the electrical characteristics. Increasing the number of winding turns N_w increases the electromagnetic torque constant:

$$k_e^* = N_w^* \tag{6.70}$$

It also increases the motor resistance since the winding length increases and the wire section decreases if the copper volume is supposed constant:

$$R_{mot}^* = N_w^{*2} \tag{6.71}$$

The number of turns also increases the inductances of the machine:

$$L_q^* = N_w^{*2} \tag{6.72}$$

Joule losses of the motor are obtained with the corresponding winding RMS current $I_{rms} = \frac{I_{peak}}{\sqrt{2}}$:

$$P_J(t) = 3 \cdot R_{mot} \cdot I_{rms}(t)^2 \tag{6.73}$$

The winding temperature is estimated by integrating the Joule losses and injecting them in their heat capacity $C_{th_{mot}}$:

$$\Theta_{mot}(t) = \frac{1}{C_{th_{mot}}} \int P_J(t) dt \tag{6.74}$$

Solving analytically the Equation 6.68 and Equation 6.69 for determining I_{peak} and V with respect to the torque T_{em} and speed Ω_{mot} requirements is intricate due to the introduction of complex solutions [47]. Hence, an optimization approach is necessary to determined current and voltage for a given operating point.

6.7.3 Optimization Problem Formulation

In the optimization problem the motor peak current is considered as a design variable. The optimizer determines the optimal current for the required torque $T_{em_{req}}$ by introducing an equality constraints that converges the required torque and the real torque. The model determines the minimum voltage required for the operating point thanks to Equation 6.69. This voltage has to remain beneath the supply voltage V_{supply} which depends on the operating quadrant. In order to increase the voltage limit, the number of winding turns N_{mot} and the angle α are considered as design variables.

In order to reduce the dimension of the peak current design variable, the peak current $I_{peak,\alpha=0}$ is first determined for no flux-weakening $\alpha = 0$. Then a factor $k_{I_{peak}}$ with relatively small dimensions (0.1 - 5.0) tunes the value of this current to compute the real peak current $I_{peak} = k_{I_{peak}} \cdot I_{peak,\alpha=0}$. These peak current has to remain lower than the maximum current supply I_{supply}. It is then used along with the inductances and angle α to compute the real electromagnetic torque T_{em}. The objective chosen is to minimize the maximum winding temperature Θ_{mot} which is an image of the Joule losses and the current required.

$$
\begin{array}{lll}
\text{minimize} & \Theta_{mot} & 1 \\
\text{with respect to} & A(t) & N \\
 & k_{I_{max}}(t) & N \\
 & \alpha(t) & N \\
 & N_{mot} & 1 \\
\text{subject to} & V(X) - V_{max}(X) \leq 0 & N \\
 & 0.85 \cdot stroke - X(t_1) \leq 0 & 1 \\
 & stroke - X(t_{deploy}) \leq 0 & 1 \\
 & V - V_{supply} \leq 0 & N \\
 & I_{peak} - I_{supply} \leq 0 & 1 \\
 & T_{em_{req}} - T_{em} = 0 & N
\end{array}
\tag{6.75}
$$

The optimization and system analysis model structure is given in Figure 6.34.

The results were obtained for $N = 200$ variables. This leads to 601 design variables and 603 design constraints. The same optimizer configurations are used than for the previous preliminary trajectory optimization.

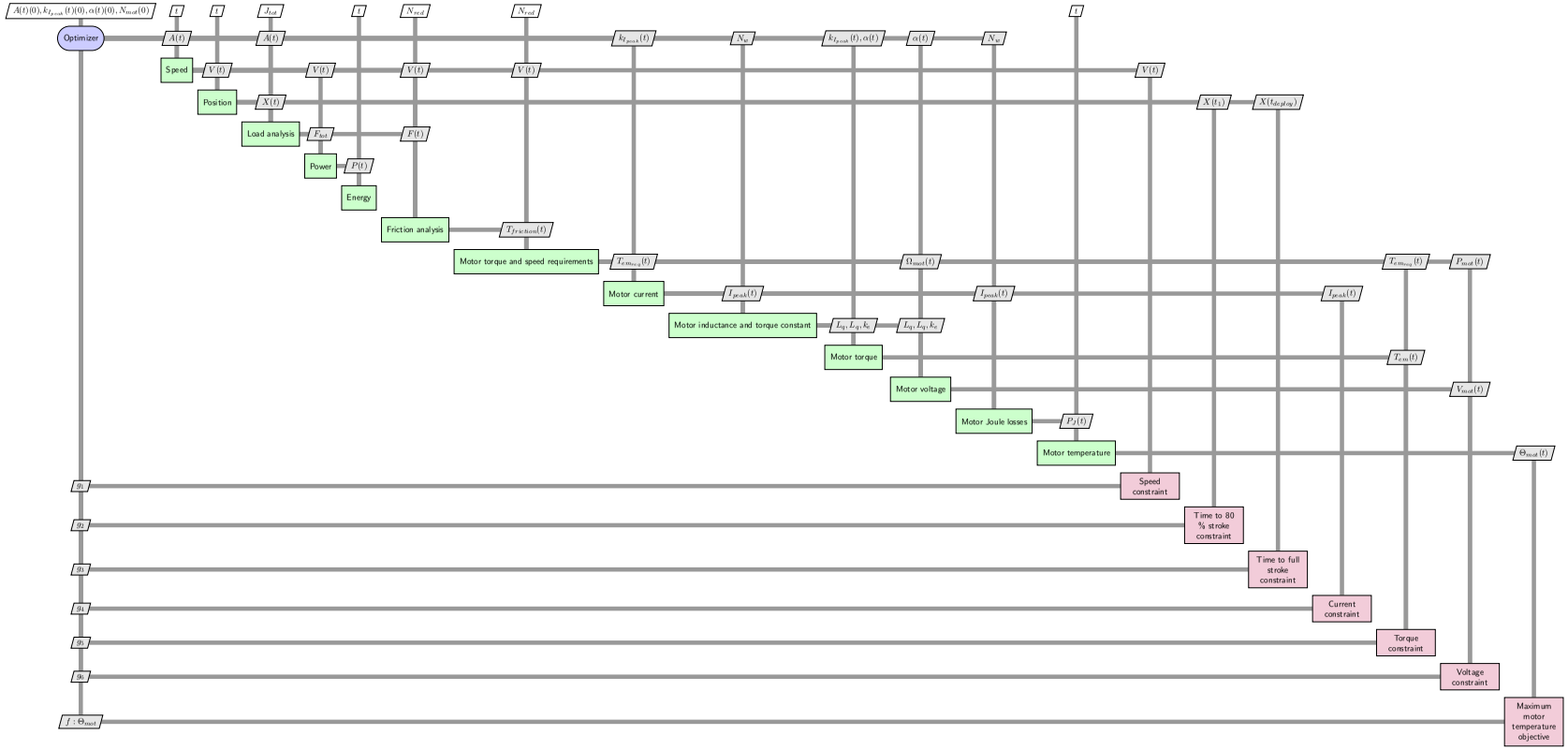

Fig. 6.34 XDSM diagram of the ETRAS trajectory and electrical power chain optimization problem

6.7.4 Results

The optimization results at system level for a cold ATO deploy and a hot ATO deploy are shown in Figure 6.35. The trajectory obtained is different than the previous trajectory optimization. This is due to the integration of friction which changes the equivalent load and also to the addition of voltage supply constraint which is equivalent to a speed constraint at high speed. Nevertheless, the speed constraint due to the overspeed phase remain respected.

Figure 6.36 give the results at motor level for both cold and hot ATO deploy profiles. During the motor quadrant phase the voltage is at its maximum which leads to the introduction of flux-weakening by tuning the angle α. The equality between the required torque and the effective torque is guaranteed.

These results show that a flux-weakening strategy is needed to enable ETRAS applications using voltages similar to the aircraft AC voltage. However, solution with boost converters or transformers can naturally offer higher voltage to inverter and motor. Exploiting fully the magnetic characteristics of the motor and applying advanced control strategies can shift the boundary where higher voltage and higher current are mandatory.

The results enables to determine whether a motor design can match a mission profile with degrees of freedoms on the number of winding turns and flux-weakening control strategy. The motor design can then be achieved by applying the most constraining operating envelop (torque vs speed) by combining the cold and hot profiles results. Once the design is fixed, it is possible tu build flux-weakening control table that determines the optimal current and angle α in terms of losses for the required operating point (torque, speed) [149]. These tables can then be embedded in the control software of the actuation system.

6.8 Conclusion

This chapter has proposed two steps to address the ETRAS sizing problem to deal with the complexity of the mission profile and the closeness of component technological limits on such application. First, a preliminary sizing study of the ETRAS was performed with a low fidelity model of the mechanical efficiencies and the mission profile along with a higher fidelity system sizing model. Then, the sizing used a higher fidelity model of the mechanical efficiencies and the mission profile along with simplified assessment on the system sizing model.

In the first part, main design drivers and sizing scenarios of an ETRAS application have been outlined. It has revealed that even in preliminary phase, the number of sizing scenarios was significant. Hence, due to this sizing problem complexity the preliminary sizing phase has to be supported by a methodology. The methodology proposed in this thesis was therefore applied to this complex sizing problem. Emphasis was placed on dynamic criterion and how to integrate dynamic simulation within the algebraic optimization framework BOA. For that surrogate models of FMU were used. New estimation models were introduced in particular for transient thermal responses in short operating application like ETRAS. The preliminary sizing optimization was achieved in order to determine the

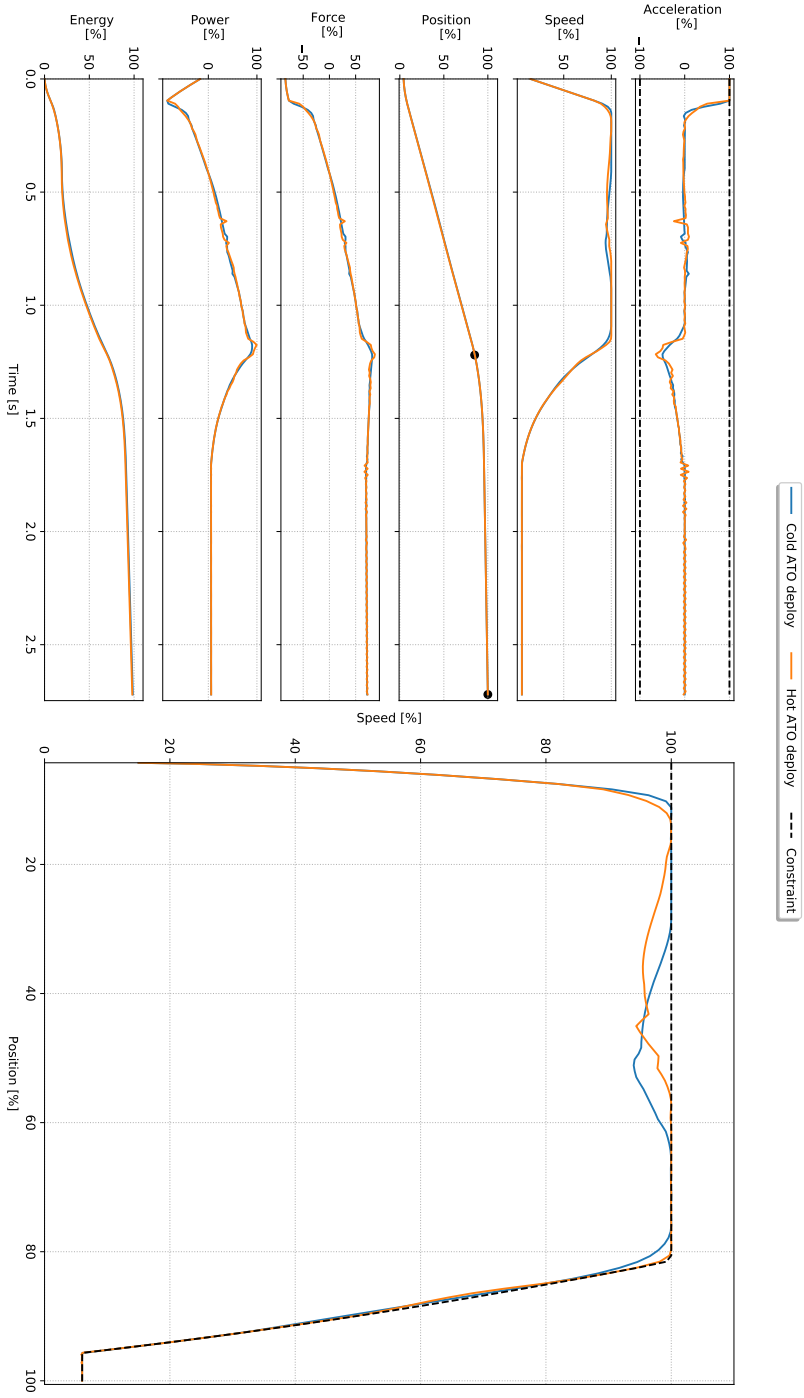

Fig. 6.35 Optimization results for system level characteristics

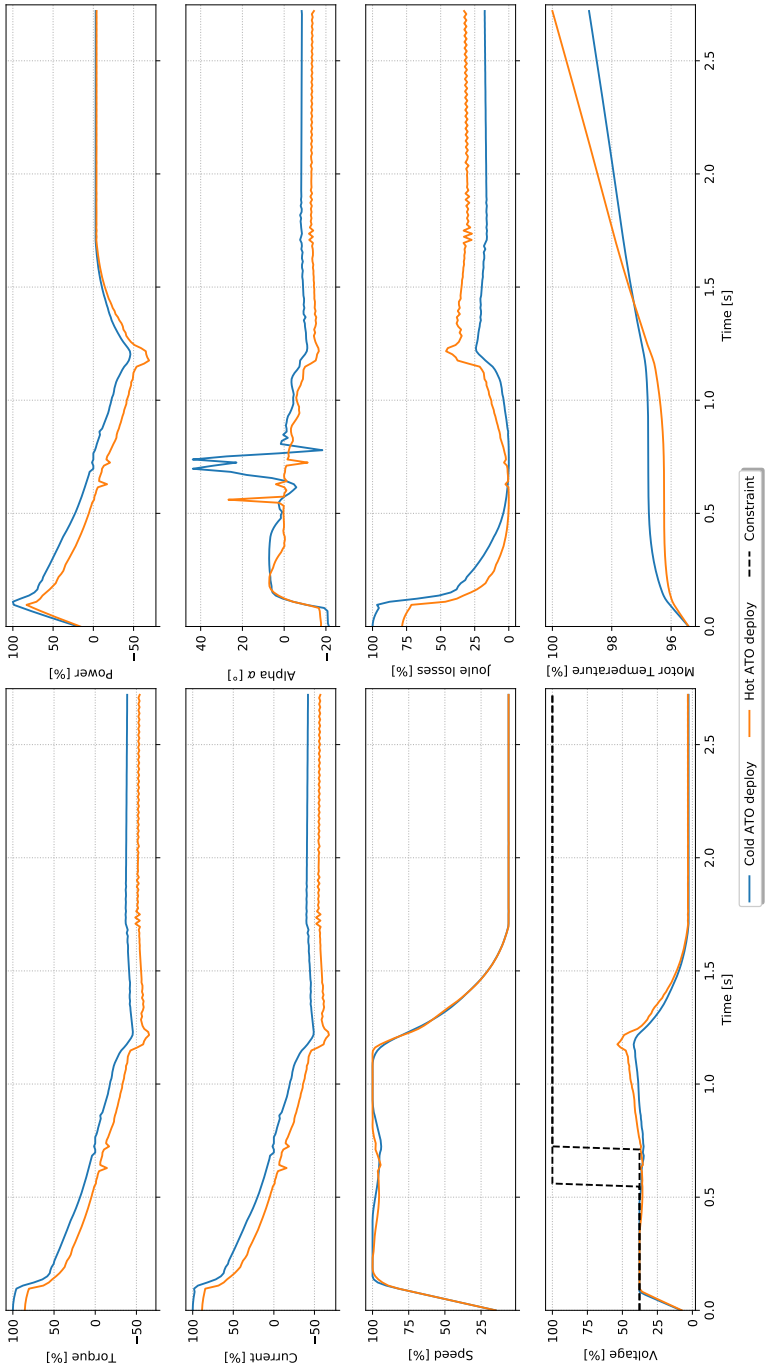

Fig. 6.36 Optimization results for motor level characteristics

main characteristics of components. The effect of slider jamming consideration in the sizing has been underlined. It has proven that for ETRAS like for many other systems, a system level compromise is necessary. Once the preliminary sizing was achieved the main components characteristics were obtained.

In the second part, it was decided to go from a trapezoidal speed profile to a discretized acceleration profile. This enabled to determine a detailed trajectory of the ETRAS. A detailed model of dynamic and static loads were then provided. A trajectory optimization problem using inverse simulation was then implemented. The effect of the objective choice on the resulting trajectory and the other variable of interest were given. It resulted that the most pertinent choice of objective was the maximum power in motor quadrant has it decreased the motor power by 50 % and therefore the power withdrawn from the aircraft electrical network. Effects of the objective choice on the trajectory smoothness have been outlined. A pseudo multi-objective approach that uses the system sizing model to tune the different objective influence has been outlined. The trajectory optimization technique was then extended to the electrical power chain design. The objective was to optimize the size of electrical component by minimizing the equivalent current. In order to make some more detailed assessment of the loads, the detailed friction models were implemented in order to consider the effect on speed and static load on the motor electromagnetic torque. The study focused on the brushless motor which is on its technological limit for the voltage and current supply configuration of this application. Hence, a flux-weakening strategy has been proposed to add some degrees of freedom to the design.

This trajectory optimization code enables to assess the effect of requirements like deploy time on the power consumption rapidly (less than an hour). Thus, power consumption versus thrust reverser braking effectiveness trade offs can be achieved. This chapter concludes another application of holistic sizing approaches to aerospace actuation systems.

Chapter 7

Conclusions

7.1 Summary and Perspectives

The context of this work has been presented in Chapter 1 to better understand the needs as well as the stakeholders involved in this thesis. The More Electrical Aircraft course of action has leaded to significant rethinks of how an aircraft with electrical technologies for subsystems and components has to be designed. The introduction of these new technologies on critical applications like commercial aircraft has to be achieved incrementally and rigorously. Hence, a design methodology is needed for the development of the forthcoming systems and subsystems. This thesis focused on electro-mechanical actuation systems and the development of a methodology to design them in a holistic and more integrated manner. Furthermore, a concern for contemporary industrial companies is the capitalization of their expertise. In addition, a better reuse of previous work was needed to enable rapid bid or trade-off studies. Thus, knowledge management was also an concern for the developed design methodology. Another motivation was to propose a new approach for designing actuation systems in order to avoid the common sequential iterative design process which results in costly human iterations. The disparate components used in actuation systems involves multiple discipline specialists. It is important to note that the results of previous thesis, the Safran company experts and Institut Clément Ader researchers have provided significant foundation and support to this work. This thesis can be seen as the continuation of Aurélien Reysset's thesis. Furthermore, an important collaboration with Florian Sanchez was settled as his thesis focused on component detailed design whereas this thesis focuses on the system level design with emphasis placed on technologies. The collaboration between the company and the laboratory was very fruitful mainly because the objectives (requirements) were clearly defined at the beginning. The main objective of this thesis was to obtained a functional sizing framework within three years. The sub-objectives were to enable knowledge capitalization, collaborative work, rapid analysis and provide optimization capabilities. Low simulation runtime is an important criteria in an industrial context where the main objective is rapid decision making during design activities especially in early bid and proposal phases. The methodology developed has been applied to different aerospace actuation systems with increasing complexity. Nevertheless, the methodology and the approaches can be extended to other products and applications.

Chapter 2 has provided a large scope of engineering design approaches. It first outlined different aircraft engineering problems to show that each had particular challenges. The common challenge in engineering design is the management of interdependencies. Embedded mechatronic system design is core part of the aerospace engineering problem solving. These particular systems require multi-level, multi-engineering specialization, multi-physical and multi-scale design approaches. In addition, as the knowledge is spread among multiple discipline specialist and engineering tools, it is harder to capitalize and to interact. Furthermore, embedded applications require high consideration for reliability, and particularity critical sizing scenarios, during their design. Additionally, design challenges appear when systems are large and multidisciplinary. In order to assist the development of complex and critical products, many Model-Based Design solution exist throughout the design process. MBSE tools provide solutions for requirements engineering, functional and organic architecture definition. Reliability analysis standards and tools enable us to conduct system reliability analysis. Preliminary sizing methods contribute to determining component specifications with respect to system specifications by making system level assessment of component geometries using 0D modelling. However, this is often achieved using spreadsheets by a single expert who masters system trade-off with respect to engineering specializations. Engineering specializations for model-based design tools are numerous and cover all the fields of engineering. They focus on high fidelity simulations of component performances, typically 2D-3D, which require high simulation runtimes. Virtual prototyping provide simulation tools based on lumped parameter models, typically 0D-1D, to represent the system overall behaviour with respect to physical parameters and to support the validation process. Co-simulation between design tools is soaring. Specific software provide such feature even in the cloud and is referred to as distributed engineering. However, these solutions often results is costly simulation runtimes. To encourage co-simulation, some model exchange standards have been develop such as the FMI standard. Surrogate modelling techniques permit to represent complicated simulation results of 0D-1D or 3D models with low computational cost. The VPLM methodology enables to generate relatively simple algebraic expressions. The state of the art of Model-Based Design tools showed that many activities were required beside the main focus of this thesis, that is sizing. Moreover, it has been outlined that sizing could also use complex simulations usually available later in the design process by using surrogate modelling.

Due to the complexity of embedded mechatronic systems, a systemic design approach is needed. Different formalism can be used to represent a system, the N2 diagram seems very adapted for multidisciplinary systems. For this purpose many approaches are used to decompose the system into multiple disciplines and coordinate them. The decomposition of a system is intricate, it depends strongly on the type of application. Mechatronic system are commonly decomposed in two main layers: system and component. None-the-less, design is an iterative process between both of these layers. The coordination of engineering design can be achieved by using graph and tearing algorithms. This task is sometimes performed by system analysis tools where algorithmic intelligence is implemented. However, such approach gives a high authority to the design tool and less flexibility to the designer. System analysis can be performed in environments that enable the connection of dataflows between

different engineering legacy tools. Algebraic computation environments can also be used for system analysis when elementary models have been reduced to algebraic expressions. Once system analysis is performed, many visualization tools are available for engineering design. Scatter plot, scatter matrix and parallel coordinates enables the visualization of large data sets and design by shopping techniques. A standardization of engineering design visualization tools could offer significant insights in terms of collaboration.

The state of the art also focused on design optimization. The most effective approach, that emphasizes a rapid search rather than a global search, is to combine gradient-based optimizers with monolithic formulations. Nevertheless, this combination is most effective when partial derivatives are analytic and the computation of system total derivatives is available. Thus, symbolic differentiation can be used for partial derivatives and the MAUD architecture for total derivative computation. To handle multi-modal functions and enhance global search, gradient-based methods can be combined with multi-start capabilities. In addition, MSDO techniques provide the theoretical foundation in order to tackle coupled engineering system analysis and optimization. The openMDAO framework is very interesting as in provides a systemic modelling approach with advanced gradient-optimization features. Uncertainty and robust optimization have not been investigated in this state of the art but are important topics in engineering design as well as sensitivity analysis.

The work presented in Chapter 3 provides a benchmark test case for MSDO formulations, a new formulation, its performances when compared to other existing formulations and a theoretic graph approach to assist MSDO problem formulations. The case study is a linear electro-mechanical actuator for Thrust Vector Control applications. EMAs are on their technological limit in terms of bandwidth for such application and are only used on small launchers. Hence, the sizing of the actuator is numerically difficult. The Normalized Variable Hybrid formulation (NVH) is monolythic, easy to implement and is well suited for sizing problems. It consists of one design variable with a relatively small dimension and a single inequality constraint whereas IDF and Hybrid require additional large dimension design variables and equality constraints which can introduce numerical difficulties. The benchmark results show that the MDF and the NVH converge rapidly. However, the NVH requires the less function calls to converge. In addition, the setting of the MDF formulation is intricate and is problem dependant which makes it less reusable. In the present application it requested to reformulate the analysis function by using the absolute function. The remarkable advantage of the NVH is it robustness to scale change. The actuation systems design inputs can change scale from an application to another (flight control, landing gear, electrical thrust reverser...) or for different aircraft size. Hence, robustness is an important criterion for reusability of the sizing code which is one sub-objective of this thesis.

However, the NVH formulation requires a non-negligible reformulation effort of the analysis functions. This is one reason why graph-based methods that assist the formulation of MSDO problems have been proposed. It provides a semi-automatic formulation of the NVH strategy. The other reasons are that as the problems get larger and coupled, human errors become numerous. The proposed

graph-based procedure enables designers to detect and correct easily potential mistakes. The use of the bipartite graph formalism and an assigned color code is very convenient. This graph procedure is implemented in the acausal Block Generator environment of the BOA framework presented in Chapter 4.

Perspectives could include the automatic formulation of different MSDO strategy whereas only the NVH formulation is proposed here. Furthermore, the graph procedure could be extended to a mix of causal and acausal models. The causal models could be not only algebraic models but FMUs or Python code. In addition, solutioning of under-constrained singularities can be automatized by adding additional variables. Nevertheless, the NVH formulation is a practical way for engineers that have no experience in multidisciplinary design analysis and optimization to tackle the complexity of these problems.

In Chapter 4, a design and sizing methodology for complex technological systems has been proposed as an answer to the main objective of this thesis. A methodology consists of a process, methods and tools. The sub-objectives were capitalization, collaborative work, rapid analysis and optimization capabilities. The methodology was outlined throughout a Thrust Vector Control electro-mechanical actuator case study.

The proposed methodology is composed of six successive steps: requirements, design drivers and sizing scenarios definition, elementary computational model generation, elementary models assembly into reusable component sizing models, component sizing models assembly into a system sizing model, analysis and optimization using the system sizing model, and design space exploration using the system sizing model.

For the first step, a formalism was presented in order that stakeholders can interact and structure their respective design constraints and needs. It proposes to decompose a sizing problem into system design drivers, component design drivers and sizing scenarios. This way modelling needs for the sizing process are better defined. For the second step, algebraic models were chosen to represent the disciplines as they provide low computational cost and can be used in an acausal modelling environment. Different algebraic modelling approaches like scaling laws and VPLM surrogate models were presented. These previous steps are not included in the sizing framework. The BOA framework is decomposed into four successive environments: Block Generation, Sizing Procedure, Design and Explore.

The third step is supported by the Block Generation environment. It consists of the assembly of elementary algebraic models. This enables to use acausal modelling for increasing reusability of models. The acausal environment was developed by combining graph-based methods and symbolic computation methods. Such methods also permit to detect computation singularities. This step enables to generate flexible inputs/outputs component sizing models composed of elementary algebraic models whilst checking their solvability.

The fourth step is supported by the Sizing Procedure environment. It consists of the assembly of component sizing models to form a total system sizing model. The method used to represent the

system model is the N2 diagram. In addition, a hierarchical decomposition method is used to deal with the complexity of system containing a large number of model elements.

The fifth step is supported by the Design environment. It enable the analysis and optimization of the system sizing model by utilizing Multidisciplinary System Design Optimization techniques. This environment is built on top of the openMDAO framework. Gradient-based methods are used with symbolic differentiation for elementary models derivatives and Unified Derivatives Equations for total derivatives. The Design environment provides low analysis and optimization runtime which is one of the sub-objective of this thesis in order to permit rapid decision making. A spreadsheet formalism adapted to optimization problems was developed in order to easily change parameters and visualize results.

The last and sixth step is supported by the Explore environment. It uses Multidisciplinary System Design Optimization techniques to achieve consistent analyses. The analyses are driven by implemented Design of Experiments methods. The parallel coordinates plot has been chosen as the visualization and filtering tool for this environment as it suited for large number of experiments and variables.

The framework also provides model library and documentation features. Furthermore, it is possible to export the optimization and exploration model as Python Serialization Object in order to be used in larger and heterogeneous problems.

The methodology proposed is a small step towards knowledge capitalization and collaborative work in engineering design. It provides very low analysis and optimization runtime. It also enables to organize the complete model with a systemic approach. Therefore, it can been used to tackle higher complexity systems like electro-mechanical primary flight control actuation system (Chapter 5) and electrical thrust reverser actuation system (Chapter 6).

The perspectives here could be the development of a standardized representation of component design drivers, systems design drivers, sizing scenarios and their interactions. The framework was developed with emphasis placed on making things simple in order to require a reasonable learning curve. However, the sizing framework can be extended to a wider range of analysis function types than simple algebraic models. The implementation of sensitivity analysis, uncertainty propagation and robust optimization capabilities for the complete system sizing model is one of the top priorities.

Chapter 5 used the previously presented framework to design and size an electro-mechanical primary flight control actuation system. This application enabled us to show how to integrate component detailed design models during the system preliminary sizing process.

A compact and easy integration rotary EMA has been sized. For that, the design drivers and sizing scenarios of primary flight control actuation systems have been outlined. This way sizing scenarios like thermal behaviour for which modelling should be emphasized were investigated with detail. Appendix B has shown a thermal behaviour investigation that suggests to use maximum torque of the flight mission profile as the operating thermal point. The different models used to size the system were presented, both the electrical power chain and the electro-mechanical power chain. Surrogate

models of FEM simulations were used for the motor losses and thermal resistance as well as the housing thermal resistance and vibratory stress. The actuator sizing model has then been extended to an integrated actuator and aileron control surface application. This more integrated concept enabled the removal of load limitation devices and consider control surface splitting as a degree of freedom. The torque density and diameter confinement of an aileron enabled us to investigate the concept of control surface splitting at actuation system level.

Effects of aileron control surface splitting on overall mass of integrated actuators and control surfaces have been studied. The main benefits come from structural components like control surface and actuator housing. The main advantage of control surface splitting is that is can lead to multi-surface actuators and thus reduce maintenance, development and production costs. Nevertheless, the results have shown that a high degree of splitting did not offer important mass gain. Thus, the number of elementary surfaces shall remain as low as possible to avoid an important number of maintenance operations. The effect of the enhance thermal configurations on the design have been studied. A better cooling of actuators could lead to competitive EMAs for next generation aircraft.

This investigation has shown the importance of interaction between actuator integrator and supplier. Such approach, supported by sophisticated sizing tools, could lead to more optimized and standardized solutions. However, more detailed studies much be achieved, especially for elevators and the rudder surfaces. In addition, the motor sizing should include the damping requirements as it will have an effect on its size. A challenging investigation would be to achieve simultaneously a wing and actuation system design that includes multiple disciplines such as structure, aerodynamics, aeroelastics, control surface allocation and actuation. Such investigation could lead to more ambitious concept like having the same actuator not only for multiple surfaces but multiple aircraft.

Conversely to Chapter 5, Chapter 6 has shown how to integrate system dynamic models during the system preliminary sizing process. This was achieved by studying an electrical thrust reverser actuation system. The mission profile of this system has an important effect on the sizing. Thus, the study was decomposed into two parts. First, a preliminary sizing study of the ETRAS was performed with a low fidelity model of the mechanical efficiencies and the mission profile together with a higher fidelity system sizing model. Then, the sizing used a higher fidelity model of the mechanical efficiencies and the mission profile together with simplified assessment on the system sizing model.

As suggested by the methodology, design drivers and sizing scenarios of the ETRAS were first outlined. It has enabled us to distinguish two phases of the deploy mission: a phase where the system operates in the motor quadrant and a phase where it operates in generator quadrant. The sizing scenario analysis has also shown that these two phases as well as the stow mission have different effects on the components sizing.

The first design case with low fidelity on the mission profile used surrogate models of lumped parameter model simulations. Simulations were achieved using FMUs generated in the Dymola software. Other algebraic models were used to represent the sizing scenarios and component estimation models. One particularity of the ETRAS is that it operates during a short time. Thus, specific thermal

model which use energies and thermal capacities were implemented. The system sizing model enabled us to obtain the preliminary characteristics of the system and its components. The effect of the slider jamming scenario on the system sizing was outlined and showed the importance of capitalizing the list of sizing scenarios. This model was implemented in the BOA framework.

The second design case used a more detailed model for the mission profile and was implemented in pure Python code using the openMDAO framework. The model is based on a discretized acceleration profile. A detailed model of dynamic and static loads were then provided. A trajectory optimization problem using inverse simulation was then implemented. The position/time and overspeed requirements were implemented as constraints. The effect of the objective choice on the resulting trajectory and the other variable of interest were given. It resulted that the most pertinent choice of objective was the maximum power in motor quadrant has it decreased the motor power by 50 % and therefore the power withdrawn from the aircraft electrical network. A pseudo multi-objective approach based on the design of experiment of the previously sizing code was proposed. It improve the trajectory smoothness but was not the most efficient when compared to the RMS power objective choice.

The trajectory optimization technique was then extended to the electrical power chain design. In order to make some more detailed assessment of the loads, the detailed friction models were implemented in order to consider the effect on speed and static load on the motor electromagnetic torque. The objective was to minimize the final temperature of the motor. The study focused on the brushless motor which is on its technological limit for the voltage and current supply configuration of this application. Hence, a flux-weakening strategy has been proposed to add some degrees of freedom to the design and validate the previous preliminary design.

This study enabled us to build a sizing process with two levels of fidelity. The trajectory optimization provided accurate assessment of the requirements on the power consumption. Thus, power consumption versus thrust reverser braking effectiveness trade offs can be achieved.

Perspectives of this study include a complete system sizing model with a high fidelity trajectory optimization. This way the selected objective can be to minimize the overall mass of the ETRAS. In addition, investigating the use analytic derivatives for components that use integration or interpolation instead of the complex step method is a challenging topic.

7.2 Contributions

The work presented in this thesis is is an answer to particular industrial needs with a large scope of scientific techniques. The main contributions can be outlined by reminding the initial objectives to which they refer:

IO1. *Develop a holistic sizing methodology and an associated software tool.*

1. The main contribution is the development of the design and sizing methodology which emphasizes knowledge capitalization, collaborative work, reusability, design optimization and rapid

decision making. The methodology have been presented by a process supported by multiple methods and tools.

2. This design methodology is supported by a desktop software named "BOA" which required thorough thinking with regard to the features and the user interface. The code development was as well a significant work effort as it occupied most of these first two years.

IO2. *The methodology shall enable knowledge capitalization and collaboration.*

3. To permit knowledge capitalization many features were implemented such as documentation, equation description, parameter uncertainties and model libraries. In order to enable collaboration, component and system models and projects can be serialized as files which can be exchanged with other users. Furthermore, the choice of algebraic models permits to most of mechatronic disciplines to contribute to the system sizing.

4. In order to facilitate model reuse, an algebraic acausal modelling environment has been developed. It required the usage of symbolic computing and graph algorithms.

IO3. *The software tool shall handle analysis and optimization of coupled systems.*

5. The software tools enables to handle coupled systems by implementing monolythic formulation except ones which require multidisciplinary solvers. The NVH formulation has been proposed as a convenient way for industrial engineers to tackle algebraic loops and multidisciplinary optimization.

IO4. *The software tool shall provide reasonable analysis and optimization times.*

6. It was proposed to use lightweight algebraic models in the software. For that, different techniques to generate such models were presented. The main contribution here was the development of a workflow which used lumped parameter model FMUs to run simulations and achieve data regression to the simulation data.

7. It was proposed to use gradient-based optimization using symbolic differentiation for elementary models. For that a symbolic differentiation module had to be implemented in order to make it transparent for the user and handle particular mathematical functions.

IO5. *The methodology and software tool shall be tested on a realistic industrial product.*

8. The methodology and software tool have been tested on three main study cases: a Thrust Vector Control EMA, a electro-mechanical primary flight control actuation system and an electrical thrust reverser actuation system.

9. A new approach for primary flight control actuation system design has been proposed. It has been proven that the concept of split control surfaces actuated by rotary actuators is worth being

thoroughly investigated in particular for structural mass gain and actuator standardization. It could have significant outcomes in terms of overall actuation system cost and will be a key enabler for thin wing concept and structural loading control.

10. The trajectory optimization using inverse simulation proposed for the ETRAS design is also a significant contribution. This has enabled on an industrial application to stay within the technological limit of the power electronics architecture and the aircraft electrical network voltage supply. It also enables to assess the effect of requirements changes such as deploy time on the ETRAS power consumption and thus permit rapid trade-offs.

Some additional scientific contributions can be given by answering the initial research questions with hindsight on these three years of work:

RQ1. *How should this sizing methodology be incorporated in the overall design process?*

The proposed methodology does not replace the upstream activities such as requirements engineering, architecture propositions and reliability analysis. It does not replace either the downstream activities of detailed design and virtual prototyping. However, the methodology should be used in between in order to transform system specifications into component specifications. This permits to make some design iterations during preliminary design instead of detailed design. This leads to a significant time reduction of the trade-off process and close to optimal designs.

RQ2. *Who will be the users of such software tool?*

The developed software is mainly a system architect tool as he has the global vision and the technical authority at the system level. However, the tool was developed such as domain experts could include their models in libraries as well as running analysis and optimization of component sizing codes.

RQ3. *How to capitalize knowledge and collaborate in a multidisciplinary design office?*

This is usually achieved through the storage of technical documents and models with attached documentation. However, reusability is difficult as engineering specialization legacy tools require significant expertise. In the thesis, it was propose to use one same algebraic modelling environment. The challenge was to generate these models using data and approaches of different engineering tools. Nevertheless, many techniques for this purpose have been presented. Regarding capitalization, it was proposed to use model documentation and model libraries in order to provide collaboration and knowledge capitalization capabilities within this common modelling environment.

RQ4. *How to interface different engineering specialization design tools?*

The first approach and most employed methods are to use distributed engineering between different engineering specialization tools. However, this often leads to high computational

times and is not well suited for knowledge capitalization. In the thesis, it was preferred to use algebraic models obtained using different techniques that are interfaced in a same algebraic computing environment.

RQ5. *Can Multidisciplinary Design Optimization techniques be made available to unexperienced users?*

It is very challenging. Here, it was proposed to use a semi-automatic implementation of the NVH formulation. However, it can be delicate and remains problem-dependent.

RQ6. *What is a reasonable computation time in a design office? What are the potential solutions to reach it?*

This time corresponds to the time to make a decision. In an actuation system design office this time shall be less than one hour but less than 10 minutes shall be the target. However, another solution is to increase the computational power by using specialized machines or clusters.

RQ7. *Is there a limit in terms of system complexity for using such sizing methodology?*

The limit can come either from the implementation difficulties because of to large and complicated models or from the numerical resolution of the problem. The software tool enables user to implement complex problems thanks to the use of hierarchical modelling. The increase of complexity will increase the time to implement the problem. From a numerical point of view a complexity limit can be reached. However, the use of gradient-based optimization permits to deal with large problems and therefore shift the limit. Nevertheless, the software seems compatible with the complexity of most aerospace actuation systems.

7.3 Limitations and Propositions for Future Work

The limitations of the work and some propositions for future work can be achieved for the design methodology part and the case study part.

The developed sizing framework is collaborative by the mean of exchanging models offline. This could be enhanced by developing it in a web environment to improve the exchange and version control of models.

The elementary models generated are then implemented by the user in the BOA framework which increases risk of typing errors. It would be interesting to smoothen this workflow by having the model generation tools within the framework.

The software only handles algebraic models, it would have been interesting to enable a wider range of models. This could have been achieved by standardizing the interfaces and implementing the corresponding numerical resolution mean.

An effort was achieved on the formulation of models and on the resolution strategy but not on high performance computing. However, multi-processing features are becoming easily usable thanks to frameworks like openMDAO. This can significantly improve computational runtimes.

Surrogate modelling is a very interesting alternative to associate multiple disciplines with different levels of fidelity. For these reasons, they have been widely used in this work. Nevertheless, it is a complex topic and requires convenient software tools and workflows to be used by industrials, and to facilitate capitalization and reuse. Thus it constitutes an important topic for future work.

The details of analysis and optimization runs are obtained through the optimizer log which is rendered in the console of the software. However, it would have been also interesting to include convergence plots when visualizing the optimization results.

The software enables to build an overall system sizing code and run some analysis or optimization. However, as the uncertainty on parameters were made available, an interesting perspective would be to provide robust optimization capabilities. Furthermore, the exploration environment could include sensitivity analysis features to permit such analysis to be conducted on coupled systems.

The Primary Flight Control EMA study was achieved for the aileron surface and virtually extended to rudder and elevators. Nevertheless, structural and thermal detailed studies should be driven on these surfaces as it was done for the aileron. In addition, the drawbacks of the concept of split control surfaces could be more accurately assessed.

The trajectory optimization of the ETRAS used a discretized acceleration vector. This needed a very large number of design variables and constraints. Thus, an other perspectives would be to evaluate the contribution of such high computational cost approach when compared to more light weight methods such as B-Splines.

References

[1] Abevi, F., Daidie, A., Chaussumier, M., and Sartor, M. (2016). Static load distribution and axial stiffness in a planetary roller screw mechanism. *Journal of Mechanical Design*, 138(1):012301.

[2] Airliners.net (2018). A380 load alleviation function. http://www.airliners.net/forum/viewtopic.php?t=774177.

[3] Akoto Chama, L. and Bertram, O. (2018). Identifying enhancement potentials of actuation systems using a criticality index. *Recent Advances in Aerospace Actuation Systems and Components, INSA Toulouse*, pages 211–218.

[4] Alavi, M. and Leidner, D. E. (2001). Knowledge management and knowledge management systems: Conceptual foundations and research issues. *MIS quarterly*, pages 107–136.

[5] Alexandrov, N. and Lewis, R. (2000). Algorithmic perspectives on problem formulations in mdo. In *8th Symposium on Multidisciplinary Analysis and Optimization*, page 4719.

[6] Allain, L. (2003). *Capitalisation et traitement des modèles pour la conception en génie électrique*. PhD thesis, Institut National Polytechnique de Grenoble-INPG.

[7] Allison, J. T., Kokkolaras, M., and Papalambros, P. Y. (2009). Optimal partitioning and coordination decisions in decomposition-based design optimization. *Journal of Mechanical Design*, 131(8):081008.

[8] Amine Bouhlel, M., Bartoli, N., Regis, R. G., Otsmane, A., and Morlier, J. (2018). Efficient global optimization for high-dimensional constrained problems by using the kriging models combined with the partial least squares method. *Engineering Optimization*, pages 1–16.

[9] Andersson, C. (2016). Methods and tools for co-simulation of dynamic systems with the functional mock-up interface. *Doctoral Theses in Mathematical Sciences*.

[10] ANSYS (2018). Ansys: Engineering simulation and 3-d design software. https://www.ansys.com/.

[11] ARP, S. (1996). 4761. *Guidelines and methods for conducting the safety assessment process on civil airborne systems and equipment*, 12.

[12] ARP, S. (2010). 4754a. *Guidelines for Development of Civil Aircraft and Systems*, 12:41.

[13] Ashok, S. V. (2013). *An integrated product–process development (IPPD) based approach for rotorcraft drive system sizing, synthesis and design optimization*. PhD thesis, Georgia Institute of Technology.

[14] Association, A. G. M. (2018). Agma standards. https://www.agma.org/standards/.

[15] Balling, R. J. and Sobieszczanski-Sobieski, J. (1996). Optimization of coupled systems-a critical overview of approaches. *AIAA journal*, 34(1):6–17.

[16] Barrett, R. and Stutts, J. (1998). Development of a piezoceramic flight control surface actuator for highly compressed munitions. In *39th AIAA/ASME/ASCE/AHS/ASC Structures, Structural Dynamics, and Materials Conference and Exhibit*, page 2034.

[17] Bartoli, N., Lefebvre, T., Dubreuil, S., Olivanti, R., Bons, N., Martins, J., Bouhlel, M.-A., and Morlier, J. (2017). An adaptive optimization strategy based on mixture of experts for wing aerodynamic design optimization. In *18th AIAA/ISSMO Multidisciplinary Analysis and Optimization Conference*, page 4433.

[18] Belegundu, A. D. and Chandrupatla, T. R. (2011). *Optimization concepts and applications in engineering*. Cambridge University Press.

[19] Blanding, D. (2007). Subsystem design and integration for the more electric aircraft. In *5th international energy conversion engineering conference and exhibit (IECEC)*, page 4828.

[20] Bloebaum, C. (1995). Coupling strength-based system reduction for complex engineering design. *Structural Optimization*, 10(2):113–121.

[21] Bostock, M., Ogievetsky, V., and Heer, J. (2011). D^3 data-driven documents. *IEEE transactions on visualization and computer graphics*, 17(12):2301–2309.

[22] Bouhlel, M. A., Bartoli, N., Otsmane, A., and Morlier, J. (2016). Improving kriging surrogates of high-dimensional design models by partial least squares dimension reduction. *Structural and Multidisciplinary Optimization*, 53(5):935–952.

[23] Braun, R. D., Moore, A. A., and Kroo, I. M. (1997). Collaborative approach to launch vehicle design. *Journal of spacecraft and rockets*, 34(4):478–486.

[24] Brochu, E., Cora, V. M., and De Freitas, N. (2010). A tutorial on bayesian optimization of expensive cost functions, with application to active user modeling and hierarchical reinforcement learning. *arXiv preprint arXiv:1012.2599*.

[25] Browning, T. R. (2001). Applying the design structure matrix to system decomposition and integration problems: a review and new directions. *IEEE Transactions on Engineering management*, 48(3):292–306.

[26] Buckingham, E. (1914). On physically similar systems; illustrations of the use of dimensional equations. *Physical review*, 4(4):345.

[27] Budinger, M. (2014). Preliminary design and sizing of actuation systems. Mémoire de HDR, UPS Toulouse.

[28] Budinger, M., Liscouët, J., Hospital, F., and Maré, J. (2012). Estimation models for the preliminary design of electromechanical actuators. *Proceedings of the Institution of Mechanical Engineers, Part G: Journal of Aerospace Engineering*, 226(3):243–259.

[29] Budinger, M., Liscouet, J., Hospital, F., and Multon, B. (2011). Chaînes de transmission de puissance mécatroniques mise en place des modèles d'estimation pour la conception préliminaire. *Techniques de l'ingénieur Mécatronique*, (bm8025).

[30] Budinger, M., Passieux, J.-C., Gogu, C., and Fraj, A. (2014a). Scaling-law-based metamodels for the sizing of mechatronic systems. *Mechatronics*, 24(7):775–787.

[31] Budinger, M., Reysset, A., Halabi, T. E., Vasiliu, C., and Mare, J.-C. (2014b). Optimal preliminary design of electromechanical actuators. *Proceedings of the Institution of Mechanical Engineers, Part G: Journal of Aerospace Engineering*, 228(9):1598–1616.

[32] Bunch, J. R. and Hopcroft, J. E. (1974). Triangular factorization and inversion by fast matrix multiplication. *Mathematics of Computation*, 28(125):231–236.

[33] Bunus, P. (2002). *Debugging and structural analysis of declarative equation-based languages*. PhD thesis, Institutionen för datavetenskap, Linköping University.

[34] Cao, W., Mecrow, B. C., Atkinson, G. J., Bennett, J. W., and Atkinson, D. J. (2012). Overview of electric motor technologies used for more electric aircraft (mea). *IEEE transactions on industrial electronics*, 59(9):3523–3531.

[35] Carnevale, C. and Resta, P. (2007). Vega electromechanical thrust vector control development. In *43rd AIAA/ASME/SAE/ASEE Joint Propulsion Conference & Exhibit*, page 5812.

[36] Carty, A. (2002). An approach to multidisciplinary design, analysis & optimization for rapid conceptual design. In *9th AIAA/ISSMO Symposium on Multidisciplinary Analysis and Optimization*, page 5438.

[37] Cellier, F. E. and Elmqvist, H. (1993). Automated formula manipulation supports object-oriented continuous-system modeling. *IEEE Control Systems*, 13(2):28–38.

[38] Chakraborty, I., Trawick, D. R., Jackson, D., and Mavris, D. (2013). Electric control surface actuator design optimization and allocation for the more electric aircraft. In *2013 Aviation Technology, Integration, and Operations Conference*, page 4283.

[39] Charier, G. A. and Gallet, F. (2015). System of compact contra-rotating propellers. US Patent 9,057,326.

[40] Chattopadhyay, A., McCarthy, T. R., and Pagaldipti, N. (1995). Multilevel decomposition procedure for efficient design optimization of helicopter rotor blades. *AIAA journal*, 33(2):223–230.

[41] Chauvin, A. (2015). *Contribution à l'optimisation globale pour le dimensionnement et la gestion d'énergie de véhicules hybrides électriques basée sur une approche combinatoire*. PhD thesis, INSA de Lyon.

[42] Ciampa, P. D. and Nagel, B. (2017). The agile paradigm: the next generation of collaborative mdo. In *18th AIAA/ISSMO Multidisciplinary Analysis and Optimization Conference*, page 4137.

[43] Coïc, C. (2016). *Model-Aided Design of a High-Performance Fly-by-Wire Actuator, Based on a Global Modelling of the Actuation System using Bond-graphs*. PhD thesis, INSA Toulouse.

[44] COMSOL (2018). Comsol multiphysics: Understand, predict, and optimize. http://www.mscsoftware.com/en-uk/product/patran.

[45] Conn, A. R., Scheinberg, K., and Vicente, L. N. (2009). *Introduction to derivative-free optimization*, volume 8. Siam.

[46] Cooper, M., Lawson, C., and Zare Shahneh, A. (2017). Simulating actuator energy consumption for trajectory optimisation. *Proceedings of the Institution of Mechanical Engineers, Part G: Journal of Aerospace Engineering*, page 0954410017710271.

[47] Daguse, B. (2013). *Modélisation analytique pour le dimensionnement par optimisation d'une machine dédiée à une chaîne de traction hybride à dominante électrique*. PhD thesis, Supélec.

[48] Deb, K., Pratap, A., Agarwal, S., and Meyarivan, T. (2002). A fast and elitist multiobjective genetic algorithm: Nsga-ii. *IEEE transactions on evolutionary computation*, 6(2):182–197.

[49] Delannoy, S. (2007). A380 roll kinematics design. *IFAC Proceedings Volumes*, 40(7):103–108.

[50] Delannoy, S. and Bertin, T. (2012). Method and device for piloting an aircraft about a piloting axis. US Patent 8,141,824.

[51] Delbecq, S., Budinger, M., Hazyuk, I., Sanchez, F., and Piaton, J. (2017a). A framework for sizing embedded mechatronic systems during preliminary design. *IFAC-PapersOnLine*, 50(1):4354–4359.

[52] Delbecq, S., Budinger, M., and Piaton, J. (2018a). A more integrated design approach for embedded mechatronic systems: Application to electrical thrust reverser actuation systems. In *International Congress of the Aeronautical Sciences*.

[53] Delbecq, S., Budinger, M., Piaton, J., and Dagusé, B. (2018b). Optimization of primary flight control actuation system using parametric sizing models of actuators, power electronics and structural analysis. *Recent Advances in Aerospace Actuation Systems and Components, INSA Toulouse*, pages 132–138.

[54] Delbecq, S., Tajan, F., Budinger, M., Maré, J.-C., and Sanchez, F. (2017b). A framework for the conceptual and preliminary design of embedded mechatronic systems. In *International Workshop on aircraft System Technologies*.

[55] Delinchant, B., Duret, D., Estrabaut, L., Gerbaud, L., Nguyen Huu, H., Du Peloux, B., Rakotoarison, H. L., Verdière, F., and Wurtz, F. (2007). An optimizer using the software component paradigm for the optimization of engineering systems. *COMPEL-The international journal for computation and mathematics in electrical and electronic engineering*, 26(2):368–379.

[56] Delinchant, B., Wurtz, F., Magot, D., and Gerbaud, L. (2004). A component-based framework for the composition of simulation software modeling electrical systems. *Simulation*, 80(7-8):347–356.

[57] Denieul, Y. (2016). *Preliminary Design of Control Surfaces and Laws for Unconventional Aircraft Configurations*. PhD thesis, INSTITUT SUPERIEUR DE L'AERONAUTIQUE ET DE L'ESPACE (ISAE).

[58] Derrien, J.-C., Tieys, P., Senegas, D., and Todeschi, M. (2011). Ema aileron covadis development. Technical report, SAE Technical Paper.

[59] Deshmukh, A. P. and Allison, J. T. (2017). Design of dynamic systems using surrogate models of derivative functions. *Journal of Mechanical Design*, 139(10):101402.

[60] Detwarasiti, A. and Shachter, R. D. (2005). Influence diagrams for team decision analysis. *Decision Analysis*, 2(4):207–228.

[61] Dieng, R., Corby, O., Giboin, A., and Ribiere, M. (1999). Methods and tools for corporate knowledge management. *International journal of human-computer studies*, 51(3):567–598.

[62] Dill (2018). dill python package: serialize all of python. https://github.com/uqfoundation/dill.

[63] Dolan, A. and Aldous, J. (1993). *Networks and algorithms: an introductory approach*. John Wiley & Sons.

[64] Dols, S. (2016). *Développement d'une nouvelle méthode de serrage intelligente pour le contrôle des assemblages boulonnés*. PhD thesis, Toulouse, INSA.

[65] Doran, T. (2006). Ieee 1220: for practical systems engineering. *Computer*, 39(5):92–94.

[66] Dudley, D. W. (1991). *Dudley's gear handbook*. Tata McGraw-Hill Education.

[67] Ellson, J., Gansner, E., Koutsofios, L., North, S. C., and Woodhull, G. (2001). Graphviz—open source graph drawing tools. In *International Symposium on Graph Drawing*, pages 483–484. Springer.

[68] Elmqvist, H. and Otter, M. (1994). Methods for tearing systems of equations in object-oriented modeling. In *Proceedings ESM*, volume 94, pages 1–3.

[69] Ersal, T., Fathy, H. K., Rideout, D. G., Louca, L. S., and Stein, J. L. (2008). A review of proper modeling techniques. *Journal of Dynamic Systems, Measurement, and Control*, 130(6):061008.

[70] Estefan, J. A. et al. (2007). Survey of model-based systems engineering (mbse) methodologies. *Incose MBSE Focus Group*, 25(8):1–12.

[71] Evans, R., Tsohou, A., Tryfonas, T., and Morgan, T. (2010). Engineering secure systems with iso 26702 and 27001. In *System of Systems Engineering (SoSE), 2010 5th International Conference on*, pages 1–6. IEEE.

[72] FAA, A. C. (1988). 25.1309-1a. *System Design and Analysis*.

[73] Faisandier, A. (2013). *Systems architecture and design*. Sinergy'Com.

[74] Fervel, M., Lecanu, A., Maussion, A., and Andrieu, L. (2013). Flight control system for an aircraft. US Patent 8,567,715.

[75] Forrester, A., Keane, A., et al. (2008). *Engineering design via surrogate modelling: a practical guide*. John Wiley & Sons.

[76] Friedl, M., Scheidl, R., Hehenberger, P., Kellner, A., Weingartner, L., and Hörl, M. (2016). A design optimization framework for multidisciplinary mechatronic systems. In *Proceedings of TMCE*, pages 3–12.

[77] Friedman, G. J. and Leondes, C. T. (1969). Constraint theory, part i: fundamentals. *IEEE Transactions on Systems Science and Cybernetics*, 5(1):48–56.

[78] Fritzson, P., Aronsson, P., Pop, A., Lundvall, H., Nystrom, K., Saldamli, L., Broman, D., and Sandholm, A. (2006). Openmodelica-a free open-source environment for system modeling, simulation, and teaching. In *Computer Aided Control System Design, 2006 IEEE International Conference on Control Applications, 2006 IEEE International Symposium on Intelligent Control, 2006 IEEE*, pages 1588–1595. IEEE.

[79] Fritzson, P. and Engelson, V. (1998). Modelica—a unified object-oriented language for system modeling and simulation. In *European Conference on Object-Oriented Programming*, pages 67–90. Springer.

[80] Gao, Z. and Grandhi, R. V. (1999). Sensitivity analysis and shape optimization for preform design in thermo-mechanical coupled analysis. *International Journal for Numerical Methods in Engineering*, 45(10):1349–1373.

[81] Garrick, I. and Reed III, W. H. (1981). Historical development of aircraft flutter. *Journal of Aircraft*, 18(11):897–912.

[82] Gasperi, M. L. and Gollhardt, N. (1998). Heat transfer model for capacitor banks. In *Industry Applications Conference, 1998. Thirty-Third IAS Annual Meeting. The 1998 IEEE*, volume 2, pages 1199–1204. IEEE.

[83] Gazaix, A., Gallard, F., Gachelin, V., Druot, T., Grihon, S., Ambert, V., Guénot, D., Lafage, R., Vanaret, C., Pauwels, B., et al. (2017). Towards the industrialization of new mdo methodologies and tools for aircraft design. In *18th AIAA/ISSMO Multidisciplinary Analysis and Optimization Conference*, page 3149.

[84] Gee, G., Vanthuyne, T., and Alexandre, P. (2007). An electrical thrust vector control system with dynamic force feedback. *Recent Advances in Aerospace Actuation Systems and Components, INSA Toulouse*, pages 75–79.

[85] Gill, P. E., Murray, W., and Saunders, M. A. (2005). Snopt: An sqp algorithm for large-scale constrained optimization. *SIAM review*, 47(1):99–131.

[86] Giraud, X. (2014). *Méthodes et outils pour la conception optimale des réseaux de distribution d'électricité dans les aéronefs*. PhD thesis, Toulouse, INSA.

[87] Giraud, X., Budinger, M., Roboam, X., Piquet, H., Sartor, M., and Faucher, J. (2016). Optimal design of the integrated modular power electronics cabinet. *Aerospace Science and Technology*, 48:37–52.

[88] Grand, S., Fervel, M., Balducci, G., and Wendling, M. (2016). Actuator control: A successful modular multi-application approach for actuation2015 and beyond. *Recent Advances in Aerospace Actuation Systems and Components, INSA Toulouse*, pages 60–65.

[89] Gray, J., Moore, K., and Naylor, B. (2010). Openmdao: An open source framework for multidisciplinary analysis and optimization. In *13th AIAA/ISSMO Multidisciplinary Analysis Optimization Conference*, page 9101.

[90] Gray, J., Moore, K. T., Hearn, T. A., and Naylor, B. A. (2013). Standard platform for benchmarking multidisciplinary design analysis and optimization architectures. *AIAA journal*, 51(10):2380–2394.

[91] Gray, J. S., Mader, C. A., Kenway, G. K., and Martins, J. R. (2017). Modeling boundary layer ingestion using a coupled aeropropulsive analysis. *Journal of Aircraft*, pages 1–9.

[92] Griewank, A. and Walther, A. (2008). *Evaluating derivatives: principles and techniques of algorithmic differentiation*, volume 105. Siam.

[93] Gross, J. and Rudolph, S. (2016). Rule-based spacecraft design space exploration and sensitivity analysis. *Aerospace Science and Technology*, 59:162–171.

[94] Grossman, B., Gurdal, Z., Haftka, R., Strauch, G., and Eppard, W. (1988). Integrated aerodynamic/structural design of a sailplane wing. *Journal of Aircraft*, 25(9):855–860.

[95] Hagberg, A., Swart, P., and S Chult, D. (2008). Exploring network structure, dynamics, and function using networkx. Technical report, Los Alamos National Lab.(LANL), Los Alamos, NM (United States).

[96] Hahn, A. (2010). Vehicle sketch pad: a parametric geometry modeler for conceptual aircraft design. In *48th AIAA Aerospace Sciences Meeting Including the New Horizons Forum and Aerospace Exposition*, page 657.

[97] Hammadi, M., Kellner, A., Choley, J.-Y., and Hehenberger, P. (2014). Mechatronic design optimization using multi-agent approach. In *14th Mechatronics Forum International Conference*, pages 310–317.

[98] Hannifin, P. (2018). Parvex electrical motors. http://ph.parker.com/us/en/electric-motors.

[99] Hansen, N. (2006). The cma evolution strategy: a comparing review. In *Towards a new evolutionary computation*, pages 75–102. Springer.

[100] Hazyuk, I., Budinger, M., Sanchez, F., and Gogu, C. (2017). Optimal design of computer experiments for surrogate models with dimensionless variables. *Structural and Multidisciplinary Optimization*, 56(3):663–679.

[101] Hehenberger, P. (2012). *Advances in model-based mechatronic design*. Trauner.

[102] Hehenberger, P. and Bradley, D. (2016). *Mechatronic Futures: Challenges and Solutions for Mechatronic Systems and their Designers*. Springer.

[103] Hehenberger, P., Vogel-Heuser, B., Bradley, D., Eynard, B., Tomiyama, T., and Achiche, S. (2016). Design, modelling, simulation and integration of cyber physical systems: Methods and applications. *Computers in Industry*, 82:273–289.

[104] Herman, A. L. and Conway, B. A. (1996). Direct optimization using collocation based on high-order gauss-lobatto quadrature rules. *Journal of Guidance, Control, and Dynamics*, 19(3):592–599.

[105] Herman, J. and Usher, W. (2017). Salib: an open-source python library for sensitivity analysis. *The Journal of Open Source Software*, 2(9).

[106] Hinze, M. and Volkwein, S. (2005). Proper orthogonal decomposition surrogate models for nonlinear dynamical systems: Error estimates and suboptimal control. In *Dimension reduction of large-scale systems*, pages 261–306. Springer.

[107] Hooke, R. and Jeeves, T. A. (1961). "direct search"solution of numerical and statistical problems. *Journal of the ACM (JACM)*, 8(2):212–229.

[108] Hopcroft, J. E. and Karp, R. M. (1973). An n^5/2 algorithm for maximum matchings in bipartite graphs. *SIAM Journal on computing*, 2(4):225–231.

[109] Hospital, F. (2012). *Conception préliminaire des actionneurs électromagnétiques basée sur les modèles: lois d'estimations et règles de conception pour la transmission de puissance mécanique*. PhD thesis, Toulouse, INSA.

[110] Hospital, F., Budinger, M., Reysset, A., and Maré, J.-C. (2015). Preliminary design of aerospace linear actuator housings. *Aircraft Engineering and Aerospace Technology: An International Journal*, 87(3):224–237.

[111] Hussain, E., Atallah, K., Odavic, M., Dragan, R., and Clark, R. (2016). Pseudo direct drive electrical machines for flight control surface actuation. In *Power Electronics, Machines and Drives (PEMD 2016), 8th IET International Conference on*, pages 1–6. IET.

[112] Hwang, J. T. (2015). A modular approach to large-scale design optimization of aerospace systems.

[113] Hwang, J. T. and Martins, J. (2017). A computational architecture for coupling heterogeneous numerical models and computing coupled derivatives. *ACM Transactions on Mathematical Software*.

[114] Iman, R. L. (2008). Latin hypercube sampling. *Wiley StatsRef: Statistics Reference Online*.

[115] Inselberg, A. and Dimsdale, B. (1987). Parallel coordinates for visualizing multi-dimensional geometry. In *Computer Graphics 1987*, pages 25–44. Springer.

[116] James, G., Witten, D., Hastie, T., and Tibshirani, R. (2013). *An introduction to statistical learning*, volume 112. Springer.

[117] Jensen, S. C., Jenney, G. D., and Dawson, D. (2000). Flight test experience with an electromechanical actuator on the f-18 systems research aircraft. In *Digital Avionics Systems Conference, 2000. Proceedings. DASC. The 19th*, volume 1, pages 2E3–1. IEEE.

[118] Jeyaraj, A. and Liscouet-Hanke, S. (2018). A model-based systems engineering approach for efficient flight control system architecture variants modelling in conceptual design. *Recent Advances in Aerospace Actuation Systems and Components, INSA Toulouse*, pages 34–41.

[119] Judt, D. M. and Lawson, C. (2016). Development of an automated aircraft subsystem architecture generation and analysis tool. *Engineering Computations*, 33(5):1327–1352.

[120] Kakosimos, P. E., Sarigiannidis, A. G., Beniakar, M. E., Kladas, A. G., and Gerada, C. (2014). Induction motors versus permanent-magnet actuators for aerospace applications. *IEEE Transactions on Industrial Electronics*, 61(8):4315–4325.

[121] Kallas, S., Geoghegan-Quinn, M., Darecki, M., Edelstenne, C., Enders, T., Fernandez, E., and Hartman, P. (2011). Flightpath 2050 europe's vision for aviation. *Report of the High Level Group on Aviation Research, European Commission, Brussels, Belgium, Report No. EUR*, 98.

[122] Kapurch, S. J. (2010). *NASA systems engineering handbook*. Diane Publishing.

[123] Karam, W. (2007). *Générateurs de forces statiques et dynamiques à haute puissance en technologie électromécanique*. PhD thesis, Toulouse, INSA.

[124] Kasper, M. (2016). *Analysis and Multi-Objective Optimization of Multi-Cell DC/DC and AC/DC Converter Systems*. PhD thesis, ETH Zurich.

[125] Keim, D. A. (2001). Visual exploration of large data sets. *Communications of the ACM*, 44(8):38–44.

[126] Kenway, G., Kennedy, G., and Martins, J. (2014). Aerostructural optimization of the common research model configuration. In *15th AIAA/ISSMO multidisciplinary analysis and optimization conference*, page 3274.

[127] Kessler, C. (2011). Active rotor control for helicopters: individual blade control and swashplateless rotor designs. *CEAS Aeronautical Journal*, 1(1-4):23.

[128] KISSsoft (2018). Kisssoft: Design software for mechanical engineering applications. http://www.kisssoft.ch/english/home/index.php.

[129] Kokkolaras, M., Louca, L., Delagrammatikas, G., Michelena, N., Filipi, Z., Papalambros, P., Stein, J., and Assanis, D. (2004). Simulation-based optimal design of heavy trucks by model-based decomposition: An extensive analytical target cascading case study. *International Journal of Heavy Vehicle Systems*, 11(3-4):403–433.

[130] Kopala, D. and Doell, C. (2001). High performance electromechanical actuation for primary flight surfaces (epad program results). *Recent Advances in Aerospace Actuation Systems and Components, INSA Toulouse*, pages 131–136.

[131] Kraft, D. (1988). A software package for sequential quadratic programming. *Forschungsbericht-Deutsche Forschungs- und Versuchsanstalt fur Luft- und Raumfahrt*.

[132] Kroo, I., Altus, S., Braun, R., Gage, P., and Sobieski, I. (1994). Multidisciplinary optimization methods for aircraft preliminary design. In *5th Symposium on Multidisciplinary Analysis and Optimization*, page 4325.

[133] Krus, P. (2008). Engineering design analysis and synthesis. Technical Report 10, Linköping University, Machine Design.

[134] Kuhn, H. W. and Tucker, A. W. (2014). Nonlinear programming. In *Traces and emergence of nonlinear programming*, pages 247–258. Springer.

[135] Lambe, A. B. and Martins, J. R. (2012a). Extensions to the design structure matrix for the description of multidisciplinary design, analysis, and optimization processes. *Structural and Multidisciplinary Optimization*, 46(2):273–284.

[136] Lambe, A. B. and Martins, J. R. R. A. (2012b). Extensions to the design structure matrix for the description of multidisciplinary design, analysis, and optimization processes. *Structural and Multidisciplinary Optimization*, 46:273–284.

[137] Lefebvre, T., Bartoli, N., Dubreuil, S., Panzeri, M., Lombardi, R., D'Ippolito, R., Della Vecchia, P., Nicolosi, F., and Ciampa, P. D. (2017). Methodological enhancements in mdo process investigated in the agile european project. In *18th AIAA/ISSMO Multidisciplinary Analysis and Optimization Conference*, page 4140.

[138] Leonard, J. (1999). Systems engineering fundamentals. Technical report, DEFENSE SYSTEMS MANAGEMENT COLL FORT BELVOIR VA.

[139] Leonard, J. B. (1985). A system look at actuation concepts and alternatives for primary flight control. Technical report, SAE Technical Paper.

[140] Liem, R. P., Mader, C. A., and Martins, J. R. (2015). Surrogate models and mixtures of experts in aerodynamic performance prediction for aircraft mission analysis. *Aerospace Science and Technology*, 43:126–151.

[141] Liscouet, J. (2010). *Conception préliminaire des actionneurs électromécaniques: Approche hybride, directe/inverse*. PhD thesis, Toulouse, INSA.

[142] Liscouët, J., Maré, J.-C., and Budinger, M. (2012). An integrated methodology for the preliminary design of highly reliable electromechanical actuators: Search for architecture solutions. *Aerospace Science and Technology*, 22(1):9–18.

[143] Liscouet-Hanke, S. (2008). *A model-based methodology for integrated preliminary sizing and analysis of aircraft power system architectures*. PhD thesis, Institut National des Sciences Appliquées de Toulouse.

[144] Livne, E. (2017). Aircraft active flutter suppression: State of the art and technology maturation needs. *Journal of Aircraft*, 55(1):410–452.

[145] Luenberger, D. G., Ye, Y., et al. (1984). *Linear and nonlinear programming*, volume 2. Springer.

[146] Maclaurin, D., Duvenaud, D., and Adams, R. P. (2015). Autograd: Effortless gradients in numpy. In *ICML 2015 AutoML Workshop*.

[147] Malmquist, D., Frede, D., and Wikander, J. (2014). Holistic design methodology for mechatronic systems. *Proceedings of the Institution of Mechanical Engineers, Part I: Journal of Systems and Control Engineering*, 228(10):741–757.

[148] Malone, B. and Papay, M. (1999). Modelcenter: an integration environment for simulation based design. In *Simulation Interoperability Workshop*.

[149] Mansouri, B. and Piaton, J. (2017). From characterisation to optimal flux-weakening control of permanent magnet synchronous motors (pmsms). In *Power and Electrical Engineering of Riga Technical University (RTUCON), 2017 IEEE 58th International Scientific Conference on*, pages 1–7. IEEE.

[150] Maré, J. (2016a). *Aerospace Actuators 1: Needs, Reliability and Hydraulic Power Solutions*. Number vol. 1 in Robotics series. Wiley.

[151] Maré, J.-C. (2016b). Requirement-based system-level simulation of mechanical transmissions with special consideration of friction, backlash and preload. *Simulation Modelling Practice and Theory*, 63:58–82.

[152] Mare, J.-C. (2017). *Aerospace Actuators: Signal-by-wire and Power-by-wire*, volume 2. John Wiley & Sons.

[153] Maré, J.-C. and Budinger, M. (2009). Comparative analysis of energy losses in servo-hydraulic, electro-hydrostatic and electro-mechanical actuators. In *The 11th Scandinavian International Conference on Fluid Power, SICFP*, volume 9, pages 2–4.

[154] Martin, J. N. (1996). *Systems engineering guidebook: A process for developing systems and products*, volume 10. Crc press.

[155] Martins, J. (2003). A guide to the complex-step derivative approximation. *World Wide Web page, http://mdolab. utias. utoronto. ca/resources/complex-step*.

[156] Martins, J. (2012). A short course on multidisciplinary design optimization. University Course Lecture Notes.

[157] Martins, J. R. and Hwang, J. T. (2013). Review and unification of methods for computing derivatives of multidisciplinary computational models. *AIAA journal*, 51(11):2582–2599.

[158] Martins, J. R. and Lambe, A. B. (2013). Multidisciplinary design optimization: a survey of architectures. *AIAA journal*, 51(9):2049–2075.

[159] Martins, J. R., Sturdza, P., and Alonso, J. J. (2003). The complex-step derivative approximation. *ACM Transactions on Mathematical Software (TOMS)*, 29(3):245–262.

[160] Maskrey, R. and Thayer, W. (1978). A brief history of electrohydraulic servomechanisms. *Moog Technical Bulletin*, 141.

[161] Mathcad, P. (2018). Ptc mathcad: Engineering math software. http://www.kisssoft.ch/english/home/index.php.

[162] MathWorks (2018a). Simscape: Model and simulate multidomain physical systems. https://www.mathworks.com/products/simscape.html.

[163] MathWorks (2018b). Simulink: Simulation and model-based design. https://www.mathworks.com/products/simulink.html.

[164] McMahon, C., Lowe, A., and Culley, S. (2004). Knowledge management in engineering design: personalization and codification. *Journal of Engineering Design*, 15(4):307–325.

[165] Meinadier, J.-P. (1998). *Ingénierie et intégration des systèmes*. Hermes.

[166] Microsoft (2016). Microsoft excel. https://products.office.com/fr-fr/excel.

[167] Miller, G. A. (1956). The magical number seven, plus or minus two: Some limits on our capacity for processing information. *Psychological review*, 63(2):81.

[168] MITCalc (2018). Mitcalc: Mechanical, industrial and technical calculations. http://www.mitcalc.com/.

[169] Močkus, J. (1975). On bayesian methods for seeking the extremum. In *Optimization Techniques IFIP Technical Conference*, pages 400–404. Springer.

[170] Monsimer, A. (2018). *Méthodologie pour l'étude conceptuelle d'un système fortement innovant -– Application au cas du circuit carburant d'un moteur d'helicoptère*. PhD thesis, Toulouse, INSA.

[171] Morentin Etayo, A. (2017). *Methods and tools for the optimization of modular electrical power distribution cabinets in aeronautical applications*. PhD thesis, Toulouse, INP.

[172] Nelder, J. A. and Mead, R. (1965). A simplex method for function minimization. *The computer journal*, 7(4):308–313.

[173] Nocedal, J. and Wright, S. J. (2006). *Sequential quadratic programming*. Springer.

[174] Nordmann, L., Thielecke, F., Lucken, P., and Hamm, M. (2018). Virtual testing of aircraft hydraulic systems. *Recent Advances in Aerospace Actuation Systems and Components, INSA Toulouse*, pages 96–102.

[175] Ozcan, M. F., Chakraborty, I., and Mavris, D. N. (2016). Impact of subsystem secondary power requirements on gas turbine sizing and performance. In *16th AIAA Aviation Technology, Integration, and Operations Conference*, page 3146.

[176] O'Brien, M. (1998). Boeing 777 thrust reverser actuation system. *Aircraft Engineering and Aerospace Technology*, 70(5):364–366.

[177] Papalambros, P. Y. and Wilde, D. J. (2000). *Principles of optimal design: modeling and computation*. Cambridge university press.

[178] Paredis, C. J., Diaz-Calderon, A., Sinha, R., and Khosla, P. K. (2001). Composable models for simulation-based design. *Engineering with Computers*, 17(2):112–128.

[179] Pate, D. J., Gray, J., and German, B. J. (2014). A graph theoretic approach to problem formulation for multidisciplinary design analysis and optimization. *Structural and Multidisciplinary Optimization*, 49(5):743–760.

[180] Pedregosa, F., Varoquaux, G., Gramfort, A., Michel, V., Thirion, B., Grisel, O., Blondel, M., Prettenhofer, P., Weiss, R., Dubourg, V., et al. (2011). Scikit-learn: Machine learning in python. *Journal of machine learning research*, 12(Oct):2825–2830.

[181] Penas, O., Plateaux, R., Choley, J.-Y., Kadima, H., Sorinao, T., Combastel, C., and Riviere, A. (2011). *Conception mecatronique. Vers un processus continu de conception mecatronique integree*. PhD thesis, SUPMECA.

[182] Penas, O., Plateaux, R., Patalano, S., and Hammadi, M. (2017). Multi-scale approach from mechatronic to cyber-physical systems for the design of manufacturing systems. *Computers in Industry*, 86:52–69.

[183] Persson, J. and Ölvander, J. (2013). Comparison of different uses of metamodels for robust design optimization. In *51st AIAA Aerospace Sciences Meeting Including the New Horizons Forum and Aerospace Exposition*, page 1039.

[184] Perullo, C. A., Tai, J. C., and Mavris, D. N. (2013). Effects of advanced engine technology on open rotor cycle selection and performance. *Journal of Engineering for Gas Turbines and Power*, 135(7):071204.

[185] Pfennig, M. and Thielecke, F. (2011). A knowledge-based approach for design and modelling of high lift actuation systems. *Proceedings of the Institution of Mechanical Engineers, Part G: Journal of Aerospace Engineering*, 225(3):302–311.

[186] Pham, T. H. and Hoole, S. R. H. (1995). Unconstrained optimization of coupled magneto-thermal problems. *IEEE transactions on Magnetics*, 31(3):1988–1991.

[187] Piaton, J. (2015). Electric motor braking system for rotolinear actuator. US Patent 9,035,511.

[188] Powell, M. J. (1994). A direct search optimization method that models the objective and constraint functions by linear interpolation. In *Advances in optimization and numerical analysis*, pages 51–67. Springer.

[189] Prieto, D., Dagusé, B., Dessante, P., Vidal, P., and Vannier, J.-C. (2012). Effect of magnets on average torque and power factor of synchronous reluctance motors. In *Electrical Machines (ICEM), 2012 XXth International Conference on*, pages 213–219. IEEE.

[190] Quora (2018). Operating principle of a modern high-bypass jet engine thrust reverser. https://www.quora.com/How-does-the-reverse-thrust-in-aircrafts-work.

[191] Radio Technical Commission for Aeronautics, Washington, D. S. C. . (1990). *Environmental conditions and test procedures for airborne equipment*. Radio Technical Commission for Aeronautics.

[192] Rahimi, F., Feng, L., Wikander, J., and Frede, D. (2017). Early phase design-optimization of mechatronic systems. In *Proceedings of the 2017 The 5th International Conference on Control, Mechatronics and Automation*, pages 42–49. ACM.

[193] Reul, A., Schwerdt, L., and Rinderknecht, S. (2016). Fast multidisciplinary design optimization in the development of mechatronic systems. In *ASME 2016 International Mechanical Engineering Congress and Exposition*, pages V011T15A022–V011T15A022. American Society of Mechanical Engineers.

[194] Reysset, A. (2015). *Conception préliminaire d'actionneurs électromécaniques-outils d'aide à la spécification et à la génération de procédures de dimensionnement pour l'optimisation*. PhD thesis, Toulouse, INSA.

[195] Reysset, A., Budinger, M., and Maré, J.-C. (2015). Computer-aided definition of sizing procedures and optimization problems of mechatronic systems. *Concurrent Engineering*, 23(4):320–332.

[196] Richardeau, F., Vinnac, S., Mosser, F., Boestch, A., Chillon, S., Hors, D., and Rashed, A. (2018). First practical evaluation of a complete fail-safe and 100fault-tolerant inverter for critical load in aerospace application. *Recent Advances in Aerospace Actuation Systems and Components, INSA Toulouse*, pages 64–68.

[197] Robbins, D., Bobalik, J., De Stena, D., Martin, N., Plag, K., Rail, K., and Wall, K. (2018). F-35 subsystems design, development & verification. In *2018 Aviation Technology, Integration, and Operations Conference*, page 3518.

[198] Rogers, J. L. (1989). A knowledge-based tool for multilevel decomposition of a complex design problem.

[199] Rohrschneider, R., Olds, J., Braun, R., Hutchinson, V., Kuhl, C., and Steffes, S. (2004). Flight system options for a long-duration mars airplane. In *AIAA 3rd" Unmanned Unlimited" Technical Conference, Workshop and Exhibit*, page 6568.

[200] Roos, F. (2007). *Towards a methodology for integrated design of mechatronic servo systems*. PhD thesis, KTH.

[201] Roos, F., Johansson, H., and Wikander, J. (2006). Optimal selection of motor and gearhead in mechatronic applications. *Mechatronics*, 16(1):63–72.

[202] Rosenbrock, H. (1960). An automatic method for finding the greatest or least value of a function. *The Computer Journal*, 3(3):175–184.

[203] Sadraey, M. H. (2012). *Aircraft design: A systems engineering approach*. John Wiley & Sons.

[204] Safavi, E., Chaitanya, M., Ölvander, J., and Krus, P. (2013). Multidisciplinary optimization of aircraft actuation system for conceptual analysis. In *51st AIAA Aerospace Sciences Meeting including the New Horizons Forum and Aerospace Exposition*, page 282.

[205] Safavi, E., Tarkian, M., Gavel, H., and Ölvander, J. (2015). Collaborative multidisciplinary design optimization: a framework applied on aircraft conceptual system design. *Concurrent Engineering*, 23(3):236–249.

[206] Saltelli, A., Annoni, P., Azzini, I., Campolongo, F., Ratto, M., and Tarantola, S. (2010). Variance based sensitivity analysis of model output. design and estimator for the total sensitivity index. *Computer Physics Communications*, 181(2):259–270.

[207] Sanchez, F. (2017). *Génération de modèles analytiques pour la conception préliminaire de systèmes multi-physiques: application à la thermique des actionneurs et des systèmes électriques embarqués*. PhD thesis, Université de Toulouse, Université Toulouse III-Paul Sabatier.

[208] Sanchez, F., Budinger, M., Delbecq, S., and Hazyuk, I. (2017a). Modelling and design approaches for the preliminary design of power electronic converters. In *ELECTRIMACS*.

[209] Sanchez, F., Budinger, M., and Hazyuk, I. (2017b). Dimensional analysis and surrogate models for the thermal modeling of multiphysics systems. *Applied Thermal Engineering*, 110:758–771.

[210] Sanchez, F. and Delbecq, S. (2016). Surrogate modeling technique for the conceptual and preliminary design of embedded actuation systems and components. In *International Congress of the Aeronautical Sciences*.

[211] Sanchez, F., Koschlik, A.-K., Budinger, M., and Hazyuk, I. (2016). Dimensional analysis and surrogate modelling technique for the sizing of actuation systems. *Recent Advances in Aerospace Actuation Systems and Components, INSA Toulouse*, pages 158–165.

[212] Sellar, R., Batill, S., and Renaud, J. (1996). Response surface based, concurrent subspace optimization for multidisciplinary system design. In *34th Aerospace Sciences Meeting and Exhibit*, page 714.

[213] Seresinhe, R. and Lawson, C. (2015). Electrical load-sizing methodology to aid conceptual and preliminary design of large commercial aircraft. *Proceedings of the Institution of Mechanical Engineers, Part G: Journal of Aerospace Engineering*, 229(3):445–466.

[214] Siddiqui, M. A. and Haq, M. S. (2013). Review of thrust reverser mechanism used in turbofan jet engine aircraft. *International Journal of Engineering*, 6(5):717–726.

[215] Simpson, T. W., Poplinski, J., Koch, P. N., and Allen, J. K. (2001). Metamodels for computer-based engineering design: survey and recommendations. *Engineering with computers*, 17(2):129–150.

[216] Sobieszczanski-Sobieski, J. (1988). Optimization by decomposition: a step from hierarchic to non-hierarchic systems.

[217] Software, M. (2018a). Patran: Complete fea modeling solution. http://www.mscsoftware.com/en-uk/product/patran.

[218] Software, S. P. (2018b). Simcenter amesim: Integrated simulation platform for multi-domain mechatronic systems simulation. https://www.plm.automation.siemens.com/global/en/products/simcenter/simcenter-amesim.html.

[219] Standard, F. (2018). Fmi: Functional mock-up interface. https://fmi-standard.org/.

[220] Stanford, B. (2017). Optimal control surface layout for an aeroservoelastic wingbox. In *58th AIAA/ASCE/AHS/ASC Structures, Structural Dynamics, and Materials Conference*, page 1813.

[221] Stefano Bianchi, E. (2005). The launchers and the vega programme and the launcher subsystems. http://www.ingaero.uniroma1.it/attachments/1609_VEGA%20%20sapienza%20small.pdf.

[222] Steward, D. V. (1965). Partitioning and tearing systems of equations. *Journal of the Society for Industrial and Applied Mathematics, Series B: Numerical Analysis*, 2(2):345–365.

[223] Stump, G., Yukish, M., Martin, J., and Simpson, T. (2004). The arl trade space visualizer: An engineering decision-making tool. In *10th AIAA/ISSMO Multidisciplinary Analysis and Optimization Conference*, page 4568.

[224] Sympy (2018). Sympy python library. http://www.sympy.org.

[225] Systemes, D. (2018a). Abaqus: Unified fea. https://www.3ds.com/products-services/simulia/products/abaqus/.

[226] Systemes, D. (2018b). Dymola: Multi-engineering modeling and simulation based on modelica and fmi. https://www.3ds.com/products-services/catia/products/dymola/.

[227] Tarjan, R. (1971). Depth-first search and linear graph algorithms. In *Switching and Automata Theory, 1971., 12th Annual Symposium on*, pages 114–121. IEEE.

[228] Thareja, R. and Haftka, R. (1986). Numerical difficulties associated with using equality constraints toachieve multi-level decomposition in structural optimization. In *27th Structures, Structural Dynamics and Materials Conference*, page 854.

[229] Thauvin, J. (2018). *Exploring the design space for a hybrid-electric regional aircraft with multidisciplinary design optimisation methods*. PhD thesis, Toulouse, INPT.

[230] Tiedeman, R. K. (1996). Jam-tolerant rotary actuator. US Patent 5,518,466.

[231] Todeschi, M. (2018). Reliability of the electronics for actuation? *Recent Advances in Aerospace Actuation Systems and Components, INSA Toulouse*, pages 48–57.

[232] Todeschi, M. and Salas, F. (2016). Power electronics for the flight control actuators. *Recent Advances in Aerospace Actuation Systems and Components, INSA Toulouse*, pages 1–9.

[233] Touré, B., Schanen, J.-L., Gerbaud, L., Meynard, T., Roudet, J., and Ruelland, R. (2013). Emc modeling of drives for aircraft applications: Modeling process, emi filter optimization, and technological choice. *IEEE Transactions on Power Electronics*, 28(3):1145–1156.

[234] Van Den Bossche, D. (2006). The a380 flight control electrohydrostatic actuators, achievements and lessons learnt. In *25th international congress of the aeronautical sciences*, pages 1–8.

[235] Van der Velden, A., Wujek, B., and Koch, P. (2008). isight-fd: A tool for multi-objective data analysis. In *12th AIAA/ISSMO Multidisciplinary Analysis and Optimization Conference*, page 5988.

[236] Van Huynh, N. and McCormick, P. J. (2018). Electronically controlled rotary actuator for an aircraft control surface. US Patent App. 15/216,963.

[237] Vanthuyne, T. (2009). An electrical thrust vector control system for the vega launcher. In *Proceeding of 13th European Space Mechanisms and Tribology Symposium, ESMATS*, pages 23–25. Citeseer.

[238] Walden, D. D., Roedler, G. J., Forsberg, K., Hamelin, R. D., and Shortell, T. M. (2015). *Systems engineering handbook: A guide for system life cycle processes and activities*. John Wiley & Sons.

[239] Wang, G. G. and Shan, S. (2007). Review of metamodeling techniques in support of engineering design optimization. *Journal of Mechanical design*, 129(4):370–380.

[240] Wang, L. (2012). *Force equalization for active/active redundant actuation system involving servo-hydraulic and electro-mechanical technologies*. PhD thesis, Toulouse, INSA.

[241] Wang, X., Bibeau, E., and Naterer, G. (2007). Experimental correlation of forced convection heat transfer from a naca airfoil. *Experimental Thermal and Fluid Science*, 31(8):1073–1082.

[242] Welstead, J. and Felder, J. L. (2016). Conceptual design of a single-aisle turboelectric commercial transport with fuselage boundary layer ingestion. In *54th AIAA Aerospace Sciences Meeting*, page 1027.

[243] Yan, X., Qiao, M., Li, J., Simpson, T. W., Stump, G. M., and Zhang, X. (2012). A work-centered visual analytics model to support engineering design with interactive visualization and data-mining. In *System Science (HICSS), 2012 45th Hawaii International Conference on*, pages 1845–1854. IEEE.

[244] Yang, X.-S. (2010). *Nature-inspired metaheuristic algorithms*. Luniver press.

[245] Zatloff, E. (2018). Spoiler and flap rotary em actuation (rema) implementation on a recently certified business jet. *Recent Advances in Aerospace Actuation Systems and Components, INSA Toulouse*, pages 15–23.

Appendix A

Thrust Vector Control Actuation System Case Study

Models

System Analysis Functions

Actuator Length

$$L_{act} = \left((0.2248 \cdot d_1 - 0.3757)^2 + (-0.9744 \cdot d_1 + d_2 - 1.172)^2\right)^{0.5} \tag{A.1}$$

Lever Arm

$$\begin{aligned} L_{arm} = ((-(-0.9744 d_1 - 1.372) \cdot (0.2248 \cdot d_1 - 0.3757) \cdot ((0.2248 \cdot d_1 - 0.3757)^2 + \\ (-0.9744 \cdot d_1 + d_2 - 1.172)^2)^{-0.5} + (0.2248 \cdot d_1 + 0.9823) \cdot ((0.2248 \cdot d_1 - 0.3757)^2 + \\ (-0.9744 \cdot d_1 + d_2 - 1.172)^2)^{-0.5} \cdot (-0.9744 \cdot d_1 + d_2 - 1.172))^2)^{0.5} \end{aligned} \tag{A.2}$$

Actuator Stroke

$$S_{act} = \Theta_{noz} \cdot L_{arm} \tag{A.3}$$

Actuator Speed

$$V_{max_{act}} = \Omega_{max_{noz}} \cdot L_{arm} \tag{A.4}$$

Actuator Maximum Load

$$F_{max_{act}} = \frac{T_{dyn_{noz}}}{L_{arm}} \tag{A.5}$$

Motor Torque Specification

$$T_{em} = k_{os} F_{max_{act}} \frac{p_{bs}}{N_{red} \eta_{mech}} \tag{A.6}$$

Motor Speed Specification

$$\Omega_{mot} = V_{max_{act}} \frac{N_{red}}{p_{bs}} \tag{A.7}$$

Stall Load Specification

$$F_{stall} = T_{em} \frac{N_{red}}{p_{bs}} \tag{A.8}$$

Limit Load Specification

$$F_{lim} = k_{sec} F_{stall} \tag{A.9}$$

Geometric Integration

$$L_{act} \geq S_{act} + L_{nut} + L_{bearing} + 2L_{rod} \tag{A.10}$$

Total Mass

$$M_{tot} = M_{mot} + M_{nut} + M_{screw} + M_{bearing} + 2M_{rod} + M_{housing} \tag{A.11}$$

Component analysis functions

Motor

Motor mass:

$$M_{mot} = M_{mot_{ref}} \left(\frac{T_{em}}{T_{em_{ref}}} \right)^{\frac{3}{3.5}} \tag{A.12}$$

Motor inertia:

$$J_{mot} = J_{mot_{ref}} \left(\frac{T_{em}}{T_{em_{ref}}} \right)^{\frac{5}{3.5}} \tag{A.13}$$

Motor maximum mechanical speed:

$$\Omega_{mot_{max}} = \Omega_{mot_{max_{ref}}} \left(\frac{T_{em}}{T_{em_{ref}}} \right)^{-\frac{1}{3.5}} \tag{A.14}$$

Motor speed constraint:

$$\Omega_{mot_{max}} \geq \Omega_{mot} \tag{A.15}$$

Motor torque consistency:

$$T_{em} \geq F_{max_{act}} \frac{p_{bs}}{N_{red} \eta_{mech}} + J_{mot} \alpha_{noz} L_{arm} \frac{N_{red}}{p_{bs}} \tag{A.16}$$

Rod-end

Rod-end mass:

$$M_{rod} = M_{rod_{ref}} \left(\frac{F_{limit}}{F_{rod_{ref}}} \right)^{\frac{3}{2}} \tag{A.17}$$

Rod-en length:

$$L_{rod} = L_{rod_{ref}} \left(\frac{F_{limit}}{F_{rod_{ref}}} \right)^{\frac{1}{2}} \tag{A.18}$$

Ball screw

Nut mass:

$$M_{nut} = M_{nut_{ref}} \left(\frac{F_{limit}}{F_{nut_{ref}}} \right)^{\frac{3}{2}} \tag{A.19}$$

Nut length:

$$L_{nut} = L_{nut_{ref}} \left(\frac{F_{limit}}{F_{nut_{ref}}} \right)^{\frac{1}{2}} \tag{A.20}$$

Nut diameter:

$$D_{nut} = D_{nut_{ref}} \left(\frac{F_{limit}}{F_{nut_{ref}}} \right)^{\frac{1}{2}} \tag{A.21}$$

Screw mass:

$$M_{screw} = Ml_{screw_{ref}} \left(\frac{F_{limit}}{F_{screw_{ref}}} \right)^{\frac{3}{2}} \cdot \frac{L_a}{2} \tag{A.22}$$

Thrust bearing

Thrust bearing mass:

$$M_{bearing} = M_{bearing_{ref}} \left(\frac{F_{limit}}{F_{bearing_{ref}}} \right)^{\frac{3}{2}} \tag{A.23}$$

Thrust bearing length:

$$L_{bearing} = L_{bearing_{ref}} \left(\frac{F_{limit}}{F_{bearing_{ref}}} \right)^{\frac{1}{2}} \tag{A.24}$$

Housing

Housing mass:

$$M_{housing} = \rho \frac{L_a ct}{2} \left(\pi \left(\left(\frac{d_{rs}}{2} + e_1 + e_2 \right)^2 - \left(\frac{d_{rs}}{2} + e_1 \right)^2 \right) + \pi \left(\left(\frac{d_{rs}}{2} + e_1 \right)^2 - \left(\frac{d_{rs}}{2} \right)^2 \right) \right) \tag{A.25}$$

Housing stress:

$$\begin{aligned}\log(\pi_0) = 124\log\left(\frac{L_a}{d_{rs}}\right) + \\ \frac{2}{23}\log\left(\frac{L_a}{d_{rs}}\right)\cdot\log\left(\frac{e_1}{d_{rs}}\right) + \\ \frac{31}{421}\log\left(\frac{L_a}{d_{rs}}\right)\cdot\log\left(\frac{e_2}{d_{rs}}\right) + \\ \frac{713}{812}\log\left(\frac{L_a}{d_{rs}}\right) + \frac{125}{892}\log\left(\frac{e_1}{d_{rs}}\right)^2 - \\ \frac{194}{911}\log\left(\frac{e_1}{d_{rs}}\right)\cdot\log\left(\frac{e_2}{d_{rs}}\right) - \\ \frac{231}{391}\log\left(\frac{e_1}{d_{rs}}\right) + \frac{13}{48}\log\left(\frac{e_2}{d_{rs}}\right)^2 + \\ \frac{704}{875}\log\left(\frac{e_2}{d_{rs}}\right) + \frac{290}{231}\end{aligned} \tag{A.26}$$

$$\sigma = \pi_0 Q_m d_{rs} \rho a \tag{A.27}$$

Optimization

Formulation

The optimization is the following:

$$\begin{array}{ll} \text{minimize} & M_{tot} \\ \text{with respect to} & N_{red}, d_1, d_2, e_1, e_2, k_{os} \\ \text{subject to} & \Omega_{mot} - \Omega_{mot_{max}} \leq 0 \\ & S_{act} + L_{nut} + L_{bearing} + 2L_{rod} - L_{act} \leq 0 \\ & \sigma - \sigma_{max} \leq 0 \\ & F_{max_{act}} \dfrac{p_{bs}}{N_{red}\eta_{mech}} + J_{mot}\alpha_{noz}L_{arm}\dfrac{N_{red}}{p_{bs}} - T_{em} \leq 0 \end{array} \tag{A.28}$$

Results

The optimization was achieved considering a reduction of motor inertia of 2 and for variable anchorage positioning.

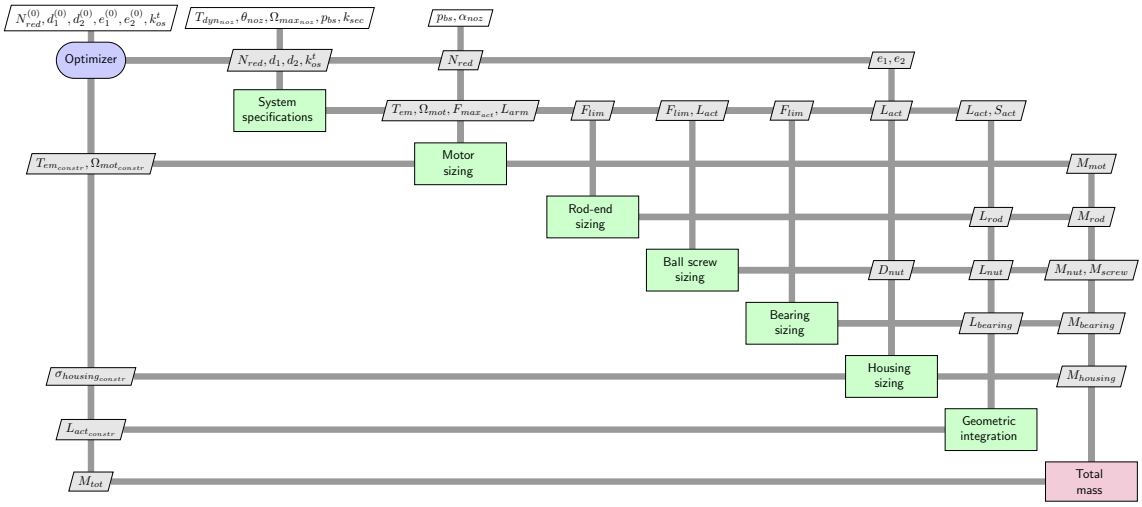

Fig. A.1 XDSM diagram of the thrust vector control electro-mechanical actuator optimization

Inputs

Table A.1 Inputs parameters values for the TVC EMA design

	Parameter	Value	Unit	Description
Requirements	α_{noz}	14.15	[rad s^{-2}]	Nozzle angular acceleration
	k_{sec}	2.0	[-]	Sizing security factor
	$\Omega_{max_{noz}}$	0.16	[rad s^{-1}]	Nozzle maximum angular velocity
	p_{bs}	1.6×10^{-3}	[-]	Ball screw pitch
	$T_{dyn_{noz}}$	48	[kN]	Nozzle dynamic peak torque
	Θ_{noz}	1×10^{-2}	[rad]	Nozzle stroke
	η_{mech}	0.7	[rad]	Mechanical transmission efficiency
Motor	$J_{mot_{ref}}$	2.9×10^{-4}	[kg m^2]	Reference motor inertia
	$M_{mot_{ref}}$	3.8	[kg]	Reference motor mass
	$\Omega_{mot_{max_{ref}}}$	754	[rad s^{-1}]	Reference motor maximum speed
	$T_{em_{ref}}$	13.4	[N m]]	Reference motor nominal electromagnetic torque
Rod-end	$F_{rod_{ref}}$	183	[kN]	Reference rod limit load
	$L_{rod_{ref}}$	61	[mm]	Reference rod length
	$M_{rod_{ref}}$	1.55	[kg]	Reference rod mass
Ball screw	$D_{nut_{ref}}$	80	[mm]	Reference nut diameter
	$F_{nut_{ref}}$	135	[kN]	Reference nut limit load
	$F_{screw_{ref}}$	135	[kN]	Reference screw limit load
	$L_{nut_{ref}}$	107	[mm]	Reference nut length
	$M_{nut_{ref}}$	2.1	[kg]	Reference nut mass
	$M_{screw_{ref}}$	9.4	[kg]	Reference screw mass
Bearing	$F_{bearing_{ref}}$	183	[kN]	Reference thrust bearing limit load
	$L_{bearing_{ref}}$	72	[mm]	Reference thrust bearing length
	$M_{bearing_{ref}}$	5.05	[kg]	Reference thrust bearing mass
Housing	Q_m	30	[-]	Quality factor of the structure assembly
	ρ	7800	[mm]	Volumic mass of the material (steel)
	σ_{max}	500	[MPa]	Limit stress of the material (steel)
	a	196	[m s^{-2}]	Acceleration during vibration test (20 g)

Design Variables, Constraints and Objective

Table A.2 Design variables, constraints and objective of the TVC EMA design

	Parameter	Value	Unit	Description
Design variables	d_1	-510	[mm]	Anchorage position parameter [-800,800]
	d_2	200	[mm]	Anchorage position parameter [-200,200]
	e_1	4.1	[mm]	Housing thickness [1,40]
	e_2	1	[mm]	Housing thickness [1,40]
	N_{red}	1.32	[-]	Spur gear reduction ratio [0.1,5]
Constraints	L_{act}	682	[mm]	Actuator length (min=313)
	Ω_{mot}	162	[rad s^{-1}]	Motor speed (max=414)
	σ	500	[MPa]	Housing resonance stress (max=500)
	T_{em}	109.2	[Nm]	Consitency constraint on motor torque (min=109.2)
Objective	M_{tot}	39	[kg]	Actuator total mass

Outputs

Table A.3 System output values for the TVC EMA design

	Parameter	Value	Unit	Description
System specifications	F_{lim}	180.355	[kN]	Actuator limit load
	$F_{max_{act}}$	38.97	[kN]	Actuator maximum load (to provide)
	F_{stall}	90.177	[kN]	Actuator stall load
	L_{act}	682	[mm]	Actuator length
	L_{arm}	1.23	[m]	Lever arm length
	$\Omega_{max_{mot}}$	1.6×10^{-3}	[rad s−1	Motor maximum speed
	S_{act}	24	[mm]	Actuator stroke
	T_{em}	109	[Nm]	Motor electromagnetic torque
	$V_{max_{act}}$	197	[mm s^{-1}]	Maximum actuator speed
Motor	J_{mot}	2.9×10^{-3}	[kg m^2]	Motor inertia
	M_{mot}	22.96	[kg]	Motor mass
	$\Omega_{mot_{max}}$	414	[rad s^{-1}]	Motor maximum speed
Rod-end	L_{rod}	60	[mm]	Rod length
	M_{rod}	1.51	[kg]	Rod mass
Ball screw	D_{nut}	92	[mm]	Nut diameter
	L_{nut}	124	[mm]	Nut length
	M_{nut}	3.24	[kg]	Nut mass
	M_{screw}	4.95	[kg]	Screw mass
Bearing	$L_{bearing}$	44	[mm]	Thrust bearing length
	$M_{bearing}$	1.18	[kg]	Thrust bearing mass
Housing	$M_{housing}$	4.2	[kg]	Housing mass
	Π_0	117.9	[-]	Stress dimensionless number
	σ	500	[MPa]	Stress at resonance frequency

Appendix B

Primary Flight Control Actuation System Case Study

EMA Thermal Behaviour Investigation

The objective of this study was to achieve an optimal sizing of an aileron linear EMA with dynamic thermal constraints. Details of this work can be found in [54]. The dynamic thermal constraints are evaluated using a lumped parameter model developed in the Dymola software [226]. The optimization is achieved using the openMDAO framework [89].

The actuator is a linear parallel gear drive EMA. The EMA is assumed to operate in a confine space environment of the wing with only natural convection cooling as illustrated in Figure B.1.

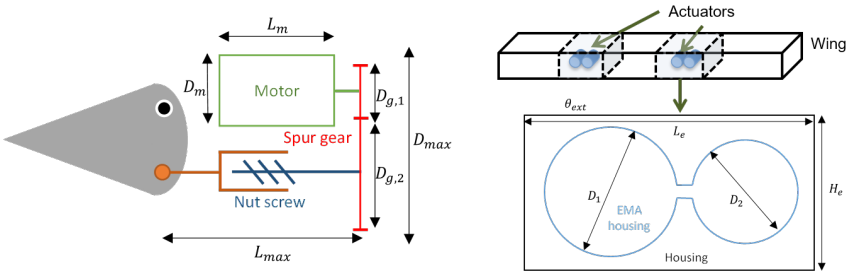

Linear geared drive with parallel axis *Natural convection in a confined space*

Fig. B.1 Actuator thermal behaviour investigation parametrization

The ball screw is assumed fixed. Only the spur gear and the motor are sized. The objective is to minimize the overall mass of the actuator. The design variables considered are the motor diameter and current density, and the spur gear reduction ratio and gear aspect ratio. The constraints of the optimization problem are the EMA maximum reflected inertia, motor maximum mechanical speed, geometric integration, and both the housing skin temperature and motor winding hot spot temperature.

In order to evaluate these temperatures over an entire flight mission profile, a lumped parameter model is constructed for which the architecture and interfaces are shown in Figure B.2.

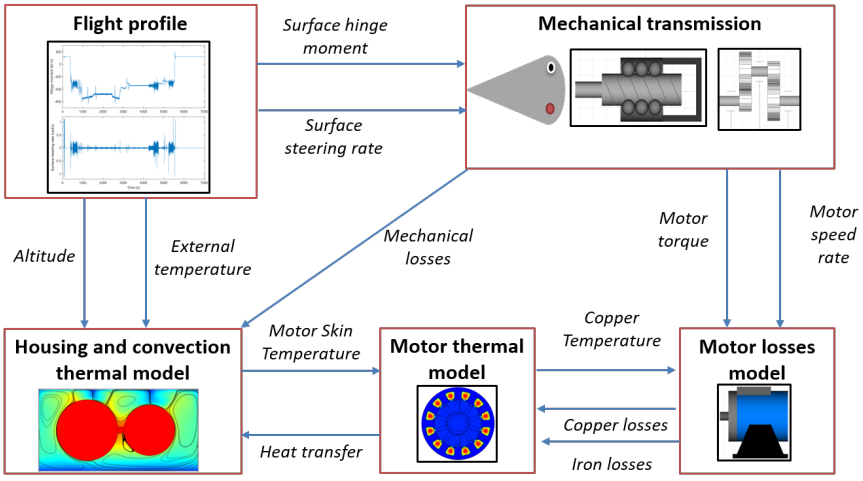

Fig. B.2 Actuator dynamic model architecture and interfaces

This model enables to assess the effect of the flight mission profile on the motor and mechanical losses, altitude and temperature on the housing thermal convection resistance, and finally the motor winding hot spot temperature and housing skin temperature.

The actuator thermal model implemented is outlined in Figure B.3.

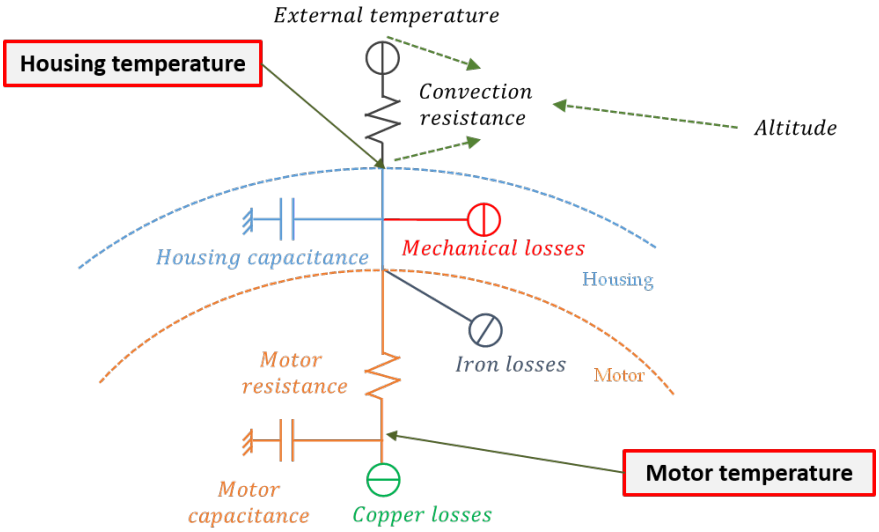

Fig. B.3 Actuator dynamic thermal model architecture and interfaces

The housing convection thermal resistance between the wing temperature and the housing temperature is altitude and temperature dependent. Mechanical and motor iron losses are injected directly in the housing whereas the Joule (copper) losses are injected in the winding. The motor is modelled as a conduction thermal resistance and a single heat capacity. Justification of this simplification can be found in [54].

The Dymola model is illustrated in Figure B.4.

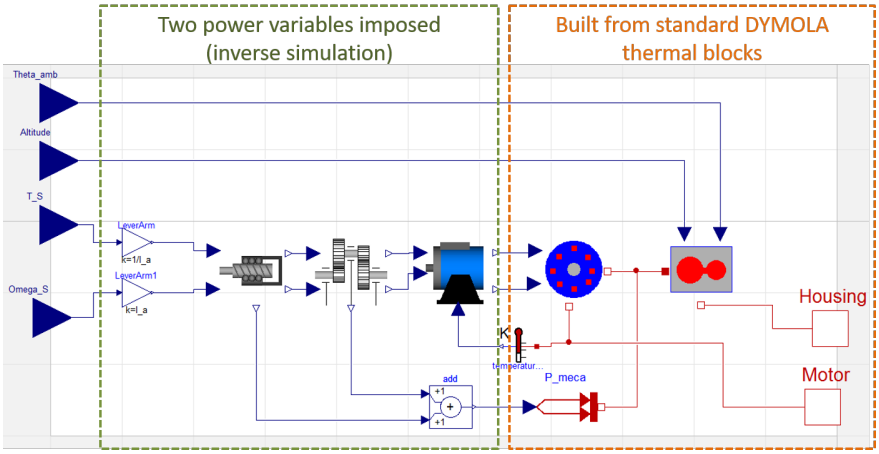

Fig. B.4 Overall architecture of the actuator Dymola model

Inverse simulation is used, thus the mission profile imposes the power flux. Conversely, the thermal model is implemented in a direct manner with common library components.

In the system sizing model, the housing thermal resistance and the motor thermal resistance depend on the actuator design. The models that link the design to the resistance values are obtained by surrogate modelling of thermal FEM simulations (Figure B.5).

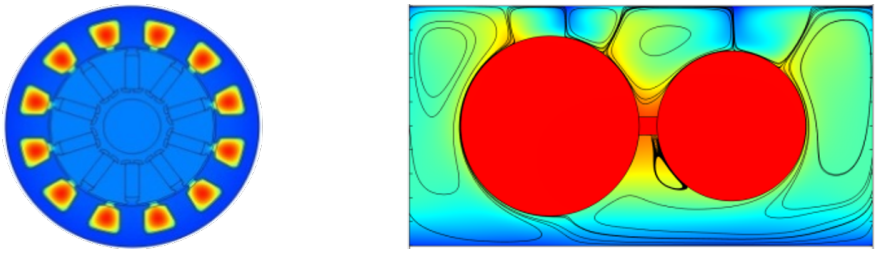

Fig. B.5 Thermal FEM simulations of the motor (left) and the actuator housing (right)

The sizing model of the actuator is implement in the BOA framework and then exported as a Python Serializer Object. The Dymola model is converted to a FMU [219] and manipulated using pyFMI [9]. A Python code is then written to implement the overall problem. Figure B.6 illustrates how the sizing model and the FMU interact.

The sizing model provides to the FMU the parameters of the actuator such as the thermal resistance, reduction ratio, torque constant, motor electrical resistances etc... Then the FMU provides the motor winding hot spot temperature and housing skin temperature to the sizing model. These temperatures are analyzing and their maximum values are passed as constraints to the optimizer. A FMU simulation is performed for for each optimizer iteration. The gradient-based optimizer SLSQP is used. The gradient of the FMU is a linearized model of the thermal model [54].

Three designs are achieved. Two use a linear steady state thermal model to evaluate the actuator temperatures. The first design is obtained for the temperatures corresponding to the maximum torque

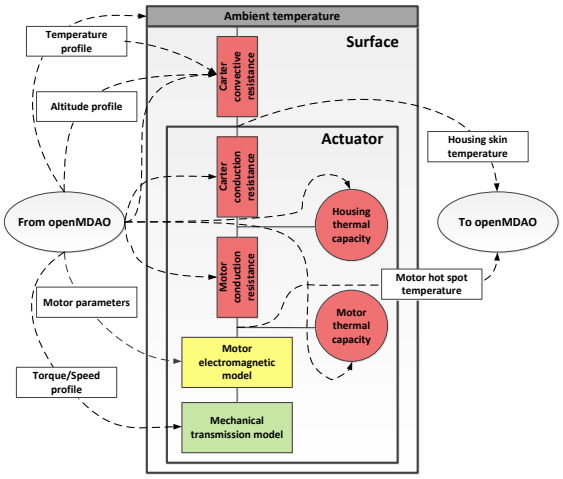

Fig. B.6 Interaction between optimization model and FMU model [54]

of the mission profile. The first design is obtained for the temperatures corresponding to the RMS torque of the mission profile. The third design is obtained for the temperatures evaluated using the dynamic model response to the entire flight profile presented previously. A validation of each design is achieved by running the dynamic model for each configuration. The thermal response for the three designs have been achieved for the same operating speed Ω_{mean}. Thermal simulation validation results are illustrated in Figure 5.12.

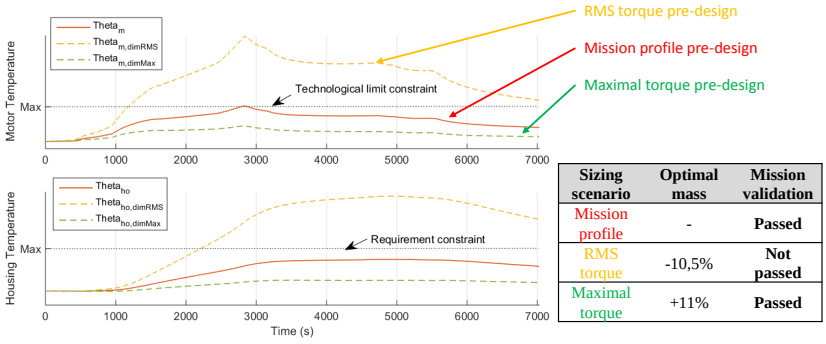

Sizing scenario	Optimal mass	Mission validation
Mission profile	-	Passed
RMS torque	-10,5%	Not passed
Maximal torque	+11%	Passed

Fig. B.7 Thermal response of preliminary design over the entire mission

The first conclusion is that the most critical flight phase for the thermal behaviour of an EMA is during cruise when the loads are high and the heat transfer is less efficient due to low air density despite that the ambient temperature is very low. The optimal mass was obtained for the complete mission profile scenario and an increase of 10 % was obtained for maximum torque. However, the sizing achieved for the RMS torque operating point was not compliant with thermal constraints. In the present study, it is therefore chosen to use the maximum torque T_{surf} to compute temperatures even

though it is not the optimum. More details of the work achieved in [54] can be found in Appendix B. The chosen operating point T_{surf} and Ω_{mean} enable to determine the losses in the different components.

As the surfaces studied operate during the entire flight, the steady state response is used to compute component temperatures. Hence, only the losses obtained for the operating point and the component thermal resistances are needed. These will be determined during the component estimation models description. The thermal losses in the Harmonic Drive are not considered during temperature estimation.

The RMS torque as chosen because is the equivalent torque to compute the motor Joule losses.

Permanent Magnet Synchronous Motor Sizing Model

The sizing model of the brushless motor used is based on the work of Sanchez [209, 207] who developed electromagnetic and thermal surrogate models based on FEM simulations illustrated in Figure B.8.

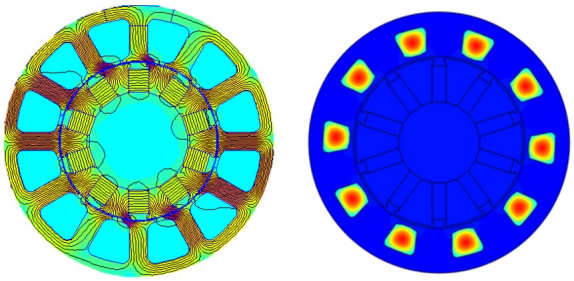

Fig. B.8 Brushless motor electromagnetic (left) and thermal (right) FEM simulations [207]

Electromagnetic Model

The linear electromagnetic torque of the motor $T_{em,l} = \frac{T_{em}}{L_{mot}}$ can be expressed using twelve physical parameters:

$$T_{em,l} = f\left(D_{mot}, D_{Si}, e_y, L_T, L_{mag}, H_{mag}, D_{Ri}, J_{cur}, \mu_0, B_r, B_{sat}\right) \tag{B.1}$$

Where D_{mot} and D_{Si} are respectively the stator outer and inner diameter, e_y the yoke thickness, L_T the teeth width, L_{mag} and H_{mag} the magnet width and height, D_{Ri} the rotor inner diameter, J_{cur} the current density in the windings, μ_0 the permeability of vacuum, B_r the induction of the magnet and B_{sat} the saturation value of the iron sheets. A sensitivity analysis on the torque density enables us to reduce the number of variables to express the linear torque:

$$T_{em,l} = f\left(D_{mot}, e_y, J_{cur}, \mu_0, B_r, B_{sat}\right) \tag{B.2}$$

Dimensional analysis enables us to express Equation B.2 in a dimensionless manner [209]:

$$\pi_0 = F\left(\pi_1, \pi_2\right) \tag{B.3}$$

Where $\pi_0 = \frac{T_{em,l}}{J_{cur}B_r D_{mot}^3}$ which represents the dimensionless linear torque, $\pi_1 = \frac{\mu_0 J_{cur} D_{mot}}{B_{sat}}$ which represents the magnetic saturation and $\pi_2 = \frac{e_y}{D_{mot}}$ which represents the quantity on iron the yoke and has a significant influence on the iron losses.

The obtained surrogate model that represents the linear electromagnetic torque is the following [207]:

$$\pi_0 = 1.72 \cdot 10^{-4} \cdot \pi_1^{1.142-0.262\log(\pi_1)+1.679\log(\pi_2)} \pi_2^{-2.256-0.721\log(\pi_2)+0.518 log(\pi_2) log(\pi_1)} \tag{B.4}$$

Thermal Model

The thermal model of the brushless motor consists of steady state response which can be represented by the conduction thermal resistance between the winding hot spot temperature and the stator external skin temperature. Sanchez has built using surrogate modelling and 2D thermal FEM simulation (Figure B.8)) a model for the conduction thermal resistance $R_{th_{cond}}$. The list of modelling assumptions can be found in [209, 207]. The main assumptions are that the thermal resistance of stator (iron) can be neglected when compared to the thermal resistance inside the winding. Hence, the losses will be dissipated through the winding. Furthermore, simulations are achieved for different sizes of motor in order to construct the surrogate model. Geometric similarity is assumed for all parameters except the Nomex insulation thickness which is considered constant.

The linear conduction thermal resistance of the motor $R_{th_{cond}} L_{mot}$ can be expressed using four physical parameters:

$$R_{th_{cond}} L_{mot} = f(D_{mot}, e_N, \lambda_w, \lambda_{ir}) \tag{B.5}$$

Where L_{mot} and D_{mot} are respectively the length and diameter of the motor, e_N is the Nomex insulation thickness, λ_w and λ_{ir} are respectively the thermal conductivity of the winding and the iron.

Dimensional analysis enables us to express Equation B.5 in a dimensionless manner [209, 207]:

$$\pi_{cond} = F(\pi_1, \pi_2) \tag{B.6}$$

Where $\pi_{cond} = R_{th_{cond}} L_{mot} \lambda_{ir}$, $\pi_1 = \frac{D_{mot}}{e_N}$ and $\pi_2 = \frac{\lambda_w}{\lambda_{ir}}$. Since the physical properties are assumed constant, π_2 is constant. The problem can then be reduced as follows:

$$\pi_{cond} = F(\pi_1) \tag{B.7}$$

The obtained surrogate model that represents the motor conduction thermal resistance is the following [207]:

$$\pi_{cond} = 84.2 \cdot \pi_1^{-1.077+0.164\log(\pi_1)} \tag{B.8}$$

Losses Model

The main losses considered in the brushless motor are the Joule and iron losses.

The Joule losses P_J in the motor are a function of the winding volume per slot pair V_w, current density J_{cur}, winding factor k_w, copper electrical resistivity σ_{cop} and the number of slots N_{slot}:

$$P_J = \frac{N_{slot}}{2} k_w \sigma_{cop} V_w J_{cur}^2 \tag{B.9}$$

The challenge to obtain an accurate Joule losses model is to have an accurate estimation of the winding volume. The winding volume per slot pair can be decomposed into the winding volume of the active part of the motor V_{slot} and the winding head V_{wh} as follows:

$$V_w = V_{slot} + V_{wh} = 2A_{slot}L_{mot} + 2\pi^2 \left(\frac{d_{tore}}{2}\right)^2 R_{tore} \tag{B.10}$$

Where A_{slot} is a single slot area, $d_{tore} = 2\sqrt{\frac{A_{slot}}{\pi}}$ the equivalent diameter of the winding head and $R_{tore} = 0.2877 \cdot D_{mot} \sin\left(\frac{\pi}{12}\right)$ the radius of the winding head from one slot to another.

Sanchez has also provided a surrogate model that estimates the slot area [207]:

$$\pi_{slot} = 2.31 \cdot 10^{-6} \cdot \pi_2^{-6.946 - 4.104\log(\pi_2) - 0.833\log(\pi_2)^2} \tag{B.11}$$

Where $\pi_{slot} = \frac{A_{slot}}{D_{mot}^2}$ and $\pi_2 = \frac{e_y}{D_{mot}}$.

The second source of losses are the iron losses. The general expression of iron losses is the following:

$$P_{ir} = A \cdot V_{ir} \cdot B^2 \tag{B.12}$$

Where $A = k \cdot \delta_{p\,\frac{1}{50}} \cdot \rho_{ir} \left(\frac{\Omega_{mot,mean} \cdot pp}{2\pi \cdot 50}\right)^{1.5}$, with k and $\delta_{p\,\frac{1}{50}}$ loss factors measured for 50 Hz, ρ_{ir} the density of iron, $\Omega_{mot,mean}$ the operating speed of the motor for the temperature computation, pp the number of pole pair, and $B = B_y + B_t$, with B_y and B_t respectively the induction level in the yoke and the teeth.

The iron losses of the motor $\frac{P_{ir}}{L_{mot}}$ can be expressed using four physical parameters:

$$\frac{P_{ir}}{L_{mot}} = f\left(A, D_{mot}, e_y, \mu_0, J_{cur}, B_{sat}, B_r\right) \tag{B.13}$$

Dimensional analysis enables us to express Equation B.13 in a dimensionless manner [209]:

$$\pi_{P_{ir}} = F\left(\pi_1, \pi_2\right) \tag{B.14}$$

Where $\pi_{P_{ir}} = \frac{P_{ir}}{A L_{mot} D_{mot}^2 B_r}$, $\pi_1 = \frac{\mu_0 J_{cur} D_{mot}}{B_{sat}}$ and $\pi_2 = \frac{e_y}{D_{mot}}$.

The obtained surrogate model that represents the motor iron losses is the following [207]:

$$\pi_{P_{ir}} = 2.361 \cdot 10^{-2} \cdot \pi_1^{-0.498 - 0.0605\log(\pi_1) + 0.496\log(\pi_1)^2} \cdot \pi_2^{-1.714 - 0.765\log(\pi_2)} \tag{B.15}$$

Mechanical Model

The diameter of the motor D_{mot} is a design variable. Conversely, the motor length L_{mot} is obtained with respect to the required electromagnetic torque Tem and the linear electromagnetic torque $T_{em,l}$ obtained previously:

$$L_{mot} = \frac{T_{em}}{T_{em,l}} \tag{B.16}$$

The inertia is obtained as follows:

$$J_{mot} = J_{mot_{ref}} \left(\frac{L_{mot}}{L_{mot_{ref}}} \right) \cdot \left(\frac{D_{mot}}{D_{mot_{ref}}} \right)^4 \tag{B.17}$$

Where $J_{mot_{ref}}$, $L_{mot_{ref}}$ and $D_{mot_{ref}}$ are respectively the inertia, length and diameter of the reference motor. The diameter term $\frac{D_{mot}}{D_{mot_{ref}}}$ represent the effect of diameter on the rotor diameter.

The mass model is obtained using surrogate modelling:

$$M_{mot} = 5945.85 L_{mot} D_{mot}^2 e_y^{0.06654} \tag{B.18}$$

The motor maximum mechanical speed is obtained using a scaling law as follows:

$$\Omega_{mot_{max}} = \Omega_{mot_{max_{ref}}} \cdot \left(\frac{T_{em}}{T_{em_{ref}}} \right)^{-\frac{1}{3.5}} \tag{B.19}$$

Where $\Omega_{mot_{max_{ref}}}$ and $T_{em_{ref}}$ are respectively the maximum mechanical speed and electromagnetic torque of the reference motor.

Electrical Model

The electrical model of the model is needed to evaluate the factor β used for the power electronics sizing.

The torque constant of the motor is derived using the DC bus voltage U_{DC} and the maximum operating speed of the motor Ω_{mot}.

$$K_e = \frac{U_{DC}}{2\Omega_{mot}} \tag{B.20}$$

The peak current can then be yielded:

$$I_{peak} = \frac{2}{3} \frac{T_{em}}{K_e} \tag{B.21}$$

The electrical resistance of one phase of the motor in obtained as follows:

$$R_{mot} = P_J \frac{2}{3} I_{peak}^2 \tag{B.22}$$

The electromotive force can also be derived for the operating point $\Omega_{mot,mean}$ used to compute the thermal response:

$$E = K_e \cdot \Omega_{mot,mean} \tag{B.23}$$

The effect of the inductor on the voltage when compared to the resistor is negligible. The phase voltage of the motor can then be obtained:

$$V = R_{mot} \cdot I_{peak} + E \tag{B.24}$$

Finally, the factor β is expressed as follows [86]:

$$\beta = 2 \cdot \frac{V}{U_{DC}} \tag{B.25}$$

Appendix C

Electrical Thrust Reverser Actuation System Case Study

Trapezoidal Speed Profiles

The trapezoidal speed profiles were develop to enable a simple parametrization of the ETRAS mission profile in terms of position, speed, acceleration and load. The models used have one degree of freedom which is the maximum speed at actuator level $V_{act_{max}}$. The bounds of the maximum actuator speed have to be computed with respect to the required deploy (or stow) time t_d (or t_s), stroke S_{act} and 80 % stroke $S_{80\%}$ to make the chosen profile valid. In addition, if the TLS zone distance X_{TLS} or speed V_{TLS}, it will have an impact on the parameter bounds. In this section, the parametrization and the mathematical models used to computed the different instants are given. The bounds of $V_{act_{max}}$ can be obtained numerically by minimizing and maximizing t_4 with respect to $V_{act_{max}}$, subject to the time sequence constraints ($t_f \geq t_5 \geq t_4 \geq t_3 \geq t_2 \geq t_1$).

Deploy

Figure C.1 illustrates the parametrization of the deploy speed profile. It enable then to obtain by derivation and integration respectively the acceleration and the position with respect to time.

The instants t_f (t_d) and t_4 are imposed by requirements because t_4 correspond to 2 seconds where 80% of full stroke has to be reached.

$$t_2 = \frac{x_{TLS}}{V_{TLS_{max}} \cdot \left(1 - \frac{k_{TLS}}{2}\right)} \tag{C.1}$$

$$t_1 = t_2 \cdot k_{TLS} \tag{C.2}$$

$$t_3 = \frac{2 \cdot (V_{act_{max}} \cdot (t_4 - t_2) - (S_{80\%} - x_{TLS}))}{V_{act_{max}} - V_{TLS_{max}}} + t_2 \tag{C.3}$$

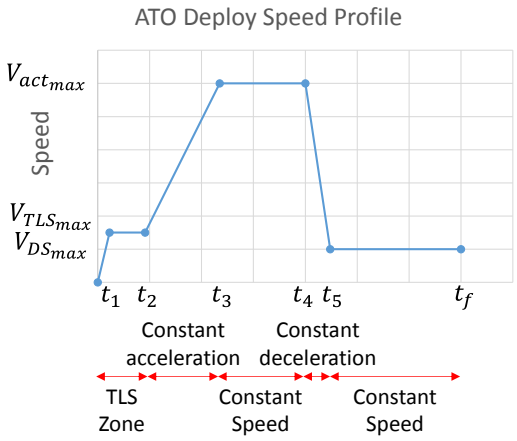

Fig. C.1 ATO Deploy speed profile principle

$$t_5 = \frac{2 \cdot (V_{ds_{max}} \cdot (t_f - t_4) - (S_{act} + x_{unc} - S_{80\%}))}{V_{ds_{max}} - V_{act_{max}}} + t_4 \tag{C.4}$$

Figure C.2 and Figure C.3 shows the resulting profiles respectively for a medium and high $V_{act_{max}}$.

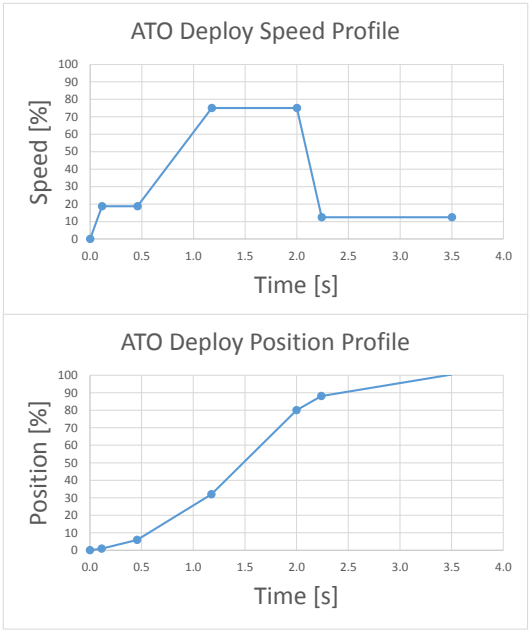

Fig. C.2 ATO Deploy speed and position for medium maximum speed

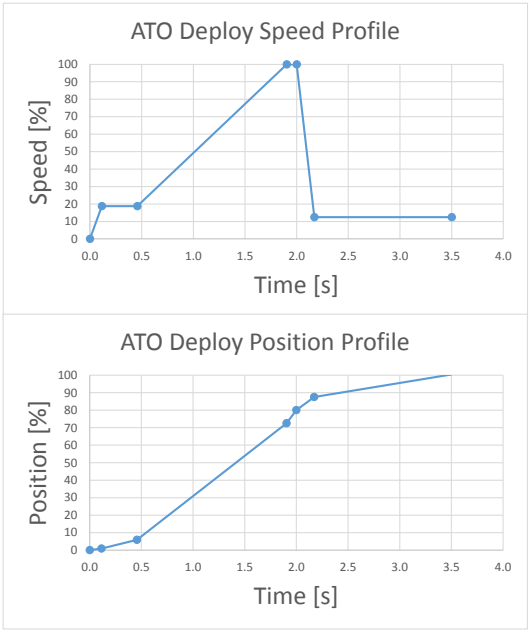

Fig. C.3 ATO Deploy speed and position for maximum speed

Stow

Figure C.4 illustrates the parametrization of the speed profile. It enable then to obtain by derivation and integration respectively the acceleration and the position with respect to time.

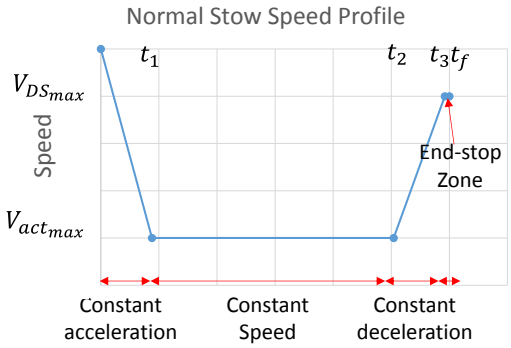

Fig. C.4 Normal Stow speed profile principle

The instant t_f (t_s) is imposed by requirements.

$$t_3 = t_f - \frac{x_{unc}}{V_{ds_{max}}} \tag{C.5}$$

$$t_1 = \frac{2 \cdot (V_{act_{max}} \cdot t_3 - S_{act})}{2 \cdot V_{act_{max}} - V_{ds_{max}}} \tag{C.6}$$

$$t_2 = t_3 - t_1 \tag{C.7}$$

Figure C.5 and Figure C.6 shows the resulting profiles respectively for a medium and high $V_{act_{max}}$.

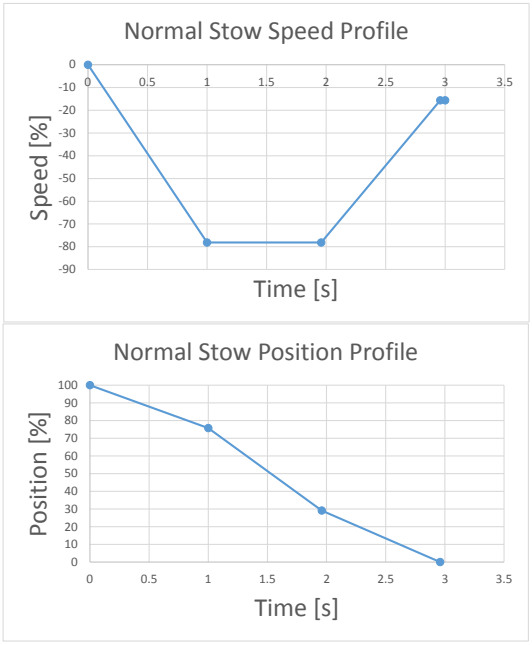

Fig. C.5 Normal Stow speed and position profile for medium maximum speed

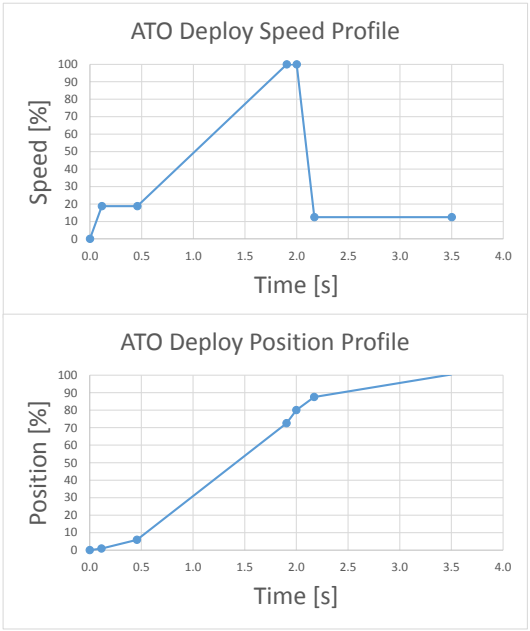

Fig. C.6 Normal Stow speed and position for maximum speed

Overspeed Limit

The overspeed limit is an envelop of position/speed configurations in which the ETRAS shall remain in order to be able to stop the motion, thanks to a braking device, despite the aerodynamic loads once the motor control loss occurs. This protects the system from overloads due to high speed arrivals on mechanical end-stops. The benefits of friction in the mechanical power chain are not considered to be conservative. The study is achieved at transcowl level.

Once the motor control losses occurs the ETRAS is considered as a single mass $M_{ref_{tot}}$ submitted to aerodynamic loads F_{aero}. After the brake engagement time t_r the mass is submitted to aerodynamic loads which tend to open the transcowl and a constant braking force F_{brake}. The behaviour of the system to motor loss of control in different initial position and speed configurations in given in Figure C.7.

It is shown that if the motor control loss occurs outside the overspeed limit envelop the ETRAS is not brought to the end-stop speed limit before reaching full stroke. The modelling and construction of this envelop is quite tricky due to the fact that the aerodynamic loads are position dependant. The system can be modelled by the following differential equation:

$$M_{ref_{tot}} \cdot \frac{\mathrm{d}^2 X(t)}{\mathrm{d}t^2} = F_{load}\left(X(t)\right) - F_{brake}(t) \tag{C.8}$$

Where the loss of motor control occurs at $t = 0$, $F_{brake}(t) = 0$ for $t < t_r$ and $F_{brake}(t) = F_{brake}$ for $t \geq t_r$.

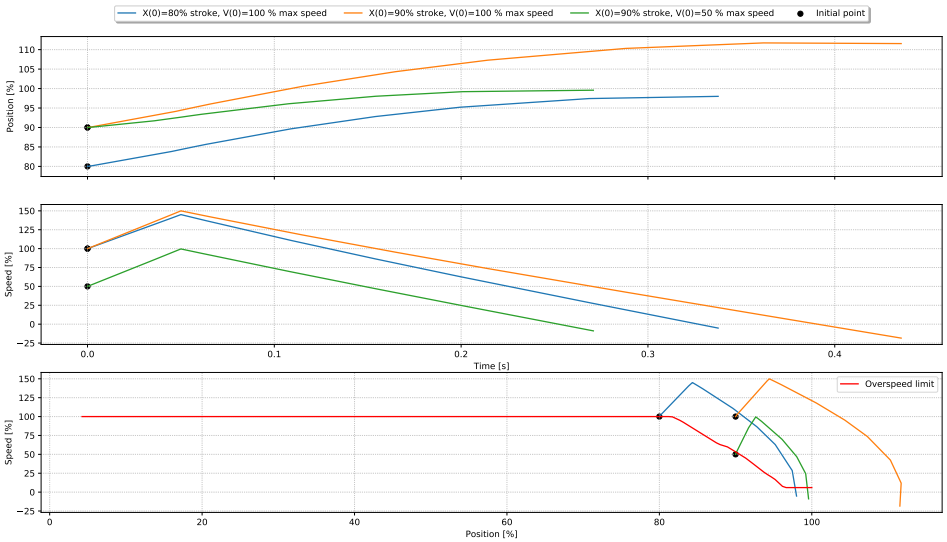

Fig. C.7 Overspeed limit principle

The overspeed limit is determined by analyzing the system response in terms of braking distance for different position and speed initial conditions. Two difficulties have to be undertaken: the position dependant load and the delay of the speed brake (hybrid system). This has to be solved numerically. To solve the problem, it is chosen to decompose the problem into two successive system of differential equations.

The first system represent the first state of the ETRAS $M_{ref_{tot}}$ when it is submitted to only aerodynamic loads for the brake reaction time duration:

$$\begin{cases} M_{ref_{tot}} \cdot \frac{\mathrm{d}^2 X(t)}{\mathrm{d}t^2} = F_{load}\left(X(t)\right) \\ \frac{\mathrm{d}X(t_0)}{\mathrm{d}t} = V_0 \\ X(t_0) = X_0 \end{cases} \tag{C.9}$$

This system is simulated for a time t_r and the final position and speed values (X_1 and V_1) are obtained. These final states of the system are the initial points of the second system of equations that represent the phase where the ETRAS $M_{ref_{tot}}$ is submitted to both the aerodynamic load and the braking force.

$$\begin{cases} M_{ref_{tot}} \cdot \frac{\mathrm{d}^2 X(t)}{\mathrm{d}t^2} = F_{load}\left(X(t)\right) - F_{brake} \\ \frac{\mathrm{d}X(t_0)}{\mathrm{d}t} = V_1 \\ X(t_0) = X_1 \end{cases} \tag{C.10}$$

The system is simulated for a fixed time. The results obtained are a the vector of position and speeds with respect to time.

The construction of the overspeed limit envelop consist of determining which have the initial position and speed (X_0 and V_0) configurations which lead to a braking distance within the stroke. The position when speed has reached the end-stroke speed limit shall be less than full stroke. In order to do that, several simulations are achieved with different initial positions and speeds. The simulations which have a successful braking time are then kept are feasible configurations as illustrated in Figure C.8. To determine the overspeed limit trajectory, a Pareto filtering that maximizes the speed and the position is achieved.

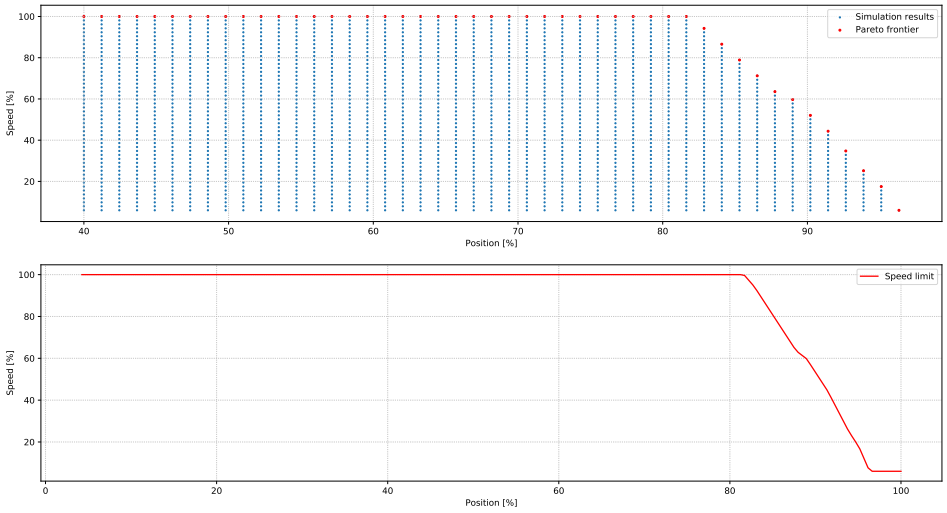

Fig. C.8 Overspeed limit construction

The braking force and the brake engagement time have a effect on the overspeed limit trajectory as shown in Figure C.9.

A high braking force and a low brake engagement time lead to less constraining overspeed limit trajectories. Hence, both of these parameters have to be taken into account during design.

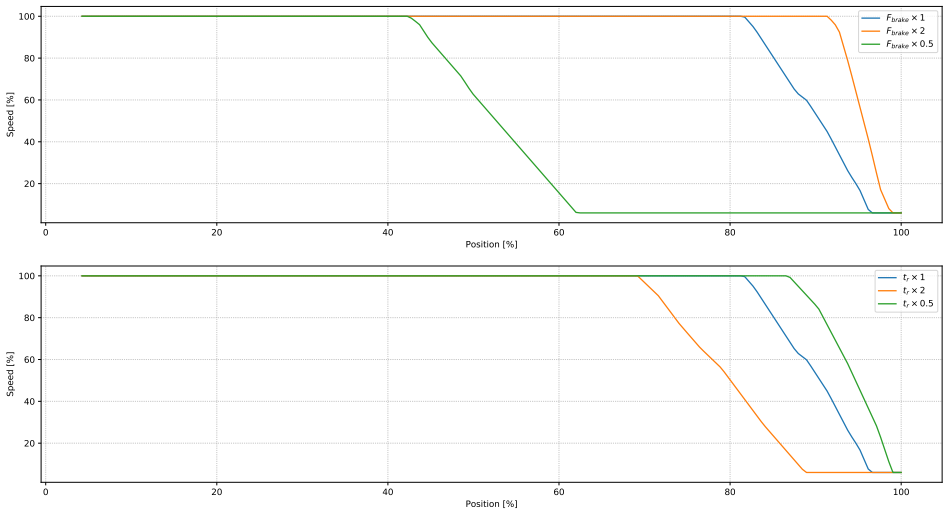

Fig. C.9 Overspeed limit parameters